Effect of stucture on digestion of proteins

Maja Napieraj

université PARIS-SACLAY

Effect of structure on digestion of proteins

Effet de la structure sur la digestion des protéines

Thèse de doctorat de l'université Paris-Saclay

École doctorale n° 571
Sciences Chimiques : Molécules, Matériaux, Instrumentation et Biosystèmes (2MIB)
Spécialité de doctorat : Physique
Graduate School : Chimie
Référent : Faculté des sciences d'Orsay

Thèse préparée dans l'unité de recherche **LLB (Université Paris-Saclay, CEA, CNRS)**, sous la direction d'**Annie BRÛLET**, Ingénieure de Recherche CNRS.

Thèse soutenue à Paris-Saclay, le 17 mai 2023, par

Maja NAPIERAJ

Composition du Jury

Membres du jury avec voix délibérative

Monique AXELOS Directrice de Recherche, INRAE, Nantes	Présidente
Laurence RAMOS Directrice de Recherche, CNRS, Montpellier	Rapporteur & Examinatrice
Denis RENARD Directeur de Recherche, INRAE, Nantes	Rapporteur & Examinateur
Anja JANSSEN Maître de conférences, Wageningen University & Research	Examinatrice
Guillaume TRESSET Directeur de Recherche, CNRS, Orsay	Examinateur

THESE DE DOCTORAT

NNT : 2023UPASF036

université PARIS-SACLAY

ÉCOLE DOCTORALE
Sciences Chimiques : Molécules, Matériaux, Instrumentation et Biosystèmes (2MIB)

Titre : Effet de la structure sur la digestion des protéines

Mots clés : Digestion, Nourriture, Structure des protéines, Gels de protéines, Rhéologie, Diffusion aux petits angles

Résumé : Les protéines sont des macronutriments irremplaçables dans l'alimentation humaine, fournissant les acides aminés essentiels aux fonctions de l'organisme. Les aliments protéiques ingérés dans le système gastro-intestinal subissent diverses modifications physico-chimiques, induites par le pH et les environnements enzymatiques (la pepsine gastrique à pH acide, puis les protéases intestinales à pH neutre).

Contrairement aux processus biochimiques de la digestion des protéines, les questions biophysiques, comme les changements des structures moléculaires (dépliement, agrégation, réticulation des protéines…) sont peu connues.
Nous abordons la question des changements structurels, lors d'une digestion gastro-intestinale simulée, des protéines de colza (la cruciférine - un grand cylindre creux et la napine - un petit ellipsoïde compact).

Dans un premier temps, nous caractérisons les comportements et les structures des protéines de colza dans des solutions natives, à divers environnements de pH et dans des conditions dénaturantes (chimiques et par la chaleur).
L'information structurale sur le mélange de ces protéines provient principalement de la structure de la plus grande cruciférine. Nous nous concentrons sur deux gels préparés par chauffage à différentes conditions de pH. Dans les gels à pH 8, les protéines sont plutôt dépliées, alors que dans les gels à pH 11, elles conservent une conformation assez repliée.

Ensuite, nous étudions les comportements de ces deux gels lors de la digestion gastro-intestinale principalement *in vitro*, par l'utilisation de la rhéologie et la Diffusion de neutrons aux petits angles (DNPA), en observant les différentes tendances des structures protéiques pour les deux gels, en fonction des conditions digestives.
Les études complémentaires de la Diffusion de rayons X aux petits angles (DXPA) ont permis de détailler et de compléter les tendances déjà observées, avec des comportements complexes des protéines lors de la digestion, impliquant des évolutions de va-et-vient avec le dépliement et le re-compactage des protéines ainsi que l'agrégation, avant les scissions finales des protéines aboutissant à des petits peptides.
Les différences de comportement des protéines entre les deux gels résultaient des états initiaux des protéines (dépliées ou compactes) affect les processus et les cinétiques de dégradation enzymatique des gels.

Ces études ont été complétées par des expériences d'imagerie, permettant d'explorer à l'échelle microscopique, c'est-à-dire la structure des gels et la taille des agrégats de protéines (imagerie confocale et neutronique), et les processus de digestion in situ des gels (fluorescence UV).
L'approche méthodologique a permis de lier les changements conformationnels des protéines au cours de la digestion aux propriétés microscopiques et macroscopiques des gels.

université PARIS-SACLAY

ÉCOLE DOCTORALE
Sciences Chimiques : Molécules, Matériaux, Instrumentation et Biosystèmes (2MIB)

Title : Effect of structure on digestion of proteins

Keywords : Digestion, Food, Protein structure, Protein gels, Rheology, Small-Angle Scattering

Abstract : Proteins are irreplaceable macronutrients in human diet, providing essential amino acids for different functions of the body.
Ingested protein food in gastro-intestinal tract undergoes various physicochemical modifications, induced by pH and enzymatic environments, i.e. gastric pepsin at acidic pH, followed by intestinal proteases at neutral pH.

Unlike biochemical processes of protein digestion, the biophysical questions, like the conformational changes of molecular structures (e.g. protein unfolding, aggregation, crosslinking) are still little known.
We address, in this thesis, the issue of structural changes during simulated gastro-intestinal digestion of canola proteins (i.e. cruciferin – a large hollow cylinder and napin – a small compact ellipsoid).

First, we characterize the behaviors and structures of canola proteins in native solutions, at various pH environments and under denaturing conditions (chemical and by heat).
The structural information on the mixture of those proteins arises mainly from the larger cruciferin's structure. We focus on two heat-set gels, prepared at different pH conditions. In the pH 8 gels, proteins are rather unfolded, whereas in the pH 11 gels, they retain a quite folded conformation.

We first studied the behaviors of these two gels upon *in vitro* gastro-intestinal digestion. By the use of rheology and SANS, we observed different trends of the protein structures for the two gels, depending on the digestive conditions.
The further studies by SAXS enabled to detail and complete the already observed trends, with complex behaviors of the proteins upon digestion, involving back-and-forth evolutions with the proteins unfolding and re-compaction together with aggregation, before the final protein scissions resulting in small peptides.
The differences in protein behaviours between the two gels resulted from the initial states of the proteins (unfolded or compact), which affected the rates the enzymatic degradation of the gels.

This studies were completed by imaging experiments, allowing to explore microscale, i.e. structure of the gels and sizes of protein aggregates (confocal and neutron imaging), and the *in situ* digestion processes of the gels (UV fluorescence).
The methodological approach allowed to link the protein conformational changes during digestion with microscopic and macroscopic properties of the gels.

Acknowledgements

First and foremost, I want to thank my supervisors Annie Brûlet and François Boué, and my encadrement Evelyne Lutton, who gave me continuous mentorship, through their knowledge and plentiful experience. Thank you for your engagement, professional and personal support, and patience. Annie, thank you for kindness and scientific rigor. François, thank you for plenty of discussions on scientific and non-scientific topics. Evelyne, thank you for your enthusiastic and friendly encouragement.

I want to thank CNRS and Laboratoire Léon Brillouin for the finantial support during the whole duration of my thesis.

Furthermore, I want to thank to all the people from Laboratoire Léon Brillouin who made it a great pleace to work, with friendly and cooperative atmosphere. Especially all the members of Matière Molle et Biophysique group, my colleagues and lab mates – for your scientific insights and the time spent together in social settings.

I would like to thank all the people who contributed in some way to the work described in this thesis, in particular: Marianne Bombled for introducting me to the lab environment and for technical support. Former Post-Doc Simeon Minić, for having time for my questions in the beginning of my PhD. Daniel Dudzinski, for your experstise along my rheological experiments and your company during Synchrotron experiments. Fabrice Cousin, for performing neutron experiments in ILL when I couldn't do it, but foremost, for always being available for my questions and for useful comments on my work. Clémence LeCœur, for enabling the access to confocal microscope in ICMPE in Thiais and for your help. I would also like to thank Frédéric Gobeaux, who enabled the access to the Zeta-potential analyser in LIONS Laboratory in CEA.

I would also like to thank scientists in Synchrotron Soleil: Frédéric Jamme and Hugo Chauvet from DISCO and Javier Pérez from SWING beamline, for their high-quality technical and scientific support during experiments. Thanks to Matteo Busci from PSI in Switzerland for a valuable contribution in neutron imaging experiments, data treatment and analysis support.

Additional thank you to: Arnaud Helary for your technical help with the SAXS sample environment. Aurore Verdier, Olivier Sineau and Sarah Même, who deserve credit for their assistance with administrative work. Gaston Exil and Remy Lautie, who provided support for any IT problems.

Last, but not least, to my family: my loving parents, my brother and my grandparents, who gave me emotional support. Mamo, Tato, dziekuje wam za możliwość edukacji i rozwijania pasji, bezgraniczną miłość i wsparcie w każdej decyzji, którą podejmuję. To my partner Nils, who has been a never-ending source of love, encouragement and motivation. To my dear friends from Poland and from France, for all your your friendship, love and unyielding support.

Table of Contents

Introduction (*en français*)

Il est maintenant reconnu que l'alimentation est plus qu'une simple somme de nutriments car de plus en plus de preuves expérimentales montrent que la qualité nutritionnelle de l'alimentation, et donc sa pertinence pour la santé, ne dépend pas seulement de la composition de l'aliment lui-même, mais aussi d'autres facteurs qui influencer sa digestion. La forme sous laquelle l'aliment est consommé, comprend ses caractéristiques physico-chimiques et sa structure spécifique, i.e. l'arrangement de tous les éléments et leurs interactions à de multiples échelles de longueur spatiale. La structure des aliments est soit naturelle, soit formée ou détruite par différents types de préparation ou de transformation, par exemple par la chaleur ou des modifications chimiques. Il peut donc avoir un impact critique sur son évolution dans le système digestif gastro-intestinal, influençant la cinétique de la digestion et son efficacité, et donc l'absorption finale des nutriments et les conséquences potentielles sur la santé.

Cette préoccupation sur la structure s'applique à toutes sortes d'aliments. Au niveau des composants simples, qui semble être le premier niveau à comprendre, le sort des glucides est probablement le plus simple. Les lipides ont été assez largement étudiés, mais ce n'est pas le cas des protéines - macronutriments complexes et irremplaçables, qui fournissent les acides aminés essentiels nécessaires à de nombreuses fonctions du corps humain. Leur complexité structurelle pourrait être l'une des raisons de leur évaluation limitée sous divers stimuli au cours de la digestion.

La structure est l'aspect de départ de cette thèse : les aliments riches en protéines sont généralement consommés sous forme solide, ce qui nécessite souvent une perturbation plus importante de leur structure. Cependant, les processus qui déterminent la vitesse et les mécanismes sous-jacents reliant les propriétés structurelles des aliments et les résultats de leur digestion ne sont toujours pas clairs.

Afin de comprendre comment la structure d'aliments spécifiques affecte leur digestion, il faut en explorer le maximum, y compris non seulement ses résultats de digestion/résultats finaux, mais aussi les processus et les comportements des protéines dans le système digestif gastro-intestinal.

La préoccupation sur la structure alimentaire en rencontre une autre – la durabilité de l'alimentation. En raison d'une population mondiale croissante, les ressources mondiales sont obligées de fournir de plus en plus de protéines, cependant, les limites des terres, ainsi que les préoccupations écologiques rendent plus nécessaire de réduire la consommation de protéines d'origine animale, en particulier dans le monde occidental, et à les remplacer par des alternatives végétales nouvelles ou existantes. Ceci est nécessaire pour assurer une production de protéines suffisante mais aussi durable.

Les protéines d'origine végétale sont généralement considérées comme inférieures aux protéines animales, compte tenu de leur qualité nutritionnelle, notamment en ce qui concerne la teneur en acides aminés essentiels; cependant, l'image inférieure des protéines végétales n'est pas toujours exacte. La graine de colza (Brassica napus), choisie pour cette thèse, est par exemple considérée comme une très bonne source de protéines de haute qualité, avec un profil d'acides aminés bien équilibré, riche en résidus essentiels. Même si les protéines de colza ne sont pas encore utilisées dans l'alimentation humaine, leur grande valeur biologique offre un fort potentiel d'utilisation en tant qu'ingrédient alimentaire humain.

Dans cette thèse, en appliquant les techniques d'étude des protéines moins explorées jusqu'à présent, nous visons à étudier la digestion des protéines végétales structurées, en abordant simultanément ces deux sujets importants.

Enfin, ces connaissances pourraient, espérons-le, fournir des informations supplémentaires utiles, par exemple dans la conception ou l'optimisation de nouveaux aliments à base de protéines avec des comportements spécifiques lors de la digestion et des effets physiologiques souhaitables.

Cette thèse porte sur la digestion gastrique et intestinale simulée des protéines de graines de colza dans leurs états natifs et transformés, c'est-à-dire les solutions protéiques et les gels thermofixés. L'effort a été mis sur l'exploration de ces modèles de structures alimentaires à différentes échelles de longueur, du nano au micrométrique, que nous détaillons ci-dessous.

Le chapitre 1 de ce manuscrit commence par une présentation des connaissances actuelles et de l'état de l'art sur la composition générale et la structure des protéines, et plus particulièrement - des protéines de graines de colza. Il montre la relation entre la structure alimentaire des protéines à plusieurs échelles de longueur avec la digestion et la nutrition, et donne un aperçu du système digestif humain et des processus de digestion des protéines. Il résume les informations de la littérature et fournit une évaluation critique de l'écart actuel de la recherche, avec la présentation de l'objectif de la thèse.

Le chapitre 2 présente les différentes techniques utilisées dans cette thèse, les méthodes de préparation des échantillons, les modes opératoires et les traitements des données.

Le chapitre 3 décrit la conformation et les caractéristiques de charge des protéines de colza (cruciférine et napine séparément et en mélange) avant la digestion, à l'aide de techniques de diffusion aux petits angles, de potentiel zêta et de spectrophotométrie. Il fournit les informations sur les états des protéines dans des solutions natives et dans différentes conditions non natives (pH, dénaturants chimiques et chaleur). La gélification des protéines induite par la chaleur a été ici plus détaillée avec des mesures de rhéologie (propriétés mécaniques) et de Diffusion aux petits et grands angles (nanostructure).

Par la suite, la digestion des protéines de colza a été étudiée.

Le chapitre 4 présente les évolutions structurales des gels de protéines de colza préparés à deux pH différents (présentant des structures différentes), au cours de la digestion gastrique et gastro-intestinale in vitro. Les structures protéiques et les propriétés des gels ont été étudiées par :

- Des techniques de rhéométrie et de diffusion de neutrons aux petits angles, sur des échantillons de tailles similaires à celles obtenues après mastication orale in vivo ;
- La diffusion des rayons X aux petits angles, sur des échantillons dans les capillaires, qui nous a fourni des informations structurelles plus détaillées sur les protéines lors de la digestion in situ et des informations dynamiques importantes sur les processus multi-échelles. C'est la partie centrale de ce manuscrit de thèse.
- La diffusion à grands angles (WAXS), pour explorer les changements dans les structures secondaires.

Le chapitre 5 complète les informations structurales à plus grande échelle, par l'utilisation de différentes techniques d'imagerie:

-L'imagerie UV-Fluorescence (10 à plusieurs 100 µm) de la diffusion et de la digestion enzymatique in-situ des gels.
- La fluorescence confocale et l'imagerie en champ noir neutronique de gels après une durée de digestion donnée, permettant l'exploration des tailles d'agrégats de protéines (de l'ordre µm).

Introduction

It is now recognized that food is more than just a sum of nutrients and there is a growing experimental evidence showing that the nutritional quality of food, and so its health relevance, depends not only on the food composition itself, but also on other factors which influence its digestion. The form in which the food is consumed, comprises its physicochemical characteristics and its specific structure, which is defined as the arrangement of all the elements and their interactions at multiple spatial length scales. The structure of food either occurs naturally or is formed or destroyed by different types of preparation or processing, e.g. by heat or chemical modifications. It can therefore have a critical impact on its evolution in the gastro-intestinal tract, influencing the digestion kinetics and its efficiency, and so the final absorption of nutrients and potential health consequences.

This concern on the structure applies to all kinds of foods. At the level of single components, which seems to be the first to understand, the fate of carbohydrates is probably the simplest. Lipids have been rather extensively studied, but it is not the case for proteins - complex, irreplaceable macronutrients, which provide essential amino acids needed in many human body functions. Their structural complexity might be one of the reasons for their limited evaluation under various stimuli during digestion.

The structure is the starting aspect in this thesis: protein-rich food is usually consumed in solid-like form, which often requires longer disruption of its structure. However, the processes that determine the rate and the underlying mechanisms linking the structural properties of foods and the results of their digestion are still not clear.
In order to understand how the structure of specific foods affects their digestion, one needs to explore the most of it, including not only its digestion outcomes/final results, but also the processes and the behaviors of the proteins within the gastrointestinal tract.
The concern on the food structure meets another one – sustainability of food. Due to an increasing global population, the world's resources are forced to provide more and

more proteins, however, the lands limitations, as well as the ecological concerns make it more necessary to reduce consumption of animal-sourced proteins, especially in western world, and to to replace them by new or existing plant alternatives. This is required to ensure sufficient but also sustainable protein production.

Proteins from plant sources are generally valued as inferior to animal ones, when considering their nutritionally quality, especially with respect to the essential amino acid content; however, the inferior image of plant proteins is not always accurate. Canola seed (*Brassica napus*), chosen for this thesis, is, for instance, considered to be a very good source of high-quality proteins, with a well-balanced amino acid profile, rich in essential residues. Even though canola proteins are not yet utilized in human nutrition, their great biological value offers a high potential in use as human food ingredients.

In this thesis, by applying the techniques to study proteins, less explored until now, we aim at studying digestion of structured plant proteins, simultaneously addressing both of these important topics

As a final point, such knowledge could hopefully provide further insight helpful e.g. in designing or optimization of new protein-based foods with specific behaviors during digestion and desirable physiological effects.

This thesis focuses on research on simulated gastric and intestinal digestion of canola seed proteins in their native and processed states, i.e. protein solutions and heat-set gels. The effort was put on the exploration of those model food structures at different length scales, from nano to micrometric, which we detail just below.

Chapter 1 of this manuscript starts with a presentation of current knowledge and state-of-the-art about general composition and structure of proteins, and specifically - canola seed proteins. It shows the relation of the protein food structure at several length scales with digestion and nutrition, and overviews the human digestive system and protein digestion processes. It summarizes information from the literature and provides a critical evaluation of the current research gap, with presentation of the aim of the thesis.

Chapter 2 presents the different techniques used in this thesis, the samples preparation methods, operating modes and data treatments.

Chapter 3 describes the conformation and charge characteristics of canola proteins (cruciferin and napin separately, and in a mixture) before digestion, with the use of Small-Angle Scattering, zeta-potential and spectrophotometric techniques. It provides information about the protein states in native solutions and under different non-native conditions (pH, chemical denaturants and heat). The heat-induced gelation of the proteins was here further monitored: by rheology (mechanical properties) and Small and Wide-Angle Scattering (nanostructure).

Subsequently, digestion of canola proteins was studied.

Chapter 4 presents the structural evolutions of the canola protein gels prepared at two different pH (owning different structures), during *in vitro* gastric and gastro-intestinal digestion. The protein structures and gels properties were studied by:

- Rheometry and Small-Angle Neutron Scattering techniques, on samples with sizes similar to the ones obtained after oral chewing *in vivo*;
- Small-Angle X-ray Scattering, on samples in capillaries, which provided us more detailed structural information about proteins during *in situ* digestion and with important dynamic information of multi-scale processes. This is the central part of the work.
- Wider scattering angles (WAXS), to explore changes in secondary structures.

Chapter 5 completes the structural information at larger scales, by the use of different imaging techniques:

- UV-Fluorescence imaging (10 to several 100 µm) of the *in-situ* enzymatic diffusion and digestion of the gels.
- Confocal fluorescence and Neutron Dark-field imaging of gels after given duration of digestion, enabling the exploration of protein aggregates sizes.

Chapter 1 Literature Review

1.1 Proteins

1.1.1 Composition and Structure

Proteins are complex biological macromolecules composed of different amino acid (AA) sequences of diverse characteristic lengths and arrangements. An amino acid is made up of a central α-carbon atom, covalently linked to an amino ($–NH_3^+$) and a carboxyl (−COO–) group, together with a hydrogen atom and a functional side chain group (R) (**Figure 1**). The size, shape, solubility and ionization of the side chain group define the unique nature of a given amino acid (polar, charged aliphatic or aromatic), and therefore the physicochemical properties of the whole protein and then its interactions with other molecules[1,2,3].

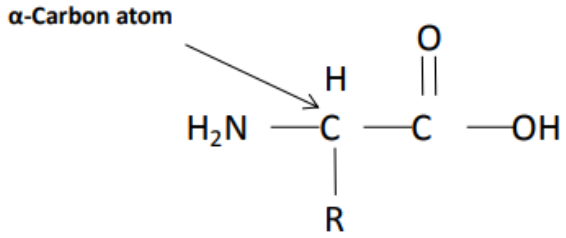

Figure 1 Schematic representation of an amino acid.

Adjacent amino acids are linked together by a covalent peptide bond into a linear sequence of AA of a given chain length (polypeptide), which represents the **primary structure** of a protein. Each type of protein owns a distinct primary structure, which drives the bonding and folding of the linear sequence, and ultimately determines further structural levels within a protein molecule, namely secondary, tertiary and quaternary structures[1,2,3]. The **secondary structure** refers to the folding pattern of the protein polypeptide chain(s), with principal motifs being α-helices and β-pleated sheets[4], all stabilized *internally* by hydrogen bonding (between amide hydrogens and carbonyl oxygens on the polypeptide chain)[1,2]. An α-helix is formed when a polypeptide chain turns around itself, forming a structural motif resembling a spiral (with 3.6 amino acid residues in its complete turn and 1.5 Å per each amino acid along its axis, resulting in

the length of 5.4 Å)[2,4.] It has a compact structure, with side chains facing outward the cylindrical core, allowing their interactions with other motifs. Due to a steric hindrance/rigidity of proline (Pro) and too high flexibility of glycine (Gly), those two amino acids are not favourable in the α-helices[6]. Thus, proteins with a predominance of α-helices exhibit an amphiphilic behaviour, with hydrophobic residues (i.e. Val, Pro, Leu, Ile, Phe, Trp, Ala, Met) remaining in the molecule's core and the hydrophilic ones on its exteriors[3,5]. A β-pleated sheet structure consists of at least two extended polypeptide chains (β-strands), with typically 3 to 10 amino acids, organized linearly side-by-side, in either parallel or antiparallel orientation in respect to each other, creating a sheet-like structure[2,6]. They are more extended and flat conformations, compared to α-helices, with 3.5 Å distance between amino acids along a strand[6]. Here, hydrogen bonds are formed not only within a single chain (backbone), which give the local stabilisation, but also between the adjacent β-strands. Besides, hydrophobic or van der Waals interactions occur between the strands in layered sandwich-like structures, when more than two polypeptides participate. Those inter-strands contacts give additional stabilization to beta-sheets, compared to α-helices[7]. Proteins with a higher content of β-sheets are considered to be more resistant against heat than the α-helical ones[3].

In globular proteins, with compact folded structures, the polypeptide chains often reverse their directions in particular turns or loops, comprised of several AA residues linking successive runs of α-helices or β-sheets. The most common motifs are there β-turn, often found on the protein surface, with their middle amino acids hydrogen-bonded with water molecules. Pro and Gly residues often occur in β turns, due to small size, flexibility and the favourable configuration[2].

The least stable secondary structure of a protein is a random coil, characterized by a of a polypeptide chain without distinctive motif elements. In other words, formation of random coils[1] can be associated with protein denaturation through a disruption of the native tertiary folding and/or the α-helices or β-sheets[1,8].

[1] More precisely, this conformation was identified with the one of Self Avoiding Walk, using SANS (Russo, D., Durand, D., Desmaril, M., Calmettes, P. (2000). *Physica B.*, 276-278, 520-52).

Folding of the secondary structure components into a global three-dimensional arrangement is defined as a **tertiary structure** of a protein. It is stabilized by a range of intramolecular interactions, including hydrogen bonding, hydrophobic and Van der Waals interactions and covalent disulfide bridges (formed between the sulfhydryl side chains of two cysteine residues, allowing distant parts of the protein to be held together)[6].

Furthermore, the several tertiary structures can assemble in a multi-subunit oligomeric structure (dimeric, trimeric, tetrameric etc), called the **quaternary structure** of the protein[3].

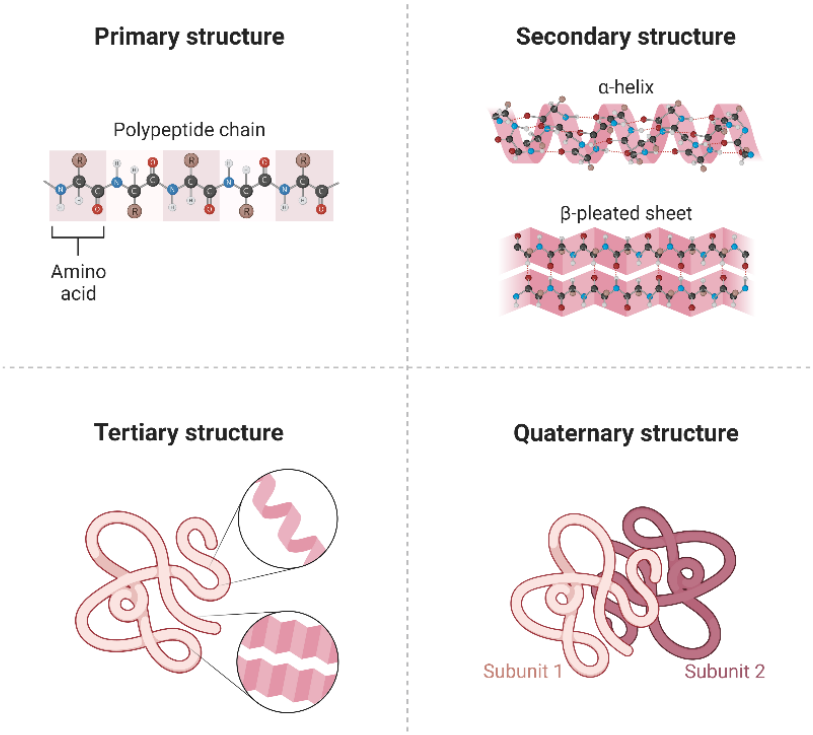

Figure 2 Schematic representation of primary, secondary, tertiary and quaternary structures of proteins. Created with BioRender.com

We can distinct globular, fibrous, membrane or disordered proteins. Globular proteins represent approximately spherical, compact molecules with their hydrophobic amino acids in the core and the charged, hydrophilic residues on the surface of the protein. Thanks to these features, globular proteins in aqueous environment can be solubilized, by participation of the charged AA side chains on the protein-water interface in weak

electrostatic interactions with water dipoles (hydrogen bonding). As the proteins become more polar, more contacts between water and protein molecules can take place, and so the protein solubility can increase[9].

1.1.2 Food Proteins

Proteins are major structural and functional components of plant and animal foods and dietary sources of amino acids. They can be categorized by their specific function, like structural, storage or transport proteins, all being vital in different human body processes, including building and repairing body tissues, muscles and bones, production of hormones and enzymes, to name a few. Human body can synthesize proteins from a combination of 20 amino acids, however, it can only produce 11 of those. The rest, referred to as essential (i.e. His, Leu, Met, Phe, Lys, Val, Iso, Thr and Try), can only be delivered externally, from food[10,11,6.] It makes the proteins indispensable macronutrients in our diets, supplying, besides the energy, the essential amino acids to meet our functional and structural needs, and providing the body development and health maintenance[12].

Majority of proteins in human diet is conventionally associated with consumption of animal products, like milk or meat, since they contain in general relatively high levels of proteins compared to plant foods. However, due to concerns about the ecological sustainability and nutrition security driven by the population growth, there is an increasing motivation worldwide to replace animal protein sources with their plant alternatives, which appear as better environmental and lower-cost options[13,14]. Moreover, an increased intake of high-quality proteins from different plant sources, such as seeds, legumes or cereals, in human nutrition is associated with beneficial effect on health[15,16,17,18]. An important share of plant proteins (with exception for e.g. gluten found in wheat) is often represented by globulins or albumins, with densely packed, well-defined secondary and ternary structures[19], with globulins (of higher molecular weights) generally predominating in legume and oil seeds, e.g. soybean or rapeseed [20].

While soy continues to dominate as an alternative plant protein source for animal-based proteins, there is a potential in other grains and vegetables as protein sources, e.g. canola seed[21].

1.1.3 *Canola Seed Proteins*

Canola plant, also known as rapeseed (from *Brassicaceae* family) is, after palm and soybean, the third source of oil seed in the world[22,23]. Apart from the oil, canola seeds contain on average 20%of protein[24] and canola "meal", which is a raw protein-rich byproduct of canola oil extraction, contains up to 40% of crude protein[25,26], making it a great protein source, competing with the ~50% protein soybean meal[27,28]. An abundant share (approx. 80%) of the total protein content of the mature canola seeds constitutes of two main storage proteins: cruciferin and napin, accounting for around 60 and 20%, respectively[29]. The relative proportions of the two proteins in canola seeds depend on the cultivar itself but also on maturation environment, presence of sulphur compounds, protein extraction and purification processes[30,31].

Cruciferin (12S or 11S) is a large-sized, neutral globulin with molecular weight of about 300 kDa. Its structure after crystallization is shown in **Figure 3** It displays an isoelectric point (IEP) around pH 7[32], contains a high level of β-sheet structures (~50%) and is rather low in α-helices (~10%)[33].

Cruciferin's native molecule is a hexamer that assembles as two trimers held together principally by non-covalent hydrophobic, electrostatic, hydrogen and van der Walls forces/bonds[34.] It shares the quaternary structure features with soy glycinin, another member of the 11S globulin family[35]. Each cruciferin's monomer comprises of two polypeptide chains: a 30 kDa α-(acidic) chain and a 20 kDa β-(basic) chain, linked covalently by a disulfide bridge[36,34]. Under denaturing conditions (e.g. low pH or in urea solutions), cruciferin's hexamer can dissociate by rupture of the intermolecular bonds into trimers or into six single subunits[37,38]. At extreme environments, e.g. under reducing conditions, the acidic and basic polypeptides of cruciferin can separate[39].

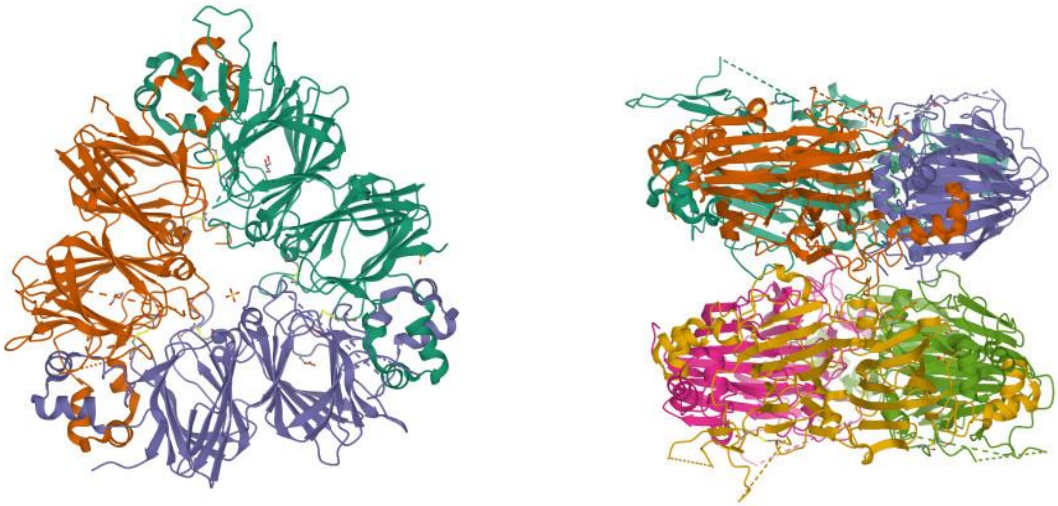

Figure 3 Crystal structure of pro cruciferin, 11S globulin from Brassica Napus (3KGL), taken from Protein Data Bank. The trigonal structure (on the left), being an antiprism of hexametric structure (on the right).

Napin (2S) is a small, alkaline albumin with molecular weight of around 12.5 to 14.5 kDa (see **Figure 4**) and the IEP between pH 9 and 11[30,40,41]. It is rich in α-helices (≈ 50 %) and poor in β-sheets (≈ 15 %) and, due to its hydrophilic character (stronger than of cruciferin) and the presence of positively charged residues on its surface, it privileges the electrostatic interactions[41]. Napin's molecule is comprised of two polypeptide chains, a small one of around 4.5 kDa and a bigger one of around 10 kDa, linked together by a pair of disulfide bridges[41,42]. The larger chain has additional two intra-chain disulfide bonds[41,42,43], which altogether greatly stabilizes and rigidizes the napin's molecule, making it resistant against denaturation and dissociation in large pH range (between pH 3 and 12)[44] and temperature (up to ~70°C)[41,34]. The compact and rigid structure of napin with four disulfide bounds provides also its higher resistance to hydrolysis, compared to cruciferin[25].

Napin has a homologous structure with a group of low molecular weight 2S albumins in other plant seeds, i.a. Brazil nuts, mustard, sunflower[40].

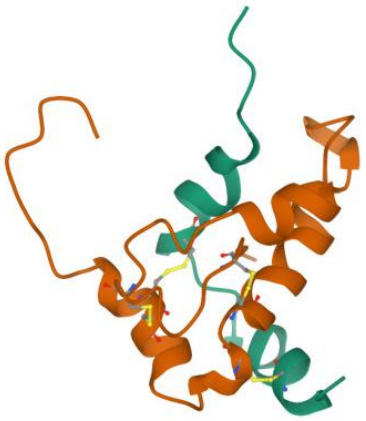

Figure 4 Schema of biological assembly of napin from Brassica Napus (1PNB) with 2 polypeptide chains, taken from Protein Data Bank.

Other types of proteins in canola seeds are the low-molecular-weight (~20 kDa) oleosins, and other minor proteins, such as thionins, trypsin inhibitors and lipid transfer proteins[30]. All the different protein fractions can be separated by chromatography, membrane filtration or electrophoretic techniques[45].

1.2 Effect of processing on protein structure

Different physical or chemical conditions applied to a native protein environment, like high temperature, pressure and shear or solvent pH/composition, can result in the protein structural modifications, involving unfolding and further proteins association (aggregation)[2,46,47]. Those structural alterations can affect the secondary, tertiary and quaternary structures of a protein, influencing mostly non-covalent bonding patterns within the molecule, but, in severe conditions, also covalent disulfide bonds (internally stabilizing the molecule[48]), yet retaining the integrity of polypeptide chain, i.e. without cleaving the peptide bonds.

Partial or complete unfolding of natively globular, compact proteins, is the effect of an exposure of the protein hydrophobic groups, initially buried into its core and, in consequence, a reorganization of its tertiary and secondary structures, often accompanied with dissociation of the quaternary structure units, and formation of more extended conformations. A significant rearrangement of the native tertiary

structure of a protein, on the way of unfolding, is defined as its denaturation. It occurs particularly under harsh conditions involving high temperatures or extremes pH. Depending on the type and severity of the denaturing environment, it may be reversible or irreversible[2,6,49]. For most proteins, irreversible denaturation can be caused by **heat**, which, increases its molecular vibrations, which can then weaken or even disrupt the hydrogen bonds, hydrophobic interactions and Van der Waals forces, which were primarily stabilizing the native protein structure[49,52].

Since almost all proteins contain some charged amino acids, they give a protein its overall net charge. Changes in the **pH** of the protein environment enable ionization of the ionisable α-amino and α-carboxyl groups of the protein, that act as a proton donor (acid) or acceptor (base) respectively, to maintain the pH of the system. An acid (H^+) added to a water solution converts the –COO– ion to a protonated –COOH group, making the amino acid positively charged and, by that, increasing the net positive charge on the protein. Correspondingly, an addition of a base (OH^-) provokes a deprotonation of the $-NH_3^+$ ion to a neutral $-NH_2$ group, resulting in a negatively charged amino acid and an increase of the net negative charge on the protein's surface. At a given pH, the net charge density depends on the protein concentration and the ionic strength[50]. The resulting charge on the protein molecules defines the strength of the electrostatic interactions between the protein themselves and between them and the solvent (e.g. the polar groups and water molecules)[3], and so influences the ionic and hydrogen bonding patterns in the protein's tertiary and quaternary structures, and modifies the protein solubility in favorable or disfavorable way.

When the pH of a protein solution is adjusted in such a way that the net protein charge becomes zero, i.e. at the protein's isoelectric point (IEP), or when salt is added, which screens electrostatic interactions[1], the protein-solvent and the protein-protein repulsive interactions weaken, and the hydrophobicity-driven and energetically-favorable protein-protein attractive forces predominate. In such conditions, globular proteins have minimum solubility and tend to precipitate and phase separate during aggregation, in protein-rich and protein-poor phases[5,49]. The IEP value depends primarily

on the AA composition, based on the combination of dissociation constants (pK) for the ionisable groups of the charged AA and so, it is specific to each protein[51].

Conversely, the greater the net charge on the protein molecule, the greater the electrostatic repulsion between the like-charged molecules, preventing their interactions and thus retaining the protein solution colloidal stability[51,49,2].

However, in extreme pH values, if the ionic attraction between the side chains within the molecule is diminished, or if strong intramolecular electrostatic repulsions occur, **protein unfolding** is provoked. An increased repulsion within the protein molecule destabilizes its folded conformation due to the greater charge density on the folded protein compared to the unfolded one, making the later one energetically favorable[52]. Acid-induced unfolding of proteins often occurs between pH 2 and 5, while base-induced unfolding can require pH 10 or higher[46]. In addition, organic solutes such as urea or guanidine hydrochloride (more soluble in water) and salts forming complexes with proteins can also induce protein denaturation[49].

Protein refolding can sometimes occur after changing/restoring the protein environment. The refolded protein is however considered as denatured since its conformation unlikely resembles the native state, due to formation of new intra-or intermolecular links[53].

Alterations in the protein structure occurring upon protein unfolding or refolding, usually lead to the formation of bonds or interactions between proteins, resulting in protein **aggregation**[53].

1.2.1 Aggregation

Aggregation occurs due to suppression of colloidal stability, e.g. via disappearance of the electrostatic repulsion at IEP, for example. It origins primarily due to weak attractive interactions, through random diffusion of proteins (by Brownian motions)

[2] If pH > IEP, the proteins will be negatively charged, and if pH < IEP, they will be positively charged.

and then, via stronger interactions/bonds, which hold the aggregated structure together[54]. When a protein unfolds, its initially buried hydrophobic residues become available to interact inter-molecularly through hydrogen bonds, electrostatic, hydrophobic interactions or covalent disulfide bonding. When many hydrophobic sites of the protein molecules are exposed, the interactions between them are inevitable, leading to their aggregation.

Those interactions between the proteins strongly depend on the protein concentration, denaturing conditions (temperature, pH, ionic strength and the processing intensity and rate), and the susceptibility/predisposition of the given (native) protein to the bonds formation and rupture in those conditions (owning to its AA composition and structure)[5,55,56]. This determines the **size, morphology and stability** of the aggregates. Wang et al. proposed a definition of a protein aggregate as a structure consisting of proteins in non-native states, having at least twice the size of the native protein[53]. Among aggregates, we can distinguish: (i) the ones formed via diffusion-controlled process, in which proteins aggregate each time they encounter each other. It is rapid and often results in **fibril-like** structures, resembling 'strings of beads'; or (ii) formed via reaction-controlled process, occurring more slowly due to electrostatic repulsions and result in coarse and open structures, favoring the particulate aggregates in which proteins weakly interact with more than one molecule at the time[57]. They are characterized by a self-similar (**fractal**) structure within some spatial length range[5,58].

We will distinguish two types of **fractal structures**: mass fractals, described by the fractal dimension D_f, with a power law dependence of a measurable quantity upon the length of the aggregate *R,* i.e. $M \sim R^{D_f}$, with *M* being its mass. D_f indicates how effectively the structure fills the available space, with D_f usually > 1 and < 3 , a higher value indicating better packing of the structure resulting in reduced void space[59]. Such structures are often characterized by a Small-Angle Scattering (SAS) power-law $1/q^{Df}$. The D_f value can vary from protein types and conditions. $D_f \sim 2$ have been reported e.g. for whey proteins[60,61], egg white proteins[62] or soy globulin[63], and its values of 1.7–1.8

were proposed for diffusion-limited aggregation and 1.9–2.2, for reaction-limited aggregation[58].

The surface fractal aggregates have a dense inner structure but a self-similar surface profile due to multi-scale (roughness of the surface; the total area is $A \sim R^{D_f}$, with D_s between 2 and 3 (larger values for more intricate, less dense surface structures[78,79]). Such structures are often characterized by a SAS power-law $1/q^{(6-Ds)}$ (for D_s = 2, on return to Porod law $1/q^4$, **cf. Chapter 2**).

Depending on the severity of the processing conditions, protein aggregation may be **reversible** - resulting from localized, short-range protein–protein interactions (e.g. hard-sphere, hydrophobic, electrostatic, van der Waals)[52] causing their self-assembly, with moderate unfolding, or **irreversible** - formed via bonds that require more energy for breaking than provided by processing, i.e. hydrogen bonds or disulfide bridges[3,5,64]. Irreversible aggregation occurs usually at high temperatures, which provide enough perturbations of the native protein conformations for their aggregation. A full unfolding of globular proteins is herein not necessary and partially unfolded molecules can be sufficient to form irreversible aggregates[3].

1.2.2 Gelation of proteins

Owing to the protein aggregation, we are able to obtain spatially organized structures, like protein **gels**[49], in which aggregates, dispersed in a continuous liquid phase, are interconnected (cross-linked) into a three-dimensional network[65,66].

To achieve this interconnection between the protein aggregates, the protein concentration in a dispersion has to be sufficient, otherwise it will result in a suspension of precipitated aggregates or macroscopically heterogeneous gels.

In case of proteins, molecular weight/hydrodynamic size of the polypeptide chain also influence the gel strength, since they are unfolded, they can act as flexible polymer

[3] Formation of disulfide bridges is favored at alkaline pH, where thiol residues can react via thiol-disulfide interchange reactions[213].

chains, i.e. can interpenetrate. Following Wang & Damodaran[67], the critical M_w of protein of about 23 kDa to form a gel.

Depending on the nature of the protein, the solvent and denaturation/gelation conditions, various types of gels can be obtained. In case of most globular food proteins, gels can form through aggregation, on the way of **temperature treatment**, where, along the heating time, more proteins denature, the aggregates increase in size/fraction and connect[68,69]. The dispersion increases in viscosity and viscoelasticity, until forming a percolated network, connected at the sample scale, yielding viscoelastic behaviour with a non-zero elastic resistance against shear stress[5,65].

Such mechanism is called gelation and, like for any aggregation, the links (called cross-links when they are point-like) are determined by protein-protein and protein–solvent interactions. Globular protein gel networks are generally established and stabilized via non-covalent cross-links such as hydrogen bonds, hydrophobic, electrostatic interactions or, but less frequently, by covalent disulfide bonds (formed via sulphydryl–disulphide interchange or sulphydryl groups oxidation reactions during heat treatment)[70].

Maintaining the network stability is accomplished by the counter balancing attraction and repulsion forces between the protein molecules[71].

By controlling the processing conditions, which influence the strength of short- and long-range electrostatic interactions in the system, one can therefore obtain a variety of protein gels with distinct microstructures, morphologies and physical properties[50,72,73,74].

For instance, **strong electrostatic repulsion**, i.e. at low ionic strength or far from the IEP of the proteins, puts two proteins the furthest from each other, favors formation of **thin strands**[66,74]. When these strands branch, it may well define characteristic distances between the crosslinks, which appear homogeneous and translucent (e.g. gelatin, pectin gels)[75]. Formation of such a gel is schematically shown in **Figure 5** (option 1).

Decreasing the electrostatic repulsion, by screening with salt or approaching the IEP, may lead to an aggregation, with microphase separation (with protein poor and protein rich phases)[50] and formation of microgels, i.e. dense and relatively uniform, spherical

aggregates[76]. Such microgel aggregates can further associate and crosslink into a so-called **particulate type of gel**[74] (see **Figure 5**, option 2). The formed network is more rigid and disordered than the fine-stranded gel. Due to the size of microgels, they scatter light more and the gel appears more turbid[77].

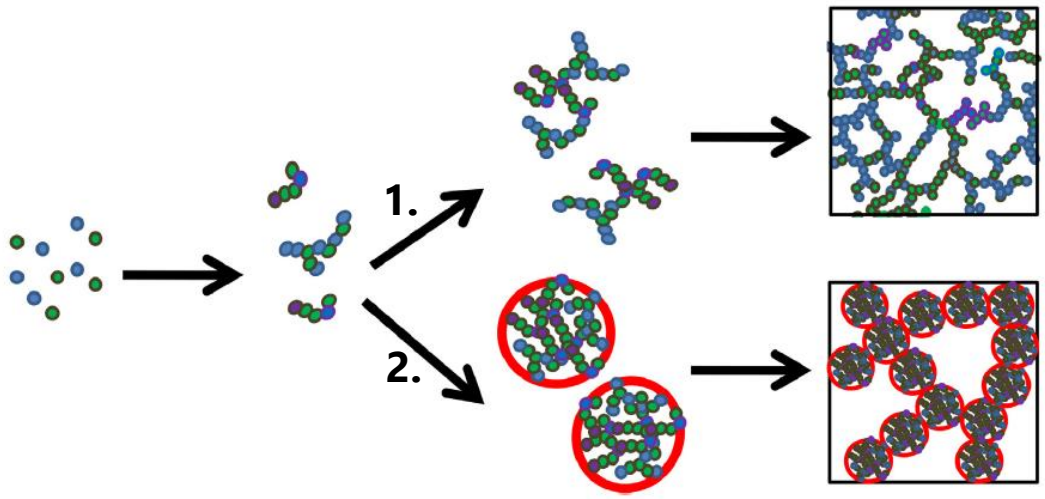

Figure 5 A schematic representation of protein gelation via formation of fine-stranded and particulate (microgels) aggregates. From (Nicolai, 2019)[50].

However, if the attractive forces start to predominate, the water is driven off the matrix and the microgels continue to grow, via a surface-tension-driven coalescence, into large spherical-shape flocs which then sediment, failing in forming a gel[76,78].

If the electrostatic repulsion is such that fractal aggregates form first, they will grow into to larger flocs and, as they aggregate - result in a network formation[74].

For the same protein concentration, fractal aggregates yield stronger gels compared to microgels, because they are less dense and therefore occupy a larger volume fraction, as reported e.g. for whey protein gels[79,78].

The physicochemical properties of protein gels containing more than one type of protein depend additionally on the interactions between them, since together, they can form either homogeneous mixtures or phase separate, with either all the proteins concentrated in two distinct phases or with the different types of proteins together in one phase separated from a protein poor phase[80].

1.2.2.1 Canola protein gels

Proteins from different sources vary in their amino acid composition, which further reflects in their different structural characteristics, gel formation and its properties. Canola proteins were reported to have good functional properties[93] and because of that, they could be used in a variety of processing applications for foods and beverages, including meat and dairy alternatives[81]. Cruciferin has particularly good gelling properties, due to its hexamer structure susceptibility towards structural changes, dissociation and unfolding upon heat and pH processing, compared to the more hydrophilic and rigid napin, which shows rather high heat and pH stability[81,82]. Cruciferin can produce gels established primarily by hydrophobic forces, thanks to its high content of hydrophobic amino acids and be stabilized and strengthened by electrostatic interactions, hydrogen and disulfide bonding[83,84].

Different gelling behaviors of the two canola proteins have been also related to their changes in solubility at different pH[32]. Napin was reported to be soluble at a broader pH range compared to cruciferin, which solubility increases at higher pH[32,85,86].

The pH plays an important role in the type of protein network formed upon gelation and it affects heat stability. Cruciferin was reported to form rather similar particulate fractal networks upon heat treatment (120°C) but with pH dependence. At pH 11, cruciferin was denatured with a rupture of disulfide bonds and, by yielding more interactions among their exposed hydrophobic groups, resulted in a gel with an increased strength and macroporus structure (as determined by rheometry and Electron Microscopy techniques)[83,84]. At pH 9, 7 or 5, cruciferin gelation was induced by its denaturation without disrupting of disulfide bonds, being the most heterogeneous at pH 5, possibly due to higher protein pre-aggregation closer to IEP (based on rheology and confocal microscopy)[85].

Cruciferin forms stronger (more crosslinked) gels than napin. Between pH 4 and 8, napin was found to be resistant against heat gelation[87], which might be related to its resistance to unfold at low pH. It achieved to form gels at alkaline pH, while below pH 4.0, it underwent modifications in its surface hydrophobicity[84].

When both napin and cruciferin are present in a mixture solution, the higher molecular weight cruciferin can overcome the weak gel-formation properties of napin and build the network anyways. Several authors reported that the mixed canola protein heat-set gels were stronger and more stable at alkaline pH than neutral or acid pH[83,88,89]. Both mixed protein isolates and individual proteins developed opaque gels[90]. We report also to our experience in **Chapter 2**.

1.3 Canola Proteins in Human Nutrition

In spite of the fact that canola meal is rich in high quality proteins, it is mostly considered as a by-product of the oil production, mainly used for animal feed[23]. In human nutrition, there was, until recently (apart from the recent food product CanolaPro®, see below), no general usage of canola proteins and thus little available *in vivo* evaluation of its nutritional value[91,92] despite their big potential to substitute other plant proteins, e.g. from the most popular soybean[93].

Nutritional quality of a protein is related to its content of essential amino acids and also its biological value, i.e. those amino acids bio-accessibility and bio-availability upon ingestion, defined as the amount of ingested AA available for absorption and their use for physiological needs, respectively[10,94,95].

When comparing to animal-based proteins, the ones coming from plant sources are considered to have overall lower nutritional values. This is due to i) limited contents of some of the essential AA (like lysine, methionine, cysteine or tryptophan), and ii) their lower digestibility[95,96], often attributed to the presence of anti-nutritional factors such as protease inhibitors, polyphenols, lectins or phytates, being often in high levels in storage proteins of cereals or legumes[16,97,98]. Protein **digestibility** is here an important factor, used to evaluate the nutritional quality of the proteins, generally by calculating the proportion of the ingested amino acids to excreted/retained after their digestion[99]. It is influenced by the rates of food hydrolysis and may affect the kinetics of nutrients delivery for their further absorption into the bloodstream and their post-absorptive metabolism[10,99,100].

In context of nutritional quality, canola proteins offer a great opportunity to provide a well-balanced amino acid profile with all essential and sulfur-containing amino acids, largely meeting the FAO/WHO/UNU requirements for adults and children, with cruciferin being particularly rich in lysine and methionine (compared to e.g. soy and pea[101]), and napin - in cysteine[93,102,103]. Incorporating both of these proteins, with their complementary AA profiles, in the diet may henceforward improve their final nutritional quality.

In context of digestibility, canola protein isolate scored 0.89 in protein digestibility-corrected amino acid score (PDCAAS)[4], which is superior to e.g. soy protein isolate. For canola protein hydrolysate, Fleddermann et al., 2013 reported the highest score (1.00), which corresponds to that of egg and milk proteins[92]. Moreover, rapeseed proteins demonstrated a high postprandial biological value, as high as that of milk proteins[91,104]. Altogether, this places canola above many other plant protein sources and even on the comparable level with some of the animal products, making it a potentially interesting plant-based protein source for human nutrition[25,26,91,92,95,105].

One obstruction for the human consumption of canola proteins could be herein the presence of antinutritional factors, like phenolic compounds, which also contribute to the characteristic dark color and bitter taste. Those inconvenient physicochemical properties are however possible to eliminate already by extraction procedures, resulting in protein isolates of interest with both enhanced nutritional and functional properties[93,106.] Eventually, recently, a few life science/food industry companies lead the research and development of new canola protein based products for human nutrition, including i.a. better protein extraction/processing methods[23]. In Europe, French company Avril together with Dutch partner DSM confirmed production of new type of canola protein isolate CanolaPRO® [107,108], while Canadian industries Corteva Agriscience, Bunge and Botaneco work together on improvement of canola protein products, serving as plant-based protein alternatives for human feed[23].

[4] Employed by FAO/WHO as the preferential method for evaluating the protein value in human nutrition (from 0 to 1.00).

In overall, the acknowledged nutritional value (and following health benefits) of canola, together with their protein functionality, gives a great potential for its wider use in human nutrition as a high-quality, sustainable source of proteins.

1.4 Overview of the human digestive system

Human digestion is a complex, multistep process during which ingested food is gradually transformed and finally broken down into the basic nutrient constituents, enabling their effective absorption to the bloodstream and use for different body functions[109]. Protein digestion takes place in different parts of the gastrointestinal tract, starting from the mouth, and continuing in the stomach and small intestine. Each of these steps has a specific physiological environment, involving pH, enzymes and mixing conditions. The protein food undergoes there different physicochemical, mechanical and enzymatic processes, like water absorption, acid hydrolysis and enzymatic reactions, resulting in swelling, disintegration and general destruction of its initial structure[110,111,112]. The kinetics of those processes depend on both the digestive environment and the food properties.

The proteolytic action of different enzymes result in cleaving of large polypeptide chains into smaller peptides and single amino acids[1,49]. The enzymes preferentially attack peptide bonds between the specific amino acids. The schematic succession of events and conditions during protein digestion is presented in **Figure 6**.

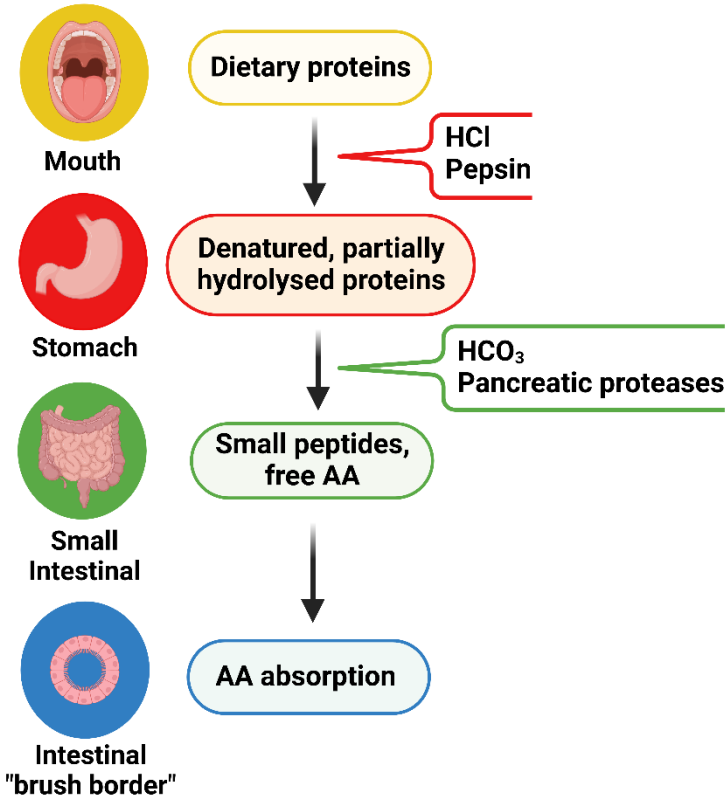

Figure 6 Scheme of the successive steps of protein digestion for humans. Created with BioRender.com.

The pH of both the protein food and its environment is here an important factor. In case of protein gels, depending on their overall charge, the external pH conditions can induce either the network's swelling or contraction/shrinking: swelling of the gel is likely to occur at pH away from the IEP of the constituting proteins and is expected to rather improve the digestion, by allowing a convective influx of the digestive fluids into the network. Contrary, at pH close to the IEP, the gel will have the lowest swelling potential[113] and will more probably contract, when crossing the zero-charge point[123], which will have a negative effect on digestion[111].

Temperature also plays an important role as it is related to the enzymes activity. Since enzymes are proteins, they can be denatured at high temperatures. The optimal temperature for human digestive enzymes is close to the human body temperature, i.e. 37°C[114].

In the first place of digestion (oral cavity), solid food undergoes physicochemical processes due to salivation and mechanical mastication; it is transformed into smaller food

pieces (<1 mm to ~ 3 mm)[217], with formation of the so called food bolus, i.e. a cohesive/solid mass that can be swallowed and enter the stomach through the esophagus[115]. Although most of the mechanical breakdown of solid foods occurs in the mouth, the factual/chemical digestion, in case of protein foods, starts in the stomach, since the salivary secretions do not contain any proteolytic enzymes (only α-amylase) and the changes in pH, which could provoke hydrolysis, are rather moderate[115].

1.4.1 Protein digestion in the stomach

In the stomach, the swallowed food bolus is mixed with the gastric juice, consisting mainly of water, hydrochloric acid and one enzymes (pepsin), accompanied with salts and ions, making altogether a mixture called chyme[116]. These gastric juice components are secreted gradually along the digestion time, through a neural feedback, to about 2-3 L per day, largely depending on the physical state of the ingested food, with larger secretions for more solid forms[117].

Contrary to other parts of the digestive tract, the gastric secretion is very acidic, having the fasted pH as low as 1.7[118]. After the food entry in the stomach, the gastric pH increases, accordingly to the food pH, composition (buffering capacity of the proteins[5]), size and consistency, and then gradually decreases back to the fasted pH[117].

The low pH of the stomach plays several important roles in the digestion of protein-rich foods. First of all, it converts inactive pepsinogen to active pepsin enzyme (to avoid self-digestion of the stomach cells)[119] and provides an optimal pH for its activity, with a maximum value between pH 1.5 and 2.5[120,121]. Pepsin remains relatively active up to pH 4[122] and irreversibly denatured above pH 8[2,120]. The rate of HCl secretion affects here not only the amount of pepsin in the stomach, but also its activity. In this context, the ability of food to acid uptake is an important factor[123,124].

[5] Buffering capacity of proteins is related to the sum of their ionisable amino-acid groups (with specific pK values), and is induced in the stomach by their bonding to hydrogen ions when food comes into contact with the gastric juice.

Moreover, the strongly acidic environment alters the ionizable protein groups and provokes the ingested proteins to lose their folded structures (unfold) and expose the hydrophobic residues and their peptide bonds, facilitating the access for pepsin attack[125]. Additional, but very important function of the acid pH is a prevention from the bacteria and germs proliferation, which can damage the gastrointestinal tract[126].

Pepsin has a broad cleavage specificity, with a preference to cleave before the hydrophobic residues (except for proline) and aromatics like phenylalanine, tryptophan, and tyrosine and leucine[127,128,129]. It was showed that pepsin has a lower ability to cleave inside the globular, tightly folded proteins[130]. It breaks approx. 10-15% of the ingested peptide bonds[128,129], generating shorter (but still relatively long) polypeptides, different-size oligopeptides, and some free amino acids, depending on the digestion efficiency[2,131].

The residence time of food in the stomach ranges from 30 min to 4 hours[132]. The rate of gastric digestion, measured by the gastric emptying rate, depends on properties of food such as nutrient content, food particle size, but also its global physical parameters, like viscosity[133,134]. Liquid meals are characterized by a rather rapid onset and linear rate of gastric emptying, compared to solid meals, in which an initial lag phase is observed. Solid foods require additional disintegration into smaller particles, obtained, along with the acid and enzymatic hydrolysis, also by muscular contractions of the stomach wall, leading to liquid flows, mixing, slight shearing etc[217]. Homogenization of the meal can be herein an important factor, which can reduce the length of the gastric digestion of solid meals. The gastric digesta, containing suitable particle sizes (2-3 mm), is being then gradually emptied into the duodenum (the first part of the small intestine)[133].

1.4.2 Protein digestion in the intestine

The gastric digesta/chyme gradually enters the duodenal part of small intestine, where it is mixed with pancreatic enzymes (proteases, lipase and amylase), bile[6],[135,136] and hormones which are secreted by the exocrine pancreas, liver and duodenum itself, respectively[137]. In addition, sodium bicarbonate $NaHCO_3$ is secreted to the pancreatic fluid, neutralizing the acidic pH of the gastric chyme (to pH ~7 in the duodenum to pH ~ 7.5 in the ileum[7]) and providing optimal activity for a continuation of the proteolysis[138].

Pancreatic enzymes are serine proteases, comprising predominating trypsin and chymotrypsin, as well as the minor elastase and carboxypeptidases A and B[139]. All these enzymes are secreted also in inactive forms and activated to their active forms by the intestinal environment[114,139].

- Trypsin is highly specific to cleave after positively-charged/basic amino acids, which, at small intestinal pH, are lysine and arginine[199]. It cleaves peptide bonds between the carboxyl site of these residues and the amino site of the adjacent ones *(except for proline)*[114.] When the lysine and arginine are adjacent to cysteine or acidic amino acids, the cleavage by trypsin occurs more slowly.
- Chymotrypsin cleaves peptide bonds at the carboxyl site of both aromatic and hydrophobic residues, most preferentially next to Tyr, Trp, Phe and Leu, unless followed by Pro[114,116,140].
- Additional elastase hydrolyses peptide bonds at the carboxyl site of small uncharged and aliphatic amino acids, i.e. Ala, Gly and Ser[128].

Trypsin, chymotrypsin and elastase are endopeptidases which cut internal (middle chain) peptide bonds and can digest proteins into small peptides, but not into single

[6] Bile is an alkaline fluid consisting of, i.a. bile salts, made of bile acids conjugated with glycine or taurine and it helps in lipid digestion by emulsifying fats and facilitating the action of lipase[135]. Conjugated bile acids were found to enhance the protein digestion by accelerating their hydrolysis by proteases from pancreas by displacing the proteins[136].

[7] Final section of the small intestine.

amino acids. This ability is given to carboxypeptidases (exopeptidases), which cleave carboxy terminus of peptide bonds to remove single AA from the C-terminal end of their substrates. Carb-A cut off aromatic, neutral, or acidic amino acid, or branched chain amino acids, while carb-B cut off basic amino acids (lysine and arginine)[116,140].

Those different intestinal proteases, put altogether, cleave both internal and terminal peptide bonds, compared to pepsin which targets only the internal ones. Due to larger number of proteolytic enzymes and their sum wider specificity, compared to the gastric step, the intestinal step is more efficient, digesting 66%–95% of proteins[130,141] and results in a mixture of short peptides (of a few residues) and single amino acids[139,142].

Nevertheless, the crucial factor for efficient intestinal proteolysis is the accessibility to the proteolytic sites. As reported by Fu et al. (2021), the pancreatic enzymes hydrolyze the peptide bonds exposed on the protein's surface and not the ones hidden in folded structures, even if they are preferential[130]. The denaturing conditions of the preceding gastric step are therefore important.

The small remaining peptides can be further hydrolyzed by the enzymes located on the "brush border" membrane of the small intestinal epithelium (majorly to single AA) and be transported into the bloodstream[142]. The not fully digested proteins will pass into the large intestine and will be eventually excreted in the feces.

In summary, a combined action of the gastric, intestinal and brush border enzymes provides the availability of free amino acids for body functions.

1.5 Methodology for Studying Protein Digestion

The fate of proteins during digestion has been studied experimentally either *in vivo* (on humans or animals), or *in vitro*, by applying simulated digestive conditions. Both methods have advantages and disadvantages/limitations.

1.5.1 *In vivo* methods

In vivo approaches usually involve feeding the human or animal subject and a subsequent blood sampling[100] or breath testing (with 13C-labelled proteins)[143], or else examination of terminal ileal samples, collected through an ileostomy or faeces, where the latter ones are heavily degraded by colonic microflora. These *non-invasive* methods allow indirect physiological/metabolic diagnostics, however they can only reveal the end-point information about the food digestion, not yielding the insights about the dynamic processes occurring in the gastrointestinal tract.

There are also possible studies of digesta taken at regular time intervals from the subject's upper stomach or small intestine. Samples taken from those parts need to be however in liquid states, so they can be aspirated through a naso-gastric or naso-jejunal tube[144] or a cannula[145], which limits studies of solid foods. From the collected samples, one can analyze the liquid digesta and reveal kinetics of the protein digestion. Such endoscopic examinations can be combined with imaging e.g. by using a wireless capsule equipped in a camera, giving additional information on the visual aspect of the food[146,147]. One has to keep in mind that those techniques are more invasive.

There also exist direct, non-invasive **imaging techniques**, including ultrasound[148] or magnetic resonance imaging (MRI)[149,150,151], which can monitor volumes in the gastrointestinal tract, and provide real-time, structural information on the spatial distribution of the food components, e.g. its heterogeneity, but also viscosity[134]. Even though human body is the gold standard for the digestion studies, its use is constrained by ethical, financial and often just technical difficulties. Here, animal experiments could serve as an alternative, however, there are also ethical objections regarding their use, as well as just the relevance in similarities/comparison to human systems.

Both human and animal *in vivo* assays require, in general, more resources and generate more concerns. Furthermore, the complexity of the physiological systems makes it very difficult to elucidate specific/individual information/mechanisms that underlie the overall digestive process. In addition, variations between individual subjects can lead to large differences in the digestion outcomes[152]. All these reasons gave a strong case

for researchers to develop simplified *in vitro* models that can simulate the conditions of the human digestive system.

1.5.2 *In vitro* methods

In vitro protocols offer a practical alternative in food, nutrition, and medical research due to their easier and faster sampling at any time point, lower cost and no ethical implications, compared to *in vivo* studies. Importantly, they can eliminate a lot of complexity of the *in vivo* systems and allow higher reproducibility when under standardized conditions. Moreover, they are better adapted to handling solid, structured foods which cannot be always tested in *in vivo* trails.

Models for studying in vitro food digestion have been reviewed e.g. by Mackie (2017)[153] or Bornhorst and Singh (2014)[154]. They involve two main actions of human digestion, i.e. i) mechanical transformation and reduction of food particle size and ii) pH-enzymatic degradation of the food sample, occurring through three main sequences, i.e. oral, gastric and intestinal step[109].

In vitro digestion models can be classified as dynamic or static.

Dynamic models can simulate the complexity of the digestive system physiology, including not only its chemical environment but also its dynamic aspects like fluid secretions, oral chewing, mixing, peristaltic contractions or gastric emptying[109,155]. Examples of such models were developed in several countries, i.e. New Zealand[156], Netherlands[157], England[158] and France[159]. Development of such models is expensive and their complexity can restrict the understanding of the individually occurring processes.

Static models, also called biochemical models, are designed to reproduce human digestion by working in static conditions of specific enzymes, pH and temperature for a given duration, using laboratory containers/test tubes[109]. They are particularly suitable for studies of simple foods or single nutrients digestion, but they are not adapted to simulate mechanical forces and dynamic processes occurring *in vivo*. In return, static models are cheaper and more practical than the dynamic models and, due to their

lower complexity, it is easier to describe and understand the individual processes occurring in digestion, unattainable with more real-life methods. Static digestion models are therefore recommended before conducting more advanced dynamic *in vitro* or *in vivo* trials[160].

Different static *in vitro* digestion methods have been used over the years, but often with varying parameters across individual assays, such as type of enzymes and their specific activities (enzyme to substrate ratios), pH conditions and the incubation/digestion times[199].

Those differences made it particularly difficult to compare the results from different studies. For that reason, Minekus et al. developed a harmonised static *in vitro* digestion protocol ***INFOGEST***. The main objectives of this protocol were to develop a static model providing digestion conditions based on human physiology, which is, at the same time, easy to set up and use, and standardized, to increase reproducibility and possibility to compare results between different laboratories[161,162]. INFOGEST protocol consists of simple oral, gastric and intestinal steps, each described by the recommended volumes of simulated fluids, pH conditions, enzymes ratios and digestion times. It is considered a robust static model to study *in vitro* human digestion.

There also exist ***in silico* models**, which use computational modelling/simulations to describe and predict different aspects of *in-vivo* digestion processes*, e.g.* mechanical disintegration of solid foods in the stomach[163] or peptide distribution after gastric hydrolysis[164]. *In silico* models can help to gain more insight into the complexity of the *in vivo* digestion. Nevertheless, they often depend on experimental data and stay limited to very specific conditions. Therefore, only with a better understanding of the experimentally studies digestion processes (as intends this thesis), will the *in silico* models be developed and universally applied.

1.5.3 Experimental techniques for monitoring digestion

Depending on the nature and purpose of the research, different methodological approaches/tools can be applied to monitor and analyse the digested food, assessing its different physicochemical or structural aspects. The toolbox for protein studies is diverse and the short descriptions of some are presented below.

Most frequently, protein food is analysed after performing the *in vitro* or *in vivo* digestion (i.e. at the endpoints of given digestion steps). Here, the common analysis of the digesta is based on the so called "degree of hydrolysis", which quantifies, by UV absorption, the soluble fraction of protein products released during the digestion reaction. Many authors studied protein digestion by the use of only this method, e.g. in studies on homogenized milk proteins[165], rapeseed and whey protein mixtures[166], cereal and milk meals[167], plant protein pasta digestion[168] or meat, milk and soy protein meals[169].

Some researchers combined this method with a chromatography technique for attaining the digested peptides size distribution: e.g. in *in vitro* gastric digestion studies on heated soy protein foods[170]; soy, pea, whey and egg white protein gels[171,172,173] or in *in vivo* studies (on pigs) of milk proteins[123,174] or almonds[175,176.]

Additionally, spectrophotometric quantitative measurements, based on the interaction of UV, visible and infrared radiation with proteins, (UV-Vis Spectroscopy, Circular Dichroism or FTIR spectroscopy) were implied to evaluate the hydrolysis and also self-organization of proteins in digestive environment, for milk protein samples[200], meat myoglobin[177], or rice protein and corn oil emulsions[178]. Also, the mass spectrometry was used for the mass analysis of amino acids, detected after enzymatic fragmentation of proteins, e.g. for cooked meat proteins[179].

All those analytical methods provide undoubtedly valuable quantitative information about the nutrients release and their sizes, however they are based on the endpoint measurements.

Alternative techniques in digestion studies of food gels rely on imaging techniques. To obtain information about the structural changes of protein foods during gastric digestion, some authors applied microscopic tools (UV-fluorescence, confocal, optical), e.g. for studying digestion of **diary protein** gels on micron to mm scales (Floury et al., 2018)[123,180], emulsions[181,214] protein-fat globules (A. Ye et al. 2016)[182] or proteins-polysaccharides complexes (J.Ø. Markussen et al. 2021)[183], as well as on egg white gels[184]. They were observing differences in structure breakdown and proteolysis kinetics attributed to specific food structure (induced by different preparation conditions, e.g. ionic strength, pH). Some other authors used electron microscopy[185,186] to investigate the μm scale structures of the protein aggregates and the relation with their digestion rates, or Magnetic Resonance Imaging[187,188], to relate microstructure and mechanical properties of differently-structured gels or the relaxation times during digestion of protein solutions or gels, highlighting the differences in digestion rates.

Flow behavior studies were also investigated: on liquid digesta of mushroom creams[189] and on cooked rice proteins in *in vivo* digestion (on pigs)[190], giving information about the viscoelastic properties, dependent on the food processing and their effect on digestion rate.

A relatively few studies were dedicated to usage of Small-Angle Scattering techniques (neutron for SANS and X-ray for SAXS) in digestion studies, even though they are powerful tools for studying soft condensed matter in a wide range of sizes (from 5 Å up to 1000 Å for the classical SAS techniques) and thus adequate for food science. Most of them concerns lipid digestion studies[191,192,193]. For proteins, Pasquier et al. (2019) studied digestion of canola gels (SAXS and SANS)[194], showing impact of food structure on digestion kinetics with the differences in digestion rates between protein gels and solutions. M. Bayrak et al. (2021)[195] focused on gastric digestion of casein gels (SANS and USANS - ultra SANS), demonstrating that gel network elasticity, governed by protein micelles size and density determines disintegration behaviour and pepsin diffusivity.

1.6 Factors influencing protein digestion

Digestion of food is currently known to depend not only on its chemical composition but also on its structure[11,154,180,206]. For that reason, to evaluate the protein food digestibility, we have to take in account not only the physicochemical properties of the native protein itself (i.e. its amino acid profile, hierarchical structure and bonding patterns), but also, external factors which can e.g. induce complexion of the protein food structure, altering its digestion kinetics and nutrients release[100].

On the level of protein composition, proline and glutamine residues (often present in α-helices) are not preferred to be cut by the small intestinal enzymes, thus their high contents (e.g. in wheat/gluten proteins) are associated with limited digestibility[196]. This particular resistance against digestion can result in relatively large peptides, being retained at the end of the digestion, that provoke immunogenic responses[197,198].

An influence of the **protein structure** on digestion has been associated with its particular resistance efficiency towards mechanical degradation (physical breakdown) and chemical hydrolysis (by pH and digestive enzymes), imposed by the accessibility of the digestive enzymes to cleavage sites[112,199]. This effect of the protein structure includes different levels in the protein structural hierarchy.

On the secondary structure level of a protein, a limited digestion, attained by both gastric and intestinal enzymes, was associated with relatively high levels of intramolecular beta-structures, due to their high hydrophobicity (involving aromatics and branched-chain AA)[200,201,202]. Hydrophobic interactions contribute here significantly to stabilization of the native structures of globular proteins. Secondary structure of a protein can be therefore a good indicator of its digestibility, however not a complete one, since proteins with similar secondary structures can differ in their digestibility[203].

The densely folded **tertiary and/or quaternary protein structures** with a presence of high number of disulfide bridges, explicitly constitutes a physical hindrance, which limits accessibility of the digestive enzymes to peptide bonds[204] and consequently slows down the digestion rate. This was shown for milk proteins[205,206].

1.6.1 Food processing

Different types of food processing can influence the protein digestion in positive or negative way, i.e. rendering the food either more susceptible or more resistant to the proteolysis. As already mentioned, **heat treatments** are common processing methods, allowing to obtain a desired physical state of the protein-rich food, by influencing the protein structure, type of formed bonds, however often not without digestion consequences.

Positive effect of heat. For native plant proteins, the heat processing can facilitate their digestion by reducing the effect of anti-nutritional factors, which can initially abate digestion efficiency, by inactivating intestinal enzymes or inducing their aggregation with proteins, as reported in many studies for different plant proteins, including ones from canola[106,207,208,209,210].

Furthermore, thermally triggered protein secondary and tertiary conformational changes, like unfolding, may improve the protein digestibility by decreasing the number of hydrogen bonds and enabling the enzymatic access to the previously buried peptide bonds, which was shown in several digestion studies on plant protein-sourced foods in-vivo[211,212] and in-vitro (i.a. on soybean and rapeseed proteins[27,28,92]).

Negative effect of heat. Formation of intermolecular β-sheet structures during the thermal treatment, and so an increased number of hydrogen bonds, has been negatively correlated with an *in vitro* protein digestibility of both animal (fish) and plant proteins (soy, corn and canola proteins)[202]. The total content of β-structures in the protein food could be therefore a good predictor for protein digestibility.

Moreover, the heat-induced formation of disulfide bonds or reactive thiol groups, or amino acid crosslinking (favoured at alkaline pH) was also associated with a decreased protein digestibility[213].

Proteins are consumed predominantly in solid-like forms, being often present in a certain multi spatial arrangement or food matrix, therefore contributing to the structure

of ingested food. In this context, protein unfolding, which makes it prone to the aggregation and the following crosslinking into more complex structures, can, conversely influence the protein digestion in a negative way. Indeed, protein foods with higher structural arrangements (in general, solid-like foods) undergo more complex process of digestion, compared to liquid foods[163,214]. Densely aggregated and highly cross-linked structures restrict their penetration by digestive enzymes and their subsequent breakdown[94,215,216]. Solid foods also require an initial disintegration to smaller food particles unlike liquids[217]. A different disintegration and penetration susceptibility among different food structures define hence the digestion rates[173], generally categorized into slow or fast, based on the time-dependent rise in plasma amino acids after the food intake[100]. Digestion of structured foods (e.g. protein gels) require more time and/or higher enzyme concentrations to achieve an effective proteolysis and thus the amino acids/peptides absorption in the small intestine, as reviewed by i.a. Turgeon and Rioux (2011)[218], Bornhorst (2014)[154] or Mackie (2017)[153].

The overall effect of the protein food structure on digestion is hence a combination of the positive (more susceptible) and negative (more resistant) factors, taking in account both the internal features of the native protein itself and the external factors of the food processing, altering its structure. The food structure constitutes thereby an important factor in its nutritional quality and thus health consequences[219].

Such an important role of the structure of protein-rich food was reported in many *in vitro* studies on gastric digestion of heat-set gels, often involving animal-sourced proteins from milk[180,185,220,221,222,] or egg white[173,184,223], and also, but in smaller extent, on plant proteins, from soy and pea[224] or rapeseed[194], as well as in a few *in vivo* studies (on pigs) with milk[174,123], almonds[175,225] or rice[190] proteins. A slower and decreased digestion for more densely-structured foods was generally found to be a result hindering enzymatic diffusion.

Another behavior has been also observed for native (not processed) proteins: differences in the hydrolysis rates/kinetics between two milk proteins. Whey proteins (majorly β-lactoglobulin) were characterized by a rather fast hydrolysis with an absorption

peak of plasma amino acids appearing shortly after ingestion. In case of casein proteins, their hydrolysis was significantly slower and constant in time. The slower digestion of casein was related to its coagulation/gelation under acidic gastric conditions, resulting in a reduced accessibility to gastric enzymes, compared to the more accessible (not gelled) whey proteins[100,172,226]. Even though native β-lactoglobulin is known to be more resistant to the enzymatic proteolysis (due to its natively compact structure, potentially impairing accessibility to the enzymes), it did not result in higher resistance to the gastric digestion, compared to the more structurally-loose casein, reported as more susceptible to the proteolysis at molecular level[181]. The effect of the pH-induced gelation of casein was herein predominating.

1.7 Identification of research gap and aim of research

The present literature provides the overall digestion studies and the problematics of food structure-digestion relation, yet it is still predominantly reported for animal-sourced proteins (milk, eggs). Due to the growing interest in new plant protein food sources, it is very useful to extend this knowledge to those type of proteins.

The current literature search shows that the digestion of canola proteins (as well as other high-quality plant proteins) is still rarely evaluated, especially regarding their structured food products (forms in which proteins are most often consumed). The existing protein digestion studies often focus on biochemical quantification of liquid digesta components at the end-points of the digestion, not providing information on the digestion processes in the gastrointestinal tract. Moreover, most of the studies focus on gastric digestion, leaving the intestinal phase neglected. Since the protein digestion is a complex, multiscale process, involving a wide range of disciplines describing it, including nutrition, chemistry, but also physics, it should not be studied only within each discipline, but rather with a multidisciplinary approach, which could provide a more complete outlook on it. The current food science is lacking the knowledge at the

interface between the physical processes and the biochemical outcomes, and the regard of the food digestion as a combination of processes at multiple, related length scales.

This thesis focuses on physicochemical aspects of both gastric and intestinal digestion of differently-structured canola protein model foods (solutions and multiscale heat-set gels). We thus fill the following gaps: **i) digestion of plant proteins**, with focus on **ii) structural aspects** and **iii) gastrointestinal digestion steps.**

Through the use of adapted tools and methods to study food structure, involving Small-Angle Scattering techniques, in conjunction with rheology and imaging, as well as other, more classical approaches, we attained the structural information on nano- to macro-scales. By this approach, we attempted to answer the questions of the physical states of the food proteins during digestion and to fill the undersupplied information in this discipline.

References

[1] Ustunol, Z. (2015). Amino acids, peptides, and proteins. *Applied food protein chemistry*. John Wiley and Sons, Ltd. 528p.

[2] Nelson, D.L. and Cox, M.M. (2017). Lehninger Principles of Biochemistry (7th ed.). W.H. Freeman, Ed., New York, 1328.

[3] Srinivasan, D., Kirk, P. and Fennema, O. (2007). Food chemistry (4th ed.), New York. Dekker. 1069p.

[4] Pauling, L., Corey, R. B. & Branson, H. R. (1951). The structure of proteins; two hydrogen-bonded helical configurations of the polypeptide chain. *Proc Natl Acad Sci USA,* 37, 205–211.

Pauling, L. & Corey, R. B. (1951). The pleated sheet, a new layer configuration of polypeptide chains. *Proc Natl Acad Sci USA,* 37, 251–256.

[5] Mezzenga, R., Fischer, P. (2013). The self-assembly, aggregation and phase transitions of food protein systems in one, two and three dimensions. *Rep Prog Phys.*, 76, 046601.

[6] Meisenberg, G., Simmons, W.H. (2017). Introduction to Protein Structure Principles of Medical Biochemistry, Chapter 2, 18-32.

[7] Cheng, P.N., Pham, J.D., Nowick, J.S. (2013). The supramolecular chemistry of β-sheets. *J Am Chem Soc*., 17, 135 (15), 5477-92. doi: 10.1021/ja3088407.

[8] Smith, L.J., Fiebig, K.M., Schwalbe, H. et al. (1996). The concept of a random coil: residual structure in peptides and denatured proteins. *Fold Des.,* 1, R95-R106.

[9] Miller, S., Janin, J., Lesk, A.M., Chothia, C. (1987). Interior and surface of monomeric proteins. *J Mol Biol*., 196 (3), 641-56. doi: 10.1016/0022-2836(87)90038-6.

[10] Gaudichon, C. (2017). Bioavailability of dietary proteins and amino acids in humans. *XXI Jornadas Nutrición Práctica*, Madrid, Spain. ⟨hal-01569102⟩.

[11] Institute of Medicine (US) Committee on Diet and Health (1992). Chapter 3, The Food We Eat in Woteki, C.E., Thomas, P.R., Ed. In: *Eat for Life: The Food and Nutrition Board's Guide to Reducing Your Risk of Chronic Disease*, Washington (DC): National Academies Press (US). https://www.ncbi.nlm.nih.gov/books/NBK235023/.

[12] Wu, G. (2016). Dietary protein intake and human health. *Food and Function*, 7 (3), 1251-1265. doi: 10.1039/c5fo01530h.

[13] Plant nutrition for food security, A guide for integrated nutrient management Food and Agriculture Organization of the United Nations Rome. (2006), FAO Fertilizer and Plant Nutrition Bulletin. https://www.fao.org/fileadmin/templates/soilbiodiversity/Downloadable_files/fpnb16.pdf.

[14] FAIRR, Plant-based profits: Investment risks & opportunities in sustainable food systems. FAIRR Briefing. (2019). http://www.fairr.org/resource/plant-based-profits-investmentrisks-opportunities-sustainable-food-systems/.

[15] Petrusan, J.I., Rawel, H., Huschek, G. (2016). Protein-rich vegetal sources and trends in human nutrition: a review. *Curr. Top. Pept. Protein Res.*, 17.

[16] Hertzler, S.R., Lieblein-Boff, J.C., Weiler, M., Allgeier, C. (2020). Plant Proteins: Assessing Their Nutritional Quality and Effects on Health and Physical Function. *Nutrients*, 12 (12), 3704. doi: 10.3390/nu12123704.

[17] Niva, M., Vainio, A., Jallinoja, P. (2017). Barriers to increasing plant protein consumption in western populations, In: *Vegetarian and Plant-Based Diets in Health and Disease Prevention*, 157–171. doi: 10.1016/B978-0-12-803968-7.00010-1.

[18] Asgar, M.A., Fazilah, A., Huda, N., Bhat, R., Karim, A.A. (2010). Nonmeat Protein Alternatives as Meat Extenders and Meat Analogs. *Compr. Rev. Food Sci. Food Saf.*, 9 (5), 513-529. doi: 10.1111/j.1541-4337.2010.00124.x.

[19] Sha, L., Xiong, Y.L. (2020). Plant protein-based alternatives of reconstructed meat: Science, technology, and challenges. *Trends Food Sci. Technol.*, 102, 51–61.

[20] Yong, S. Jie Sim, Hong Chiang, J., Jeyakumar Henry, Ch. (2021). Plant Proteins for Future Foods: A Roadmap, *Foods*, 10 (8), 1967. doi:10.3390/foods10081967.

[21] Schwartz, J.M., Guéguen, V.é, J., Ropers, M.H., Riaublanc, A., Anton, M. (2015). Partial replacement of β-casein by napin, a rapeseed protein, as ingredient for processed foods: Thermoreversible aggregation, *LWT - Food Science and Technology*, 63 (1), 562-568. doi: 10.1016/j.lwt.2015.03.084.

[22] Production of major vegetable oils worldwide from 2012/13 to 2022/2023, by type, *Statistica*. (2023). https://www.statista.com/statistics/263933/production-of-vegetable-oils-worldwide-since-2000/.

[23] Grown on Canadian farms, consumed around the world, *Canola Council of Canada* (2022). https://www.canolacouncil.org/about-canola/industry/.

[24] Uppstrom, B. (1995). Brassica oilseeds: production and utilization. *Seed Chemistry*. In: Kimber DS, McGregor DI, Ed., Wallingford, England: *CAB International*, 217–42.

[25] Wanasundara, J.P.D., McIntosh, T.C., Perera, S.P., Thushan, S. Withana-Gamage, T.S. & Mitra, P. (2016). Canola/rapeseed protein-functionality and nutrition. *OCL-Oilseeds and fats, Crops and Lipids*, 23 (4) D407. doi: 10.1051/ocl/2016028.

[26] Pedroche, J., Yust, M.M., Lqari, H., Girón-Calle, J., Alaiz, M., Vioque, J., Millán, F. (2004). Brassica carinata protein isolates: chemical composition, protein characterization and improvement of functional properties by protein hydrolysis. *Food Chemistry*, 88 (3), 337-346. doi: 10.1016/j.foodchem.2004.01.045.

[27] Peng K., Chen X., Lu H., Zhao J., Chen Y., Li C., Li H., Huang W. (2022). Effect of dietary soybean meal on growth performance, apparent digestibility, intestinal digestive enzyme activity, and muscle growth–related gene expression of Litopenaeus vannamei. *Frontiers in Marine Science*, 9. doi: 10.3389/fmars.2022.945417.

[28] Holtshausen, L., Benchaar, C., Kröbel, R., Beauchemin, K.A. (2021). Canola Meal versus Soybean Meal as Protein Supplements in the Diets of Lactating Dairy Cows Affects the Greenhouse Gas Intensity of Milk. *Animals,* 31, 11 (6), 1636. doi: 10.3390/ani11061636.

[29] Hoglund, A.-S., Rodin, J., Larsson, E., & Rask, L. (1992). Distribution of napin and cruciferin in developing rape seed Embryos. *Plant Physiology*, 98, 509-515.

[30] Bérot, S., Compoint, J.P., Larré, C., Malabat, C., Guéguen, J. (2005). Large scale purification of rapeseed proteins (Brassica napus L.). *Journal of Chromatography B*, 818 (1), 35-42. doi: 10.1016/j.jchromb.2004.08.001.

[31] Tzeng, Y. M., Diosady, L. L. and Rubin, L. J. (1990). Production of canola protein materials by alkaline, extraction, precipitation, and membrane processing. *Journal of Food Science,* 55, 1147–1151.

[32] Wanasundara, J. P. D., S. Tan, A. M. Alashi, F. Pudel, and C. Blanchard. (2017). Proteins from canola/rapeseed: Current status. In: *Sustainable protein sources*, Nadathur, S.R., Wanasundara, J.P.D. and Scanlin, L., Ed., 285–304. London: Academic Press.

[33] Zirwer, D., Gast, K., & Welfle, H. (1985). Secondary structure of globulins from plant seeds: a reevaluation from circular dichroism measurements. *International Journal of Biological Macromolecules*, 7, 105-108.

[34] Dalgalarrondo, M., Robin, J-M, Azanza, J-L. (1986). Subunit composition of the globulin fraction of rapeseed (Brassica napus L.). *Plant Science*, 43 (2), 115-124, doi: 10.1016/0168-9452(86)90151-2.

[35] Adachi, M, Kanamori, J., Masuda, T., Yagasaki, K., Kitamura, K., Mikami B., Utsumi, S. (2003). Crystal structure of soybean 11S globulin: glycinin A3B4 HOmohexamer. *Proceedings of the National Academy of Sciences of the United States of America*, 100, 7395-400. doi: 10.1073/pnas.0832158100.

[36] Schwenke, K.D., Raab, B., Plietz, P. and Damaschun, G. (1983). The structure of the 12 S globulin from rapeseed (*Brassica napus L.*). *Food/Nahrung*, 27, 165-175. doi: 10.1002/food.19830270208.

[37] Schwenke, K.D., Linow, K.J. (1982). A reversible dissociation of the 12 S globulin from rapeseed (Brassica napus L.) depending on ionic strength. *Food/Nahrung*, 26 (1), K5–K6. Doi: 10.1002/food.19820260139.

[38] Perera, S.P., McIntosh, T.C., Wanasundara, J.P. (2016). Structural Properties of Cruciferin and Napin of Brassica napus (Canola) Show Distinct Responses to Changes in pH and Temperature. *Plants*, 7, 5 (3), 36. doi: 10.3390/plants5030036.

[39] Inquello, V., Raymond, J., Azanza, J.L. (1993). Disulfide interchange reactions in 11S globulin subunits of Cruciferae seeds. Relationships to gene families. *Eur. J. Biochem.,* 217, 891-895.

[40] Lönnerdal, B. Janson, J.-Ch. (1972). Studies on Brassica seed proteins: I. The low molecular weight proteins in rapeseed. Isolation and characterization. *Biochimica et Biophysica Acta (BBA) - Protein Structure*, 278 (1), 175-183. doi: 10.1016/0005-2795(72)90119-5.

[41] Schwenke, K.D., Drescher, B., Zirwer, D., Raab, B. (1988). Structural Studies on the Native and Chemically Modified Low-Molecular Mass Basic Storage Protein (Napin) from Rapeseed (Brassica napus L.). *Biochemie und Physiologie der Pflanzen*, 183 (2–3), 219-224, doi: 10.1016/S0015-3796(88)80104-5.

[42] Schwenke, K.D. (1990). Structural studies on native and chemically modified storage proteins from rapeseed (Brassica napus L.) and related plant proteins. *Food/Nahrung*, 34, 225-240., doi: 10.1002/food.19900340307.

[43] Shewry, P.R., Napier, J.A., & Tatham, A.S. (1995). Seed storage proteins: Structures and biosynthesis. *The Plant Cell*, 7, 945–956. doi: 10.1105/tpc.7.7.945.

[44] Schmidt, I., Renard, D., Rondeau, D., Richomme, P., Popineau, Y. and Axelos, M.A.V. (2004). Detailed physicochemical characterization of the 2S storage protein from rape (*Brassica napus* L.). *Journal of Agricultural Food and Chemistry*, 52 (19), 5995-6001.

[45] Chabanon, G., Chevalot, I., Framboisier, X., Chenu, S., Marc, I. (2007). Hydrolysis of rapeseed protein isolates: Kinetics, characterization and functional properties of hydrolysates, *Process Biochemistry*, 42, 10, 1419-1428, doi: 10.1016/j.procbio.2007.07.009.

[46] Konermann, L. (2012). Protein Unfolding and Denaturants. eLS. Chichester, UK: John Wiley & Sons, Ltd. doi: 10.1002/9780470015902.a0003004.

[47] Wang, CH., Damodaran, S. (1991). Thermal gelation of globular proteins, influence of protein conformation on gel strength. *Journal of Agricultural and Food Chemistry*, 39 (3), 433-438.

[48] Betz, S.F. (1993). Disulfide bonds and the stability of globular proteins. *Protein Science*, 2 (10), 1551-8. doi: 10.1002/pro.5560021002.

[49] Arakawa, T., Prestrelski, S.J., Kenney, W.C., Carpenter, J.F. (2001). Factors affecting short-term and long-term stabilities of proteins. *Adv. Drug Deliv. Rev.,* 1, 46 (1-3), 307-26. doi: 10.1016/s0169-409x(00)00144-7.

[50] Nicolai, T., Chassenieux, Ch. (2019). Heat-induced gelation of plant globulins. *Current Opinion in Food Science*, 27, 18-22. doi: 10.1016/j.cofs.2019.04.005.

[51] Yang, A.-S., Honig, B. (1993). On the pH Dependence of Protein Stability. *Journal of Molecular Biology*, 231, 2, 459-474. doi: 10.1006/jmbi.1993.1294.

[52] Dill, K. A. (1990). Dominant forces in protein folding. *Biochemistry*, 29, 7133–7155.

[53] Wang, W., Nema, S., Teagarden, D. (2010). Protein aggregation-Pathways and influencing factors. *International Journal of Pharmaceutics,* 390, 89-99.

[54] Meakin, P. and Jullien, R. (1988). The effects of restructuring on the geometry of clusters formed by diffusion-limited ballistic and reaction-limited cluster-cluster aggregation. *The Journal of Chemical Physics*, 89, 246-250.

[55] Kilara, A., Sharkasi, T.Y. (1986). Effects of temperature on food proteins and its implications on functional properties. *Crit. Rev. Food Sci. Nutr.,* 23, 323-395.

[56] Chopra, H. and Panesar, P. (2010). Food chemistry. United Kingdom. Alpha Science International Limited.

[57] Ikeda, S., Foegeding, E.A., and Hagiwara, T. (1999). Rheological study on the fractal nature of the protein gel structure. *Langmuir*, 15, 8584-8589.

[58] Meakin, P. (1988). Fractal Aggregates. *Advances in Colloid and Interface Science*, 28, 249-331.

[59] Anitas, E. M. (2018). Small-Angle Scattering from Mass and Surface Fractals. Complexity in Biological and Physical Systems - Bifurcations, Solitons and Fractals. doi: 10.5772/intechopen.70870.

[60] Mahmoudi, N., Mehalebi, S., Nicolai, T., Durand, D., Riaublanc, A. (2007). Light-scattering study of the structure of aggregates and gels formed by heat-denatured whey protein isolate and β-lactoglobulin at neutral pH. *J. Agric. Food Chem.*, 55, 3104–11.

[61] Baussay, K., Le Bon, C., Nicolai, T., Durand, D., Busnel, J-P. (2004). Influence of the ionic strength on the heat-induced aggregation of the globular protein Î2-lactoglobulin at pH 7. *Int. J. Biol. Macromol.*, 34, 21–8.

[62] Weijers, M., Visschers, R.W., Nicolai, T. (2002). Light scattering study of heat-induced aggregation and gelation of ovalbumin. *Macromolecules*, 35 (12), 4753-4762, doi: 10.1021/ma0120198.

[63] Chen, N., Zhao, M., Chassenieux, Ch., Nicolai, T. (2016). Structure of self-assembled native soy globulin in aqueous solution as a function of the concentration and the pH. *Food Hydrocolloids*, 56, 417-424. doi: 10.1016/j.foodhyd.2015.12.028.

[64] Chi, E.Y., Krishnan, S., Randolph, T.W., Carpenter, J.F. (2003). Physical stability of proteins in aqueous solution: mechanism and driving forces in nonnative protein aggregation. *Pharm. Res.*, 20, 1325-1336.

[65] Banerjee, S., & Bhattacharya, S. (2012). Food Gels: Gelling Process and New Applications. *Crit. Rev. Food Sci. Nutr,* 52 (4), 334-46. doi: 10.1080/10408398.2010.500234.

[66] Matsumura, Y. and Mori, T. (1996). Gelation. In: *Methods of testing protein functionality*, 153- 158. Hall, G.M., Ed., Chapman and Hall, New York, N.Y.

[67] Wang, Ch, H. & Damodaran, S. (1990). Thermal gelation of globular proteins: weight-average molecular weightdependence of gel strength. *Journal of Agriculture and Food Chemistry*, 38, 1157–1164.

[68] de Jongh, H.H.J. (2003). Chapter III Globular proteins. *Progress in biotechnology*. Elsevier, 31–86.

[69] Gerrard, J.A. (2002). Protein–protein crosslinking in food: methods, consequences, applications. *Trends Food Sci Technol.*, 13, 391-399.

[70] Jensen, E.V. (1959). Sulfhydryl-Disulfide Interchange. *Science*, 130 (3385), 1319–1323.

[71] Uruakpa, F. (2012). Gelling Behavior of Plant Proteins and Polysaccharides in Food Systems. *Food Science* and *Engineering*, 2, 247.

[72] Mehalebi, S., Nicolai, T., & Durand, D. (2008). The influence of electrostatic interaction on the structure and the shear modulus of heat-set globular protein gels. *Soft Matter*, 4, 893. doi: 10.1039/B718640A.

[73] Jung, J.-M., Savin, G., Pouzot, M., Schmitt, C., & Mezzenga, R. A. (2008). Structure of heat-induced b-lactoglobulin aggregates and their complexes with sodiumdodecyl sulfate. *Biomacromolecules*, 9, 2477e2486.

[74] Doi, E. (1993). Gels and gelling of globular proteins. *Trends in Food Science & Technology*, 4, 1-5.

[75] Weijers, M., de Hoog, E.H.A., Cohen Stuart, M.A., Visschers, R.W., Barneveld, P.A. (2005). Heat induced formation of ordered structures of ovalbumin at low ionic strength studied by small angle X-ray scattering. *Colloids and Surfaces A*, 301, 270–1.

[76] Nicolai, T. (2019). Gelation of food protein-protein mixtures. *Advances in Colloid and Interface Science*, 270, 147-164, doi: 10.1016/j.cis.2019.06.006.

[77] Munialo, C.D., van der Linden, E., Ako, K., & de Jong, H.H.J. (2015). Quantitative analysis of the network structure that underlines the transitioning in mechanical responses of pea protein gel. *Food Hydrocolloids,* 49, 104–117. doi:10.1016/j.foodhyd.2015.03.018.

[78] Kharlamova, A., Nicolai, T., Chassenieux, Ch. (2020). Gelation of whey protein fractal aggregates induced by the interplay between added HCl, CaCl2 and NaCl. *International Dairy Journal,* 111, 104824. ff10.1016/j.idairyj.2020.104824ff.

[79] Moitzi, C., Donato, L., Schmitt, C., Bovetto, L., Gillies, G. and Stradner, A. (2011). Structure of beta-lactoglobulin microgels formed during heating as revealed by small-angle x-ray scattering and light scattering. *Food Hydrocolloids,* 25, 1766–74.

[80] Polyakov, VI., Grinberg, V.Y., Tolstoguzov, V.B. (1997). Thermodynamic incompatibility of proteins. *Food Hydrocolloids*, 11, 171–80.

[81] U.S. Canola Association, Canola Meal and Protein. https://www.uscanola.com/nutrition-cooking/canola-protein/.

[82] Wanasundara, J.P.D., Abeysekara, S.J., McIntosh, T.C. and Falk, K.C. (2012), Solubility Differences of Major Storage Proteins of Brassicaceae Oilseeds. *J. Am. Oil. Chem. Soc.,* 89, 869-881. doi: 10.1007/s11746-011-1975-9.

[83] Léger, L.W., Arntfield, S.D. (1993). Thermal gelation of the 12S canola globulin. *J. Am. Oil. Chem. Soc.,* 70, 853–861. doi: 10.1007/BF02545343.

[84] Yang, C., Wang, Y., Vasanthan, T., Chen, L. (2014). Impacts of pH and heating temperature on formation mechanisms and properties of thermally induced canola protein gels. *Food Hydrocolloids*, 40, 225-236. doi: 10.1016/j.foodhyd.2014.03.011.

[85] Ntone, E., Kornet, R., Venema, P., Meinders, M. B.J., van der Linden, E., Bitter, J. H., Sagis, L. M.C., Nikiforidis, C. V. (2022). Napins and cruciferins in rapeseed protein extracts have complementary roles in structuring emulsion-filled gels. *Food Hydrocolloids*, 125. doi: 10.1016/j.foodhyd.2021.107400.

[86] Krzyzaniak, A., Burova, T., Haertlé, T. and Barciszewski, J. (1998). The structure and properties of Napin-seed storage protein from rape (*Brassica napus* L.). *Food/Nahrung*, 42, 201-204.

[87] Folawiyo, Y.L., Owusu Apenten, R.K. (1997). The effect of heat- and acid-treatment on the structure of rapeseed albumin (napin). *Food Chemistry*, 58, 3, 237-243, doi: 10.1016/S0308-8146(96)00221-X.

[88] Schwenke, K.D., Dahme, A. & Wolter, T. (1998). Heat-induced gelation of rapeseed proteins: Effect of protein interaction and acetylation. *J. Amer. Oil. Chem. Soc.,* 75, 83–87. doi: 10.1007/s11746-998-0015-x.

[89] Tan, S. H., Mailer, R. J., Blanchard, Ch. L., Agboola, S. O., Day, L. (2014). Gelling properties of protein fractions and protein isolate extracted from Australian canola meal. *Food Research International*, 62, 819-828. doi: 10.1016/j.foodres.2014.04.055.

[90] Krause, J.P., Schwenke, K.D. (2001). Behaviour of a protein isolate from rapeseed (Brassica napus) and its main protein components - globulin and albumin - at air/solution and solid interfaces, and in emulsions. *Colloids and Surfaces B: Biointerfaces,* 21, 29-36.

[91] Bos, C., Airinei, G., Mariotti, F., Benamouzig, R., Bérot, S., Evrard, J., Fénart, E., Tomé, D. & Gaudichon, C. (2007). The Poor Digestibility of Rapeseed Protein Is Balanced by Its Very High Metabolic Utilization in Humans. *The Journal of Nutrition*, 137, 594-600. doi: 10.1093/jn/137.3.594.

[92] Fleddermann, M., Fechner, A., Rößler, A., Bähr, M., Pastor, A., Liebert, F. & Jahreis, G. (2012). Nutritional evaluation of rapeseed protein compared to soy protein for quality, plasma amino acids, and nitrogen balance - a randomized cross-over intervention study in humans. *Clinical Nutrition,* 32 (4), 519-26. doi: 10.1016/j.clnu.2012.11.005.

[93] Tan, S.H., Mailer, R.J., Blanchard, C.L., Agboola, S.O. (2011). Canola proteins for human consumption: extraction, profile, and functional properties. *Journal of Food Science,* 76 (1), R16-28. doi: 10.1111/j.1750-3841.2010.01930.x.

[94] Friedman, M. (1996). Nutritional Value of Proteins from Different Food Sources. A Review. *Journal of Agricultural and Food Chemistry*, 44 (1), 6-29. doi: 10.1021/jf9400167.

[95] Protein and amino acid requirements in human nutrition. Report of a joint FAO/WHO/UNU Expert Consultation. Geneva: WHO. (2007). Report no. 724. http://apps.who.int/iris/bitstream/10665/43411/1/WHO_TRS_935_eng.pdf?ua=1.

[96] Gorissen, S.H.M., Crombag, J.J.R., Senden, J.M.G., Waterval, W.A.H., Bierau, J., Verdijk, L.B., van Loon, L.J.C. (2018). Protein content and amino acid composition of commercially available plant-based protein isolates. *Amino Acids*, 50 (12), 1685-1695. doi: 10.1007/s00726-018-2640-5.

[97] Sarwar Gilani, G., Wu Xiao C., Cockell, K.A. (2012). Impact of antinutritional factors in food proteins on the digestibility of protein and the bioavailability of amino acids and on protein quality. *Br J Nutr*., 108, Suppl 2, S315-32. doi: 10.1017/S0007114512002371.

[98] Guillamón, E., Pedrosa, M. M., Burbano, C., Cuadrado, C., de Cortes Sánchez, M., & Muzquiz, M. (2008). The trypsin inhibitors present in seed of different grain legume species and cultivar. *Food Chemistry*, 107 (1), 68–74. doi: 10.1016/J.FOOD-CHEM.2007.07.029.

[99] Watts, S.A., Lawrence, A.L., Lawrence, J.M. (2020). Chapter 10 – Nutrition. Lawrence, J.M., Ed. In: *Developments in Aquaculture and Fisheries Science*, Elsevier, 43, 191-208. doi: 10.1016/B978-0-12-819570-3.00010-X.

[100] Boirie, Y., Dangin, M., Gachon, P, Vasson, M.P., Maubois J.L., & Beaufrère, B. (1997). Slow and fast dietary proteins differently modulate postprandial protein accretion. *Proceedings of the National Academy of Sciences of the United States of America*, 94 (26), 14930-5. doi: 10.1073/pnas.94.26.14930.

[101] Day, L. (2013). Proteins from land plants - potential resources for human nutrition and food security. *Trends in Food Science and Technology*, 32, 25–42. doi: 10.1016/j.tifs.2013.05.005.

[102] FAO/WHO/UNU. (1985). Energy and protein requirements. Report of a Joint FAO/WHO/UNU Expert Consultation. WHO Technical Report Series, Geneva.

[103] Chmielewska, A., Kozłowska, M., Rachwał, D., Wnukowski, P., Amarowicz, R., Nebesny, E. & Rosicka-Kaczmarek, J. (2020). Canola/rapeseed protein – nutritional value, functionality and food application: a review. *Critical Reviews in Food Science and Nutrition*. doi: 10.1080/10408398.2020.1809342.

[104] Boutry, C., Fouillet, H., Mariotti, F. *et al.* (2011). Rapeseed and milk protein exhibit a similar overall nutritional value but marked difference in postprandial regional nitrogen utilization in rats. *Nutrition & Metabolism (Lond),* 8, 52. doi: 10.1186/1743-7075-8-52.

[105] Ivanova, P., Chalova, V., Uzunova, G., Koleva, L., Manolov, I. (2016). Biochemical Characterization of Industrially Produced Rapeseed Meal as a Protein Source in Food Industry. *Agriculture and Agricultural Science Procedia*, 10, 55-62. doi: 10.1016/j.aaspro.2016.09.009.

[106] Tomé, D. (2013). Digestibility issues of vegetable versus animal proteins: Protein and amino acid requirements-functional aspects. *Food and Nutrition Bulletin*, 34, 272-274. doi: 10.1177/156482651303400225.

[107] Groupe Avril. (2020). https://www.groupeavril.com/.

[108] DSM, CanolaPRO® plant protein. (2021). https://www.dsm.com/corporate/markets/food-beverage/canolapro-plant-protein.html.

[109] Guerra, A., Etienne-Mesmin, L., Livrelli, V., Denis, S., Blanquet-Diot, S., Alric, M. (2012). Relevance and challenges in modeling human gastric and small intestinal digestion. *Trends in Biotechnology*, 30 (11), 591-600. doi: 10.1016/j.tibtech.2012.08.001.

[110] Bornhorst, G.M. and Singh, R.P. (2012), Bolus Formation and Disintegration during Digestion of Food Carbohydrates. *Comprehensive Reviews in Food Science and Food Safety*, 11, 101-118. doi: 10.1111/j.1541-4337.2011.00172.x.

[111] Van der Sman, R.G.M., Houlder, S., Cornet, S., & Janssen, A. (2020). Physical chemistry of gastric digestion of proteins gels. *Current Research in Food Science*, 2, 45-60. doi: 10.1016/j.crfs.2019.11.003.

[112] Deng, R., Mars, M., Van Der Sman, R.G.M., Smeets, P.A.M., Janssen, A.E.M. (2020). The importance of swelling for in vitro gastric digestion of whey protein gels. *Food Chemistry*, 330, 127182, doi: 10.1016/j.foodchem.2020.127182.

[113] Betz, M., Hörmansperger, J., Fuchs, T., Kulozik, U. (2012). Swelling behaviour, charge and mesh size of thermal protein hydrogels as influenced by pH during gelation. *Soft Matter*, 8, 2477-2485. doi: 10.1039/C2SM06976H.

[114] Bhagavan, N. V. (1992). Medical biochemistry. Boston: Jones and Bartlett Publishers, Boston.

[115] Mulet-Cabero, A-I., Rigby, N.M., Brodkorb, A., Mackie, A.R. (2017). Effect of Dairy Structures on Gastric Behaviour and Nutrient Digestion Kinetics using a Semi-Dynamic Model Dairy food structures influence the rates of nutrient digestion through different in vitro gastric behavior. *Food Hydrocolloids*, 67, 63-73. doi: 10.1016/j.foodhyd.2016.12.039.

[116] Boisen, S., Eggum, B.O. (1991). Critical evaluation of in vitro methods for estimating digestibility in simple-stomach animals. *Nutrition Research Reviews*, 4 (1), 141-62. doi: 10.1079/NRR19910012.

[117] Malagelada, J-R., Longstreth, G.F., Summerskill, W.H.J., Go, V.L.W. (1976). Measurement of Gastric Functions During Digestion of Ordinary Solid Meals in Man. *Gastroenterology*, 70, (2), 203-210. doi: 10.1016/S0016-5085(76)80010-8.

[118] Dressman, J.B., Berardi, R.R., Dermentzoglou, L.C., Russell, T.L., Schmaltz, S.P., Barnett, J.L., Jarvenpaa, K.M. (1990). Upper gastrointestinal (GI) pH in young, healthy men and women. *Pharmaceutical Research*, 7 (7), 756–761. doi: 10.1023/a:1015827908309.

[119] Kageyama, T. (2014). Pepsinogens, progastricsins, and prochymosins: Structure, function, evolution, and development. *Cellular and Molecular Life Sciences CMLS*, 59, 288–306. doi: 10.1007/s00018-002-8423-9.

[120] Johnston, N., Dettmar, P.W., Bishwokarma, B., Lively, M.O., & Koufman J.A. (2007). Activity/stability of human pepsin: implications for reflux attributed laryngeal disease. *Laryngoscope*, 117 (6), 1036-9. doi: 10.1097/MLG.0b013e31804154c3.

[121] Piper, D.W., & Fenton, B.H. (1965). pH stability and activity curves of pepsin with special reference to their clinical importance. *Gut*, 6 (5), 506-508. doi: 10.1136/gut.6.5.506.

[122] Kondjoyan, A., Daudin, J.D., Santé-Lhoutellier, V. (2015). Modeling of pepsin digestibility of myofibrillar proteins and of variations due to heating. *Food Chemistry*, 172, 265-271.

[123] Floury, J., Bianchi, T., Thévenot, J., Dupont, D., Jamme, F., Lutton, E. & Le Feunteun, S. (2018). Exploring the breakdown of dairy protein gels during in vitro gastric digestion using time-lapse synchrotron deep-UV fluorescence microscopy. *Food Chemistry*, 239, 898-910. doi: 10.1016/j.foodchem.2017.07.023.

[124] Bornhorst, G.M., Rutherfurd, S.M., Roman, M.J., Burri, B.J., Moughan, P.J., & Singh, R.P. (2014). Gastric pH Distribution and Mixing of Soft and Rigid Food Particles in the Stomach using a Dual-Marker Technique. *Food Biophysics*, 9 (3), 292-300. doi: 10.1007/s11483-014-9354-3.

[125] Herman, R., Yong Gao, Y., Storer, N. (2006). Acid-induced unfolding kinetics in simulated gastric digestion of proteins, *Regulatory Toxicology and Pharmacology*, 46 (1), 93-99. doi: 10.1016/j.yrtph.2006.05.010.

[126] Smith, J.L. (2003). The role of gastric acid in preventing foodborne disease and how bacteria overcome acid conditions. *Journal of Food Protection,* 66 (7), 1292-303. doi: 10.4315/0362-028x-66.7.1292.

[127] Rawlings, N.D. & Salvesen, G., Ed. (2013). Handbook of Proteolytic Enzymes (3rd ed.), Academic Press, Cambridge, MASS, USA. doi: 10.1016/C2009-1-60990-4.

[128] Fruton, J.S. (1970). The specificity and mechanism of pepsin action. *Advances in Enzymology and Related Areas of Molecular Biology*, 33, 401–443.

[129] Goodman, B.E. (2010). Insights into digestion and absorption of major nutrients in humans. *Adv. Physiol. Educ.*, 34 (2), 44-53. doi: 10.1152/advan.00094.2009.

[130] Fu, Z., Akula, S., Thorpe, M. and Hellman, L. (2021). Marked difference in efficiency of the digestive enzymes pepsin, trypsin, chymotrypsin, and pancreatic elastase to cleave tightly folded proteins. *Biological Chemistry*, 402 (7), 861-867. doi: 10.1515/hsz-2020-0386.

[131] Berg, J.M., Tymoczko, J.L., Stryer, L. (2002). Biochemistry. (5th ed.), (Section 23.1). Proteins Are Degraded to Amino Acids.

[132] Lin, H.C., Prather, C., Fisher, R.S., Meyer, J.H., Summers, R.W., Pimentel, M., McCallum, R.W., Akkermans, L.M., Loening-Baucke, V. (2005). AMS Task Force Committee on Gastrointestinal Transit. Measurement of gastrointestinal transit. *Digestive Diseases and Sciences*, 50 (6), 989-1004. doi: 10.1007/s10620-005-2694-6.

[133] Hellström PM, Grybäck P, Jacobsson H. (2006). The physiology of gastric emptying. *Best Pract Res Clin Anaesthesiol*., 20(3), 397-407. doi: 10.1016/j.bpa.2006.02.002.

[134] Marciani, L., Gowland, P.A., Spiller, R.C., Manoj, P., Moore, R.J., Young, P., Fillery-Travis, A.J. (2001). Effect of meal viscosity and nutrients on satiety, intragastric dilution, and emptying assessed by MRI. *Am. J. Physiol. Gastrointest. Liver Physiol*., 280 (6), G1227-33. doi: 10.1152/ajpgi.2001.280.6.G1227.

[135] Boyer, J.L. (2013). Bile formation and secretion. *Comprehensive Physiology*, 3, 1035-1078. doi: 10.1002/cphy.c120027.

[136] Gass, J., Vora, H., Hofmann, A.F., Gray, G.M., Khosla, C. (2007). Enhancement of dietary protein digestion by conjugated bile acids. *Gastroenterology,* 133, 16-23. doi: 10.1053/j.gastro.2007.04.008.

[137] Kalantzi, L., Goumas, K., Kalioras, V., Abrahamsson, B., Dressman, J. B., & Reppas, C. (2006). Characterization of the human upper gastrointestinal contents under conditions simulating bioavailability/bioequivalence studies. *Pharmaceutical research*, 23 (1), 165-176.

[138] Aburub, A., Fischer, M., Camilleri, M., Semler, J. R., & Fadda, H. M. (2018). Comparison of pH and motility of the small intestine of healthy subjects and patients with symptomatic constipation using the wireless motility capsule. *International Journal of Pharmaceutics*, 544, 158–164.

[139] Hedstrom, L. (2002). Serine protease mechanism and specificity. *Chemical Reviews*, 102 (12), 4501-24. doi: 10.1021/cr000033x.

[140] Barrett, A.J., Rawlings, N.D., Woessner, J.F. (2004). Handbook of Proteolytic Enzymes, 2nd Ed; Academic Press: London.

[141] Chung, Y.C., Kim, Y.S., Shadchehr, A., Garrido, A., Macgregor, I. L., Sleisenger, M.H. (1979). Protein digestion and absorption in human small intestine. *Gastroenterology*, 76 (6), 1415-1421. doi: 10.1016/0016-5085(79)90410-4.

[142] Roger H. Erickson, R.H. and Kim, Y.S. (1900). Digestion and Absorption of Dietary Protein. *Annual Review of Medicine*, 41 (1), 133-139.

[143] Sanaka, Masaki & Nakada, Koji. (2010). Stable isotope breath tests for assessing gastric emptying: A comprehensive review. *Journal of smooth muscle research = Nihon Heikatsukin Gakkai kikanshi*, 46, 267-80. doi: 10.1540/jsmr.46.267.

[144] Sullivan, L., Kehoe, J., Barry, L., Buckley, M., Shanahan, F., Mok, K., & Brodkorb, A. (2014). Gastric digestion of α-lactalbumin in adult human subjects using capsule endoscopy and nasogastric tube sampling. *British Journal of Nutrition*, 112 (4), 638-646. doi: 10.1017/S0007114514001196.

[145] Le Feunteun, S., Barbe, F., Remond, D., Ménard, O., Le Gouar, Y., et al. (2014). Impact of the dairy matrix structure on milk protein digestion kinetics: mechanistic modelling based on mini-pig [In vivo data. *Food and Bioprocess Technology*, 7 (4), 1099-1113. doi: 10.1007/s11947-013-1116-6.

[146] Iddan, G., Meron, G., Glukhovsky, A., Swain, P. (2000). Wireless capsule endoscopy. *Nature*, 25, 405 (6785), 417. doi: 10.1038/35013140.

[147] Kloetzer, L., Chey, W.D., Mccallum, R.W., Koch, K.L., Wo, J.M., Sitrin, M., Katz, L.A., Lackner, J.M., Parkman, H.P., Wilding, G.E., Semler, J.R., Hasler, W.L. and Kuo, B. (2010). Motility of the antroduodenum in healthy and gastroparetics characterized by wireless motility capsule. *Neurogastroenterology & Motility*, 22, 527-e117. doi: 10.1111/j.1365-2982.2010.01468.x.

[148] Szarka, L.A. and Camilleri, M. (2009). Methods for measurement of gastric motility. *American Journal of Physiology-Gastrointestinal and Liver Physiology*, 296 (3), G461-G475.

[149] Camps, G. (2020). The Stomach, the Mouth, or the Food? The Puzzle of Gastric Emptying. *Journal of Nutrition,* 19, 150 (11), 2852-2854. doi: 10.1093/jn/nxaa290.

[150] Al-Maliki, S., Lutton, E., Boue, F., Vidal, F. (2018). MRI Gastric images processing using a multiobjective fly algorithm. *International Conference on Parallel Problem Solving from Nature, PPSN,* Coimbra, Portugal. ⟨hal-02266292⟩.

[151] Freitas, D., Boué, F., Benallaoua, M., Airinei, R., Benamouzig, F., Lutton, E, Jourdain, L., Dubuisson, R-M., Maitre, X., Darrasse, L., Le Feunteun, S. (2022). Glycemic response, satiety, gastric secretions and emptying after bread consumption with water, tea or lemon juice: a randomized crossover intervention using MRI. *European Journal of Nutrition*. doi: 10.1007/s00394-021-02762-2.

[152] Bornhorst, G.M., Gouseti, O., Wickham, M.S.J. and Bakalis, S. (2016). Engineering Digestion: Multiscale Processes of Food Digestion. *Journal of Food Science*, 81, R534-R543. doi: 10.1111/1750-3841.13216.

[153] Mackie, A. (2017). Food: More than the Sum of Its Parts. *Current Opinion in Food Science*, 16, 120-124. doi: 10.1016/j.cofs.2017.07. 004.

[154] Bornhorst, G. M., & Singh, R. P. (2014). Gastric digestion in vivo and in vitro: how the structural aspects of food influence the digestion process. *Annual Review of Food Science and Technology*, 5 (1), 111–132. doi: 10.1146/annurev-food-030713-092346.

[155] Wickham, M., Faulks, R., Mills, C. (2009). In vitro digestion methods for assessing the effect of food structure on allergen breakdown. *Mol. Nutr. Food Res.,* 53 (8), 952-8. doi: 10.1002/mnfr.200800193.

[156] Kong, F. & Singh, R.P. (2010). A Human Gastric Simulator (HGS) to Study Food Digestion in Human Stomach. *Journal of Food Science*, 75, E627-E635. doi: 10.1111/j.1750-3841.2010.01856.x.

[157] Minekus, M. (2015). The TNO Gastro-Intestinal Model (TIM). In: *The Impact of Food Bioactives on Health: in vitro and ex vivo models*. Verhoeckx, K., Cotter, P., López-Expósito, I., Kleiveland, C., Lea, T., Mackie, A., Requena, T., Swiatecka, D., Wichers, H., Ed. Cham (CH): Springer. Chapter 5.

[158] Thuenemann, E.C., Mandalari, G., Rich, G.T., Faulks, R.M. (2015). Dynamic Gastric Model (DGM). In: *The Impact of Food Bioactives on Health: in vitro and ex vivo models*. Verhoeckx, K., Cotter, P., López-Expósito, I., Kleiveland, C., Lea, T., Mackie, A., Requena, T., Swiatecka, D., Wichers, H., Ed. Cham (CH): Springer. Chapter 6.

[159] Ménard, O. & Picque, D. & Dupont, D. (2015). The DIDGI®system. In: *The Impact of Food Bioactives on Health*, 73-81. Springer, Cham. doi: 10.1007/978-3-319-16104-4_8.

[160] Alegría, A., Garcia-Llatas, G., Cilla, A. (2015). Static Digestion Models: General Introduction. In: *The Impact of Food Bioactives on Health: in vitro and ex vivo models*. Verhoeckx, K., Cotter, P., López-Expósito, I., Kleiveland, C., Lea, T., Mackie, A., Requena, T., Swiatecka, D., Wichers, H., Ed. Cham (CH): Springer. Chapter 1.

[161] Minekus, M., Alminger, M., Alvito, P., Ballance, S., Bohn, T., Bourlieu, C., Carrière, F., Boutrou, R., Corredig, M., Dupont, D., Dufour, C., Egger, L., Golding, M., Karakaya, S., Kirkhus, B., Le Feunteun, S., Lesmes, U., Macierzanka, A., Mackie, A., Marze, S., McClements, D.J., Ménard, O., Recio, I., Santos, C.N., Singh, R.P., Vegarud, G.E., Wickham M.S., Weitschies, W. & Brodkorb, A. (2014). A standardised static in vitro digestion method suitable for food - an international consensus. *Food Function*, 5, 1113-1124. doi: 10.1039/c3fo60702j.

[162] Brodkorb, A., Egger, L., Alminger, M. *et al.* (2019). INFOGEST static *in vitro* simulation of gastrointestinal food digestion. *Nature Protocols,* 14, 991–1014. doi: 10.1038/s41596-018-0119-1.

[163] Kong, F., Singh, R.P. (2009). Modes of Disintegration of Solid Foods in Simulated Gastric Environment. *Food Biophysics,* 4, 180–190. doi: 10.1007/s11483-009-9116-9.

[164] Tonda, A., Grosvenor, A., Clerens, S., Le Feunteun, S. (2017). *In silico* modeling of protein hydrolysis by endoproteases: a case study on pepsin digestion of bovine lactoferrin. *Food Function*, 8 (12), 4404-4413. doi: 10.1039/c7fo00830a.

[165] Le Roux, L., Hacon, R., Dupont, D., Jeantet, R., Deglaire, A., Nau F. (2020). *In vitro* static digestion reveals how plant proteins modulate model infant formula digestibility. *Food Research International*, 130, 108917. doi: 10.1016/j.foodres.2019.108917.

[166] Skejovic Joehnke, M., Rehder, A., Sørensen, S., Bjergegaard, C., Sørensen, J. C. and Ejdrup Markedal, K. (2018). *In Vitro* Digestibility of Rapeseed and Bovine Whey Protein Mixtures. *Journal of Agricultural and Food Chemistry*, 66 (3), 711-719. doi: 10.1021/acs.jafc.7b04681.

[167] Kung, B., Turgeon, S.L., Rioux, L.-E., Anderson, G.H., Wright, A. J. and Goff, H.D. (2019). Correlating *in vitro* digestion viscosities and bioaccessible nutrients of milks containing enhanced protein concentration and normal or modified protein ratio to human trials. *Food Function*, 10, 7687-7696. doi: 10.1039/C9FO01994D.

[168] Gallego, M., Arnal, M., Barat, J.M., Talens, P. (2021). Effect of Cooking on Protein Digestion and Antioxidant Activity of Different Legume Pastes. *Foods*, 10 (1), 47. doi: 10.3390/foods10010047.

[169] Ding, M., Huang, Z., Jin, Z., Zhou, C., Wu, J., Zhao, D., Shan, K., Ke, W., Zhang, M., Nian, Y., Li, C. (2022). The effect of fat content in food matrix on the structure, rheological properties and digestive properties of protein. *Food Hydrocolloids*, 126, 107464, doi: 10.1016/j.foodhyd.2021.107464.

[170] Duque-Estrada, P., Berton-Carabin, C. C., Nieuwkoop, M., Dekkers, B. L., Janssen, A. E. M. and Jan van der Goot, A. (2019). Protein Oxidation and In Vitro Gastric Digestion of Processed Soy-Based Matrices. *Journal of Agricultural and Food Chemistry,* 67 (34), 9591-9600, doi: 10.1021/acs.jafc.9b02423.

[171] Pozdnyakov, N., Shilov, S., Lukin, A. *et al.* (2022). Investigation of enzymatic hydrolysis kinetics of soy protein isolate: laboratory and semi-industrial scale. *Bioresour. Bioprocess.* 9, 37. doi: 10.1186/s40643-022-00518-2.

[172] Mandalari, G., Adel-Patient, K., Barkholt, V., Baro, C., Bennett, L. *et al.* (2009). *In vitro* digestibility of β-casein and β-lactoglobulin under simulated human gastric and duodenal conditions: A multi-laboratory evaluation. *Regulatory Toxicology and Pharmacology*, 55 (3), 372-381. doi: 10.1016/j.yrtph.2009.08.010.

[173] Luo, Q., Boom, R.M. & Janssen, A.E.M. (2015). Digestion of protein and protein gels in simulated gastric environment. *LWT Food Science and Technology*, 63(1), 161-168. doi: 10.1016/j.lwt.2015.03.087.

[174] Dupont, D. (2020). Time profile of blood amino acids content after digestion of milk /dairy gels. In: *Milk proteins: Digestion and absorption in the gastrointestinal tract*. Dupont, D., & Tomé D., Ed., Academic Press. (3rd ed.), Elsevier, 978-0128152515. doi: 10.1016/B978-0-12-815251-5.00020-7.

[175] Bornhorst, G.M., Drechsler, K.C., Montoya, C.A., Rutherfurd, S.M., Moughan, P. J. and Singh, R.P. (2016). Gastric Protein Hydrolysis of Raw and Roasted Almonds in the Growing Pig. *Food Chemistry*, 211, 502–508. doi: 10.1016/j.foodchem.2016.05. 085. 15.

[176] Kong, F. and Singh, R.P. (2009a). Digestion of Raw and Roasted Almonds in Simulated Gastric Environment. *Food Biophysics* 4(4), 365–377. doi: 10.1007/s11483-009-9135-6.

[177] Li, Q., Zhao, D., Liu, H., Zhang, M., Jiang, S., Xu, X., Zhou, G., Li, C. (2020). Rigid structure is a key determinant for the low digestibility of myoglobin. *Food Chemistry*, 7, 100094. doi: 10.1016/j.fochx.2020.100094.

[178] Zang, X., Yue, C., Wang, Y., Shao, M., Yu, G. (2019). Effect of limited enzymatic hydrolysis on the structure and emulsifying properties of rice bran protein. *Journal of Cereal Science*, 85, 168-174. doi: 10.1016/j.jcs.2018.09.001.

[179] Denis, S., Sayd, T., Georges, A., Chambon, C., Chalancon, S., Santé-Lhoutellier, V., Blanquet-Diot, S. (2016). Digestion of cooked meat proteins is slightly affected by age as assessed using the dynamic gastrointestinal TIM model and mass spectrometry. *Food Function*, 7(6), 2682-91. doi: 10.1039/c6fo00120c.

[180] Guo, Q., Ye, A., Lad, M., Dalgleish, D. & Singh, H. (2014). Effect of gel structure on the gastric digestion of whey protein emulsion gels. *Soft Matter*, 10, 1214-1223. doi: 10.1039/C3SM52758A.

[181] Macierzanka, A., Sancho, A.I., Mills, E.N.C., Rigby, N.M. and Mackie, A.R. (2009). Emulsification alters simulated gastrointestinal proteolysis of beta-casein and beta-lactoglobulin. *Soft Matter*, 5(3), 538–550.

[182] Ye, A., Cui, J., Dalgleish, D., Singh, H. (2017). Effect of homogenization and heat treatment on the behavior of protein and fat globules during gastric digestion of milk. *Journal of Dairy Science*, 100 (1), 36-47. doi: 10.3168/jds.2016-11764.

[183] Markussen, J.Ø., Madsen, F., Young, J.F., Corredig, M. (2021). A semi dynamic in vitro digestion study of milk protein concentrate dispersions structured with different polysaccharides. *Current Research in Food Science*, 4, 250-261. doi: 10.1016/j.crfs.2021.03.012.

184 Somaratne, G., Nau, F., Ferrua, M.J., Singh, J., Ye, A., Dupont, D., Singh, R.P, & Floury, J. (2020). In-situ disintegration of egg white gels by pepsin and kinetics of nutrient release followed by time-lapse confocal microscopy. *Food Hydrocolloids*, 98, 105228. doi: 10.1016/j.foodhyd.2019.105228.

[185] Pinto, M.S., Léonil, J., Henry, G. et al. (2014). Heating and glycation of β-lactoglobulin and β-casein: Aggregation and in vitro digestion. *Food Research International*, 55, 70-76.

[186] Homer, S., Williams, R., Williams, A., Logan, A. (2021). WPI Gel Microstructure and Mechanical Behaviour and Their Influence on the Rate of In Vitro Digestion. *Foods*, 10 (5), 1066. doi: 10.3390/foods10051066.

[187] Deng, R., Seimys, A., Mars, M., Janssen, A. E.M., Smeets, P. A.M. (2022). Monitoring pH and whey protein digestion by TD-NMR and MRI in a novel semi-dynamic in vitro gastric simulator (MR-GAS). *Food Hydrocolloids*, 125, doi: 10.1016/j.foodhyd.2021.107393.

[188] Deng, R., Janssen, A. E.M., Vergeldt, F. J., Van As, H., de Graaf, C., Mars M., Smeets, P. A.M. (2020). Exploring *in vitro* gastric digestion of whey protein by time-domain nuclear magnetic resonance and magnetic resonance imaging. *Food Hydrocolloids*, 99, 105348. doi: 10.1016/j.foodhyd.2019.105348.

[189] Gallego, M., Ribes, S., Grau, R., Talens, P. (2023). Food matrix impact on rheological and digestive properties of protein-enriched and texture-modified mushroom creams. *Food Hydrocolloids*, 135, 108-143. doi: 10.1016/j.foodhyd.2022.108143.

[190] Bornhorst, G.M., Ferrua, M.J., Rutherfurd, S.M., Heldman, D.R. and Singh, R.P. (2013). Rheological Properties and Textural Attributes of Cooked Brown and White Rice During Gastric Digestion in Vivo. *Food Biophysics*, 8 (2), 137–150. doi: 10.1007/s11483- 013-9288-1.

[191] Salentinig, S., Amenitsch, H. & Yaghmur, A. (2017). In Situ Monitoring of Nanostructure Formation during the Digestion of Mayonnaise. *ACS Omega*, 2, 1441–1446. doi: 10.1021/acsomega.7b00153.

[192] Yaghmur, A., Lotfi, S., Ariabod, A., Bor, G., Gontsarik, M., Salentinig, S. (2019). Internal Lamellar and Inverse Hexagonal Liquid Crystalline Phases During the Digestion of Krill and Astaxanthin Oil-in-Water Emulsions. *Front. Bioeng. Biotechnol.*, 7, 384.384. doi: 10.3389/fbioe.2019.00384.

[193] Rezhdo, O., Di Maio, S., Le, P., Littrell, K.C., Carrier, R.L., Chen, S.H. (2017). Characterization of colloidal structures during intestinal lipolysis using small-angle neutron scattering. *J Colloid Interface Sci*., 499, 189-201. doi: 10.1016/j.jcis.2017.03.109.

[194] Pasquier, J., Brûlet, A., Boire, A., Jamme, F., Perez, J., Bizien, T., Lutton, E., Boué, F. (2019). Monitoring food structure during digestion using small-angle scattering and imaging techniques. *Colloids and Surfaces A: Physicochemical and Engineering Aspects*, 570, 96-106. ff10.1016/j.colsurfa.2019.02.059ff. ffhal-02561464f.

[195] Bayrak, M., Mata, J., Raynes, J. K., Greaves, M., White, M., Conn, C. E., Floury, J., A. Logan, A. (2021). Investigating casein gel structure during gastric digestion using ultra-small and small-angle neutron scattering. *Journal of Colloid and Interface Science*, 594, 561-574. doi: 10.1016/j.jcis.2021.03.087.

[196] Woychik, J. H., Boundy, J. A., and Dimler, R. J. (1961). Wheat Gluten Proteins, Amino Acid Composition of Proteins in Wheat Gluten. *Journal of Agricultural and Food Chemistry*, *9* (4), 307-310. doi: 10.1021/jf60116a020.

[197] Shan, L., Qiao, S.W., Arentz-Hansen, H., Molberg, O., Gray, G.M., Sollid, L.M., Khosla, C. (2005). Identification and analysis of multivalent proteolytically resistant peptides from gluten: implications for celiac sprue. *J. Proteome Res.,* 4, 1732–1741.

[198] Shan, L., Molberg, O., Parrot, I., Hausch, F., Filiz, F., Gray, G.M., Sollid, L.M., Khosla, C. (2002). Structural basis for gluten intolerance in celiac sprue. *Science,* 297, 2275–2279.

[199] Fuller, M. F. (1991). In vitro digestion for pigs and poultry. C.A.B. International, Wallingford, England.

[200] Carbonaro, M., Maselli, P., Nucara, A. (2012). Relationship between digestibility and secondary structure of raw and thermally treated legume proteins: a Fourier transform infrared (FT-IR) spectroscopic study. *Amino Acids,* 43, 911-921.

[201] Martínez-Velasco, A., Alvarez-Ramirez, J., Rodríguez-Huezo, E., Meraz, M., Vernon-Carter, E. J., Lobato-Calleros, C. (2018). Effect of the preparation method and storage time on the in vitro protein digestibility of maize tortillas. *Journal of Cereal Science*, 84. 10.1016/j.jcs.2018.09.016.

[202] Bai, M., Qin, G., Sun, Z., Long, G. (2016). Relationship between Molecular Structure Characteristics of Feed Proteins and Protein In vitro Digestibility and Solubility. *Asian-Australas J Anim Sci*., 29(8), 1159-65. doi: 10.5713/ajas.15.0701.

[203] Delisle, J., Amiot, J., Goulet, G. et al. (1984). Nutritive value of protein fractions extracted from soybean, rapeseed and wheat flours in the rat. *Qual Plant,* 34, 243-251.

[204] Clemente, A., Vioque, J., Sánchez-Vioque, R. et al. (2000). Factors affecting the in vitro protein digestibility of chickpea albumins. *J. Sci. Food. Agr.,* 80, 79-84.

[205] Ye, A., Cui, J., Dalgleish, D., and Singh, H. (2016). Formation of a Structured Clot during the Gastric Digestion of Milk: Impact on the Rate of Protein Hydrolysis. *Food Hydrocolloids*, 52, 478–486.

[206] G. Hu *et al.* (2017). Effects of high hydrostatic pressure, ultraviolet light-C, and far-infrared treatments on the digestibility, antioxidant and antihypertensive activity of α-casein. *Food Chemistry*, 1860-1866. doi: 10.1016/j.foodchem.2016.10.088.

[207] Sarwar Gilani, G., Wu Xiao, C., Cockell, K.A. (2012). Impact of antinutritional factors in food proteins on the digestibility of protein and the bioavailability of amino acids and on protein quality. *British Journal of Nutrition,* 108, 315-332. doi: 10.1017/S0007114512002371.

[208] Hertzler, S.R., Lieblein-Boff, J.C., Weiler, M., & Allgeier, C. (2020). Plant Proteins: Assessing Their Nutritional Quality and Effects on Health and Physical Function. *Nutrients*, 12 (12), 3704. doi: 10.3390/nu12123704.

[209] Shimelis, E., Rakshit, S. (2007). Effect of processing on antinutrients and in vitro protein digestibility of kidney bean (Phaseolus vulgaris L.) varieties grown in East Africa. *Food Chemistry,* 103, 161–172. doi: 10.1016/j.foodchem.2006.08.005.

[210] Wang, Y., Xie, Y., Wang, A., Wang, J., Wu, X., Wu, Y., Fu, Y., Sun, H. (2022). Insights into interactions between food polyphenols and proteins: An updated overview. *Journal of Food Processing and Preservation*, 46, e16597. doi: 10.1111/jfpp.16597.

[211] Abdollahi, M.R., Ravindran, V., Wester, T.J. et al. (2011). Influence of feed form and conditioning temperature on performance, apparent metabolisable energy and ileal digestibility of starch and nitrogen in broiler starters fed wheatbased diet. *Anim. Feed Sci. Technol.,* 168, 88-99.

[212] Van der Poel, A.F.B., Blonk, J., Huisman. J. et al. (1991). Effect of steam processing temperature and time on the protein nutritional value of Phaseolus vulgaris beans for swine. *Livest. Prod. Sci.,* 28, 305-319.

[213] Trivedi, M.V., Laurence, JS, Siahaan, T.J. (2009). The role of thiols and disulfides on protein stability. *Curr. Protein Pept. Sci.*, 10 (6), 614-25. doi: 10.2174/138920309789630534.

[214] Luo, N., Ye, A., Wolber, F.M., & Singh, H. (2021). Effect of Gel Structure on the In Vitro Gastrointestinal Digestion Behaviour of Whey Protein Emulsion Gels and the Bioaccessibility of Capsaicinoids. *Molecules*, 26, 1379. doi: 10.3390/molecules26051379.

[215] Carbonaro, M., Cappelloni, M., Nicoli, S., Lucarini, M., Carnovale, E. (1997). Solubility-digestibility relationship of legume proteins. *J. Agric. Food Chem.*, 45, 3387–3394.

[216] Sarkar, A., Juan, J.-M., Kolodziejczyk, E., Acquistapace, S., Donato-Capel, L., Wooster, T.J. (2015). Impact of protein gel porosity on the digestion of lipid emulsions. *J. Agric. Food Chem.*, 63 (40), 8829–8837.

[217] Kong, F. and R. P. Singh. (2008b). Disintegration of Solid Foods in Human Stomach. *Journal of Food Science,* 73 (5), R67–R80. doi: 10. 1111/j.1750-3841.2008.00766.x.

[218] Turgeon, S. L. and L.-E. Rioux. (2011). Food Matrix Impact on Macronutrients Nutritional Properties. *Food Hydrocolloids*, 25 (8), 1915–1924. doi: 10.1016/j.foodhyd.2011.02.026.

[219] Fardet, A., Dupont, D., Rioux, L., & Turgeon, S.L. (2019). Influence of food structure on dairy protein, lipid and calcium bioavailability: A narrative review of evidence. *Critical Reviews in Food Science and Nutrition*, 59, 13. doi: 10.1080/10408398.2018.1435503.

[220] Thévenot, J., Cauty, C., Legland, D., Dupont, D., & Floury, J. (2017). Pepsin diffusion in dairy gels depends on casein concentration and microstructure. *Food Chemistry*, 223, 54-61. doi: 1016/j.foodchem.2016.12.014.

[221] Barbe, F., Ménard, O., Le Gouar, Y., Bu ffiere, C., Famelart, M.-H., B. Laroche, Le Feunteun, S., Dupont, D., and Remond, D. (2013). The Heat Treatment and the Gelation Are Strong Determinants of the Kinetics of Milk Proteins Digestion and of the Peripheral Availability of Amino Acids. *Food Chemistry*, 1203–1212. doi: 10.1016/j.foodchem.2012.09.022.

[222] Guo, Q., Ye, A., Lad, M., Ferrua, M., Dalgleish, D. and Singh, H. (2015). Disintegration Kinetics of Food Gels during Gastric Digestion and Its Role on Gastric Emptying: An in Vitro Analysis. *Food & Function,* 6, 756–764. doi: 10.1039/C4FO00700J.

[223] Hyattsville, M.D., Nyemb-Diop, K., Causeur, D., Jardin, J., Briard-Bion, V., Guerin-Dubiard, C., Rutherfurd, S.M., D. Dupont, D. and Nau, F. (2016). Inves- 20 Chapter 1: Introduction tigating the Impact of Egg White Gel Structure on Peptide Kinetics Profile during in Vitro Digestion. *Food Research International,* 88, 302–309. doi: 10.1016/j.foodres.2016.01.004.

[224] Opazo-Navarrete, M., Altenburg, M.D., Boom, R.M, & Janssen, AEM. (2018). The Effect of Gel Microstructure on Simulated Gastric Digestion of Protein Gels. *Food Biophysics,* 13, 124–138. doi: 10.1007/s11483-018-9518-7.

[225] Kong, F. and R.P. Singh (2009a). Digestion of Raw and Roasted Almonds in Simulated Gastric Environment. *Food Biophysics,* 4 (4), 365–377. doi: 10.1007/s11483-009-9135-6.

[226] Lambers, T.T., van den Bosch, W.G. & de Jong, S. (2013). Fast and Slow Proteins: Modulation of the Gastric Behavior of Whey and Casein In Vitro. *Food Digestion,* 4, 1–6. doi: 10.1007/s13228-012-0028-7.

Chapter 2 Materials and Methods

This chapter provides practical information about the preparation procedures of the protein solutions and gels, as well as the digestive solutions used in this thesis. It further presents the experimental techniques used to study the protein samples, together with the experimental procedures and data analysis.

2.1 Materials

2.1.1 Canola proteins

A food-grade canola seed protein isolate was purchased from Teutexx Proteins (Oakville, Canada) by W. N. Ainis and kindly donated to us by A. Boire, BIA-INRAe. As reported by manufacturer, it consisted of 92% protein, with a mix of cruciferin and napin, in proportions of about 54% and 46%[1] (volume fractions) respectively. The remaining components were moisture (6%), ash (1%) and fat (0.6%), with traces of phenolic compounds[1]. Cruciferin and napin isolates were extracted from canola meal and obtained after passing through successive chromatographic separations and purification steps (at pH 8.5 condition), carried out at BIA laboratory (INRAe, Nantes), described precisely in [2].

2.1.2 Enzymes and other reagents

Pepsin from porcine gastric mucosa (3200-4500 $U.mg^{-1}$ protein; EC 3.4.23.1) for gastric digestion and pancreatin from porcine pancreas (P1750-100G; 4 x USP specifications; EC 232-468-9) with porcine bile extract (0.93 mM of bilar salts per g of bile) for intestinal digestion were purchased from Sigma-Aldrich Chemical Co. (St. Louis, MO, USA). The enzymes and the bile were stored at -20 °C until used. Milli-Q water (with electrical resistivity of 18.2 MΩ cm at 25 °C, Purelab ultra, ELGA) was used in all sample preparation steps.

Trichloroacetic acid (TCA, 6.1 N, ~100% (w/v)) and N-α-p-Tosyl-L-Arginine methyl ester (TAME, ≥98% (TLC)), used in enzymatic assays were purchased from Sigma-Aldrich (St. Louis, MO, USA).

Human hemoglobin for pepsin activity assay was kindly given by Dr. Stéphane Longeville from Laboratoire Léon Brillouin, who obtained it from the hospital patients.

Sodium Chloride (NaCl) and Sodium Azide (NaN_3) were used for protein solutions preparation, for stabilization and against bacterial growth, respectively. Hydrochloric

[1] Volume fractions have been determined by fitting the SANS curves. This is described in Chapter 3

acid (HCl) and sodium hydroxide (NaOH) were used for pH adjustments for protein solutions and sodium bicarbonate solution ($NaHCO_3$) - for intestinal digestive solution.

Guanidine Hydrochloride (GdnHCl), used in protein denaturation experiments, and Rhodamine B Isothiocyanate, used for protein labeling, were purchased from Sigma-Aldrich (St. Louis, MO, USA). All the used reagents were of analytical grade.

2.2 Sample preparation methods

2.2.1 Canola protein solutions

Canola protein isolates were dispersed in 85 mM NaCl and 15 mM NaN_3 aqueous solution, to reach the protein concentration of 100 g/L. The dispersions were left under gentle agitation overnight at room temperature and centrifuged (Centrifuge 5810r, Eppendorf) at 10.000 rpm for 20 min at 20°C, with a subsequent repeat. The final supernatants were adjusted from the native pH ~8 (resulting after mixing the protein isolate in the buffer) to chosen pH, with 1M or 2M HCl and 2M or 5M NaOH.

Denaturation. Canola protein (napin, cruciferin and cruciferin-napin mix) concentrated solutions were mixed with the buffer with 7.5M GndHCl stock solution and gently stirred overnight to obtain the concentration of protein of 100g/L in 3M or 6M GndHCl.

2.2.2 Protein gels

***Cm-size samples*.** In order to induce gelation, 2 mL of the protein solution was transferred into 13 mm diameter (for rheometry) or 15 mm (for SANS) sealed Luer Lock syringes, slightly lubricated with paraffin oil to ease gel removal, and immersed upright in a water bath at 95°C for 30 min. During the first 5 min of the heating, the syringes were rapidly but gently tapped, in order to remove air bubbles from the volume of solutions. After the heating, the solution appeared gelled (with changed color to lighter), with a small amount of supernatant on the top. The protein gel was pushed out from the syringes and cut with a razor blade in cylindrical slices, with thickness adapted for each technique.

Samples in capillaries. Gels for SAXS experiments were prepared directly in borosilicate glass capillaries (70 mm length, about 1.5 mm outer diameter; WJM-Las, Germany) or kapton capillaries (Polyimide tubing, 1.42 mm, Microlumen, USA). 35 µL of the protein solution the protein solution was injected into the capillary and closed with a plastic foil and parafilm. The appearing air bubbles were removed from the volume by rapid shaking down of the capillaries. The capillaries were then vertically supported in a capillary tube holder during the heating. The resulting gel appeared homogenous, with a small amount of foam on the top - the residual, partly evaporated meniscus (< 2 mm height).

Gels for confocal imaging. Samples for confocal imaging were prepared by mixing the protein solutions (for 1h at 20°C) with a fluorescent dye Rhodamine B Isothiocyanate (final concentration 0.001% w/w) prior to heating. After the heating, the formed gels were let cool down at the room temperature for 30 min and stored at in the fridge prior to use (up to one week). The protein gels were then cut with a blade to small and thin slices and placed onto the microscopic glass slides with a spacer (thickness of 50 µm) and covered with #1.5 glass coverslips (170 µm thick). The space between the slide and the coverslip was sealed with an adhesive paste to prevent drying of the gels during the analysis.

2.2.3 Digestive solutions

The preparation of the digestive solutions, with the proportions of enzymes and pH conditions, was based on the standardized INFOGEST protocol[3,4] and followed through all digestion experiments. The amounts of enzymes, added in each digestion phase, were function of their specific activities (in units per mL) and calculated for the total volume of the digestion mixture (i.e. the gel sample plus the digestive juice). The ratio of the sample (gel or solution) to a digestive juice (gastric or intestinal) in the total digestive mixture was 1:2 (vol:vol) unless stated differently.

2.2.3.1 Gastric solution

The gastric solution was prepared by mixing a fresh pepsin aqueous solution (2000 U.mL^{-1} in final mixture, i.e. sample and gastric solution) with water and 1 M HCl, to provide the pH of 2 of the gastric mixture. All the components were mixed together shortly before being added to the sample.

Pepsin activity. The initial activity of pepsin was measured by a standardized assay with TCA-soluble products, using hemoglobin as substrate. The mixtures of hemoglobin at pH 2 and pepsin (1 mg/mL) were prepared in several Eppendorf tubes and incubated at 37°C for a given digestion time. The hydrolysis reaction was then stopped by addition of 5 % (w/v) TCA and filtered through a 0.45 µm syringe filter and the absorbance at 280 nm versus air for was recorded each filtered solution for each vial. In a blank sample, the TCA was mixed with the substrate prior to the enzyme addition. The specific pepsin activity (in units per mg of solid protein) was calculated from the relation that one unit produces a ΔA_{280} of 0.001 per minute at pH 2.0 and 37°C, as described in [3]. The initial activity of pepsin was of 3564 U/mg, with its greatest loss appearing in first hour after and then, decreasing slowly with an exponential decay, to the level of ~1000 U/mg after 24 h (see **Figure 2.1b**).

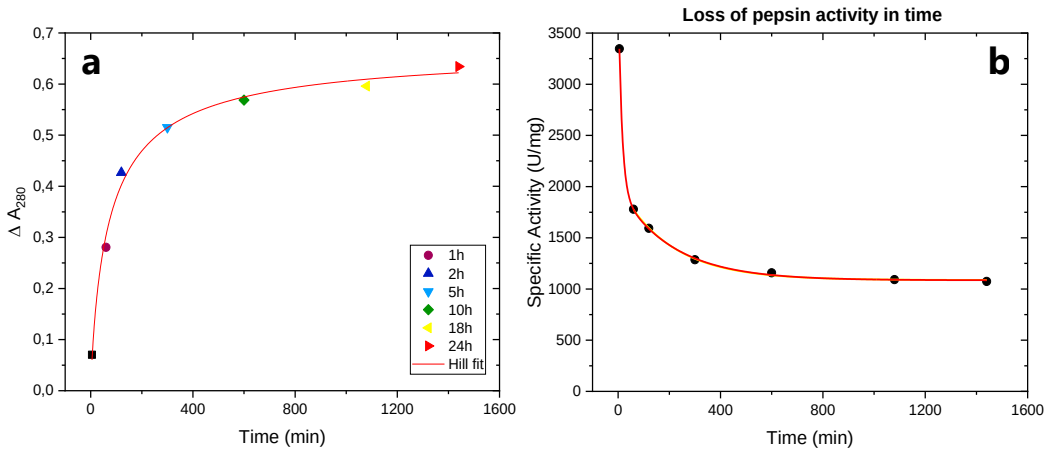

Figure 2.1 a) Change of absorbance at 280 nm of pepsin-hemoglobin reaction products, fitted with the Hill function ($v = V_{max}\frac{x^n}{k^n+x^n}$, with v - reaction velocity, V_{max} - maximal velocity, K - Michaelis constant and cooperative sites n fixed to 1), so the model behaved like Michaelis-Menten function, with V_{max} of 0.67 ΔA_{280}/min and K_m of 75 min. **b)** Pepsin activity loss with digestion time.

2.2.3.2 Intestinal solution

The intestinal solution was composed of pancreatin[2] (100 U mL^{-1} in final solution), bile (at 10 mM in intestinal solution), water and sodium bicarbonate solution (2 M). It was required to neutralize the gastric mixture to pH 7 and inactivate pepsin. All the components were mixed together shortly before being added to the substrate sample. The amount of added pancreatin depended the activity of trypsin.

Trypsin activity. Trypsin activity was based on p-toluene-sulfonyl-L-arginine methyl ester (TAME) as a substrate, with 1 unit of trypsin hydrolyzing 1 µmol of TAME per min at pH 8.2 and 25°C, as described in [3]. 0.01 M TAME was mixed with 0.046M tris-HCl buffer at pH 8.1 in several Eppendorf tubes and equilibrated at 25°C. Then, trypsin (20µm/mL) was added to each tube and incubated at 25°C in the Eppendorf Shaker for a given digestion time. The enzyme activity was determined from the change in absorbance at 247 nm per time unit when the enzyme decomposed the substrate, from initial linear part of the curve. We obtained the trypsin activity of 189 TAME U/mg (see **Figure 2.2a**).

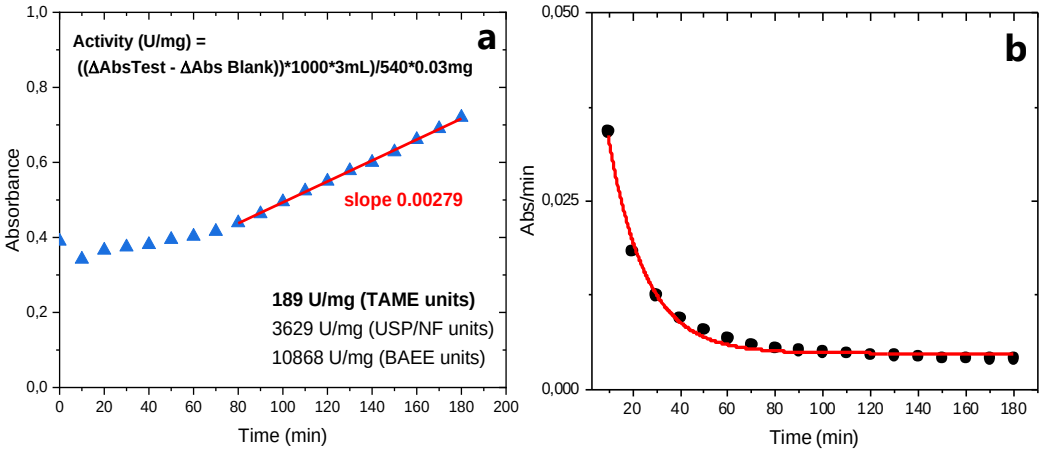

Figure 2.2 a) Absorbance at 247 nm of trypsin-TAME reaction products as a function of time; the solid line is a linear function. **b)** Absorbance change per min as a function of digestion time; the solid line represents an exponential decay fit.

[2] Mixture of pancreatic enzymes with proteases like trypsin, chymotrypsin, elastase.

A pancreatin stock solution was prepared by magnetic stirring in cold room (4 °C) for minimum 30 min, until a complete solubilization. The appearing mucous lumps were removed. After two successive centrifugations (10.000 rpm, 20 min, 4 °C), the final supernatant was recovered and stored at 4 °C for a maximum one day, or at – 20 °C.

A bile stock solution was prepared by strong magnetic stirring in a cold room (4 °C) for minimum 30 min. After two successive centrifugations (10.000 rpm, 20 min, 18 °C), the supernatant was recovered and stored at 4 °C for one day maximum, or at – 20 °C for longer storage time.

2.3 Digestion protocols adapted to different instruments

According to the INFOGEST protocol, the oral digestion is recommended for the solid protein samples, when they are relatively large, i.e. not possible to swallow directly *in vivo*. In all digestion experiments presented in this thesis, the gel samples dimensions were small enough to neglect the oral mastication step (i.e. of masticated food particle sizes). The simulated protein digestion consisted therefore of a gastric step, followed by an intestinal step. For protein gels both digestion steps were performed in static conditions, i.e. with constant temperature, enzyme concentration, pH and with no agitation. For digestion of protein solutions, the samples were mixed with each digestive solution in 2 mL Eppendorf tubes and placed in a shaking incubator (Thermomixer comfort, Eppendorf) at 37°C.

2.3.1 *In situ* digestion (on rheometer)

Prior to digestion experiments, the temperature of the plates of rheometer was lowered to 4 °C and then, the cylindrical gel slice (2.5 +/-0.5 mm thick) was immersed in the enzymatic solution (as shown in **Figure 2.3**) with not optimal activity pH, to allow a diffusion of inactive enzymes through the gel sample without starting the proteolysis. For the gastric digestion, the sample was kept in such conditions for 1 hour, after which the HCl was added to lower the solution to pH ~2. After 15 min of the acid diffusion into the sample, the solution surrounding the sample was removed, the temperature

was then raised to 37 °C in a few minutes, activating the enzyme and initiating the digestion at the beginning of the first measurement. Such an approach enabled us monitoring the rheological changes during *in situ* digestion.

Figure 2.3 Left) The glass ring, posed on the lower geometry plate of the rheometer, was used as a container for the piece of gel and digestive juice; during the digestive juice infusion to the sample the temperature of the plate was set to 4°C. **Right)** the gel sample after the infusion time, before lowering the upper geometry plate and starting the digestion measurements *in situ*; during the measurements, the temperature was set to 37°C and the temperature bonnet was covering the sample setup.

For the subsequent intestinal digestion, the temperature was once again lowered to 4 °C and the sample was immersed into the $NaHCO_3$ solution, raising the pH to 5 (able to inactivate pepsin[24] without the acid denaturation of the upcoming pancreatin enzymes). The pancreatin was then added to the solution and allowed to diffuse in cold for 30 min (we needed to limit the diffusion because of being at a pH which did not completely deactivated trypsin). At the end of diffusion, the pH was increased to the optimal value of 7. The rheological measurements started when the sample was put in contact with the rheometer geometry plates and the temperature reached 37°C.

2.3.2 *In vitro* digestion (in Falcon tube)

This protocol was used for SANS, neutron imaging and confocal imaging experiments. Cylindrical gel slices and the pepsin solution[3] were introduced in a Falcon centrifugation tube. The tube was immerged in an ice bath for 1 h, to give enough time for the gel penetration by pepsin. HCl was then added to reach pH of 2, and the tube was kept for minimum 10 min at 0 °C. The gel slices were then removed from the tube

[3] 1:2 (vol:vol) of the gel to digestive solution for imaging, and an excess volume (factor 100) for SANS.

for the preheating time (at 37 °C) and placed back into the tube for a chosen gastric digestion time (between 10 min and 2.5 h) at 37 °C. Swelling of the gel pieces was often observed after typically 15 min, resulting in more transparent slices, while in parallel, a slight decrease in mass could be inferred.

For the subsequent intestinal digestion, performed after t_{GAS} = 15 or 30 min of gastric digestion, the gel slices were permeated by the pancreatic solution, in a tube placed in an ice bath for 1 hour (adequately to the gastric step). Intestinal digestion was then performed at 37 °C for a chosen intestinal digestion time t_{INT} (between 10 and 30 min), before quenching at 0 °C. The digestion resulted in a fast (a few min) decrease in size.

For SANS, one or several slices were used to fill the 15 mm diameter cell; for neutron imaging, one digested gel slice was used; for confocal imaging, the gel slice was cut into smaller pieces (~5 mm diameter) after digestion. For neutron imaging, the samples in neutron cells were frozen in carbon ice, due to the need of transportation (24h), and kept below 0°C until the measurements.

2.3.3 Digestion in SAXS capillary

The digestion of the protein gels in a capillary was initiated by a gentle injection of the gastric solution (twice the volume of a gel, i.e. 70 µm) using a long-needle syringe, to provide the contact of the solution with the top of the gel without interfering mechanically in the gel itself.

For ***in situ* measurements**, the capillaries were then quickly transferred on the sample holder of the SAXS spectrometer, thermalized at 37±1°C and measured for given time (t_{GAS} between 35 min and 15.5 h). Prior to intestinal digestion, the supernatant gastric solution was gently absorbed with a syringe (leaving the volume close to the gel-sample interface, which contained digested proteins). The intestinal solution was then introduced in the same manner as for the gastric step and measured for t_{INT} (between 35 min and 15.5 h). After 15.5 h of intestinal digestion, the supernatant digestive solution was absorbed from the capillary and replaced by a fresh solution and the sample was digested for 2 h more.

For very long digestion times (30 h gastric and 96 h intestinal), the digestion was performed in the capillaries placed in an incubator (HERATherm, Thermo Scientific) thermalized at 37°C and stopped after given time by cooling down to 4°C until being measured.

The visual effect of progressive diffusion of the digestive juices downward the capillary along digestion time was evident, with the gel showing different aspect along the capillary; an increased transparency closer to the gel-liquid interface was observed, especially after long intestinal digestion (15 h and more). An example picture of the capillaries with digested gels are shown in **Figure 2.4**.

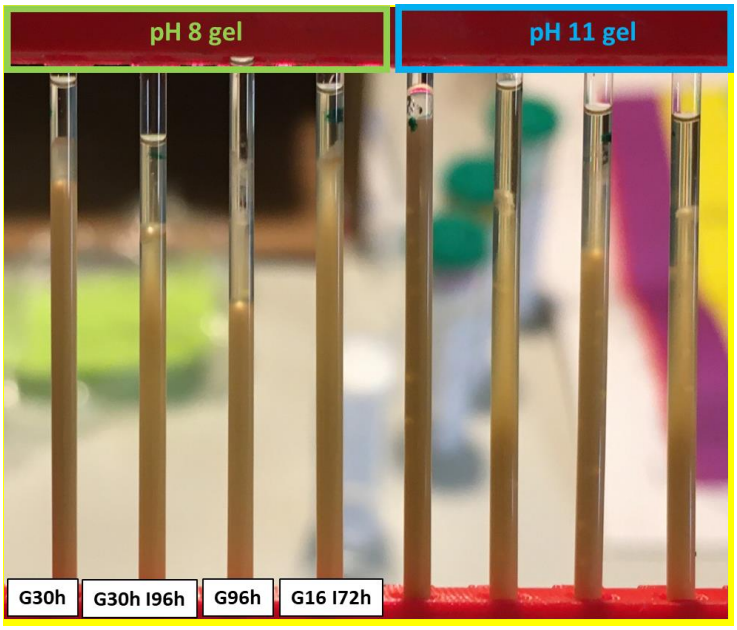

Figure 2.4 Images of capillaries containing the digested canola protein gels. **From left**: 4 pH 8 gel samples: after 30 h of gastric digestion (G30h); 30 h of gastric and 96 h of intestinal digestion (G30h I96h); 96 h of gastric digestion (G96h); 16 h of gastric and 72 h of intestinal digestion (G16h I72h). The 4 next capillaries correspond to the pH 11 gel samples.

2.3.4 Digestion of gels for deep UV-fluorescence imaging

Approximately 200-300 mg of protein gel sample (with a drop of buffer solution at given pH) was cut with a blade, to obtain very small gel pieces of interest (~100-300 µm size). The gastric and intestinal digestion was performed *in situ* during the imaging experiments, by pouring the digestive juices over the gel sample inside the infusion cell (as described later, in section 2.4.7) to an excess volume of the digestive solution (1160 μm^3).

2.3.5 Digestion of gels for spectrophotometric analysis

5 g of protein gel were weighted, cut up into small pieces (~5 mm diameter, as for confocal microscopy) and placed in a 50 mL Falcon tubes, where digestion was performed, as described above, in section 2.3.2. The digestion reaction was stopped at different times: 0, 30, 60, 90 and 120 min of gastric and 0, 15, 30, 60, 90, 120 min) of intestinal digestion, by adding TCA to digested samples to a final concentration of 10% (w/v). The mixtures were vortexed, incubated for 15 min and centrifuged at 4000× g for 20 min and passed through 0.2 µm syringe filters, to remove the insoluble parts before being analyzed. The filtrate consisted of digestion residues: small peptides and amino acids.

2.4 Experimental techniques

2.4.1 Small-Angle Scattering with X-rays and Neutrons

Small-angle (X-ray or Neutron) scattering techniques probe the nano-scale organization of matter by measuring the elastically averaged scattered intensity of a sample as a function of the modulus of scattering vector q ($q = \left(\frac{4\pi}{\lambda}\right)\sin\theta$, with 2θ the scattering angle and λ the photon/neutron wavelength). The scattering intensity $I(q)$ is the Fourier Transform of the correlation function of the electron or nuclear density of the sample, and reveals the spatial correlations in the sample in reciprocal relationship between the dimension of the fluctuations (scattering objects) and the scattering vector q. An example for a lattice parameter $d = 2\pi/q$.

The schematic layout of a SAXS instrument is shown in **Figure 2.5**

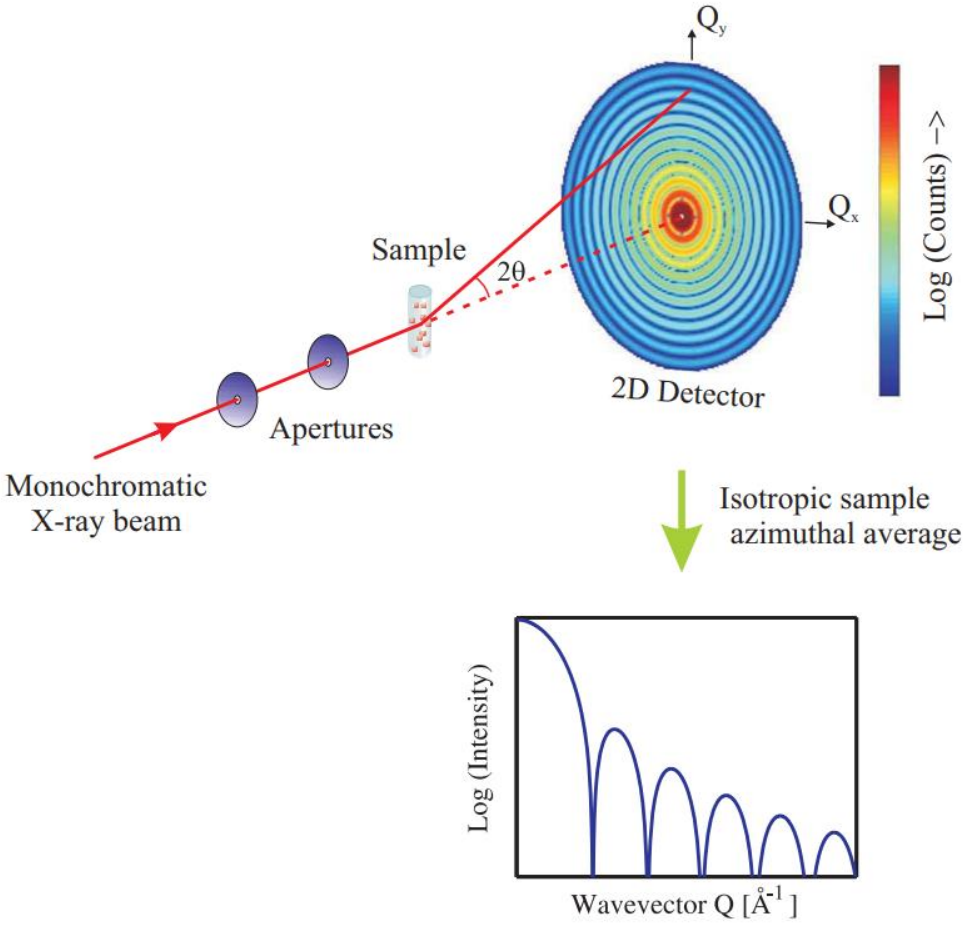

Figure 2.5 Schematic layout of a Small-Angle X-ray scattering beamline from ref. 5. An incident monochromatic X-ray beam is collimated using a set of apertures (placed at collimation distance, usually of the order of the sample-detector distance) and interacts with the sample. The scattered beam is detected on a two-dimensional XY detector. The measured signal is proportional to the incident flux, the "illuminated" area of the sample, its transmission. For isotropic samples, the scattering is azimuthally averaged to obtain the scattering intensity versus the modulus of the scattering vector *q*.

SAXS measurements of the initial protein solutions, presented in chapter 3 were carried out on the Xeuss 2.0 apparatus of Laboratoire Léon Brillouin, installed in the SWAXSLab (Saclay, France). The instrument uses a microfocused Genix^{3D} source (Cu Kα wavelength of 1.54 Å, 8 keV), coupled with scatterless slits (Xenocs, France) and a Pilatus3 1M detector (Dectris, Switzerland).

For measurements of **protein solutions**, a sample to detector distance was set to 0.539 m with a collimated beam size of 0.8 × 0.8 mm^2, to achieve good resolution in a *q* range from 2 10^{-2} $Å^{-1}$ to about 3 10^{-1} $Å^{-1}$. Each measurement was performed in the middle (x and *z* axis) of the capillary at ambient temperature, with the acquisition time of 1 hour.

Synchrotron SAXS. The **protein gels digestion kinetics** measurements were performed on the SWING beamline at the Synchrotron SOLEIL (Saint Aubin, France), with Eiger X4M detector. The sample-to-detector distance was fixed at 3.546 m and X-ray energy was of 12 keV, giving the scattering vector *q* range from 0.0018 $Å^{-1}$ to 0.22 $Å^{-1}$. The capillaries were vertically scanned (always in the x-axis center) by a narrow beam (50 μm in height and 300 μm in width) on 67 positions with 150 μm interval at each digestion time. The acquisition time of one measurement was 1250 ms, with a 625 ms interval, giving 2 min per full capillary scan. Kinetics experiments were performed during 15 to 20hours leading to a huge amount of SAXS data.

For **temperature ramp kinetics** and measurements of long digested gels (30h and 96h), in both SAXS and WAXS (wide-angle X-ray scattering), the measurements were performed with an acquisition time of 100 ms, at 2 sample-to-detector distances: 6.2 m and 0.5 m at 12 keV, corresponding to the *q* ranges of 10^{-3} to 0.18 $Å^{-1}$ and 1.6×10^{-2} to 1.8 $Å^{-1}$, respectively. The temperature kinetics measurements were performed using a Linkam oven environment, in which a quartz capillary was heated from 25 to 95 °C, with a rate of 5 °C per min.

SANS measurements on protein gels were performed on the PAXY spectrometer of the Laboratoire Léon Brillouin (CEA Saclay, France). Three *q*-ranges were chosen: at high *q* (1 m, 6 Å), medium *q* (3 m, 6 Å) and low *q* (6.7 m, 15 Å) covering a whole *q* range from 2.10^{-3} $Å^{-1}$ to 4.10^{-1} $Å^{-1}$. The gel samples were placed in the middle of a spacer ring of 1 mm thickness and sandwiched in between two quartz windows. The measurements were performed at 4 °C in dry nitrogen, owing to a temperature-regulated bonnet. External condensation of water on the quartz windows was avoided by a multi-jets airflow. Acquisition time for each sample was about 3 hours.

For SAXS and SANS measurements, 2D raw data were normalized to the sample thickness and transmission. Absolute intensity per sample volume (cm^{-1}) was obtained using either a reference sample (a capillary filled of water that scatters .016cm^{-1} or the direct incident flux measurement method[6]). Corrections for the detector sensitivity (for SANS) and background noise were applied[7].

For SAXS, the contribution scattering from the capillary, buffer and air (empty beam), were subtracted from the total scattering intensity using:

$$I(q) = I_{Sample}\,(q) - I_{Buffer}\,(q) + 10\%\,(I_{Buffer} - I_{EmptyCapillary}) \quad \textbf{(2.1)},$$

with $I_{Buffer} - I_{EmptyCapillary}$ being the constant value obtained at large q for $I_{Buffer}(q) - I_{EmptyCapillary}(q)$. 10 % is the volume fraction of buffer in the gels.

2D patterns reduction by radial averaging to 1D curves and their normalization were obtained using either PASiNET software (for data obtained at Laboratoire Léon Brillouin) or Foxtrot software (for SWING data at SOLEIL).

Small-Angle scattering Data analysis. The scattering *I*(*q*) data of protein solutions were analyzed by direct modeling, with Guinier function and shape-dependent models (using SASView software[8]), as well as by model independent approach, i.e. requiring an Indirect Fourier Transformation of the scattering curves to provide the pair distance distribution function *P*(*r*) (using BioXTAS RAW software[9]).

The **Guinier approximation**[10] of the scattering intensity follows:

$$I(q) = I_{(q\to 0)}\, exp(-\frac{q^2 R_g^2}{3}) \quad \textbf{(2.2)},$$

where *I(q->0)* is the intensity at zero scattering angle in absolute units. $\boldsymbol{R_g}$ and $\boldsymbol{I_{(q->0)}}$ are determined through linear fitting of $Ln\ I(q)\ vs.\ q^2$. The region of the Guinier fit was chosen for sufficiently small angles, so $q.R_g \leq 1.3$.

Molecular weights M_w of proteins were calculated using[11]:

$$M_W = \frac{N_A\, I_{(q\to 0)}}{c\, \Delta\rho_M{}^2} \quad \textbf{(2.3)},$$

where c is the protein concentration in mg.ml^{-1}, N_A the Avogadro number and $\Delta\rho_M{}^2$ being the scattering contrast per mass. $\Delta\rho_M$ equals $[\rho_{M,prot} - (\rho_{solv}\bar{v})]r_o$, with $\rho_{M,prot}$ = 3.22 10^{23} e.g^{-1} (n° electrons per mass of dry protein), ρ_{solv}= 3.34 10^{23} e.cm^{-3} (n° electrons per volume of aqueous solvent), $\bar{v}$ = 0.74 cm^3.g^{-1} (partial specific volume of the protein) and r_o = 2.8179 10^{-13} cm (scattering length of an electron).

The **shape dependent models** used to describe the scattering by a centrosymmetric assembly of scattering particles follows:

$$I(q) = N_p \Delta\rho^2 V_p{}^2 P(q) S(q) = \phi_p \Delta\rho^2 V_p P(q) S(q) \quad \textbf{(2.4)},$$

where N_p is the number density of scattering particles (cm^{-3}), V_p the volume of one particle (cm^3) and ϕ_p their volume fraction[4]. $\Delta\rho^2$ (the scattering contrast in cm^{-4}) is the square of the difference between the scattering length densities of the particle and the surrounding media. $P(q)$ is the form factor of the scattering particle, and $S(q)$ their structure factor[12].

The form factor $P(q)$ is the square of the scattering amplitude of the particle, $F(q)$, normalized by the particle volume V:

$$P(q) = \frac{1}{V^2} F^2(q) \quad \text{with} \quad P(q \to 0) = 1$$

[4] In most models of SASView, if the scattering length densities of particles and solvent are set to their theoretical values and the scattering intensity are in absolute units, the fit parameter named **scale** is the volume fraction of particles in the system.

The **ellipsoid form factor model** was used to fit the SAS curves of some napin solutions. The scattering amplitude of an ellipsoid is:

$$F_{ellipsoid}(q,r,\alpha) = V.\frac{3(\sin qr - qr\cos qr)}{(qr)^3} \quad \textbf{(2.5)},$$

with $r = [R_e^2 sin^2\alpha + R_p^2 cos^2\alpha]^{1/2}$, α being the angle between the axis of the ellipsoid and the scattering vector $\vec{q}$, R_p the polar radius along the rotational axis, R_e the equatorial radius perpendicular to the rotational axis of the ellipsoid. *V* is the volume of the ellipsoid.

The **hollow cylinder form factor model** was used to fit the SAS curves of some cruciferin solutions. The form factor of a hollow cylinder is

$$P(q) = \int_0^1 \Psi^2\left[q, R_{outer}(1-x^2)^{1/2}, R_{core}(1-x^2)^{1/2}\right]\left[\frac{sin(qHx)}{qHx}\right]^2 dx \quad \textbf{(2.6)},$$

$$\Psi(q,y,z) = \frac{1}{1-\gamma^2}[\Lambda(qy) - \gamma^2\Lambda(qz)]$$

$$\Lambda(\alpha) = 2J_1(\alpha)/\alpha$$

$$\gamma = R_{core}/R_{outer}$$

$$V_{shell} = \pi({R_{outer}}^2 - {R_{core}}^2)L$$

where J_1 is the 1st order Bessel function, R_{core} the cylinder core radius, R_{outer} the cylinder outer (external) radius and *L* , the cylinder length (height *H=L/2*).

The **pair-distance distribution function** *P*(*r*) is the r^2 weighted histogram of all possible pairs of atoms in the sample. It was calculated from the whole SAXS curve through indirect Fourier transform, by using BioXTAS RAW software[13], which runs GNOM program[14], following:

$$P(r) = \frac{r^2}{2\pi^2}\int_0^\infty q^2 I(q)\frac{sin(qr)}{qr}dq \quad \textbf{(2.7)}$$

The Small Angle scattering curves of protein gels during the kinetics of digestion were fitted using as shape independent function, the **two Lorentzian model**:

$$I(q) = \frac{A}{1+(q\xi)^n} + \frac{C}{1+(q\Xi)^m} + Bkg \quad \textbf{(2.8)}$$

The left-hand term of **Equation 2.8** corresponds to a high *q* range, which characterizes the scattering from the proteins-size objects (i.e. individual proteins or small "local" protein aggregates, made up of a few molecules or protein units). The right-hand term corresponds to low *q* and characterizes the scattering from the aggregated proteins, hence the structural order and interactions between the high *q* components. ξ and Ξ are the correlation lengths of the domain sizes, which give the estimations of gel and mesh sizes. *n* and *m* exponents give indications of compaction of the gel components (proteins and aggregates, respectively), with their values close to 4 revealing compact structure conformations with sharp interfaces (Porod law[15]) and close to 2 - unfolded structures, resembling Gaussian chains. Parameters *A* and *C* are the respective scale factors and *Bkg* is an incoherent (weak) remaining background signal.

To fit the kinetics SAS curves, we used a homemade algorithm developed by Evelyne Lutton, which provided a more automated batch fitting process of all the scattering curves of a capillary scan (67 scattering curves/scan). Fits were performed on the *q* range 0.007-0.1 $Å^{-1}$. Some fit results were verified by using the SASView software.

2.4.2 Rheometry

Rheological measurements were carried on a Modular Compact Rheometer MCR 302 (Anton Paar GmbH, Austria). Rheocompass® software (v.1.20, Anton Paar) was used to the instrument handling and data recording. The measurements were conducted with the use of stainless-steel parallel plate geometry with diameter of 15 mm and a profiled surface (PP15/P3, Anton Paar), to prevent slippage. In all the measurements, the rheometer measures the torque, generated by the resistance of the sample to shearing, and the resulting deflection angle. The rheological parameters (the elastic (*G'*) and viscous (*G''*) moduli) are then automatically calculated.

Preliminary strain amplitude tests. Strain sweep tests were carried in order to test the slippage and determinate the linear viscoelastic region of the protein gels. The cylindrical protein gel slice was placed on the lower plate of the rheometer's measuring system and then gently compressed in the normal direction by moving the upper plate downwards, with the gap width ~ 2 mm[5]. The *G*′ and *G*′′ were recorded as a function of the strain, in a range between 0.01 and 10%, at a constant angular frequency of 6.3 rad.s^{-1} and at a fixed temperature of 20 and 37˚C. The strain sweep results showed that a strain of 0.1% was within the linear viscoelastic region for all samples. Care was taken to prevent the sample slippage, which was not observed below 90 rad.s^{-1}.

Small-oscillatory frequency sweeps. The sample were first allowed to equilibrate at 37 °C for 2 min prior to the rheological tests. The viscoelastic moduli were recorded in the frequency range from 0.1 to 250 rad.s^{-1}, at strain of 0.1%. One frequency sweep took 10 min (with an interval rest time of 40 s), and such measurements was looped for 2 h of gastric then 2 h of intestinal digestion. All studies were carried out at least in triplicate. To prevent the sample evaporation during the measurements, a thin layer of paraffin oil was applied on the edge of the rheometer geometry plates and a cotton tissue imbibed with water was placed inside the bonnet, around the sample, to maintain water-saturated atmosphere at its edges.

Temperature ramp tests. The trends of *G*′ and *G*″ of the initial protein solutions were recorded as a function of temperature from 25˚C to 95˚C, with a ramp rate of 1.5˚C/min, at a constant strain of 1% and frequency of 1 Hz. The same method as in frequency sweeps was applied for prevention of the sample evaporation. These measurements required long efforts, but were at the end quite reproducible.

[5] Compressing the gel when closing the gap was based on the increase of the normal force (< 0.1 N) and visual aspect of the sample, so that the gel was in contact with the plate but without its syneresis.

2.4.3 Zetametry

Zeta-potential measures the magnitude of the repulsion/attraction forces between particles. Zeta-potential measurements of diluted (1 g/L[6]) and filtered (0.45 μm) canola protein solutions (napin, cruciferin and cruciferin-napin mix) were performed as a function of pH, at 25°C, by the Zetasizer Nano-ZS analyzer (Malvern Instruments, Ltd., United Kingdom), with an automatic titrator unit, equipped with a quartz sample container and a peristaltic pump (by curtesy of LIONS Laboratory, NIMBE (CEA). The protein solutions were titrated from the "native" pH values (~7.5) down to pH 3 using 0.1 M HCl and up to pH 11 using 0.1 M KOH under constant stirring. Duplicate measurements with 3 consecutive runs for each pH value were performed. **ζ**-potentials were determined through the electrophoretic mobility of proteins in solution using the Henry equation:

$$\mu_E = \frac{2\,\varepsilon\,\zeta\,f(\kappa a)}{3\,\eta} \quad \textbf{(2.9)},$$

where μ_E is the electrophoretic mobility, ε the dielectric constant, κ the reciprocal electrical double layer (dependent on the ionic strength of the solution), a the radius of the molecule, $f(\kappa a)$ - Henry's function and η viscosity of the solution[16].

2.4.4 UV-Vis spectroscopy

The absorption of a sample is related to the incident light intensity at a given wavelength (I_0) and transmitted light intensity (I) by Lambert-Beer law ($A = log\frac{I_0}{I} = \varepsilon cl$), with molar extinction coefficient ε ($M^{-1}cm^{-1}$), molar concentration c and path length l in cm[17]. It depends on the sample thickness (path length) and concentration.

Absorption spectra. UV–Vis absorbance spectra were recorded for diluted canola protein solutions (1 g/L) in the range from 500 to 200 nm, with a scan speed of 30 nm per min and a sampling interval of 0.05 nm, using Varian Cary 300 UV-Vis Spectrophotometer (Agilent Technologies Inc., Santa Clara, California, USA) with

[6] To limit aggregation and to obtain high signal-to-noise, reproducible data.

software version 4.20. Samples were measured in quartz cuvettes with 1 cm pathway. 0.5% NaCl 0.1% NaN_3 buffer was used for the baseline correction for native proteins experiments and 6M GndHCL buffer for denaturation experiments. The measurements were repeated 3 times and the results were averaged.

Digestion experiments. The soluble protein fraction released from the digested samples was determined by measuring absorbance at 280 nm[7] against a blank prepared with appropriate digestive solutions. **Degree of protein hydrolysis** (DH), reported as the percentage of the total protein concentration before digestion, was calculated from **Equation 2.10**, according to[18]. Bovine serum albumin was used as the standard for determination of protein concentration

$$DH(\%) = \frac{soluble\ protein\ content\ in\ TCA\ (mg) x\ 100}{total\ protein\ content\ (mg)} \quad \textbf{(2.10)}$$

Fluorescence. The emission spectra were recorded for diluted protein solutions (1 g/L) using quartz cuvettes (1 cm path width) by using Cary Eclipse spectrofluorometer (Varian, USA). The spectra were recorded at 20 °C between 280 and 800 nm with an excitation wavelength of 275 nm, with 0.5 nm step, 30 nm/min. Both excitation and emission slit widths were set at 5.0 nm. The background intensities of the buffer solutions/water were subtracted from the protein emission spectra. The Rayleigh scattering harmonic (at λ = 550 nm) was eliminated from the recorded spectra and the fluorescence intensities measured above 300 nm were then summed.

[7] Amino acids with aromatic side chains (Trp, Tyr, Phe) exhibit strong UV light absorption at 280 nm.

2.4.5 Neutron Imaging

Neutron Dark Field Imaging measures the modification of fringes produced by interferometry, caused by the small-angle scattering from a sample, introduced in the optical path of the interferometry device. The amplitude of the fringes is called a DFI contrast and its decrease is the relative loss of visibility (v_s/v_0). Its measure as a function of a probed correlation length ξ resembles a real space correlation function of the scattering structure $G(\xi)$ (see **Equation 2.11**) and it is reduced for lower scattering angles q. This method can be understood as a spatial transform of SANS, but being able to resolve larger length scales (from 0.3 up to 3 μm - a range analogues to q range of USANS), here the sizes of large protein aggregates. Each point of the sample illuminated area is analyzed separately, giving an image of the averaged DFI contrast:

$$DFI(\xi) = \frac{v_s(\xi)}{v_0(\xi)} = e^{\Sigma_s t(G(\xi)-1)} \quad \textbf{(2.11)},$$

where Σ_s is the total small-angle neutron scattering cross section (comprising the volume fraction of proteins in ϕ (0.07), the contrast $\Delta\rho^2$ (6.1 10^{-20} cm^{-2})[8], wavelength λ (3.5 or 4.5 Å) and the sample thickness t[19]:

$G(\xi)$ is related to the SANS intensity $I(q)$ through the Hankel transform[20]:

$$G(\xi) = \frac{1}{2\pi\xi}\int_0^\infty J_0(q\xi)I(q)qdq \quad \textbf{(2.12)},$$

where J_0 is the zeroth-order Bessel function of the first kind, q is the scattering vector.

The Dark Field Neutron Imaging experiments were carried on the ICON beamline in Swiss Spallation Neutron Source (SINQ) of Paul Scherrer Institüt in Switzerland. The sample holder hosted 4 circular cells (with diameter of 40 mm, 1 mm or 2 mm thick; see **Figure 2.6**). The digested samples (gastric 30 or 60 min and intestinal 10 or 30 min)

[8] $\Delta\rho^2 = (SLD_{protein} - SLD_{solvent})^2$.

were thermalized down to 6°C to quench further digestion. External condensation on the quartz windows was avoided by a multi-jets airflow[9].

Figure 2.6 Image of the gel samples in neutron cells before the measurements. The metal cover was closed for the measurements time, to providing a better thermal control and avoiding condensation when submitted to the air jets.

The measurements were done on a Talbot–Lau grating interferometer, which schematic setup is shown on **Figure 2.7**. One position of the sample holder (distance to grating G2) corresponds to one value of scattering vector q and thus one real correlation length of the scattering structures ξ, by relation:

$$\xi = (\lambda L_s)/p \qquad \textbf{(2.13)},$$

with L_s - sample to analysis grating distance in cm (max 350 cm), p - G_2 grating period (25 µm) and λ - wavelength in Angstroms, giving ξ in microns.

Scanning the sample-grating distance enabled then obtaining the DFI contrast (damped interference fringes at G_2) as a function of ξ.

[9] Together with P. Judeinstein (LLB) and C. Garvey (TUM, Munich), we carried on additional measurements on calcium carbonate suspensions of known size (1-40 µm) to test different effects (sample thickness, contrast (with D_2O), neutron λ), in order to work in the good DFI decay range.

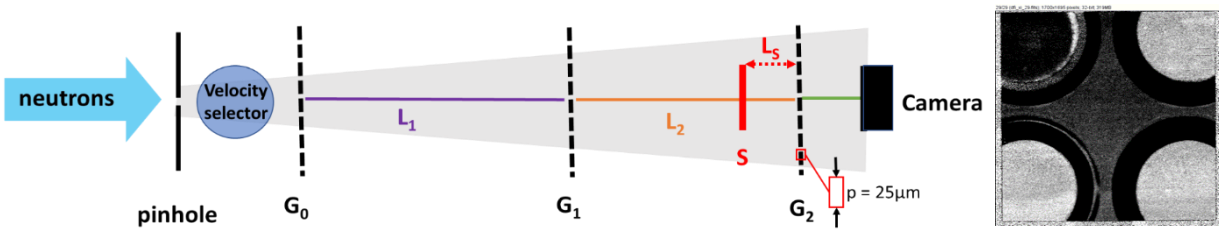

Figure 2.7 Schematic representation of the (Talbot–Lau neutron) grating interferometer setup for dark-field imaging, with a source absorption grating G_0, a phase grating G_1, generating an interference (Talbot) pattern and an analyzer absorption grating G_2, at a fractional Talbot distance matching the period of the interference pattern. The interference patterns of the individual coherent beams from G_0 add constructively at G_2. SANS from a sample reflects in the intensity modulation of the fringes, induced and analyzed by the different gratings. It results in a damping of the interference fringes at G_2, seen as loss of visibility. The detector (camera) resolves the interference pattern in pixels.

Data Acquisition. 15 distances (ξ values) were measured for each sample, with 3 images per step per 1 minute. An Andor iKon-M CCD camera was used as the detector, operated with a mirror and optical lens system (100 mm Nikkor). The DFI contrast was extracted from the resulting images pixel by pixel using Fourier analysis. The image area was 1024×1024 pixels corresponding to a field of view of approximately 67×67 mm^2. A sample region of interest could be selected using *ImageJ* software[21] and the mean grey value over its area (sum divided by the number of pixels) was calculated. We could vary the ROI and show some differences inside the samples, in particular when submitting them to a diffusion gradient of digestive juice (these preliminary observations are not shown in this work).

Data analysis. The scattering of large protein aggregates was modeled assuming polydisperse interacting spheres, with the form factor of spheres (see **Equation 2.14**) and the structure factor of interacting hard-spheres (see **Equation 2.15**).

$$P(q) = \frac{1}{V^2}F^2(q), \text{ with } F(q,r) = 3V\frac{sin(qr)-qr\,cos(qr)}{(qr)^3} \quad \textbf{(2.14)},$$

where *F*(*q*,*r*) is the scattering amplitude and *r* is the sphere radius.

$$S(q,r) = \frac{1}{1+24\varphi\frac{Y(2qr)}{2qr}} \quad \textbf{(2.15)},$$

with *S(q,r)* being the Percus–Yevick expression[22], where Y(*x*) function is:

$$\boldsymbol{Y(x) = \alpha\frac{sin(x)-x\,cos(x)}{x^2} + \beta\frac{2x\,sin(x)+(2-x^2)\,cos(x)-2}{x^3} + \gamma\frac{-x^4\,cos(x)+4[3x^2-6)\,cos(x)+(x^3-6x)\,sin(x)+6]}{x^5}} \quad \textbf{(2.16)},$$

with $= \frac{(1+2\varphi)^2}{(1-\varphi)^4}$, $\beta = -6\varphi\frac{(1+\frac{\varphi}{2})^2}{(1-\varphi)^4}$, $\gamma = \frac{\varphi\alpha}{2}$.

Polydispersity of the spheres a log-normal size distribution P(r) was applied to the model, expressed by[20]:

$$P(r) = \frac{1}{r\sigma\sqrt{2\pi}}e^{\frac{-(ln\,r-\mu)^2}{2\sigma^2}} \quad \textbf{(2.17)},$$

with the mean μ and the standard deviation of the logarithm of the sphere radius σ.

2.4.6 Confocal Fluorescence Imaging

The microstructures of the initial and digested gels were visualized by the Confocal Laser Scanning Microscopy (Zeiss Axio Imager, LSM 700), at Institut de Chimie et des Matériaux Paris-Est, ICMPE (Thiais, France). Rhodamine B in protein gels was excited with 561 nm and the fluorescence emission was recorded at 570-790 nm. Samples were imaged through Zeiss objectives: 5x (Plan-Apochrom. 5x/0.16) and 20x (Plan-Neofluar 20x/0.5) air-immersion, and 63x oil-immersion (Plan-Apochrom. 63x/1.4). A schematic setup of confocal microscope is shown in **Figure 2.8**.

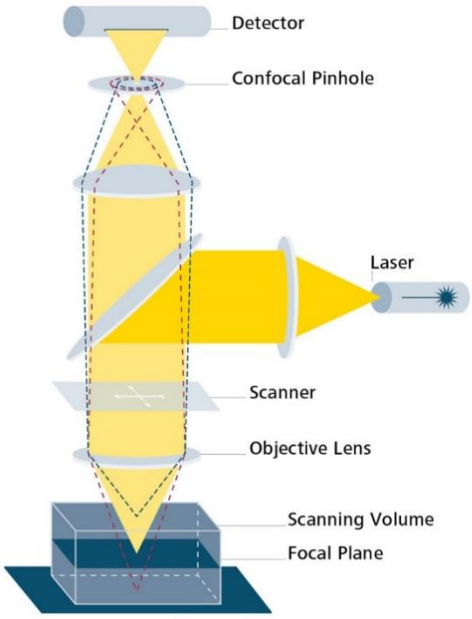

Figure 2.8 Schema of confocal microscope, comprising a laser light source, dichroic mirror, objective lenses, scanning device and detection system (photomultiplier), detecting the light from the confocal pinhole. Yellow color represent the in-focus information and red and blue dashed lines – the information out of focus. From Zeiss website: https://www.zeiss.fr/microscopie/produits/confocal-microscopes/lsm-900-pour-materiaux-non-contact-surface-topography-en-3d.html.

The advantage of the confocal microscopy is its high-resolution, provided by elimination of the out-of-focus light and detection of the emitted light confined to a single point in the specimen by the confocal pinhole. The image from the whole sample area is obtained through scanning across the sample[23], which requires some time: several minutes for a 2D image and tens of minutes for scanning at different depths to obtain a 3D image.

Data acquisition. Images were acquired through Zeiss ZEN 3.6 software, at different locations of the sample with a scanning rate of 400 Hz in 1024×1024 pixel resolution and 8×line averaging mode.

Image analysis. The confocal images were analyzed by *ImageJ* software. The FFT bandpass filter was used to enhance protein structures by filtering out the high and low spatial frequencies (selecting minimum and maximum feature sizes). This enabled better thresholding of the images to get the binary images. The selection of the

threshold segmentation was made with the Otsu algorithm, based on a visual validation. An example of thresholding segmentation is present on **Figure 2.9.**

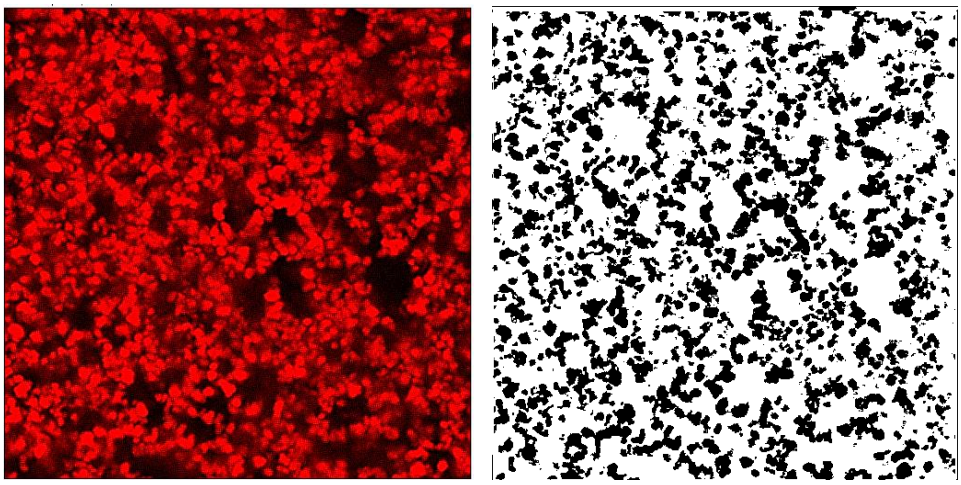

Figure 2.9 A confocal image of canola protein gel (**left**) and after thresholding (**right**).

The quantification of the thresholded images were done by the *Analyze Particles* function, which measures all the selected regions of interest as individual objects, giving the results of the parameters of interest (here the Feret's diameter).

2.4.7 Synchrotron UV fluorescence imaging

The *in situ* monitoring of the 100-300 µm gel pieces during gastric and intestinal digestion were performed on the DISCO beamline with deep X Ray UV at Synchrotron SOLEIL (Saint Aubin, France). The gels pieces were cut directly before the data acquisition (with a bit of buffer solution to prevent sample evaporation) and placed in an open infusion cell (see **Figure 2.10**). The infusion cell was then closed with a glass cover and placed on the temperature-controlled plate on the microscope, regulated at 37°C. The gel pieces were kept in the center of the cell during injection of digestion liquids thanks to a set of small vertical columns (0.5 x 3 mm) arranged in a circle in the center of the cell.

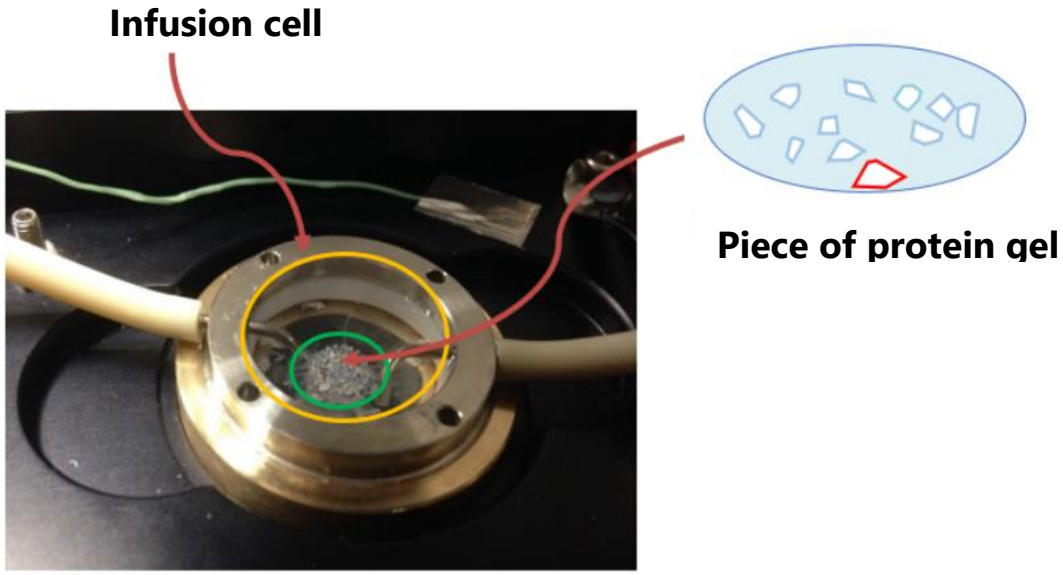

Figure 2.10 The open infusion cell used in the experiment; it was made of brass for good thermal conductivity, its bottom part was composed of very thin quartz glass and provided a short distance from the objective. It was positioned in the middle of the light beam; the gel pieces were placed in the middle part marked by green circle and the digestive solutions were injected to the volume marked by yellow circle, through syringes and connected tubes (one for gastric and one for intestinal solution). The cover glass, placed on the top, prevented the water condensation.

Data acquisition. The selected gel piece/pieces were imaged with full-field microscope TELEMOS (excitation: 275 nm; Dichroic Mirror 300 nm, emission: 327-353 nm) by the 40x objective, with successive exposures of UV (10 s) and visible (100 ms) light. One image was recorded per minute.

Under UV exposure, the fluorescence of the (majorly) tryptophan residues in the illuminated gel pieces was initially monitored for 20 min without starting the digestion. During this time period, the fluorescence was decreasing fast, due to phenomenon of photo-bleaching of the fluorophores[10].

[10] This effect is difficult to estimate by calculations. We measured it, separately, on several samples, for long durations (> 2 h) for further data treatments.

Then, by the use of a remote control peristaltic syringe-pump, the gastric solution was gently poured on the gel pieces (with rate of 200 µm per min). A very delicate step was to keep the same gel pieces in the imaged (illuminated) area. It was therefore sometimes necessary to readjust the sample stage in order to recenter the field of view.

The gel pieces were monitored throughout all the time. For intestinal digestion, a new piece of gel was chosen and the intestinal solution was injected in the same way, through the second tubing.

Image correction. The applied corrections of raw images included darkfield (for compensation of eventual hot pixels coming from the instrument) and brightfield (for background illumination compensation), with the use of the formula:

*Corrected image = (Sample Image - Darkfield)/(Brightfield - Darkfield) * 255*[11].

The capture of darkfield image was done by blocking the light path (with the microscope light on) and the brightfied - with an open light path, without the sample.

Image analysis in ImageJ. The chosen piece/pieces of gel were thresholded manually for each image[12], corresponding for given digestion time, with the use of the Otsu algorithm. The selection of the segmentation, was based on a visual validation, giving the most precise contours of the gel pieces over the full digestion sequence.

The mean fluorescence intensity and the gel piece/pieces area were then measured for each image in the sequence. More data treatments are detailed in Chapter 5.

[11] For 8 bit images.

[12] The changing contrast levels between the gel sample and the background solution during digestion did not allow a precise automatic segmentation.

References

[1] Ainis, W., Ersch, C., & Ipsen, R. (2018). Partial replacement of whey proteins by rapeseed proteins in heat-induced gelled systems: Effect of pH. *Food Hydrocolloids*, 77, 397-406. doi: 10.1016/j.foodhyd.2017.10.016.

[2] Pasquier, J., Brûlet, A., Boire, A., Jamme, F., Perez, J. et al. (2019). Monitoring food structure during digestion using small-angle scattering and imaging techniques. *Colloids and Surfaces A: Physicochemical and Engineering Aspects*, 570, 96-106. ff10.1016/j.colsurfa.2019.02.059ff. ffhal-02561464f.

[3] Minekus, M., Alminger, M., Alvito, P., Ballance, S., Bohn, T., Bourlieu, C., Carrière, F., Boutrou, R., Corredig, M., Dupont, D., Dufour, C., Egger, L., Golding, M., Karakaya, S., Kirkhus, B., Le Feunteun, S., Lesmes, U., Macierzanka, A., Mackie, A., Marze, S., McClements, D.J., Ménard, O., Recio, I., Santos, C.N., Singh, R.P., Vegarud G.E., Wickham M.S., Weitschies W. & Brodkorb, A. (2014). A standardised static in vitro digestion method suitable for food - an international consensus. *Food Function*, 5, 1113-1124. doi: 10.1039/c3fo60702j.

[4] Brodkorb, A., Egger, L., Alminger, M. *et al.* (2019). INFOGEST static in vitro simulation of gastrointestinal food digestion. *Nature Protocols,* 14, 991–1014. doi: 10.1038/s41596-018-0119-1.

[5] Als-Nielsen, J. and McMorrow, D. (2011). Elements of Modern X-ray Physics. John Wiley & Sons, West Sussex, United Kingdom.

[6] Cotton, J.P. (1991). In: Neutron, X-Ray and Light Scattering, Eds. P. Lindner, Th. Zemb, p.19, Elsevier, North-Holland, Delta series.

[7] Brûlet, A., Lairez, D., Lapp, A., Cotton, J.-P. (2007). Improvement of data treatment in SANS. *Journal of Applied Crystallography,* 40, 165-177. doi: 10.1107/S0021889806051442.

[8] SasView. http://www.sasview.org.

[9] Nielsen, S. S., Noergaard Toft, K., Snakenborg, D., Jeppesen, M. G., Jacobsen, J. K., Vestergaard, B., Kutteraand, J. P., Arleth, L. (2009). BioXTAS RAW, a software program for high-throughput automated small-angle X-ray scattering data reduction and preliminary analysis. *Journal of Applied Crystallography*, 42, 959-964.

[10] Guinier, A. and Fournet, G. (1955). Small-Angle Scattering of X-Rays. Wiley-VCH Verlag GmbH & Co., New York.

[11] Feigin, L.A. & Svergun, D.I. (1987). Structure Analysis by Small-Angle X-ray and Neutron Scattering. New York: Plenum Press.

[12] Pedersen, J.S. (1997). Analysis of small-angle scattering data from colloids and polymer solutions: modeling and least square fitting. *Advances in Colloid and Interface Science,* 70, 171–210.

[13] Nielsen, S.S., Noergaard Toft, K., Snakenborg, D., Jeppesen, M.G., Jacobsen, J.K., Vestergaard, B., Kutteraand, J.P., Arleth, L. (2009). BioXTAS RAW, a software program for high-throughput automated small-angle X-ray scattering data reduction and preliminary analysis. *Journal of Applied Crystallography*, 42, 959-964.

[14] Svergun D.I. (1992). Determination of the regularization parameter in indirect-transform methods using perceptual criteria. *J. Appl. Crystallogr.,* 25, 495-503.

[15] Ciccariello, S., Goodisman, J., Brumberger, H. (1988). On the Porod law. *Journal of Applied Crystallography,* 21, 117-128. doi: 10.1107/S0021889887010409.

[16] Schultz, N., Metreveli, G., Franzreb, M., Frimmel, F.H., Syldatk, C. (2008). Zeta potential measurement as a diagnostic tool in enzyme immobilisation. *Colloids Surf. B Biointerfaces*, 1, 66(1), 39-44. doi: 10.1016/j.colsurfb.2008.05.004.

[17] Nelson, D.L. and Cox, M.M. (2017). Lehninger Principles of Biochemistry (7th edition), W.H. Freeman, New York, 1328.

[18] Hartree, E.F. (1972). Determination of protein: a modification of the Lowry method that gives a linear photometric response. *Analytical Biochemistry,* 48, 422-427. doi: 10.1016/0003-2697(72)90094.

[19] Strobl, M. (2014). General solution for quantitative dark-field contrast imaging with grating interferometers. *Scientific Reports*, 4, 7243.

[20] Andersson, R., Van Heijkamp, L.F., De Schepper, I.M., Bouwman, W.G. (2008). Analysis of spin-echo small-angle neutron scattering measurements. *Journal of Applied Crystallography*, 41, 868–885.

[21] Schneider, C.A., Rasband, W.S., & Eliceiri, K.W. (2012). NIH Image to ImageJ: 25 years of image analysis. *Nature Methods*, 9 (7), 671–675. doi: 10.1038/nmeth.2089.

[22] Ashcroft, N.W., March, N.H. (1967). Structure factor and direct correlation function for a classical hard sphere fluid. *Proc. R. Soc. London. Ser. A. Math. Phys. Sci.*, 297, 336–350.

[23] Földes-Papp, Z., Demel, U., Tilz, G.P. (2003). Laser scanning confocal fluorescence microscopy: an overview. *International Immunopharmacology*, 3, (13–14), 1715-1729. doi: 10.1016/S1567-5769(03)00140-1.

Chapter 3
Preliminary Characterization of Canola Proteins

This chapter presents the results obtained from characterization of canola proteins (napin, cruciferin and their mixture) in solutions and in gels, **before digestion experiments**. We describe here the conformations of the proteins and their charge characteristics with the use of Small-Angle X-ray Scattering, zeta-potential and spectrophotometric techniques. We compare the "native" states of the proteins in solutions to the ones at different denaturing conditions (pH, chemical denaturants and heat). We further present the heat-induced gelation of the proteins, monitored by rheology (mechanical properties) and Small- and Wide-Angle Scattering (nanostructure). At last, we describe the differences in mechanical properties and nanostructure between the two gels formed at different pH conditions (pH 8 and 11).

3.1. Canola Proteins in Aqueous Solutions

3.1.1. Conformation of "native" canola proteins

Prior to studying the effect of digestion on canola proteins, we will characterize their native states, i.e. after their dissolution in water plus salt solutions, giving, without other modifications, pH ~7.5.

From the Small-Angle X-ray Scattering curves of the two native canola protein solutions (**Figure 3.1a**), we can directly distinguish the characteristic molecular features, like general shape, size and mass of napin and cruciferin. For **napin**, the low *q* signal is not high and relatively flat, telling us that it is a rather small and low mass protein. Then, for higher *q*, its scattering signal goes down due to a certain compactness of napin: a general expectation is the stronger the decay (slope) towards higher *q*, the more compact the object. A power law exponent close to -4 indicates a compact object and -2, some extended conformation[1].

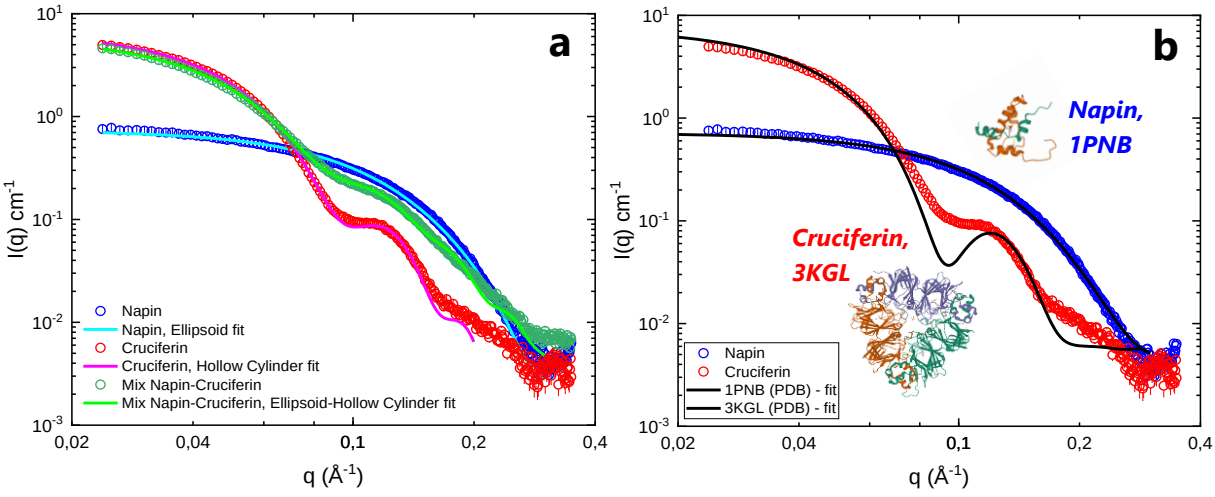

Figure 3.1 SAXS of "native" canola protein solutions (pH~7.5, c=0.1 g/cm^3): **a)** napin (blue), cruciferin (red), their mixture (green). Lines represent the best fits: ellipsoid for napin (with *R*= 22 Å and *r*= 12 Å), hollow cylinder for cruciferin (with *R*= 46 Å, *r* = 10 Å and *L*= 55 Å) and the mix of both form factors (with volume fractions 47% - 53%). **b)** The same data for napin and cruciferin with the simulations of the corresponding 1PNB and 3KGL Protein Data Bank (PDB) structures from CRYSOL software.

[1] More precisely, -2 is for a random walk.

Cruciferin's SAXS profile at low q is less flat and with higher intensity, informing about its larger size and mass, compared to napin. The oscillation visible from q ~ 0.1 $Å^{-1}$ comes from the toroidal shape of cruciferin, shown on **Figure 3.1b** by its atomic structure representation from Protein Data Bank (PDB). By the use of CRYSOL program[1], we could also evaluate our results, by comparing the experimental SAXS curves to the reference curves obtained after fittings with the known PDB structures, i.e. 3KGL for native cruciferin and 1PNB for native napin (black solid lines). We obtain a very good correlation of our experimental SAXS data with the crystallographic data. The more pronounced oscillation for the PBD fit, likely comes from a better signal-to-noise ratio for protein crystals, compared to proteins in solution.

In the **mixed sample**, napin and cruciferin coexist, as individual molecules or in their mixed local assemblies. In the scattering signal, the cruciferin is the predominantly scattering component (owing to its higher molecular weight), thus we can see a similarity of the mix and cruciferin curves, however "attenuated" mainly at high q due to the signal coming from the small napin.

The scattering intensity of a protein solution is proportional to the protein concentration in the dilute regime, usually for c of order of a few percent. Here, for native canola protein solutions, the concentration of ~10 w.% (i.e. volume fraction of protein of 0.1/1.35=0.074) is high with that respect. However, the scattering does not display interpenetration nor attraction-repulsion interactions, nor evident aggregation, giving a strong upturn in the scattering pattern at lower q (at least in the measured q range by the lab-SAXS instrument). The use of relatively high concentration had the great advantage of obtaining a sufficient signal-to-noise ratio for our protein samples.

From the SAXS spectra, we could obtain several characteristic parameters of the scattering objects, including the molecular weight, maximum dimension D_{max} and radius of gyration R_g. The latter could be extracted directly from the SAXS data by using the **Guinier approximation**[2] (see **Equation 2.2**, **Chapter 2**). For native canola proteins

it was determined to be equal **19.7 Å** for napin, **37.3 Å** for cruciferin and **39 Å** for the napin-cruciferin mix.

Kratky representation ($q^2I(q)\ versus\ q$) enables a general qualitative assessment of the degree of compactness of the scattering objects, by accenting particular features of the scattering profile, explicitly the oscillations or curvatures in high/middle q region. For a more sensitive analysis of the protein compactness and flexibility, SAXS data have been shown on dimensionless Kratky plot, $(qR_g)^2 I(q)/(I(q \to 0))\ vs\ qR_g$. As can be seen in **Figure 3.2**, the curves for cruciferin and cruciferin-napin mix show the well-defined, almost exact same maxima of ~1.1 at qR_g of √3, which position (marked by the crossings of the grey dash lines) corresponds to a compact geometry of a globular protein[3]. Compared to the one of cruciferin, napin's maximum position is shifted to the right (at qR_g > √3), which denotes a well-folded but more asymmetric shape, like an **ellipsoid.**

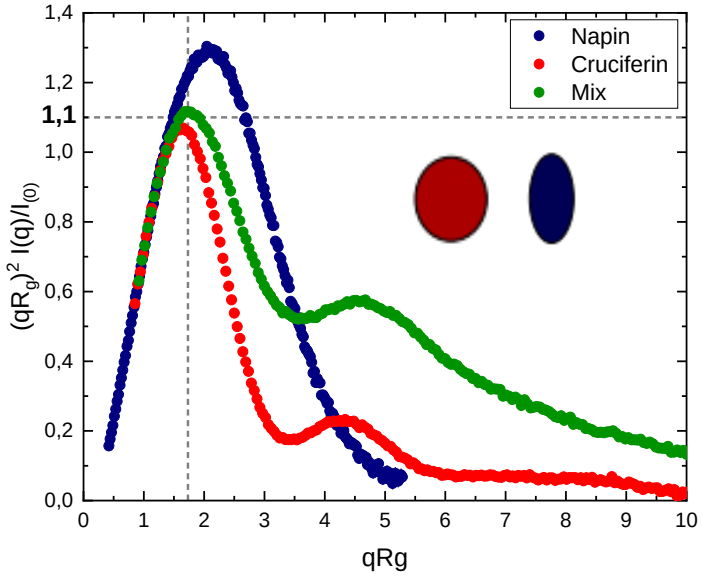

Figure 3.2 Dimensionless Kratky plots, $\frac{(qR_g)^2 I(q)}{I(q \to 0)}\ vs\ qR_g$, which normalize scattering profiles by mass and concentration; for napin (blue), cruciferin (red) and napin-cruciferin mix (green). The figures show the deduced shapes of cruciferin (red) and napin (blue), without the aspect of their sizes.

When comparing results obtained alternatively from the pair distance distribution ***P(r)***, which uses fitting from the whole SAXS curves (see **Equation 2.7**, **Chapter 2**), we attained broader size and shape information about a given protein (i.e. its radius but also the maximum size D_{max}). We estimated napin's radius to be of ~18 Å (from the peak of the bell-shape *P*(*r*) curve), however an additional minor peak could be identified around 55 Å. Indeed, it can be due to flexible regions present in the napin's structure, rendering its more elongated, ellipsoidal shape. The *P*(*r*) profile for napin goes down to D_{max} around 80 Å.

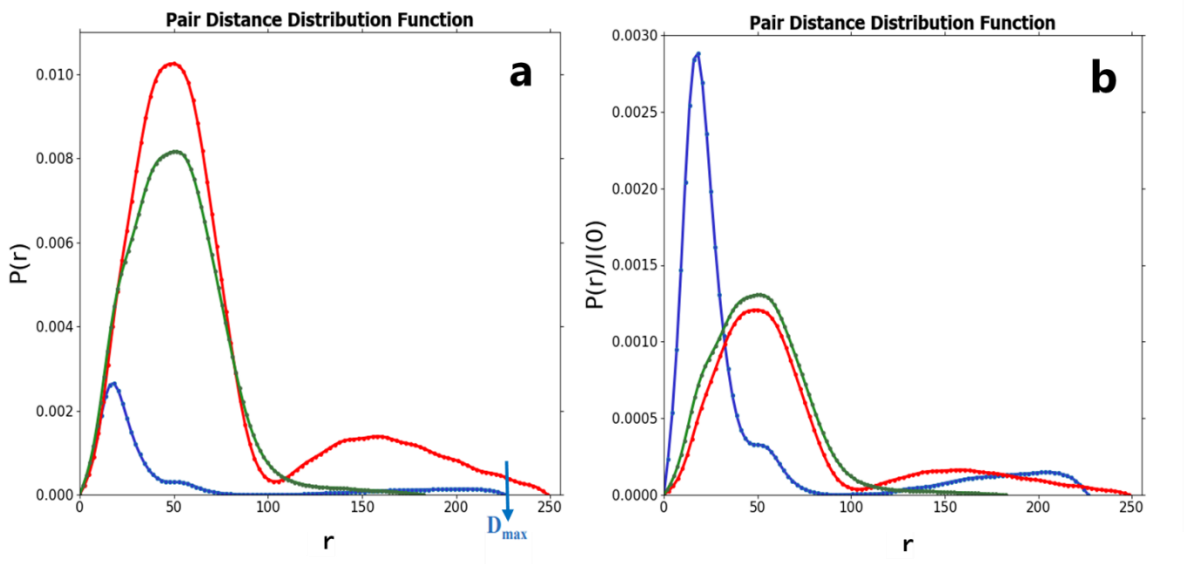

Figure 3.3 a) Pair distribution function *P*(*r*) for napin (blue), cruciferin (red) and napin-cruciferin mix (green). **b)** The same curves but normalized by X-ray scattering intensity at zero angle, $I(q \to 0)$.

The profiles of cruciferin and cruciferin-napin mix have very similar shapes and positions of the main peak, being around 50 Å, but the protein mix have an additional small shoulder visible for ~20 Å. This less distinct *P*(*r*) feature, compared to cruciferin alone, can tell us about association of napin with cruciferin, resulting in more disordered assemblies, washing out distinct *P*(*r*) features. For cruciferin alone, some smaller fraction of large sizes (~150 Å) appears together with D_{max} of almost 250 Å. This dual feature can represent a larger number of possible conformations of cruciferin, in respect to mix solution.

The radii obtained from $P(r)$ are in agreement with values of R_g from Guinier analysis. The Kratky plots and $P(r)$ analysis are clearly consistent with the notion that canola proteins in native solutions are predominantly in the folded states, being a small ellipsoid for napin, larger globule for cruciferin and their compact assembly for cruciferin-napin mix.

Fitting with geometrical model

For more precise descriptions of the protein geometries, the SAXS curves were fitted with particle form factors $P(q)$, characterizing the shapes of a given protein molecule (see **Equation 2.5** and **2.6** in **Chapter 2**). A hollow cylinder[4] form factor (torus) was applied for cruciferin and an ellipsoid[5] for napin. The best fitting parameters are listed in **Table 3.1**.

Table 3.1 Best fitting parameters obtained with the ellipsoid form factor for napin and the hollow cylinder for cruciferin, in native (~ pH 8) protein solutions (100g/L).

	Radius (Å)		***Height L (Å)***
Napin	***r polar***	***R equatorial***	
	11.8±0.1	22.±0.1	-
Cruciferin	***r core***	***R external***	55±0.1
	9.6±0.1	45.7±0.1	

The dimensions of the canola proteins obtained from the form factor fittings are in reasonable agreement with those obtained from $P(r)$ and Guinier analysis. It allows us to obtain additional geometry information. In particular, for the cruciferin molecule, the height of the hollow cylinder, 55 Å, is large compared to its external radius, 46 Å; this can corresponds well to the total height of two trimers, e.g. assembled perpendicularly to each other, leading to a hexamer.

Based on the scattering intensities at zero scattering angle $I(q \to 0)$ for the proteins (i.e. 6.8 cm^{-1} for cruciferin, 0.8 cm^{-1} for napin), we can estimate the molecular weights of the proteins: 11.9 kDa for napin, 92 kDa for cruciferin. The value for napin is in fair

agreement with the literature value (12.6 kDa[6]), however for cruciferin, it is much lower than the value for the expected hexamer assembly, 300 kDa[7]. It is tempting to assume here a rather trimeric structure, but it is contradictory with the hexameric conformation to which was pointed by the height of the molecule (55 Å).

The discrepancy in the molecular weight could be explained by the effect of hydration of cruciferin, which is decreasing of its contrast with the buffer. Indeed, the contrast for cruciferin can decrease by more than a factor two when we consider that only a fifth of the all labile hydrogens of the protein are replaced by water molecules. This could happen because native cruciferin has been first extracted, by using severe chemical reaction, which could have altered its hydrophobicity. In addition, the hollow cylindrical shape of cruciferin could be favorable to a higher hydration (especially in the core), than for napin, which is small and shows a compact ellipsoid shape.

From the fitting parameters of the napin-cruciferin mix (green curve in **Figure 3.1**), we could extract their relative proportions in the mixture. We used a model being a sum of the scatterings of an ellipsoid and of a hollow cylinder. We obtained 47% napin and 53% cruciferin for the volume fractions.

3.1.2. Canola proteins denaturation

Unfolding of proteins is not only characterized by the disappearance of the well-defined three-dimensional structure but can also lead to less dense, more open protein structures. In this case, protein unfolding can be well visualized by the Kratky representation, $q^2I(q)\ vs\ q$ which will be very different for flexible-chain-like/unfolded and for compact protein conformations, as shown in **Figure 3.4**. As example, the scattering at large angles from well-folded, compact molecules approximates to $1/q^4$ (Porod law[8]), exhibiting a parabolic (bell-shape) Kratky transform, converging towards the background signal at higher q, with a defined maximum indicating a characteristic real-space global size of the scattering object. Conversely, the scattering from completely unfolded objects (Gaussian chains) scales as $1/q^2$, exhibiting hence a parabolic growth of the Kratky curve, approaching a plateau at higher q values[9]. In

case of partial unfolding or a high molecule's flexibility, a peak with a much slower intensity decay or a plateau over a specific q range, followed by a linear/monotonic increase at larger q in the Kratky plot are expected, as e.g. for branched thin polymers chains. In case of proteins, this increase at larger q is attributed to the linear dimension of the chain at short length scales resulting from the amino acid backbone stiffness and it displays an intermediate state between the folded protein and of the random chain.

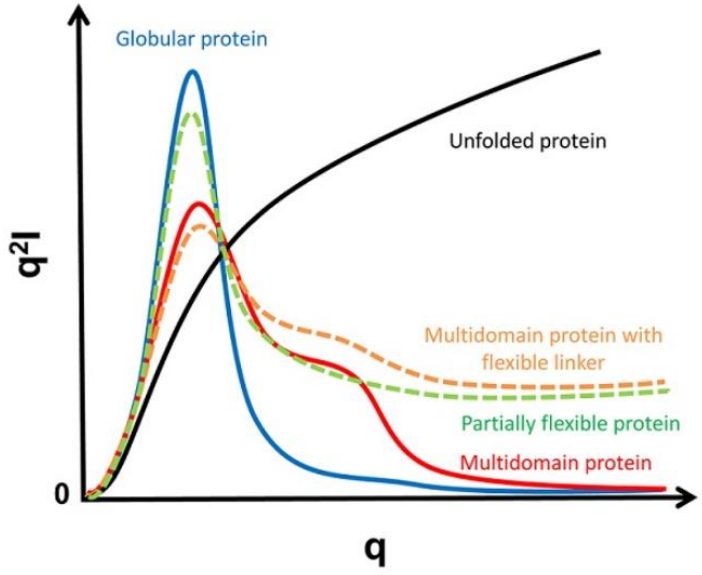

Figure 3.4 Schema of Kratky plots, $q^2I(q)\ vs\ q$, for proteins with different levels of unfolding/flexibility (from www-ssrl.slac.standford.edu). For the unfolded protein case, it is necessary to choose a sufficiently unfolded structure and especially with a large enough R_g to see the plateau at high q.

The Kratky curves for native canola proteins shown above (**Figure 3.5**) are close to bell shapes, representing therefore compactly folded conformations. We can tell at this point, that the proteins from the used isolate powders have conserved their natively-folded conformations, i.e., they were not denatured by the extraction and/or purification processes, which is advantageous for their later use in studying the effect of pH, heat, and finally digestion on their structural/conformational changes.

Chemical denaturation

In order to make comparisons, different severe conditions can be used to induce protein unfolding[10]. Here, a strong denaturing agent guanidine hydrochloride (GndHCl) was used to provoke protein denaturation, by interacting with their polar parts. While the Kratky plots of the natively folded proteins present clear maxima, the ones treated with 3M GndHCl (**Figure 3.5a**) exhibit larger, less sharp peaks, displaying more unfolded shapes. Nevertheless, some level of protein folding is still preserved, seen from the attenuated, but still visible, parabolic shapes of the curves, which trail off back to zero at higher q values. This indicates a relative robustness of canola proteins against chemical denaturation. The effect of urea (6 and 8 M) was also tested, however it did not provoke a sufficient protein unfolding (not shown).

The values of the protein geometries, obtained after fittings with ellipsoid for napin and with hollow cylinder for cruciferin in 3 M GdnHCl, are presented in **Table 3.2.** They confirm some elongation of the proteins and, in case of napin, we can assume the elongation along its initially shorter axis, changing its shape to less ellipsoidal.

Table 3.2 Fitting parameters obtained for napin (ellipsoid form factor), for cruciferin (hollow cylinder form factor) and for the protein mix (cylinder form factor) in native protein solutions and in 3M GndHCl solutions. c=0.1g/cm^3 (i.e. a volume fraction of protein of 0.1/1.35=0.074) for all the solutions. $\Delta\rho^2$ is the theoretical contrast between the protein and the solvent assuming the density of proteins of 1.35g/cm^3. Note that the best fit values for the scale of proteins in 3M GndHCl samples are lower than the volume fraction of proteins (.074) in the solutions: this is due to hydration of molecules upon denaturation.

	Contrast* $\Delta\rho^2$ *(Å^{-4})	***Scale***	***Radius (Å)***		***Height L (Å)***
			r polar	***R equatorial***	
Napin *native*	7.45E+20	0.059±5E-5	11.3±0.02	22±0.1	-
+3M GndHCl	4.84E+20	0.02±9E-5	16.9±0.6	19.7±0.3	-
			r core	***R external***	***Height L (Å)***
Cruciferin *native*	7.49E+20	0.038±2E-5	10.3±0.02	45.7±0.1	54.2±0.1
+3M GndHCl	4.88E+20	0.0014±2E-5	13±0.06	49.2±0.1	49.1±0.1
			Radius		***Height L (Å)***
Mix *+3M GndHCl*	4.87E+20	0.012±3E-5	14.7±0.1		170±4

Compared to the individual proteins, the unfolding of the protein mix with 3M GndHCl was much stronger (see **Figure 3.5a**, green curve); the hollow cylinder oscillation observed for native cruciferin has vanished. The SAXS curve could be well fitted with a cylinder model, with a radius of 15 Å and length of ~170 Å. These values likely correspond to an extended structure. Denaturation effect could be seen also by the much lower value of $I(q \to 0)$ for the protein mix, compared to cruciferin alone, explained, as for cruciferin, by the hydration of the unfolded proteins. The stronger effect of unfolding for the protein mix might be due to association of the two proteins.

Finally, for the highest concentration of denaturant, **6 M GndHCl**, the Kratky plots for all the protein solutions showed a greater unfolding. It can be seen from the shapes of the curves, tending at large *q* not towards zero but to a plateau (preceded however by a wide and soft maximum, hence slightly different from the case of completely unfolded structures (see **Figure 3.5b**). The increase signals at *q* values above 0.2 Å^{-1} comes from an incomplete subtraction of the buffer.

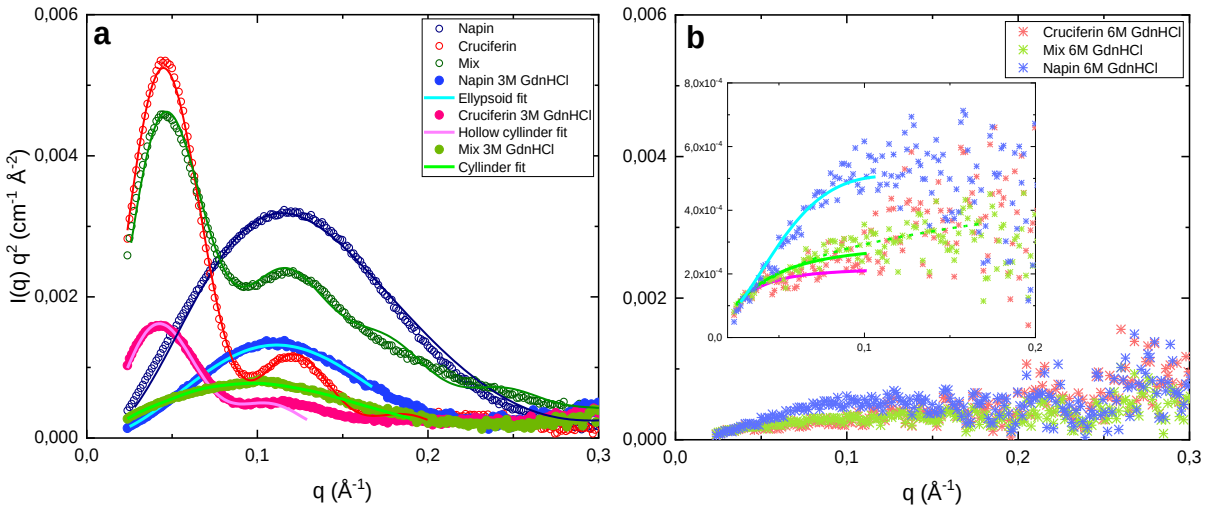

Figure 3.5 Kratky plots of SAXS for napin (blue), cruciferin (red) and mix (green) solutions (100g/L): **a)** in native states (pH ~8) (open symbols) and in 3M GndHCl (full symbols); lines are fits shown in **Figure 3.1** for native states and for 3M GndHCl solutions (cf. Table 3.2: napin (*r*=17 Å, *R*=20 Å), cruciferin (r=13 Å, R= 49 Å, L= 49 Å) and the protein mix (*R*=15 Å, *L*=170 Å). **b)** in 6M GndHCl; inset: enlarged plot. Lines are Lorentzian fits for napin (ξ =13 Å and exponent of 3.3), cruciferin (ξ =33 Å and exponent of 2.1) and mix (ξ = 30 Å and exponent of 2).

Here, napin seemed to be the most resistant towards the harsh denaturing conditions, still retaining some compactness. This can be better seen on the inset of **Figure 3.5b** with the enlarged plot. Here, the green curve, corresponding to the protein mix, was divided by a prefactor 1.7, enabling a better visual comparison with cruciferin (red curve). We could there see that both cruciferin and mix are closer to representing completely unfolded structures. The elevated $I(q \to 0)$ for the protein mix compared to the individual proteins, can suggest that the two proteins are likely assembled together (giving bigger mass of the scattering objects)

Based on the Guinier analysis of the 6M GndHCl protein solutions (see **Table 3.3**), all the proteins experienced significant increase in size, as expected for the protein unfolding. The radius of gyration of the denatured canola protein mix was 48 Å. The SAXS curves could be also well fitted with a Lorentzian function, $(q) = \frac{scale}{1+(q\xi)^n}$. Up to q $\leq$ 0.1 Å^{-1}, we obtained a correlation length ξ = 29 Å (thus R_g = 50 Å, from the relation $R_g^2 = 3\xi^2$, valid for non-interacting scattering molecules in good agreement with the R_g of the Guinier analysis), and an exponent n = 1.9, which additionally confirms the extended Gaussian coil conformations[2].

Table 3.3 Values of radii of gyration R_g and scale ($I(q \to 0)$ determined from the Guinier analysis for native proteins, and proteins in 3M GndHCl and 6M GndHCl solutions.

	Native		***3M GndHCl***		***6M GndHCl***	
	Scale	R_g (Å)	*Scale*	R_g (Å)	*Scale*	R_g (Å)
Napin	0.8	19.7	0.3	15	0.2	27.5
Cruciferin	6.6	37.3	2.5	41	0.3	46.3
Mix	6.2	39	0.7	42	0.5	48

The great decrease of the scattering intensity for the denatured proteins, compared to the native states, is likely due to a decreased contrast, which arises from i) a higher

[2] Exponent 2 in neutral solvent/random walk or 5/3 in good solvent/self-avoiding walk.

scattering length density of the 3M and 6M GndHCl solutions[3] (not to be neglected) and ii) the hydration of the unfolded proteins, which is likely when the labile hydrogens are exposed.

3.1.3. Influence of the pH on canola proteins solutions

3.1.3.1. Zeta-potential measurements

To better understand the influence of the pH on structural alterations of our proteins, the zeta-potentials of napin, cruciferin and their mixture were measured as a function of pH. The zeta-potential is a very useful parameter for understanding electrostatic colloidal dispersion stability. It indicates the charge that a molecule acquires in a particular environment, here at certain pH, and is characteristic for a particular protein. The magnitude of the zeta potential indicates the degree of electrostatic repulsion between adjacent, similarly charged particles in a dispersion.

As can be seen in **Figure 3.6**, **napin** (blue curve) keeps rather high positive values of zeta potential at pH 3, suggesting its relatively high electrostatic stability. With increasing pH, up to pH 5, its net charge decreases, and remains relatively stable up to pH 8. Then again, the net charge decreases with increasing pH, passing through the zero-charge at **pH ~9.8** (**IEP**, **isoelectric point**), at which napin is the least stable. Up to pH 11, the napin's charge continues to increase in absolute value on the negative charge scale, giving, again, an increased stability. Napin is an alkaline protein and in the literature, its IEP was found to be at pH between 9 and 11[7] or around ~11[11,12], being in agreement with our findings. Our IEP at pH 9.8 is also relatively consistent with the theoretical value at pH 8.7, calculated from the amino acid sequence for *2SSI_BRANA UniProt* sequence[13,14].

[3] Scattering length density of protein =1.22E+11 cm^{-2}; native buffer= 9.51E+10 cm^{-2}; 3M GndHCl= 1.004E+11 cm^{-2}; 6M GndHCl =1.057E+11 cm^{-2}.

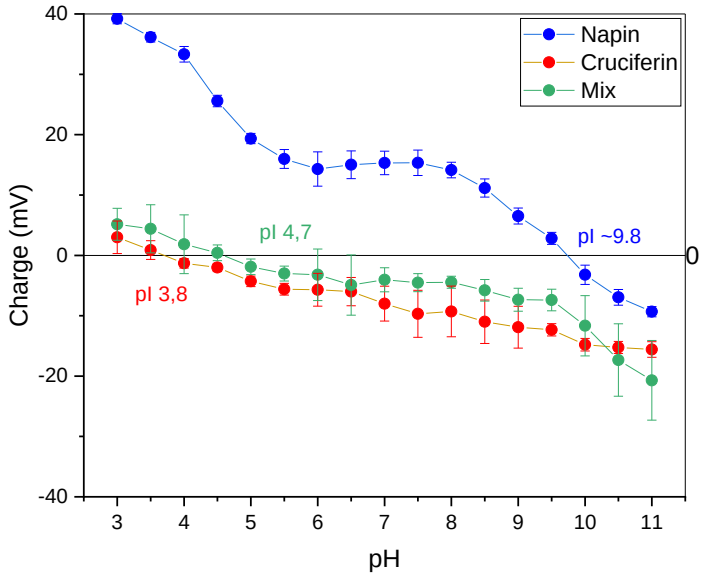

Figure 3.6 Zeta potential in the pH range from 3 to 11 for 1g/L native protein solutions in 10 mM NaCl: napin (blue), cruciferin (red), napin-cruciferin mix (green). The marked points indicate the zero-charge values.

Cruciferin (red curve in **Figure 3.6**) has, in general, a lower net charge compared to napin, being therefore less electrostatically stabilized and possibly proner to aggregation. In contrary to napin, cruciferin acquires relatively low positive charge at pH 3, which decreases until crossing the zero-charge point already at **pH 3.8**. Then, for pH > IEP, cruciferin acquires negative charges, however with a potential not lower than -20 mV, giving, in general, a rather moderate/low stability of cruciferin in this pH range. The IEP of cruciferin was reported in the literature to be in neutral pH ~7[15], which corresponds well to the acidic and basic chain structure of the molecule and the theoretical IEP value (pH 6.6), calculated for one unit of cruciferin (CRUA_BRANA[16]). Other authors reported, however, the IEP for cruciferin in broader pH range, from 4 to 8[12] or even around pH 3.5[17], which corresponds better to our measurements (IEP 3.8). The differences between these theoretically calculated and experimentally determined isoelectric points can result from the different genetic types of the protein used, as well as from the experimental conditions (see **section 2.4.3**). Note that the zeta-potentials, which are measured in diluted protein solutions (here at 1 g/L) can differ from the

values for more concentrated solutions; nevertheless, they can be close enough to give useful indications about the protein charge.

The zeta potential is an overall mean average, thus, for the **cruciferin-napin mix** (green curve), the overall effective charge is dominated by the cruciferin contribution. Cruciferin and cruciferin-napin mix present, in general, a similar zeta-potential tendency in the studied pH range. The mix is slightly shifted towards the positive values and its isoelectric point was found at **pH 4.7** (to compare with 3.8 for cruciferin alone). These features likely result from the contribution of napin, which is much more charged.

To sum up, napin is rather highly stable in pH between 3 and 5, having positive charge up to its IEP at pH 9.8, while cruciferin is comparatively less stable at pH between 3 and 9, with the lowest charge at pH 3.8. At the isoelectric point, proteins are the most unstable and can tend to coagulate or flocculate (some kinds of aggregation), when in larger concentrations.

It is also important to notice, that in a large pH range (from ~4 to 10), cruciferin and napin possess opposite net charges, which means that electrostatic attractive interactions may induce additional association of the two proteins.

3.1.3.2. Small-Angle X-Ray Scattering

SAXS was used to probe the effect of the pH on the unfolding of the cruciferin-napin mix in solutions. SAXS spectra and their Kratky plots of the proteins at pH values from 11 to 3 are shown in **Figure 3.6a-b**, respectively.

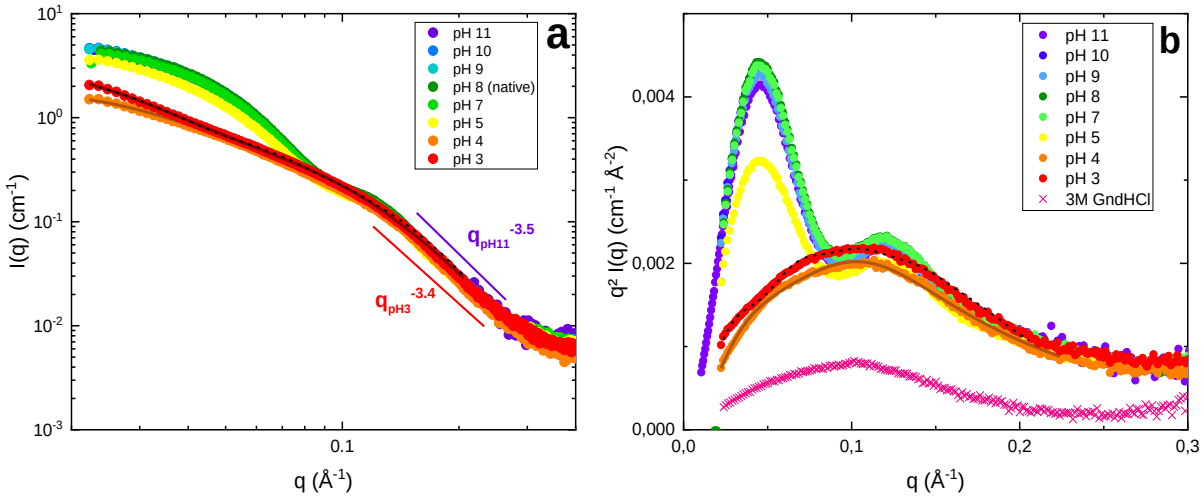

Figure 3.6 SAXS of solutions of the mix cruciferin-napin in a function of pH (100 g/L). **a)** $I(q)\ vs\ q$ **b)** Kratky representations $q^2I(q)\ vs\ q$ of the same data. The curve (pink stars), representing the 3M GndHCl protein solution, exhibits lower intensity due to lower contrast of protein in 3M GndHCl[3].

No evident difference was observed for the proteins at pH between 11 and 7: all the Kratky curves are bell-shaped, representing native-like conformations. Below pH 5, a stronger decrease of the scattering intensity was evident, due to hydration after unfolding, or to lower solubility of protein, which was visually apparent from the phase separation of the protein solution. Going into more detail, we can see that intensities from **Figure 3.6a** extrapolated[4] to $q\rightarrow0$ are varying with the pH of the protein solution (see **Figure 3.7**), decreasing moderately from pH 10 to pH 5 and then much more (by factor 2) for pH 4; pH 11 was an exception without the highest value. Those results can indicate the differences in hydration of proteins depending on the solution pH.

[4] Extrapolations to $q\rightarrow0$ were obtained from rather high q values. The intensities are thus not the most accurate values of $I(q \rightarrow 0)$.

From the Kratky plots (**Figure 3.6b**), no evident difference can be distinguished for the spectra at pH between 11 and 7: they are all bell-shape curves, representing folded conformations. For pH 5 (yellow curve), the toroid oscillations intensity decreased, and for pH 4 (orange curve) and 3 (orange curve), they vanished, together with a visible widening of the Kratky plot maximum. This indicates the unfolding, induced by the low pH through exposure of ionizable residues to the solvent. At pH 3 (red curve), precipitation/aggregation started to occur, with some increase of the low q upturn. Compared to the denaturation by guanidinium chloride (**Figure 3.6b**, pink star curve), here, the proteins appeared to stay still globally more compact, as if some parts of the protein (or its dissociated units) retained a folded nature, like in a molten-globule state[18]. The Guinier analysis gave R_g of 46 Å for pH 4 sample, confirming an increase in size with the unfolding and possible aggregation. This value is close to R_g of 48 Å, obtained for the 6M GndHCl sample.

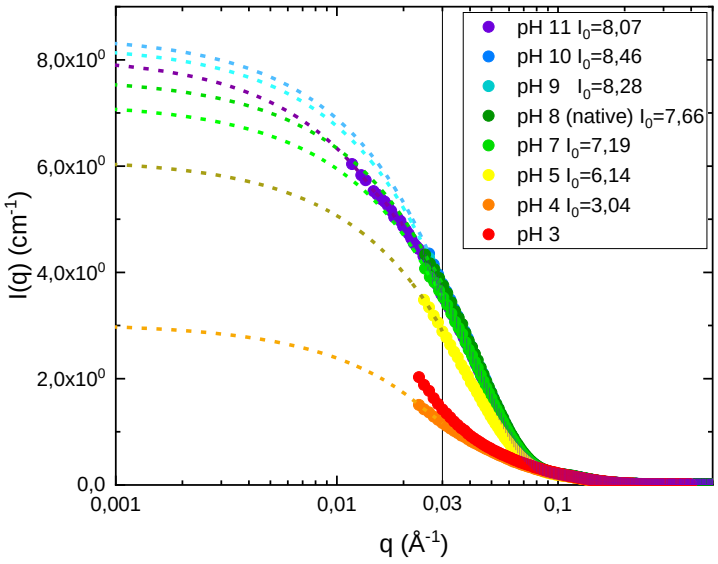

Figure 3.7 $I(q)$ *vs* $log\ q$ for canola protein solutions (100 g/L), in a function of pH, from 11 (purple) to 3 (red). The dashed lines are linearly extrapolated SAXS curves from q < 0.03 Å $^{-1}$. The legend shows the extrapolations to $q \rightarrow 0$.

3.1.3.3. UV-absorbance and fluorescence

The spectral properties of a protein are very sensitive to the pH changes since they influence the molecular environment and the mobility of the protein's chromophores (aromatic rings of Trp, Tyr, Phe (with absorption maxima at 275-290 nm) and His (225-240 nm), peptide bonds (190 nm) and disulfide bridges (250-260 nm).

When decreasing the pH of solutions of mixture cruciferin-napin from 10 to 3, we observed a general decrease of the absorbance, being consistent with the lower solubilization of proteins at higher pH values

Between pH 2 and 4, and also between pH 6 and 8, we noticed, however, a more pronounced decrease in the absorbance, while at pH 10, its level was the highest but described by an enlargement of the signal towards lower wavelengths (blue shift), similar to the one observes for pH 2-4. These spectral features can possibly indicate some precipitation of the protein molecules close to IEP, which, by looking back at our zeta-potential measurements, is indeed expected around pH ~ 4 (for cruciferin) and 10 (for napin).

On the corresponding emission spectra (**Figure 3.8a**), we distinguish the same spectral tendency as a function of pH, with an apparent decrease in the signal and a higher intensity blue edge of the spectra at pH 2-4. These features are likely related to lower polarity of the acid solvent. Here, two subpopulations can exist in solution: i) unfolded, not aggregated states, in which the formerly solvent-accessible chromophores at the folded protein surface, became more buried in less polar environment, and ii) aggregates formed by some unfolded structures, which contribute to burial of Trp residues and so the signal decrease. The observed emission feature on the blue edge can arise from Tyr emission ~305 nm in unfolded states or elastic scattering caused by the aggregation.

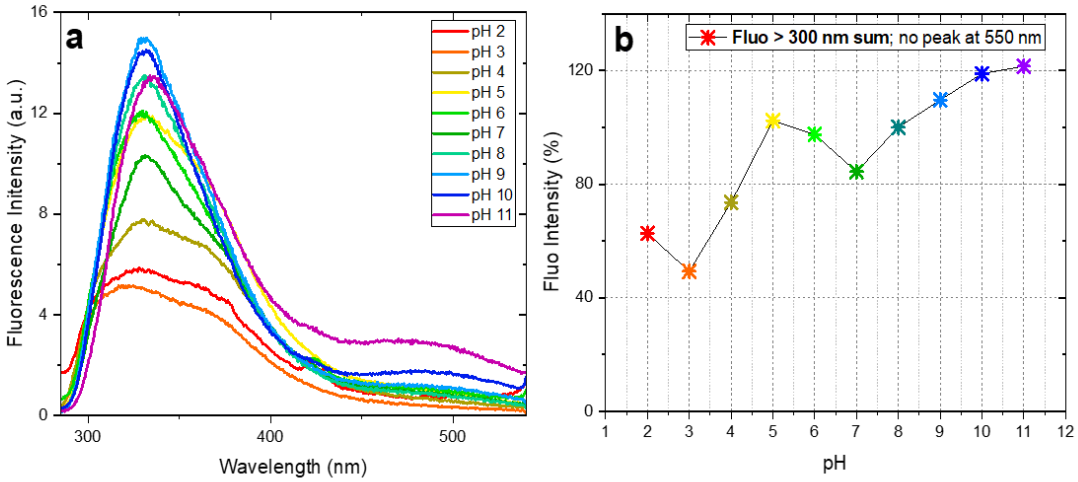

Figure 3.8 a) Fluorescence spectra of canola proteins solutions (1g/L) at pH from 2 (red) to 11 (purple); **b)** percentage of fluorescence intensity sum from the spectra in a function of pH from 2 to 11 (same colors as in **a**); the 550 nm peak was excluded from the sum.

The blue shift spectral effect of acid pH is distinct from the effect of the chemical denaturants, which, by being polar solvents, triggered red shift of emission spectra, from λ_{max} of ~330 nm to 356 nm for GndHCl (**Figure 3.9**). This is close to the value expected for fully accessible Trp (350 nm)[19]. We deduce therefore that Trp fluorescence maximum around 340 nm corresponds to folded protein states, and its red shift occurs upon chemical unfolding, rendering the exposure of Trp residues from the less-polar interior of the protein to the polar solvent and their more or less full solvation. The shape of the emission spectrum of the GndHCl-induced unfolded states is more uniform compared to the pH 3 sample, revealing no aggregation induced by GndHCl denaturation.

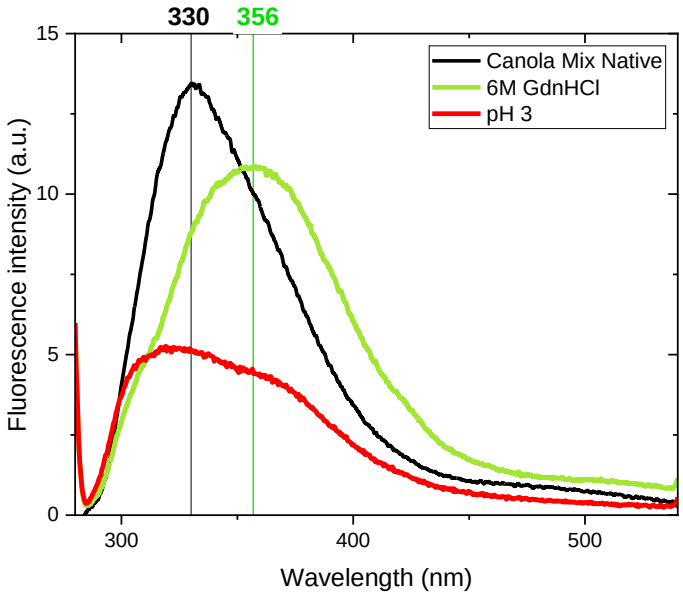

Figure 3.9 Fluorescence emission spectra for canola protein mix solutions (1g/L): native pH ~8 (black), at pH 3 (red) and in 6 M GndHCl solution (green).

In conclusion of all these measurements as function of pH, the SAXS studies of cruciferin-dominated solutions revealed major conformational changes occurring at acidic pH, nevertheless resulting in not fully unfolded structures. Determination of the isoelectric point of cruciferin around pH 4 shed light on the origin of these changes, favoring precipitation of proteins at the IEP and formation of insoluble aggregates, which was confirmed by spectrophotometry. On the other hand, strong chemical denaturation provoked an unfolding of proteins to extended conformations, with an evident increase in the radius of gyration.

3.2. Influence of temperature on canola protein mixtures

Influence of temperature on the canola protein mixture in solution was monitored using rheometry and Wide-Angle X-ray Scattering (WAXS). It is interesting and useful to understand the formation of the gels.

3.2.1. X-ray scattering

SAXS. During the heat treatment, protein molecules can experience some unfolding alterations and dissociation of their conformation. **Figure 3.10** summarizes beautifully the particularly neat temperature-triggered changes in the initially "natively" folded cruciferin-dominated structures, starting from 25°C and finishing at 95°C. Following the $q^2I\ vs\ q$ curves from the initial spectrum (navy blue curve), we can tell that the proteins experience a progressive unfolding upon the temperature increase, with a disappearance of the well-defined double oscillation at q below 0.2 Å^{-1}, coming from the hollow cylinder form factor (marked by the red frame in **Figure 3.10a** and highlighted on the Kratky plot in **Figure 3.10b**). The heat-treatment resulted in transformation of proteins into more elongated conformations, finally reaching a $I(q) \sim q^{-2}$ behaviour of a completely unfolded structure (dark red curve). Finally, we obtain the dark brown curve at 95°C suggesting a smaller R_g, with a slight maximum. This may come from sub-units dissociated at high temperature, and only partially unfolded.

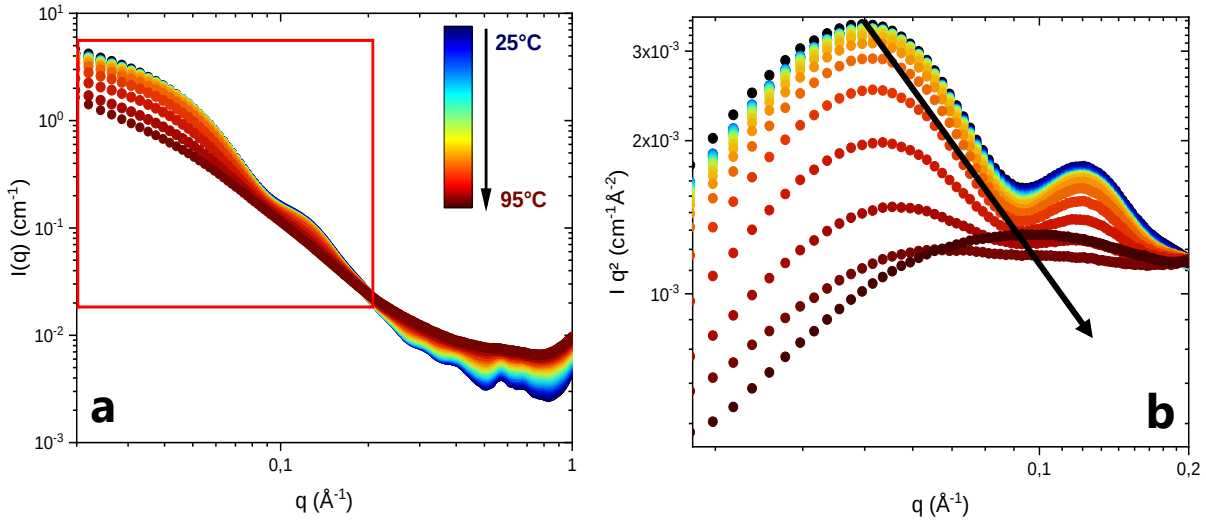

Figure 3.10 An evolution of the synchrotron X-ray scattering of a canola protein solution (at pH native ~8) upon a fast temperature increase (by 5°C/min from 20°C to 95°C). Both graphs are presented on logarithmic scale; **a)** $I(q)\ vs\ q$. **b)** Kratky representation, $q^2I(q)\ vs\ q$. The colors indicate the temperature: from navy blue (25°C) to brown (95°C).

WAXS. Most of the structural information in the WAXS data appears in the form of low intensity correlation peaks above 0.2 $Å^{-1}$ (see **Figure 3.11**). The q values of maximum intensity positions correspond to correlation (mean nearest-neighbor) distances between and/or within the protein structure ($d \approx 2\pi/q$), like the intramolecular structure: the protein subunits (0.15 - 0.25 $Å^{-1}$), the secondary structures, e.g. α helices or β-sheets (0.25 - 0.6 $Å^{-1}$) and interatomic correlations (> 0.6 $Å^{-1}$)[20,21]. Indeed, in the native WAXS signal of the mix solution, we distinguish 4 relatively visible oscillations (at q of 0.31, 0.4, 0.52, 0.7, and a small one ~0.8 $Å^{-1}$). Before observing the effect of heating, let us first try to use a model for their description.

We made such attempt on a similar basis as the evaluation of SAXS data with PDB structures by CRYSOL (paragraph 3.1.1): we have compared the WAXS curve to the one generated by the WAXSiS[22,23] software (**Figure 3.11**, black and red curve, respectively). WAXSiS calculates a histogram of the lengths of all interatomic vectors in the protein from atomic coordinate set, based on explicit solvent MD simulations[5].

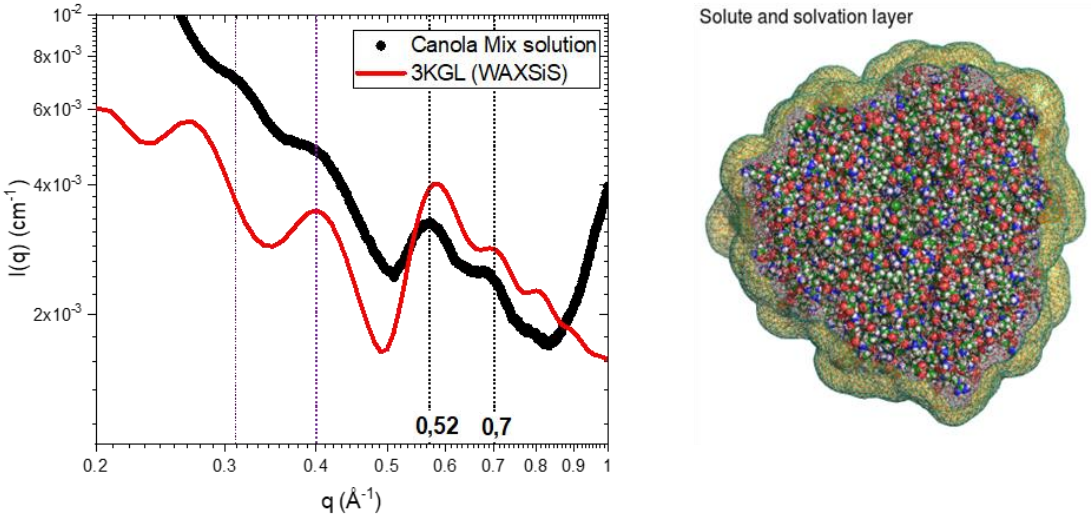

Figure 3.11 WAXS profile for the native cruciferin-dominated solution (100g/L, black curve). The red line is the 3KGL cruciferin structure from PDB and its molecular representation, with hydration layer (left hand side), computed from the molecular dynamic simulation by WAXSiS software.

[5] In contrast to Crysol, WAXSiS does not fit the parameters of the solvent (density of hydration shell, excluded volume) and it includes thermal fluctuations for the protein atoms, giving likely more precise results, especially in larger q.

Apart from the differences in the scattering intensity levels of the oscillations (which could be due to lower contrast and attenuation by the napin's signal), their maxima appearing at **0.4, 0.52** and **0.7 Å^{-1}** are coherent with the 3KGL PDB structure of cruciferin. The upturn at very high *q* of the WAXS data comes from the uncertainty of the subtraction of the buffer signal. The position of the oscillation found at **0.31 Å^{-1}** is shifted in relation to the one at 0.25 Å^{-1} for 3KGL. Together with the oscillation at 0.4 Å^{-1}, they can be attributed to the sub-maxima of the cruciferin's form factor/subunits. The maxima positions at 0.52 and 0.7 Å^{-1} correspond to 12.1 Å and 9.1 Å and, based on these characteristic lengths, their origin could be related to different secondary structures[20,21,24] with interactions between the helices (~12 Å) and β-sheets (precisely 9.08 Å)[25].

Effect of heat treatment. During the heat treatment, a progressive disappearance of WAXS oscillations was clearly observed (see **Figure 3.12**). It could be read as a transformation of the secondary structures, likely an unfolding of α-helices, with their stronger signal flattening from ~ 54°C.

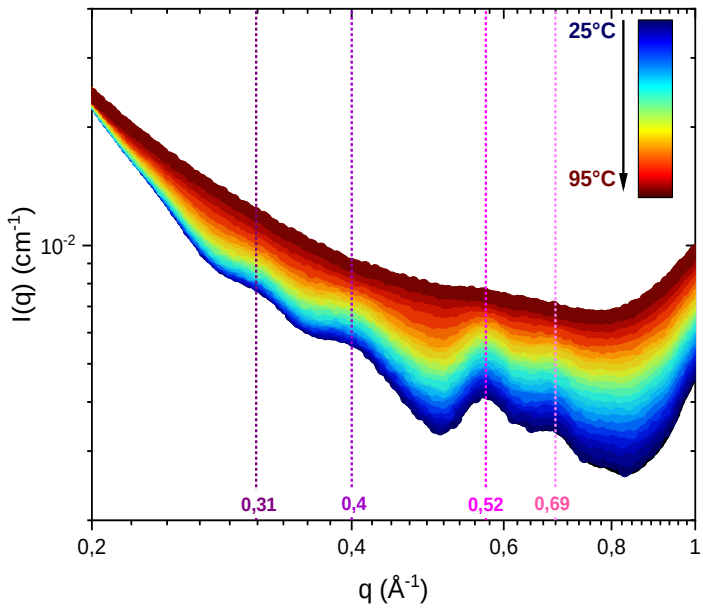

Figure 3.12 X-ray scattering curves of canola protein solution upon temperature increase from 25°C to 95 °C. Same data as in **Figure 3.10a** in a *q* range above 0.2 Å^{-1}. The lines indicate the *q* positions of the low intensity peaks.

These results correspond well to the data obtained from far-UV Circular Dichroism spectroscopy by following the ellipticity at 222 nm in a function of temperature from 25 to 95°C (not shown). The absorbance at this wavelength comes from the α-helix content and can be used to monitor thermal melting of proteins[26]. We observed a gradual decrease in ellipticity, with some pronounced decay around 56°C, suggesting some structural alterations, with likely an onset of unfolding and loss of secondary structures. A stronger decrease was observed above 70ºC, with melting temperature estimated for 74 ºC, i.e. temperature at which proteins became denatured.

3.2.2. Rheology

Temperature dependence. The rheological behaviors of canola protein solutions were monitored to investigate the establishment of interactions among proteins under heating (leading to a gel eventually). We have chosen to compare the native (pH 8) solution and the pH 11 solution, which showed distinct behavior. **Figure 3.14** shows the temperature dependence of storage modulus *G'* (stiffness, elasticity) and loss modulus *G''* (dissipated energy, viscous response)[27] of those two samples.

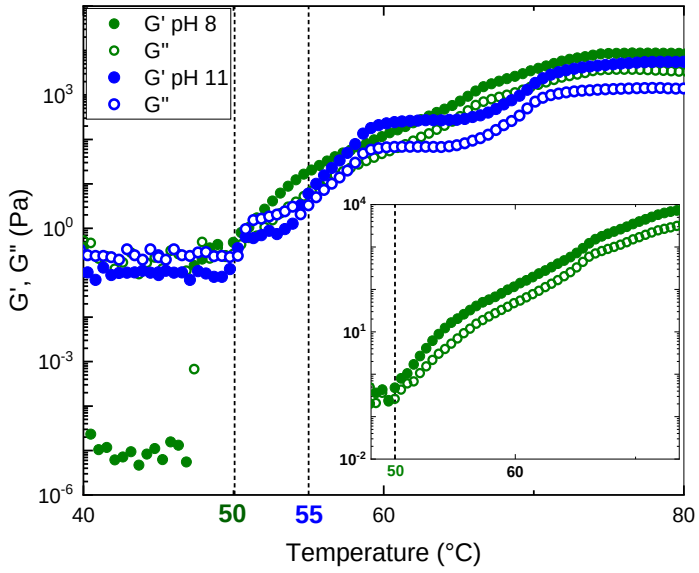

Figure 3.14 Elastic *G'* (closed circles) and viscous *G''* (open circles) moduli dependence on the temperature, here shown from 40 to 80 °C, for pH 8 (green symbols) and pH 11 sample (blue symbols); at angular frequency of 6.28 rad.s^{-1} (1 Hz). The dashed lines point out the *G'*-*G''* crossover temperatures, corresponding to the two gels. Inset: enlarged plot for the pH 8 gel.

The temperature at the crossover point of G' and G'' curves (6.28 rad.s^{-1}) was characterized as an approximate value of T for the sol-gel transition, i.e. a gelation temperature. The crossover points were observed when increasing temperature, around 50°C for pH 8 and 55°C for pH 11 sample, suggesting the transition from liquid to solid-like behaviors, taking place when heating the protein solutions. Due to the gradual unfolding of the proteins (even minimal), their reactive sites could start to interact and be progressively incorporated into the network, increasing the number of crosslinks and, consequently, resulting in the gels with certain elasticity (G').

For the pH 11 sample, the increase of G' seemed to progress in a few steps rather than steadily (as for the pH 8 sample), suggesting a more difficult unfolding of the proteins or some different mechanism of the crosslink formation.

Frequency dependence. Finally, for the two resulting heat-set gels, the solid-like behavior, with G' predominating G'' ($tan\ \delta = G''/G' < 1$), was true in the whole range of the tested angular frequency ω. For pH 8 gel, G' at chosen frequency of 1.15 rad.s^{-1} reached 1518 Pa, being over 10 times greater than the corresponding viscous modulus G''. This describes relatively strong network. Heating the solution at pH 11 resulted in a gel with higher elastic modulus (precisely by 187 Pa at 1.15 rad.s^{-1}) and less frequency dependence, compared the one formed at pH 8.

The mechanical properties of mixed protein gels depend on how the proteins interact with each other during gelation and it can be influenced by the electrostatic interactions in the system (pH), resulting in different types of aggregates, even if the proteins were mixed homogeneously before aggregation. Indeed, in a study on whey protein gels, an increase of the pH above the zero-charge pointed towards the fact that the proteins negative charge induced an increase of the gel's strength[28]. Here, at pH 11, both cruciferin and napin are above their IEP values, which could potentially explain the higher moduli of this gel. This is also consistent with literature cited in chapter 1, reporting that canola protein gels prepared at alkaline conditions have higher G' compared to the gels prepared at lower pH[29,30].

From the visual observations, both gels were opaque and appeared to be homogenous. However, they slightly differed from each other in color and texture properties, with the pH 11 gel being brighter (thus scattering more light), and more rubbery in touch. The lower modulus of the pH 8 gel, compared to the pH 11 one, could suggest a correlation of G' to the size of aggregates. However, it could be also due to a different crosslinking between proteins, resulting from differences in interactions as a function of ionic strength.

The initial G', G'' versus angular frequency ω curves of the two gels (shown later, in **section 4.1**) presented a viscoelastic behavior with both G' and G'' moduli being stable in the range from 0.5 to 10 rad.s^{-1}, with the moduli increase at higher ω, and with G'' being more frequency-dependent ($tan\ \delta$ increase from 0.1 to 0.14). Such behavior can be explained by fully crosslinked network, with relatively strong connectivity above a certain threshold in size, corresponding to the mesh size of the whole network. There exists shorter relaxation times internal to the mesh at higher frequencies[31]. Such an increase at larger frequencies (similarly to the well-known profile for polymer solutions) was also reported in literature, e.g. for BSA gels[32].

3.3. Structure of canola gels measured by SANS

In a previous work, we have observed that the Small-Angle Neutron Scattering (SANS) profiles of cruciferin-napin mix gels prepared at pH 6 and 9 were similar[33], very close to the one prepared from the "native" solution at pH~8. Hence, because the access to synchrotron or neutron beams is rare and limited, we have chosen only the pH 8 and the pH 11 samples, as model gels, for further digestion studies. We previously discussed their differences, in their rheological properties and charge features. We now describe their structure.

The SANS curves of the two chosen pH (8 and 11) gels (**Figure 3.13**) are characterized by a strong upturn from around 0.02 Å^{-1} towards lower q values, indicating attractive inter-particle interactions, characteristic for strongly aggregated,

gelled sample. Such feature was not observed for the native protein solutions. This signal upturn continues also for lower *q* values, which are not shown on this figure.

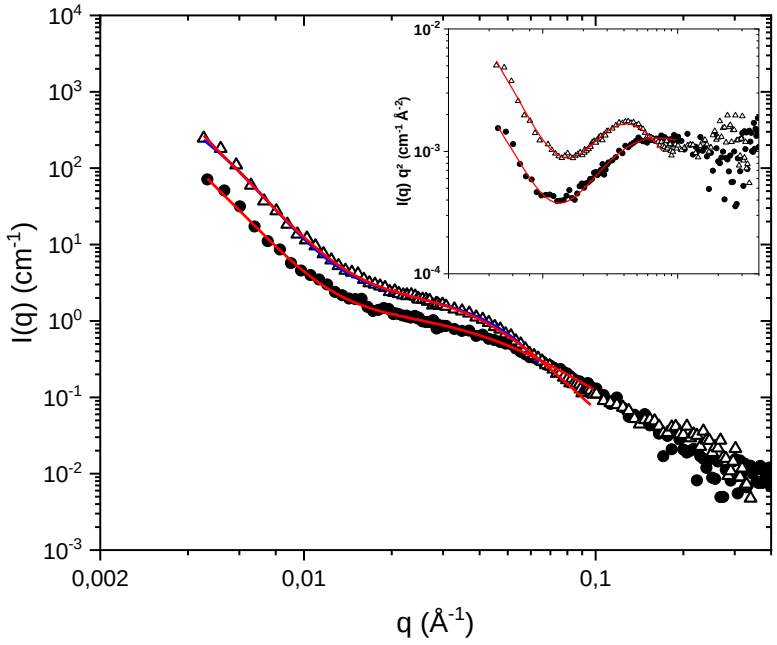

Figure 3.13 Small-Angle Neutron Scattering of canola protein gels prepared at pH 8 (closed circles) and at pH 11 (open triangles). Solid lines represent the best fits to a two Lorentzian function[34]. Inset: Kratky representations of same data. (Figure of reference[35]).

The local slopes indicate characteristic compactness/density of the gel structural components, as explained in a previous paragraph with the Porod law for high *q*. For low scattering angles, the power law exponent close to -4, as in the case of both obtained gels can result from i) dense packing of the aggregates with well-defined interfaces, thus representing compact objects with sharp interfaces (as in **Figure 3.14**), or from ii) strong sample heterogeneity of a microphase separation between regions poor and rich in proteins.

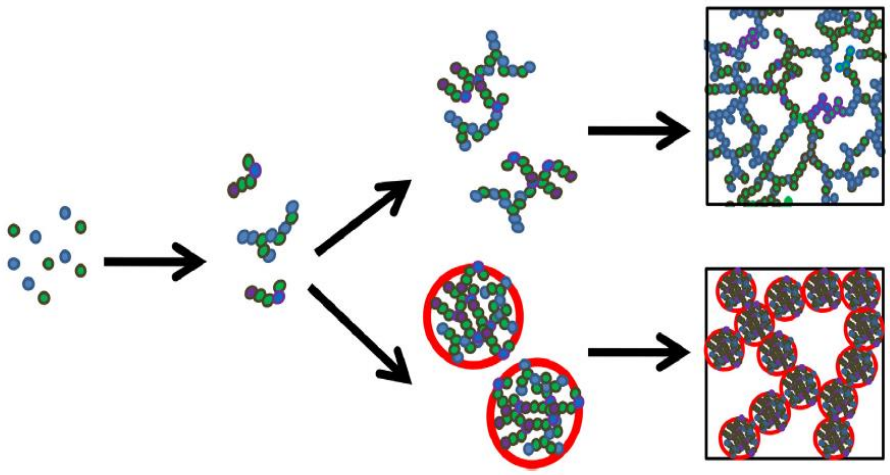

Figure 3.14 A schematic representation of globular protein aggregation and formation of fine-stranded network or particulate network (via microphase separated microgels, marked by red circles). From Nicolaï et al.[36].

The gels prepared at pH 8 and at pH 11 exhibit several differences, which can be seen directly on the curves, and more precisely from the parameters obtained from the spectra fits with a two-Lorentzian function (**Equation 2.8**, **Chapter 2**). First of all, the low q signal contribution is higher for the pH 11 gel, which, in agreement with higher elastic modulus, can be a sign of a stronger (more aggregates and crosslinked) gel. It is however not possible to distinguish whether it is due to bigger aggregate fraction or to their bigger size, since the two quantities contribute to the scale factor of the power law. The sizes of the aggregates for these two gels will be discuss in chapter 5.

Here, at higher scattering angles (>0.035 $Å^{-1}$), we observe a $q^{-3.7}$ decay (close to Porod law[37]) for pH 11 and a slower $q^{-2.5}$ decay for the pH 8 gel. This tells us that the proteins constituting the gel prepared at alkaline pH retained more compact conformations (spheres with sharp interfaces with the surrounding solvent), compared to the pre-unfolded proteins at pH 8.

Zetametry results can explain those different conformations: indeed, the proteins at pH 11 could be better stabilized by repulsive forces between the negatively charged proteins, counter-balancing the hydrophobic interactions induced by the temperature and preventing from their complete unfolding.

The Kratky plot (inset of **Figure 3.13**) for the pH 11 gel does not resemble, however, an ideal bell-shape, as for completely folded objects. We assume that the proteins are rather in intermediate situation, with non-native level of compactness. On the pH 8 gel curve, the cruciferin's form factor oscillation is much less visible, indicating more unfolded proteins in this gel. At this pH, cruciferin and napin carry opposite electric charges, which can give additional attractive interaction during gelation and influence the structures unfolding. Neither in this case, does the $q^2I(q)\ vs\ q$ show a full plateau at high q, indicating that proteins of the pH 8 network partly retained some levels of compactness.

With very different values of exponents for the two networks proteins (2.5 and 4), their ξ[6] values are only marginally different, i.e. 24 Å for the pH 8 and 25 Å for the pH 11 gel. This could mean that the structures of the pH 8 gel are composed of separated protein units, while the ones of the pH 11 gel - of a few of them.

The gel formation could be induced by the proteins aggregation and further crosslinking even without undergoing much unfolding (like in pH 11 sample), or otherwise by aggregation with more reactive sites of unfolded protein (in pH 8 sample). The resulting gel structures are convolutions of the temperature induced hydrophobic effect and the effect of solvation/electrostatic interactions, controlled by the preparation pH.

[6] We found **ξ =** 24 Å, close to $R_{g0}/\sqrt{3}$, ***R*****$_{g0}$** = 39 Å, being the radius of gyration of native cruciferin. Let us make a simplistic analogy with a polymer solution. With a mass of cruciferin M_0 = 300 kDa and a native R_{g0} = 39 Å, the overlapping concentration between two proteins $c^* = M_0/N_{av} \,/\, \left(\frac{4\pi}{3}\ R_{g0}^3\right)$ is about 2g/cm^3. In the gel at 0.1g/cm^3, cruciferin is well below ***c****. Even if proteins are connected to each other in the gel, we use a solution-like description: the elementary meshes of the gel scatter as non-overlapping entities containing one protein, like end-linked chains in a gel following the c* theorem [ref. De Gennes, P.G. (1979). *Scaling concepts in Polymer physics*. Cornell Univ. Press].

Summary

We characterized the conformations of canola proteins (napin and cruciferin) separately and in the protein mix in "native" solutions (~ pH 8) by SAXS, distinguishing the ellipsoidal shape of napin and the hollow cylindrical shape of cruciferin.

We then monitored the changes in the shapes and sizes of those protein structures under chemical denaturation, provoking the unfolding of the proteins to extended conformations, with evident increase in size, and also revealing the relative resistance of the proteins towards complete denaturation, especially for the small napin. We further compared the effect of the denaturant-induced unfolding to the effect of pH on the cruciferin-dominated mix solution. The measurements as a function of pH revealed major conformational changes occurring at acidic pH (pH 3 and 4), however resulting in not fully unfolded structures (less than after treatment with the chemical denaturant). Determination of the isoelectric points of the proteins, with IEP of cruciferin around pH 4, shed light on the origin of these changes, favoring precipitation of proteins at this IEP point and formation of insoluble aggregates, which was confirmed by spectrophotometric measurements. Some minor but present differences were also observed for the protein solutions at pH between 7 and 11. Those effects could influence the formation of different structures during temperature gelation.

Through temperature-induced changes in the protein structures, we distinguished different levels of unfolding and aggregation between the gels formed at pH 8 and pH 11. The pH 11 gel was characterized by compactly folded protein conformations, higher level of aggregation and higher elastic modulus. We perceive that the temperature alone could lead to unfolding of certain regions of proteins, keeping the others in their native-like conformations (pH 11 gel), while the stronger interplay between the pH and temperature could induce more unfolded states (pH 8 gel).

References

[1] Svergun, D.I., Barberato, C. & Koch, M.H.J. (1995). CRYSOL - a Program to Evaluate X-ray Solution Scattering of Biological Macromolecules from Atomic Coordinates. *Journal of Applied Crystallography,* 28, 768-773. doi: 10.1107/S0021889895007047.

[2] Guinier, A. and Fournet, G. (1955). Small-Angle Scattering of X-Rays. Wiley-VCH Verlag GmbH & Co., New York.

[3] Gräwert, T.W., Svergun, D.I. (2020). Structural Modeling Using Solution Small-Angle X-ray Scattering (SAXS). *Journal of Molecular Biology*, 432, 3078–3092.

[4] SasView. Hollow Cylinder model. https://www.sasview.org/docs/user/models/hollow_cylinder.html.

[5] SasView. Ellypsoid model. https://www.sasview.org/docs/user/models/ellipsoid.html.

[6] Schwenke, K.D., Drescher,B., Zirwer, D., Raab, B. (1998). Structural Studies on the Native and Chemically Modified Low-Molecular Mass Basic Storage Protein (Napin) from Rapeseed (Brassica napusL.). *Biochemie und Physiologie der Pflanzen*, 183, (2–3) 219-224. doi: 10.1016/S0015-3796(88)80104-5.

[7] Wanasundara, J.P.D., McIntosh, T.C., Perera, S.P., Thushan, S. Withana-Gamage, T.S. & Mitra, P. (2016). Canola/rapeseed protein-functionality and nutrition. *OCL-Oilseeds and fats, Crops and Lipids*, 23 (4) D407. doi: 10.1051/ocl/2016028.

[8] Ciccariello, S., Goodisman, J., Brumberger, H. (1988). On the Porod law. *J. Appl. Crystallography,* 21, 117-128. doi: 10.1107/S0021889887010409.

[9] Hammouda, B. (1993). SANS from Homogeneous Polymer Mixtures: A Unified Overview. *Advances in Polymer Science*. SpringerVerlag, 86–133. doi: 10.1007/bfb0025862.

[10] Arakawa, T., Prestrelski, S.J., Kenney, W.C., Carpenter, J.F. (2001). Factors affecting short-term and long-term stabilities of proteins. *Advanced Drug Delivery Reviews*, 1, 46 (1-3), 307-26. doi: 10.1016/s0169-409x(00)00144-7.

[11] Monsalve, R.I., Rodriguez, R. (1990). Purification and Characterization of Proteins from the 2S Fraction from Seeds of the Brassicaceae Family. *Journal of Experimental Botany*, 41 (1), 89–94. doi:10.1093/jxb/41.1.89.

[12] Lönnerdal, B., Janson, J.C. (1972). Studies on Brassica seed proteins: I. The low molecular weight proteins in rapeseed. Isolation and characterization. *Biochimica et Biophysica Acta - Protein Structure*, 278 (1), 175-183.

[13] UniProt. P24565, 2SSI_BRANA. https://www.uniprot.org/uniprotkb/P24565/entry.

[14] The UniProt Consortium, UniProt: the Universal Protein Knowledgebase. (2023). *Nucleic Acids Research*, 51 (D1), D523–D531. doi: 10.1093/nar/gkac1052.

[15] Wanasundara, J.P.D., Tan, S., Alashi, A.M., Pudel, F., and Blanchard, C. (2017). Proteins from canola/rapeseed: Current status. In: *Sustainable protein sources*. Nadathur, S.R., Wanasundara, J.P.D., and Scanlin, L., Ed., 285–304. London: Academic Press.

[16] UniProt. P11090, CRUA_BRANA. https://www.uniprot.org/uniprotkb/P11090/entry.

[17] Pedroche, J., Yust, M.M., Lqari, H., Girón-Calle, J., Alaiz, M., Vioque, J., & Millán, F. (2004). Brassica carinata protein isolates: Chemical composition, protein characterization and improvement of functional properties by protein hydrolysis. *Food Chemistry*, 88, 337–346. doi: 10.1016/j.foodchem.2004.01.045.

[18] Ohgushi, M., Wada, A. (1983). 'Molten-globule state': a compact form of globular proteins with mobile side-chains. *FEBS Lett.*, 28, 164 (1), 21-4. doi: 10.1016/0014-5793(83)80010-6.

[19] Duy, C., Fitter, J. (2006). How aggregation and conformational scrambling of unfolded states govern fluorescence emission spectra. *Biophys. Journal,* 15, 90(10), 3704-11. doi: 10.1529/biophysj.105.078980.

[20] Hirai, M., Iwase, H., Hayakawa, T., Miura, K. & Inoue, K. (2002). Structural hierarchy of several proteins observed by wide-angle solution scattering. *J. Synchrotron Radiat.,* 9, 202–205.

[21] Makowski, L. et al. (2008). Molecular crowding inhibits intramolecular breathing motions in proteins. *J. Mol. Biol.*, 375, 529–546.

[22] Po-chia, Ch. & Hub, J.S. (2014). Validating solution ensembles from molecular dynamics simulations by wide-angle X-ray scattering data. *Biophys. J.*, 107, 435-447.

[23] Knight, C. J. & Hub, J. S. (2015). WAXSiS: a web server for the calculation of SAXS/WAXS curves based on explicit-solvent molecular dynamics. *Nucleic Acids Res.*, 43, W225-W230.

[24] Phan-Xuan, T., Bogdanova, E., Millqvist Fureby, A., Fransson, J., Terry, A.E., Kocherbitov, V. (2020). Hydration-Induced Structural Changes in the Solid State of Protein: A SAXS/WAXS Study on Lysozyme. *Molecular Pharmacy*, 8, 17 (9), 3246-3258. doi: 10.1021/acs.molpharmaceut.0c00351.

[25] Chelvanayagam, G., Knecht, L., Jenny, T., Benner, S., Gonnet, G. (1998). A combinatorial distance-constraint approach to predicting protein tertiary models from known secondary structure. *Folding and Design*, 3, 3,149-160, doi: 10.1016/S1359-0278(98)00023-6.

[26] Greenfield, N. (2006). Using circular dichroism spectra to estimate protein secondary structure. *Nature Protocols,* 1, 2876–2890. doi: 10.1038/nprot.2006.202.

[27] Mezger, T.G. (2006). The rheology handbook: for users of rotational and oscillatory rheometers. (2nd ed.). Hannover: Vincentz Network GmbH and Co KG.

[28] Van Camp, J., Huyghebaert, A. (1995). A comparative rheological study of heat and high pressure induced whey protein gels. *Food Chemistry*, 54, 357-364. doi: 10.1016/0308-8146(95)00040-P.

[29] Léger, L.W. & Arntfield, S.D. (1993). Thermal gelation of the 12S canola globulin. *Journal of the American Oil Chemists' Society*, 70, 853–861. doi: 10.1007/BF02545343.

[30] Yang, C., Wang, Y., Vasanthan, T., Chen, L. (2014). Impacts of pH and heating temperature on formation mechanisms and properties of thermally induced canola protein gels. *Food Hydrocolloids*, 40(10), 225-236. doi: 10.1016/j.foodhyd.2014.03.011.

[31] Huang, T., Tu, Z.C., Wang, H., Liu, W., Zhang, L., Zhang, Y. & ShangGuan, X. (2017). Comparison of rheological behaviors and nanostructure of bighead carp scales gelatin modified by different modification methods. *Journal of Food Science and Technology*, 5, 1256-1265. doi: 10.1007/s13197-017-2511-1.

[32] De Maria, S., Ferrari, G. & Maresca, P. (2015). Rheological Characterization Bovine Serum Albumin Gels Induced by High Hydrostatic Pressure. *Food and Nutrition Sciences*, 6, 770-779. doi:10.4236/fns.2015.69080.

[33] Pasquier, J., Brûlet, A., Boire, A., Jamme, F., Perez, J., Bizien, Th., Lutton, E., Boué, F. (2019). Monitoring food structure during digestion using small angle scattering and imaging techniques. *Colloids and Surfaces A*, 570, 96-106. doi: 10.1016/j.colsurfa.2019.02.059.

[34] SasView. Two Lorentzian model. https://www.sasview.org/docs/user/models/two_lorentzian.html.

[35] Napieraj, M., Brûlet, A., Lutton, E., Randrianarisoa, U., Boire, A., Boué, F. (2022). Monitoring food structure in plant protein gels during digestion: Rheometry and Small Angle Neutron Scattering studies. *Food structure,* 32, 100270. doi: 10.1016/j.foostr.2022.100270.

[36] Nicolaï, T., Chassenieux, Ch. (2019). Heat-induced gelation of plant globulins. *Current Opinion in Food Science*, 27, 18-22. doi: 10.1016/j.cofs.2019.04.005.

[37] Ciccariello, S., Goodisman, J., Brumberger, H. (1998). On the Porod law. *Journal of Applied Crystallography*, 21, 117-128. doi: 10.1107/S0021889887010409.

Chapter 4
Digestion of Canola Protein Gels

This chapter focuses on digestion experiments of canola protein gels, prepared at pH 8 and pH 11. We present results obtained by Small-Angle Scattering (by neutrons and X-rays), providing nanometer scale structural information, and by rheometry, allowing exploration of their macroscopic mechanical behavior.

The results will be presented in three sections:

1) Digestion of cm-size gels monitored by SANS and *in-situ* small-oscillatory rheology.

2) *In situ* digestion of gels in capillaries monitored by SAXS.

3) Changes of secondary structures during digestion observed by WAXS.

4.1. Digestion of "food size" gels: rheology and Small-Angle Neutron Scattering

In this section, the canola protein gels prepared at pH 8 and pH 11, characterized in Chapter 3, are studied under gastric and intestinal conditions (see section 2.3.1 and 2.3.2. in Chapter 2). The dimensions of the studied samples were 10 and 15 mm in diameter several mm thick for rheology, and 10 mm 1-2 mm for SANS. We consider their geometry close to the one of chewed food pieces arriving *in vivo* in the stomach.

4.1.1 *In-situ* digestion performed on the rheometer

The digestion kinetics are presented separately for the two gels in **Figure 4.1** (pH 8) and **Figure 4.3** (pH 11), which show variations of G' and G'' with angular frequency ω, during 30 min of gastric digestion and subsequent 2-hour intestinal digestion *in situ* (with 10 min interval). The solid-like nature of the two gels (i.e. $G' > G''$ at the whole ω range) was preserved throughout the whole digestion experiments of the two gels. Surprisingly, at frequencies above 50 rad.s^{-1}, G', G'' showed strong upturns with ω (**Figure A.1, Appendix 1**). These increases, which, to our knowledge, have no equivalent presented in the literature (frequency range is often limited to 10-20 rad.s^{-1}), look like the Rouse dynamics of a polymer chain (here a protein "chain"). These results are, however, difficult to explain and in the following descriptions of the G', G'' variations, we will concentrate on the ω range from 0.1 to 50 rad.s^{-1}.

4.1.1.1 Frequency variation for pH 8 gel

Figure 4.1 corresponds to the gel prepared at pH 8 with its initial state marked by black symbols. After 30 min of gastric digestion (**red symbols**), only a slight decrease of the viscoelastic moduli over the whole frequency range could be observed. Values of $tan\ \delta$ between 1 and 35 rad.s^{-1} increased similarly as for the initial gel, before digestion, from 0.1 to 0.13, suggesting an essentially unchanged internal network structure. The reduction in G' can be attributed to two phenomena occurring in parallel: i) due to low gastric pH, a weakening of the interactions (hydrogen bonds, electrostatic

forces) between proteins participating to the network, equivalent to a reduction of crosslinks density, and ii) scission of peptide bonds by pepsin, resulting in shorter protein parts and a loss of connectivity. These phenomena could also affect some large scale structures, this will be discussed later in the light of scattering measurements. The scission effect, which can be extremely efficient at long digestion durations, appears to be weak at this stage, and thus should be of rather minor extent. This demonstrates a low efficiency of gastric step and/or slow action of pepsin.

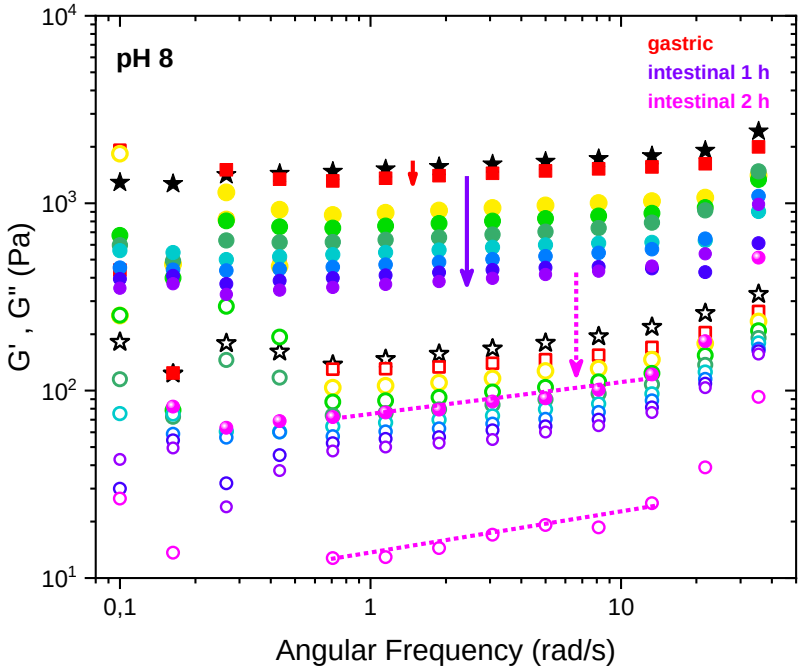

Figure 4.1 Frequency sweep tests on the canola protein gel prepared at pH 8 during the digestion process: storage moduli (*G'*, closed symbols) and loss moduli (*G''*, open symbols) as a function of oscillating frequency (0.1-50 rad.s-^{1}). The arrows indicate the direction of the digestion: 1st step – from initial gel (black) to 30 min of gastric digestion (red), 2nd step – intestinal digestion kinetics during 60 min with 10 min per sweep (t_0 – yellow, t_{60} – violet); after 2 hours of intestinal digestion (magenta).

In the **intestinal digestion step** (**yellow to violet circles**, with 10 min interval between each curve, performed in the following hour), a much stronger decrease of the moduli (compared to the gastric step) was immediately visible (by ~35% after the first 10 min). The further apparent decreasing rate was likely due to the loss of enzymatic activity, as expected from longer digestion times (see **section 2.2.3.1**). After one hour of this intestinal step (violet circles), *G'* at 1.15 rad.s^{-1} decreased from 1360

to 370 Pa (by~73%) and the frequency dependence became more pronounced (with *tan δ* rising from 0.13 to 0.19). This suggests a gradual internal deconstruction of the network, as expected with de-percolation, creating a size distribution of connected zones, and therefore a distribution of times. This trend continued for an additional hour of intestinal digestion[1], showing a substantial reduction of the moduli and a stronger angular frequency dependence of both *G'* and *G''* after the total 2-hour step (magenta curves). Interestingly, within the 10 last minutes of this step, an abrupt reduction of *G'* (from 193 Pa to 76 Pa) and an increase of *tan δ* (from 0.14 to 0.19) at 1.15 rad.s^{-1} occurred, suggesting an acceleration of the de-percolation of the gel.

Visual aspect of the samples

Visual aspect of the samples may give an additional information about the ongoing processes during the digestion. The images shown in **Figure 4.2** correspond to given kinetics curves from **Figure 4.1**: 30 min of gastric digestion (red **a**), plus intestinal digestion of 10 min (yellow **b**), 1 hour (blue **c**) and 2 hours (magenta **d**).

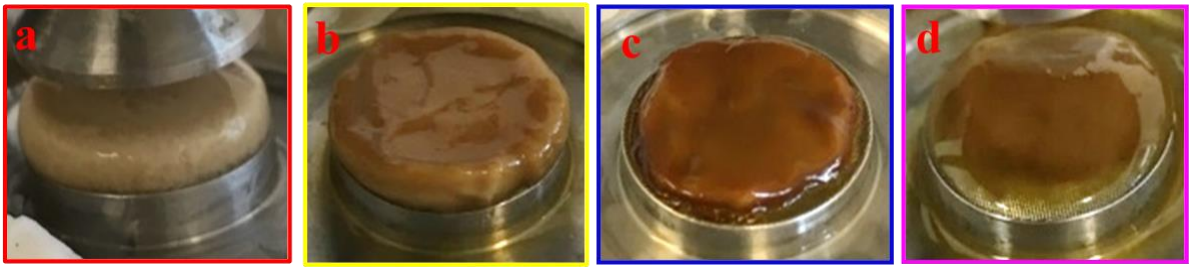

Figure 4.2 Images of canola protein pH 8 gel upon digestion: after 30 min of gastric digestion **a)**; 30 min of gastric + 10 min of intestinal digestion **b)**; 30 min of gastric + 1 h of intestinal digestion **c)**; 30 min of gastric + 2 h of intestinal digestion **d)**.

[1] The 1st hour of intestinal digestion was performed *in-vitro* (in a Falcon tube), before the digestion that was continued *in-situ* (and recorded) on the rheometer for the 2nd hour (see details in Chapter 2). All he G', G'' curves corresponding to the 2nd hour are shown in **Figure A1.2**, **Appendix 1**.

The effects of gastric digestion on the gels resulted in a slight change to lighter color (**a**), suggesting a possible aggregation induced by the gastric conditions with very acidic pH. A slight increase in the size, indicating swelling of the gel, was also observed. For the successive intestinal digestion steps, we observed progressive modifications of the gels morphology, starting from the surface dissolution by the enzymes and exhibiting pasty-like property in the first 10 min (**b**). At the same time, a gel appeared less white, possibly because of the disappearance of some large protein aggregates. After 1 h (**c**), an increased gel heterogeneity was more evident, due to a progressive appearance of regions slightly different in colors (i.e. darker center areas, with the transparent edges). After 2 h (**d**), this trend was enhanced, with the gel's edges being completely transparent: a big part of the aggregates, responsible for the whitish aspect due to scattering of light, disappeared. This step corresponds to the de-percolation of the gel – a curve marked by magenta color on **Figure 4.2**. The gel appeared definitely heterogeneous in color but also possibly in modulus. The intestinal digestion effect was likely due to the enzymatic diffusion towards the inside of the gel, but also due to some diffusion of the digestion residues towards the outside of the gel.

4.1.1.2 Frequency variation for pH 11 gel

Figure 4.3 shows the evolutions of $G'(\omega)$ and $G''(\omega)$ during digestion of the gel formed at pH 11. During 30 min of gastric digestion **(red symbols**), a surprising apparent increase of the viscoelastic moduli was observed, being opposite to the effect of gastric digestion of the pH 8 gel. This effect was observed repeatedly and we eliminated the possibility of this behavior to be due to the sample drying at 37 °C, by performing the same experiment on gels without the gastric juice, and obtaining no variations of G' and G'' moduli with time (Figure SI in ref. 1). The observed increase in elasticity of the gel during this gastric step must be therefore an effect of either pH or pepsin, or a combination of both. As described in Chapter 3 (section 3.2.2.), the pH 11 gel is initially stronger (with higher moduli and less frequency dependence) than the pH 8 gel, therefore one can expect its more difficult digestion. Moreover, the inherently

low efficiency of gastric digestion, as seen for the former gel, might be even less efficient to cope with the more crosslinked network. However, we detected here an increase of the density of crosslinks: this tells us about either some reduction of volume – not recorded, or more interactions after proteins rearrangements. Note that the network at pH 11 can be more sensitive to very low pH.

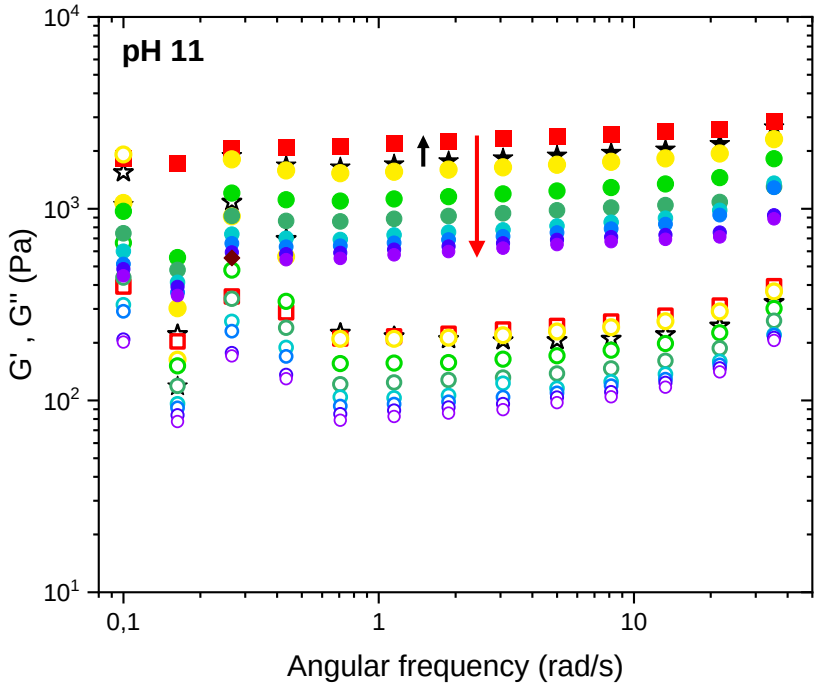

Figure 4.3 Frequency sweep tests on the canola protein gel prepared at pH 11 during the digestion process: storage moduli (*G'*, closed symbols) and loss moduli (*G"*, open symbols) as a function of oscillating frequency (0.1-50 rad/s). The arrows indicate the direction of the digestion: 1st step – from initial gel (black) to 30 min of gastric digestion (red), 2nd step – intestinal digestion kinetics during 60 min with 10 min per sweep (t_0 – yellow, t_{60} – violet). (Figure 2 from ref. 1).

During the subsequent **intestinal digestion**, we return back to a trend of the moduli decrease, similar to the one for the pH 8 gel. In the first 10 min, *G'* dropped down from 2183 to 1556 Pa (by 29%), and then continued to decrease with lower rate (similarly to a decrease for the pH 8 gel), reaching 351 Pa (decrease by 84%) at the end of the 2-hour intestinal step. This suggests a less effective digestion than for the pH 8 gel. Both storage and loss moduli were also becoming more frequency-dependent throughout this digestion time. However the final $G'(\omega)$ and $G''(\omega)$ curves for the pH 11 gel did not result in the percolation-like behavior, as it took place at the end of 2-hour

step for the pH 8 gel (see **Figure 4.5**, last point). Evidently, the pH 11 gel experienced similar intestinal digestion trend, but slowed down, compared to the pH 8 gel, which can be explained by the increased modulus before the intestinal digestion (in gastric step), or just already in initial state.

4.1.1.3 Variation of G' G'' at ω =1.15 rad.s^{-1} as a function of digestion time

We also evidenced the opposite effects of the gastric step for the two gels, and their development with time throughout a 2-hour **gastric digestion**, by plotting their viscoelastic moduli, as a function of time, at a given frequency 1.15 rad.s^{-1} (**Figure 4.4**).

For the **pH 8 gel** (circle symbols), the moduli-decreasing tendency was slow but sure, which generally slightly continued with a gradually slower rate: while after 30 min, the value of *G'* dropped by ~10%, after 2 hours, it further reduced only by ~4%, with a slight increase of *tan δ* from 0.095 to only 0.105. In overall, there was not much change in the network's strength. Compared to intestinal digestion, this effect is rather minor. **Figure 4.4** enables to see more clearly the unexpected effect of gastric digestion of the **pH 11 gel** (triangle symbols), namely the elastic response gradually increasing with digestion time. At first glance, it comes to mind that this behavior can be purely an effect of the substantial pH change (from 11 to 2), as evoked above. In fact, soaking an alkaline pH gel in acidic gastric juice could result in ionization of the negatively-charged dissociated acidic groups of AA, through binding of protons from the HCl. In such case, the electrostatic stabilization of the proteins could reduce and their subsequent unfolding could promote some attractive interactions between the exposed proteins domains. In addition, when changing the pH from 11 to 2, both the IEP of napin (9.8) and of cruciferin (3.8) was crossed, likely provoking extra interactions. This all could further lead to an additional protein aggregation (increase in aggregates size or number fraction) and result in reinforcement of the gel network (strengthening the modulus). Such an enhanced solid-like behavior was not observed for the other gel (pH 8), possibly due to its already initially more unfolded proteins.

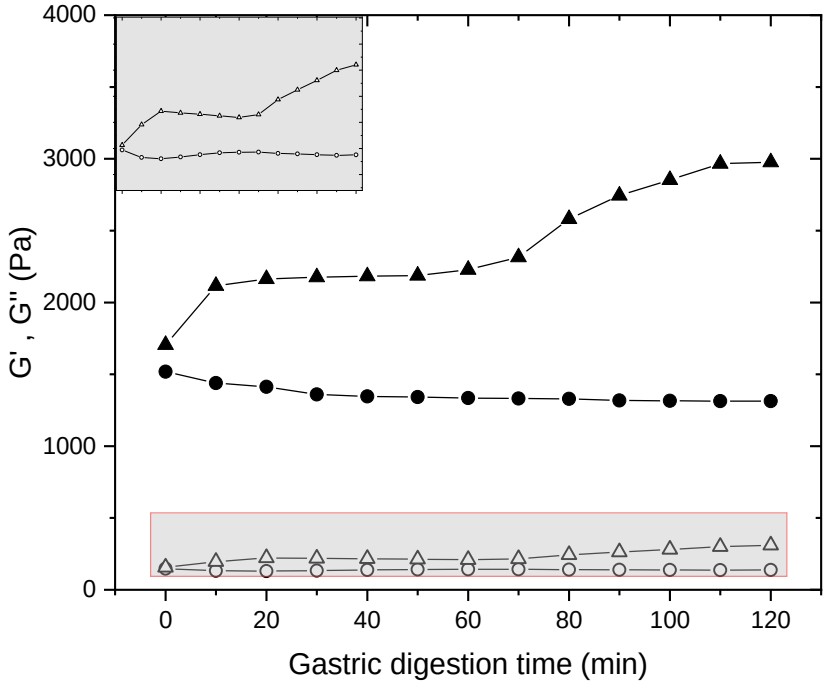

Figure 4.4 Variations of *G'* (closed symbols) and *G''* (open symbols) at 1.15 rad.s^{-1} as function of gastric digestion time. Round symbols represent the pH 8 gel and triangles – the pH 11 gel. Inset: enlargement on the variations of *G''*. (Figure 3a from ref. 1).

As control experiment, we have verified the effect of the HCl without pepsin on both gels. Indeed, it induced an increase of the elasticity, but only in the case of the pH 11 gel (not shown). This supports our former assumption of the acid-ionization effect on the gel. Nevertheless, this HCl-induced increase was immediate, with no continuous increase of the moduli with time. During gastric digestion, on the contrary, **a two-step *G'* increase** took place. The first one occurred already during 10 min (with *G'* from 1705 to 2116 Pa), followed by an hour of a very smooth rise (up to 2315 Pa). The second, more pronounced *G'* increase (up to 2976 Pa) occurred at 70 min. Such a multistep behavior could be a result of combined actions of acid pH and pepsin. The acid-induced unfolding and aggregation could be responsible for the first *G'* rise – e.g. because protons are faster to diffuse. The further increase could be caused by the ongoing processes of unfolding and enzymatic scission. Even if most proteins were at some point incorporated in the network, the enzymatic scission could progressively give rise to new reactive protein parts. They could then react with proteins of the

network and create new strands. They could also form smaller aggregates: if the connection between the aggregates contributes to the modulus, a smaller aggregate size would result in the modulus increase, following the theory of rubber elasticity. All this could happen gradually during digestion.

During the subsequent 2 hours of **intestinal digestion**, the variation of moduli looks very similar for the two pH gels (see **Figure 4.5**). In both cases, a decrease of *G'* was observed upon digestion, with two time-constants of an exponential decay, equal 6 and 77 min for pH 8 gel and 16 and 151 min for pH 11 gel, i.e. longer time for the more crosslinked pH 11 gel.

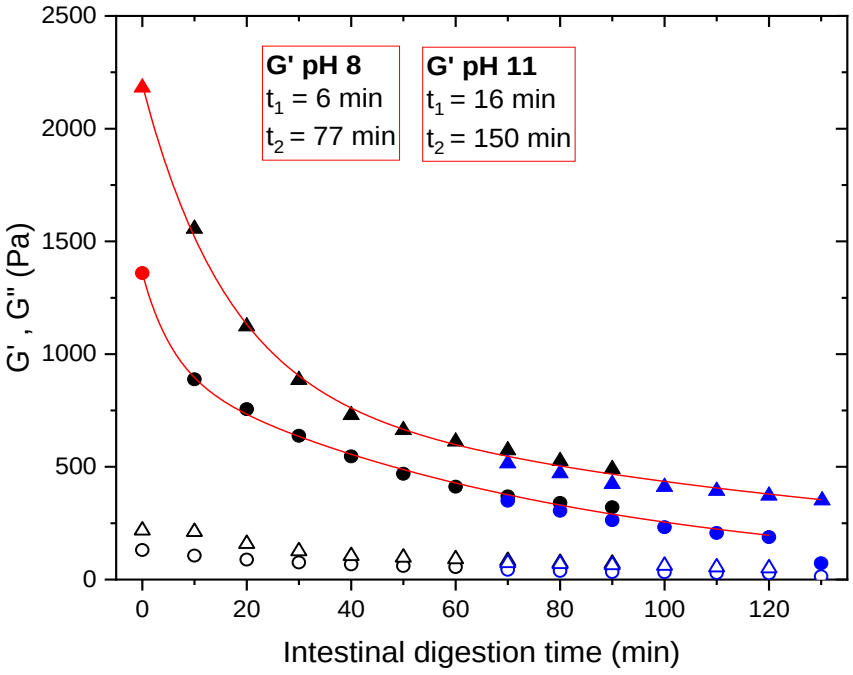

Figure 4.5 Variations of *G'* (closed symbols) and *G''* (open symbols) at frequency of 1.15 rad.s^{-1} as function of intestinal digestion time. Round symbols - pH 8 gel ; triangles - pH 11 gel. Blue symbols correspond to the gels digested for the 1st one hour *in vitro* (outside the rheometer) and continued from the 2nd hour *in situ* (on rheometer). Lines are the fits of *G'* to a double exponential decay; t_1 and t_2 are the corresponding characteristics decay times. (Figure 3b from ref. 1).

As a final remark, we wish to insist on the reproducibility of the presented results, observed when using either 2 hours *in situ* (on rheometer) or 1 hour *in vitro* (in Falcon tube, see digestion protocol in Chapter 2) plus 1 hour *in situ* (on rheometer).

In conclusion, we see that the pH of the protein solution can significantly influence the gel structure, and further influence its evolution during digestion. The specific gel structure can determine its particular moduli, which generate its specific resistance to the digestion conditions (pH, enzymes).

Summary of rheology measurements

The pH 11 gel showed greater moduli (*G*', *G*'') than the pH 8 gel, before and during the gastro-intestinal digestion.

During the gastric step, *G*' of the pH 11 gel displayed two successive increases, while *G*' for the pH 8 gel was continuously decreasing.

We perceive that the pH of the protein solution can significantly influence the gel structure, and further influence its evolutions during digestion.

4.1.2 Small-Angle Neutron Scattering

In this section, we present the SANS results of digestion of canola protein gels. We describe separately gastric and intestinal digestion and compare their effects on the pH 8 and the pH 11 gels, regarding the structural information on nanometric scale, at two distinct size ranges: the one of protein and their small aggregates (medium and large q ranges), and the one of larger protein aggregates (low q range).

In the following, the scattering intensities $I(q)$ shown in $I(q)\ vs\ q$ plots have been, for some digested samples, divided by a prefactor of 1.5 or higher. Changing the prefactor does not affect any of the curves' parameters determining the shape of the scattering objects; it was applied only to better visualize the curves on common plots. On the other hand, the Kratky representations, $q^2I(q)\ vs\ q$ (insets of $I(q)\ vs\ q$ plots) present the unchanged measured $I(q)$ values. Let us specify that the intensity level variation occurs due to a poor control of the sample volume in the neutron cell when filling it with digested gel pieces. Sometimes, the cell filling could result in squeezing of the gel pieces, which lead to its deswelling (increasing concentration and thus scattering

intensities). However, whatever was the filling of the cell, it did not affect the shape of the curve, and consequently of the local protein conformation.

All the SANS curves were fitted with the double Lorentzian function (see **section 2.4.1**, **Equation 2.8**): high *q* parameters (correlation length ξ, exponent ***n*** and scale factor ***A***) describe the conformation of proteins, and those of the low *q* range (Ξ, ***m***, ***C***), describe the large protein aggregates. The best fit parameters for the studied gels are listed in **Table 4.1**.

4.1.2.1 Gastric digestion

Figure 4.6 shows the scattering for the **pH 8 gel** in the initial state, after 30 min (red) and 2 hours (mustard) of gastric digestion. The first visible effect of the gastric digestion is a considerable reduction of the low *q* scattering intensity and a transformation of its upturn (it appears as a shift to lower *q* values). The upturn at low *q* is however, still present after the short and the long gastric digestion. Its shift towards lower values gives an impression of its reduced steepness; however, the exponent *m* remains close to 4. A decrease of the prefactor shows a reduction of the specific surface of the protein aggregates. It can be interpreted in two different ways: i) a decrease of the number of aggregates of constant size, or ii) an increase of the aggregates size (which seems unlikely in the present situation). One reason detailed above (*visual aspect of the samples*) is the decrease of the opacity of the sample, which is not likely to occur if the aggregates size increases; this will be discussed later. We hence favor an indication of a primary but not complete degradation (or coalescence) of the compact large protein aggregates. The biggest reduction of low *q* intensity occurred in the first 15 min of digestion (see **Figure A1.3**, **Appendix 1**). Then, between 30 min and 2 hours, the signal continued to decrease, however much less, suggesting a slower rate of digestion.

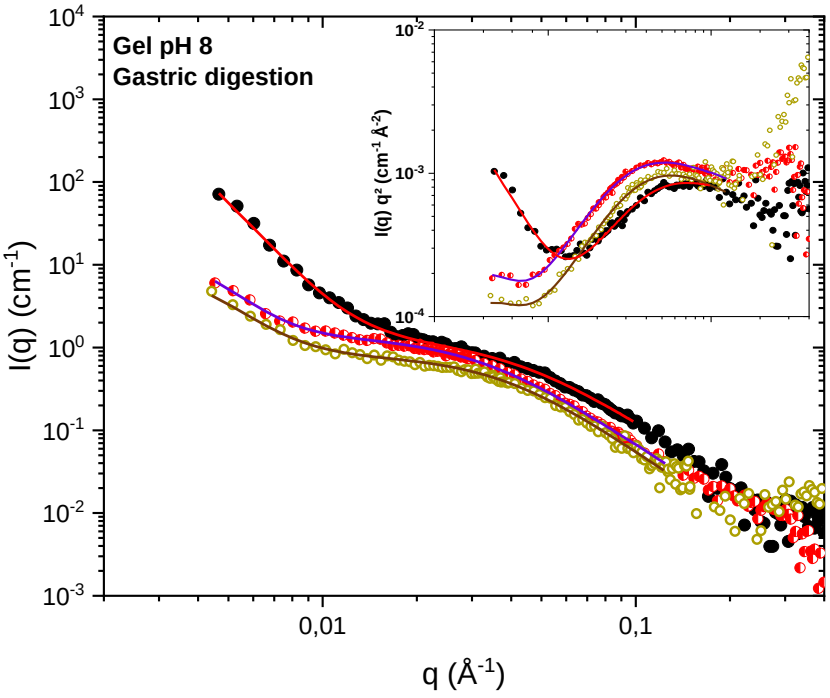

Figure 4.6 SANS of canola protein gels prepared at pH 8: initial sample (black), gastric 30 min (red) and gastric 120 min (mustard). Solid lines are fits to a double Lorentzian function. Inset: Kratky plots of same data (without the prefactor; see text at the beginning of section 4.1.2). (Fig. 5 from ref. 1).

The second effect of gastric digestion can be seen in the high q region. Before digestion, the Kratky plot shows a very broad oscillation, being close to flat for q>0.05 Å $^{-1,}$ due to unfolded proteins after heating. After 30 min of gastric digestion (red curve), a bump appears (clearly seen on the Kratky plot inset), together with a large shift to the low q region. This is evidenced more quantitatively in the fitting parameters, by a large increase of ξ (from 24 Å to ~33 Å) and suggests what we will call the "local aggregation", i.e. involving several proteins or protein units. It may come from the already unfolded proteins of this gel. This effect started already after 15 min and was continued for the 45 min step of gastric digestion (**Figure A1.3**, **Appendix 1**) to increase of ξ to 37 Å. The changes in ξ are combined with the high q exponents, which were varying between 2.4 and 2.6, suggesting a rather steady level of unfolding of those protein structures.

Between **30 and 120 min** of gastric digestion, the shape of the Kratky plots at large *q* does not change. Nonetheless, we can see a reversed evolution of the abscissa of the maximum, i.e. back to higher *q*, giving a decrease of ξ back to 28 Å (closer to the initial value). Here, the "local aggregates" appear to be suppressed and re-formed into smaller, unfolded structures.

The general evolution of the initial **pH 11 gel** (**Figure 4.7**) resembles the one of pH 8 gel only in one part: **at low *q***, after **30 min** of gastric digestion (red curve), the intensity factor and upturn were very similarly, neatly reduced. After **150 min** (mustard curve), the signal decay continued but the curve's upturn slightly raised.

At medium *q*, after **30 min** gastric digestion, the Kratky plot inset shows a widening of the initially well-pronounced bell-shaped curve for this pH 11 gel. This behavior was visible between 15 to 45 min of gastric digestion (see **Figure A1.4**, **Appendix 1**). This widening of the two sides of the oscillation was evidenced quantitatively, by an increase of ξ (from 25 Å to 34 Å) for the left side, and a decrease of the exponent (from 3.7 to 2.9) for the right side. Those two features together tell us, in this case, about an ongoing unfolding of the initially compactly folded proteins.

At **150 min** of gastric digestion, the trend was partly reversed and the curve is now described by a disappearance of the left side enlargement of the Kratky plot oscillation and so a decrease of the ξ (down to 30 Å), whereas it shows only a slight decrease of the exponent *n* to 2.8. At this point, the unfolding of proteins could be combined with the apparent effect of the enzymatic scission, resulting in smaller-sizes proteins. Together with the low *q* upturn at 150 min, it can suggest some restructuration, e.g. formation of new aggregates from the cleaved protein fragments.

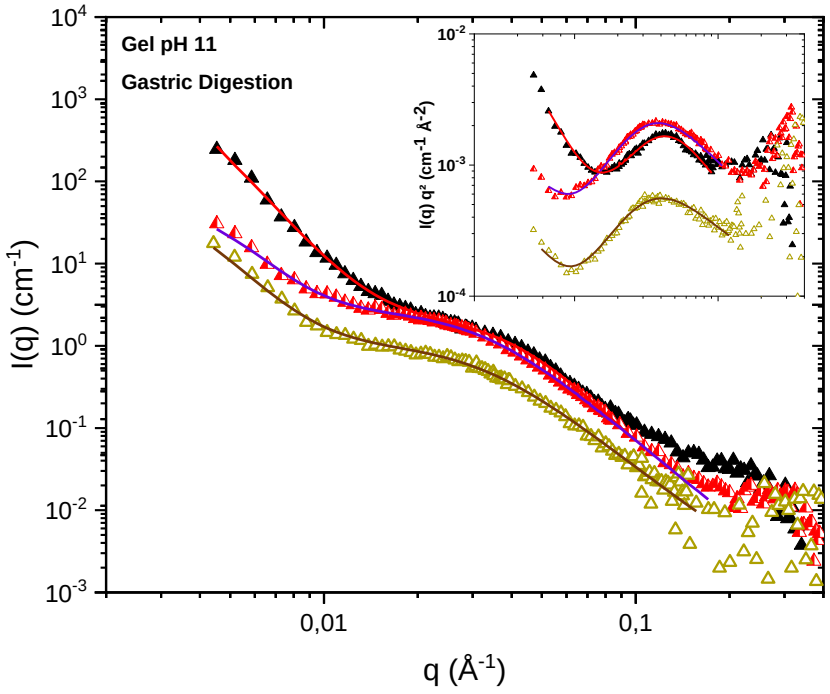

Figure 4.7 SANS of canola protein gels prepared at pH 11: initial state (black), gastric 30 min (red) and gastric 150 min (mustard). Solid lines are fits to a double Lorentzian function. Inset: Kratky plots of same data (without the prefactor; see text at the beginning of section 4.1.2). (Figure 6 from ref. 1).

4.1.2.2 Intestinal digestion

Intestinal digestion was performed after 30 minutes of gastric digestion step. In case of the **pH 8 gel**, already after the first 10 minutes (**Figure 4.8**, green curve), an important effect was clearly visible (compared to the red curve for gastric 30 min): we can observe a notably more pronounced bump in the $q^2I(q)$ *vs* q plot. This corresponds to a major increase of exponent from 2.5 to 3.4 at large q, together with a decrease of ξ from 33 to 26 Å. Those features indicate the further local aggregation, combined with a simultaneous compaction (towards much more compact structures than before digestion). All that was confirmed by similar results obtained also for 10 min of intestinal digestion, preceded with only 15 min of gastric step (not shown).

Even though this intestinal compaction effect seem to continue the trend of the 30 min-gastric step (but it is much amplified), it differs from the effect of longer (120 min) gastric digestion (described above, **Figure 4.6**).

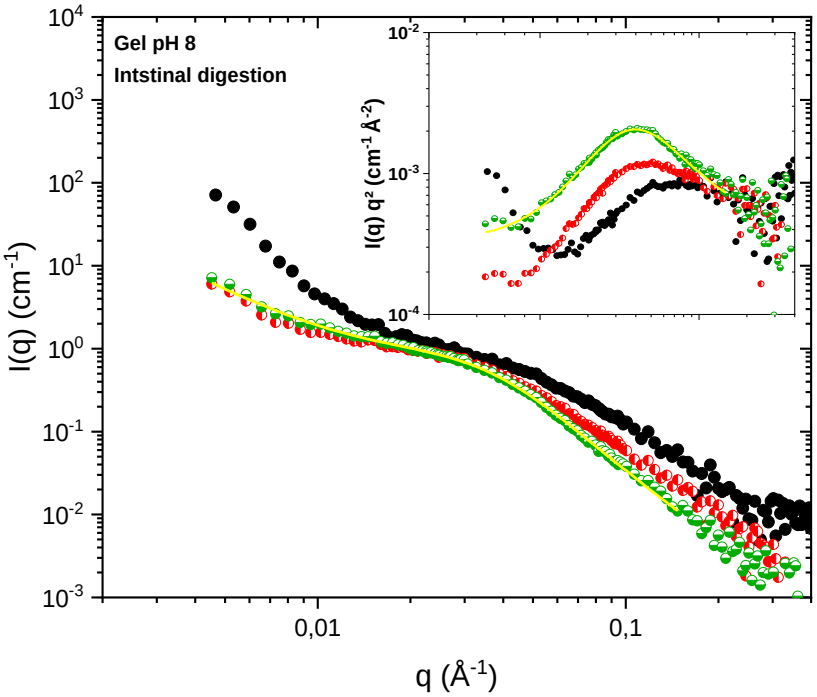

Figure 4.8 SANS of canola protein gels prepared at pH 8: initial state (black), gastric 30 min (red) and gastro 30 min - intestinal 10 min (green). Solid lines represent fits to a double Lorentzian function. Inset: Kratky representations of same data (without the prefactor; see text at the beginning of section 4.1.2). (Figure 7 from ref. 1).

For the **pH 11 gel**, intestinal digestion step (**Figure 4.9**, blue) also resulted in a narrower bell-shape of the Kratky plot (i.e. protein re-compaction), compared to 30-min of gastric step (red). However, this time, the bump is slightly shifted towards higher q (see inset of **Figure 4.9**). Translated into numbers, in the first 10 min, ξ decreased from 31 to 26 Å and exponent increased from 3.2 to 3.8. These features reveal an appearance of smaller, more compact protein structures. Nevertheless, since the proteins in this gel were less unfolded after 30 min the preceding gastric step, this re-compaction was thus softer, compared to the pH 8 gel.

For other gels, prepared at pH 6 and pH 9, we have also observed the protein compaction in 10-30 min intestinal digestion (not shown).

The reason for this apparent compaction of the protein structures of the studied gels could be a combined result of i) a harsh pH change from 2 to 7, resulting in ionization of the AA and ii) the more efficient action of the pancreatic enzymes.

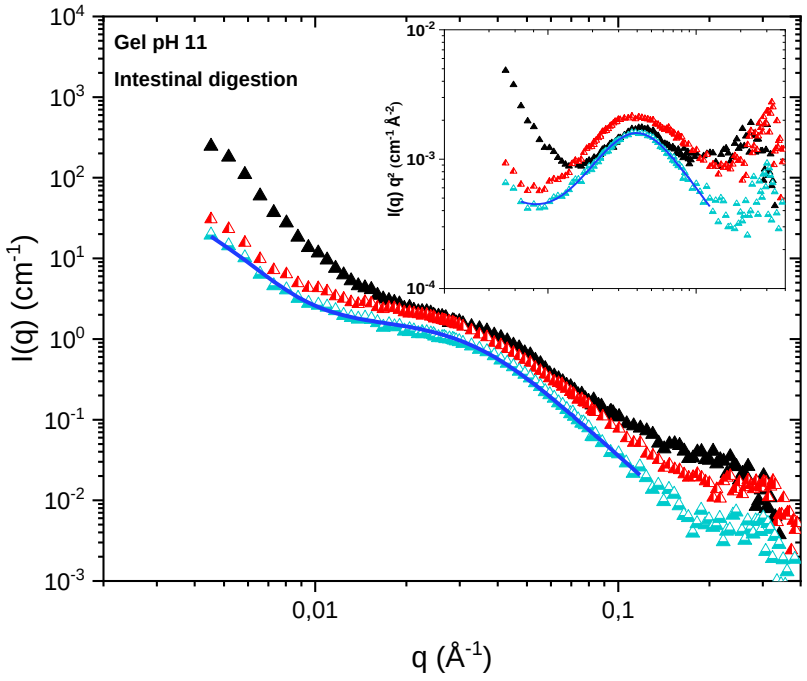

Figure 4.9 SANS of canola protein gels prepared at pH 11: initial state (black), gastric 30 min (red) and gastro 30 min - intestinal 15 min (blue). Solid lines represent fits to a double Lorentzian function. Inset: Kratky plots of same data. (Figure 8 from ref.1).

4.1.2.3 (ξ, n) diagram

In order to present all the results of gastro-intestinal digestion of the two gels, in a less cumbersome way, we gathered their high *q* fitting parameters (exponent *n* and correlation length *ξ*) and displayed them in a form of diagram (**Figure 4.10**). We can clearly distinguish from it the trends followed by proteins during gastric (red) and intestinal (green) digestion, for pH 8 (circles) and pH 11 gel (triangles). A consistent picture for these two gels arises from this diagram, pointed out by the arrows showing directions of the proteins evolution.

In **gastric digestion,** the protein sizes tend to increase to a certain point, after which this trend is reversed and, for longest times, they become smaller. This evolution is marked by the red arrows forming half-loops on (*ξ*, *n*) diagram. Some differences can be distinguished between the two gels.

Namely, for the **pH 11 gel**, the exponent decreases a lot and gradually, while for the **pH 8 gel**, it varies only slightly (firstly increasing, then reducing back and increasing

again). This difference between the two gels arises from the different initial states of their proteins (initially high *n* for the pH 11 gel). To reach smaller protein entities, on the way of the enzymatic scission, it takes a long time for two different reasons: for the pH 11 gel, because of the long process of protein unfolding, and for the pH 8 gel – because of the formation of intermediate aggregates from already unfolded proteins. The outcome of **intestinal digestion** is alike for the two gels, provoking rapid reduction in ξ, along with an increase of the exponents. As pointed out before, this likely results from more efficient protein scission combined with a pH-induced contraction of the resulting structures.

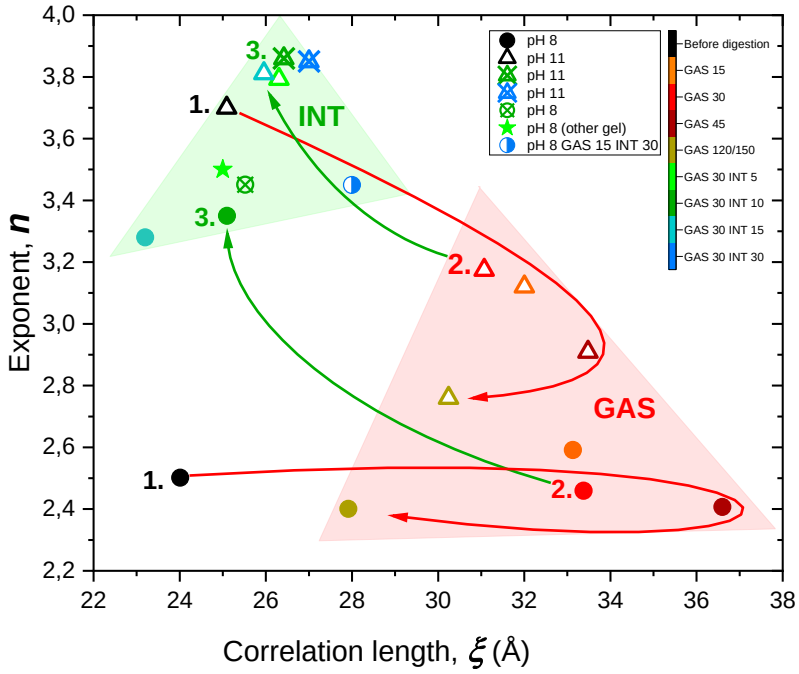

Figure 4.10 Diagram presenting the high *q* range parameters of the SANS curves: each digestion states characterized through a fit to Equation 48 (section 2.4.1.), by the exponent *n* (in ordinate) and the correlation length **ξ**. The closed circles represent the pH 8 gels and the open triangles – pH 11 gels. The umbers indicate the main digestion steps (**1** – initial, **2** – gastric 30 min and **3** – gastric 30 min plus intestinal 10 min). The colors indicate the different digestion steps: orange, red, brown and yellow correspond to 15, 30, 45 and 120/150 min of gastric digestion, respectively; dark green, light green, light blue and dark blue correspond to 30 min gastric step followed by 5, 15 and 30 min of the intestinal step. The crossed symbols represent data from complementary sets of experiments. (Figure 9 from ref. 1).

From the presented diagram, one can conclude that long (120 min) gastric digestion ends with more unfolded and cleaved protein parts, while short gastro- (30 min) intestinal (10 min) digestion results in more compact assemblies of protein fragments. We noticed that some evolutions of the protein structures during digestion reversed back towards the initial, pre-digested states (i.e. the size decrease at the end of the gastric digestion of the pH 8 gel and the re-compaction in intestinal step for pH 11 gel). Nonetheless, it is worth to distinguish that those states (i.e. initial and reversed towards initial), even if described by similar (ξ, n) pairs, most likely differ from each other, since their way through structural evolutions (unfolding, aggregation) cannot be reversed back in the same manner.

4.1.3 Relation between rheological properties and nanostructural evolutions

4.1.3.1 Gastric digestion

In general, the effects of gastric digestion on rheological properties (the values of viscoelastic moduli and their frequency-dependence) of the studied gels were relatively minor, in comparison with those of intestinal digestion. However, under the gastric conditions, the two gels behaved in an opposite way (see **Figure 4.4**): the gel prepared at pH 8 (softer) experienced a slow but decreasing variation of G' with time, as expected for a degradation of a gel upon digestion, but a very limited one, while for the gel prepared at pH 11 (stronger), the time variation of G' was an evident but unexpected increase. We can now discuss these results in the light of the known structures of the gels, not only of their initial state (distinct level of protein unfolding, see Chapter 3), but also of their evolutions.

Relation with large aggregates. From the point of view of scattering, upon gastric digestion, both gels experienced diminishing of the large aggregates signal, although being less pronounced for the pH 11 gel. Although it is difficult to conclude undoubtedly, because we do not know their sizes, it suggests that the aggregates of pH 11 gel are more resistant, which can be assumed to be related to their compact

and/or more dense structures, hindering the access of the enzymes and slowing down their dissociation.

Relation with local structures. The reason for the increase of the pH 11 gel's moduli upon gastric digestion may be also the local structures alterations. More precisely, when the proteins are in folded states, as in the pH 11 gel, the enzymatic action can modify the electric charge and induce the unfolding of the molecules, leading to increased number of interactions (repulsion, small aggregates formation, etc.) and possible higher crosslinking, which would increase the gel modulus. Indeed, in presence of the enzyme, at 30 min of gastric digestion, the proteins experienced both an unfolding and a local aggregation. These processes continued at longer times, so as the increase of the moduli. Additionally, at this pH, both proteins of the gel were likely to cross their isoelectric point, when going down to the gastric pH, rendering the gel more affected by the acid addition compared to the pH 8 gel. Furthermore, in a longer digestion process, protein fragments, released from the cut aggregates, have more time to progressively re-form into local aggregates. This process can explain the second increase in G' for the pH 11 gel. As a result, all along the duration of the gastric digestion, the processes described above, which potentially increase the modulus, could dominate over the degradation of the aggregates.

In conclusion, the different moduli behavior observed during gastric digestion cannot be at this stage directly related to the existence and connection of the aggregates, for which information is not sufficient. Concerning local structural changes, since differences are clear, it is natural to propose that those may modify the moduli, directly or via their effect on the aggregates.

4.1.3.2 Intestinal digestion

Intestinal digestion worked faster and more intensely. The progressive decrease of the moduli, together with a stronger dependency on ω was clear for both gels. This was evidently a signature of deconstruction of the gel networks, possibly due to an enzymatic destruction of the initial links, between either aggregates, individual proteins, or residues inside the proteins. SANS showed local protein re-compaction, likely resulting from the combined action of pancreatic enzymes and pH change.

Anyhow, some differences between the two gels can be pointed out: the couples of the two relaxation times (t_1, t_2) (**Figure 4.15**) showed a longer digestion process for pH 11, in agreement with the kinetics of gastric digestion. The level of compactness before intestinal digestion clearly influenced its kinetics: for the pH 8 gel, a further decrease in the protein size was seen already after 15 min, and for the more compact pH 11 gel - after 30 min (and with slighter effect). Compaction could slow down the enzymatic action if creating denser gel structures. But if it occurred together with disconnection of the proteins/protein parts involved in the network, it could explain the G' decay.

Concerning the limited decrease of the low q signal, we could hypothesize that the enzymatic hydrolysis resulted in some external erosion of the gel, which would not be seen by SANS (when filling in the neutron cells with the non-eroded gel pieces). This erosion would come from the fact that the digestion residues escape more easily at the borders than in the center part of the gel pieces. Such resulting inherent gradient of concentration would further affect enzymatic degradation, with faster digestion on the borders. This erosion effect would be even more pronounced if the residues, staying for a long time in the middle of the gel, created additional interactions, which would further hinder the enzymatic diffusion and reaction.

Table 4.1 Best fit parameters of SANS curves of canola gels to the double Lorentzian function (Equation 2.8). (Table 1 in ref. 1).

Sample name	Correlation length		Exponent		Scale factor	
	Low q	High q	Low q	High q	Low q	High q
	Ξ (Å) ±50 Å	ξ (Å) ±1 Å	***m*** ±0.1	***n*** ±0.1	***C*** ±10%	***A*** ±10%
ID 10% pH 8	330	24	4	2.56	340	1.2
ID 10% pH 8 GAS 15 min	370	33	4	2.6	60	1.6
ID 10% pH 8 GAS 30 min	270	33.4	4	2.46	15	1.4
ID 10% pH 8 GAS 45 min	370	36.6	3.85	2.4	30	1.4
ID 10% pH 8 GAS 120 min	270	28	4	2.4	15	1.3
ID 10% pH 8 GAS 30 INT 10 min	250	25.5	4	3.4	80	1
ID 10% pH 8 GAS 30 INT 20 min	260	23	4	3.3	200	1
ID 10% pH 8 GAS 15 INT 30 min	250	28	3.9	3.45	90	2.85
ID 10% pH 11	310	25	4	3.7	900	2
ID 10% pH 11 GAS 15 min	270	32	4	3.1	70	3
ID 10% pH 11 GAS 30 min	250	31	4	3.2	90	4
ID 10% pH 11 GAS 45 min	260	33.5	4	2.9	40	3
ID 10% pH 11 GAS 150 min	320	30.2	4	2.8	60	1
ID 10% pH 11 GAS 30 INT 5 min	270	26	4	3.75	80	2
ID 10% pH 11 GAS 30 INT 10 min	280	26.6	4	3.83	500	1.2
ID 10% pH 11 GAS 30 INT 15 min	270	26	4	3.8	70	1.6
ID 10% pH 11 GAS 30 INT 30 min	260	27	4	3.8	400	1.4
Mel 10% pH 9	770	26	4	2.8	59000	2
Mel 10% pH 11	460	25	3.5	3.9	3000	4
Mel 10% pH 9 GAS 30 min	350	31	4	2.8	2800	1.5
Mel 10% pH 11 GAS 30 min	360	29.5	4	3.9	1000	5

Summary of Rheology and SANS results

For the two gels (different preparation pH), some rheological behaviors were unexpected, in echo with different nanometric structure evolutions and with the unfolding states of the initial gels.

In the **gastric digestion**, the opposite rheological behaviors (i.e. a slight decrease of the elastic modulus for the initially unfolded pH 8 gel, and an increase for the yet folded pH 11 gel) can be explained by the competition between:

i) the unfolding and or crossing the IEPs of the napin and cruciferin (both in case of pH 11 gel), which increases the interactions between the gel components, increasing the elastic modulus,

ii) the enzymatic scission, which lowers the gel elasticity,

iii) reduced scission in the more crosslinked gel.

In the **intestinal digestion**, differences in behaviors of the two gels were much attenuated, because both of them have undergone the effects of gastric digestion with progressive loss of the moduli and the proteins experiencing re-compaction.

4.2 Digestion of gels in capillaries: Small-Angle X-Ray Scattering

To better describe the nanostructures of the canola protein gels under digestion, we have undertaken experiments using synchrotron SAXS. We used this technique to monitor the digestion of the gels in capillary cells, by submitting them to a one-dimensional pH-enzymatic diffusion-reaction process. This process was monitored *in situ* as a function of time *t,* and capillary position *z,* by vertical scanning of the whole capillary sample. The rapid data collection, almost simultaneously at all sample positions, allowed tracking the pH-enzymatic diffusion, governing the digestion reaction and progressing downward the capillary for times reaching tens of hours (much slower than in the previously described digestion protocol).

The further presented SAXS curves were fitted, as in case of SANS, with the Two-Lorentzian function. The extended data analysis allowed us to precisely characterize changes in the shapes and sizes of protein structures, by distinguish their compact, unfolded or aggregated states (in high *q* range), as well as to describe the evolutions of large protein aggregates (low *q* range). The fitting parameters are presented in forms of digestion diagrams, in analogy to **Figure 4.10** for SANS. The kinetics measurements on different positions in the capillary showed consistently the same features appearing temporally delayed on more distant *z* positions from the gel surface. Through many of such (*z, t*) pairs, we could reconstruct the complete pathways of the digestion processes, by associating the position in capillary (space) to the degree of digestion hydrolysis (time). This allowed a more precise monitoring of the protein evolutions, providing structural information at the resolution of a few Å and insights into the dynamics of multi-scale processes occurring along the gastric and intestinal digestion. The capillary conditions, in which digestion is limited by the slow enzymatic diffusion, positively allowed studying the whole processes of protein digestion in details. This was a limiting factor in SANS measurements, especially in case of the intestinal digestion, in which the dissolution of the gel was proceeding too fast, and thus this step was limited to only 30 min. In capillary SAXS experiment, both gastric and intestinal digestion steps lasted for much longer times. Here also, the problem of the poor sample volume control during the digestion was solved, allowing us to follow also the scattering intensity changes, which provide very important information. Finally, another advantage is the simultaneous measurement of a wide range of *q*, down to 0.005 $Å^{-1}$ and up to 0.25 $Å^{-1}$.

4.2.1 Gastric digestion

In this paragraph, we will present the SAXS results obtained for the pH 11 and pH 8 gels during 10 hours of gastric digestion.

4.2.1.1 pH 11 gel

Figure 4.11 presents an example of such digestion kinetics for the **pH 11 gel**, at one capillary position, close to the gel's surface[2]. Each $log\ I(q)\ vs\ log\ q$ spectrum informs us on the gel's state at the given digestion time (from blue to brown). The inset plot is the corresponding Kratky representation. The latter unveils the main variations in the high q (~5. 10^{-2} Å^{-1}), showing a decrease of compactness (less pronounced bump), together with a shift to low q (increase of ξ), marked by the red arrow.

We will thus focus first on the description of the high q features of the gels (corresponding to protein size range). From the fitted curves of the gastric digestion kinetics, we obtained high q parameters, which are summarized on the (ξ, n) master diagrams, within a color map indicating the digestion time.

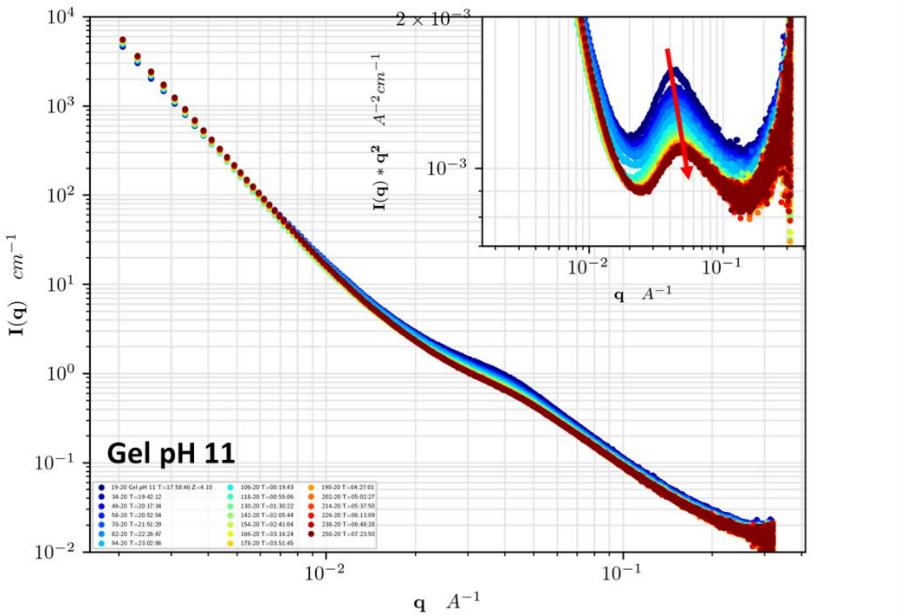

Figure 4.11 SAXS spectra presenting the digestion kinetics of canola protein pH 11 gel for one z position in the capillary. Spectra were recorded every 30 min. Colors denote the digestion time and red arrow shows the direction of its progression. Inset: Kratky representations of the same data.

[2] i.e. at the first z position below the foamy top gel layer - the residual protein solution meniscus, formed during heating).

Figure 4.12a presents the fitting results including the ones for seven different *z* positions of the capillary (marked by different symbols). The observed evolution of the proteins allows us to follow the progressive conformational changes occurring in the gastric conditions. First of all, we can tell that the initially folded (compact) proteins (here the pH 11 gel is concerned), described by ξ^3 of 22 Å and *n* ~3.5, undergo an **unfolding process**, seen mostly by a decrease of the exponent to 3 (i.e. a decrease in the oscillation slope to high *q* in **Figure 4.11**). Throughout this step, high *q* intensity was gradually decreasing (see Figure A1.5, Appendix 1), being in agreement with protein unfolding (via protein hydration and decrease of the scattering contrast).

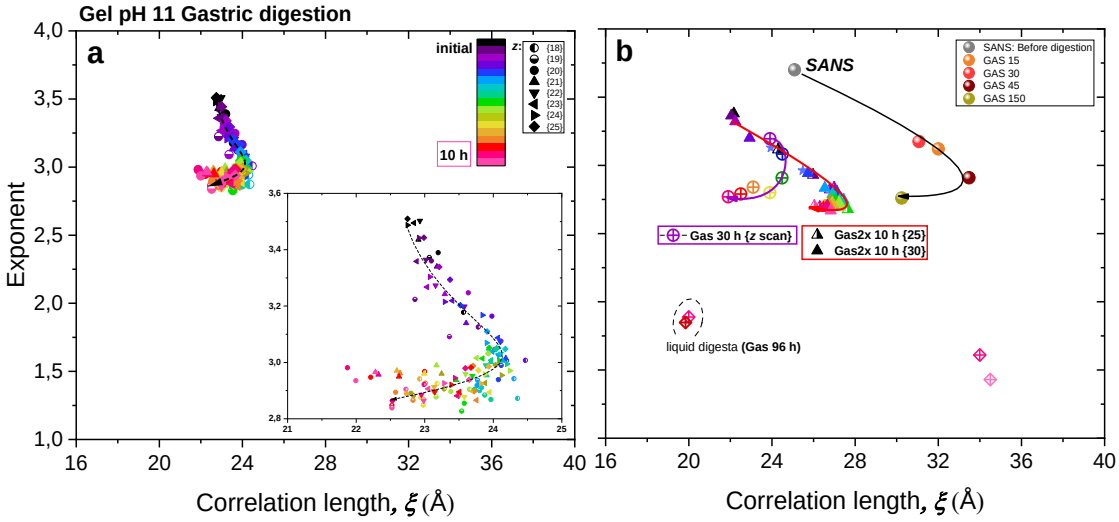

Figure 4.12 Diagram presenting temporal evolution of high *q* scattering parameters (exponent *n* as a function of correlation length ξ) for pH 11 gel; each point represents one SAXS curve. **a)** 10 hours gastric digestion kinetic, for 8 *z* positions in the capillary (different symbols; *z*=18-25, with a 150 µm interval); bottom right) enlargement of the plot. **b)** 10 hours gastric digestion kinetic with double dose of pepsin (triangles, 2 *z*); scan on 8 *z* after 30 h of gastric digestion (crossed circles); after 96 h of digestion in "liquid digesta" (crossed diamonds); SANS results for 15, 30, 45 and 120 min of gastric digestion (closed circles; data in ref. 1). Colors represent the digestion time from black to light pink. Arrows indicate the evolution directions for clarity.

[3] As indicated in Chapter 3, ξ is considered as a size of proteins, since they are never interpenetrated, even during digestion.

The second conformational change after the unfolding was an apparent decrease in the size ξ at the end of this 10-hours kinetics, indicating an enzymatic cleavage, thus **scission** and reduction of the polypeptide chain length. Those two subsequent comportments (unfolding and scission) are coherent with the observations from the previous SANS experiments (plotted also on **Figure 4.12b**). SANS results appear to be, however, shifted to larger ξ values (by about 5-6 Å). This difference between the two techniques can be due to differences in scattering contrast for x-rays and neutrons, for example its influence on the scattering from the hydration shell of the proteins. Another difference may come from the samples themselves. Indeed, for SANS, the slices of gels after each digestion step are put back in the SANS cell, and by doing so, small residues of digestion could have remained in the digestion tube, thus not measured in SANS. For SAXS, the small reaction residues remain inside the capillaries, they are parts of the samples. Therefore, the apparent size of proteins can appear smaller in SAXS than in SANS. Apart from this ξ shift, gastric digestion seems to proceed in a very similar manner from the results of the two techniques.

Together with SANS results, on **Figure 4.12,** we gathered fitting results from several other gastric digestion experiments for the pH 11 gel, where different degrees of the protein unfolding appear. **Gas2x** sample (10-hours kinetics, 2 *z* values, and with double dose of pepsin; *triangles*) experienced bigger (faster) extension of the local structures, confirming effect not solely of the acid pH but also of the enzymatic hydrolysis itself in the unfolding. **Gas30h** digestion effect (scan after 30 hours of gastric digestion; *crossed circles*) resembles the unfolding observed in the first 10 hours experiment but is followed by the enzymatic scission (with a decrease of ξ to 22 Å).

On **Figure 4.12b**, we also present a few points obtained for very long (**96 hours**) gastric digestion, and after renewing the pancreatic enzymes (*crossed diamonds*). That resulted in much unfolded structures (*n* below 2 and ξ ~35 Å). The 3 points inside the dashed circle, for ξ ~20 Å, describe the most digested state of the proteins after this step, resembling rather extended protein residual fragments. They were measured at *z* very close to the gel's initial surface, which during digestion became close to dissolved (less

gel-like). This state, which we will denote as a "liquid digesta", represents a relatively low weight-by-mass proportion of the solid.

Altogether, the results from all presented experiments coherently suggest the gastric digestion pattern comprising of two directions: i) protein unfolding and ii) protein scission. The results indicate also that the gastric unfolding is not only related to the pH environment, but rather to its combined work with pepsin. Confirmation of this finding has been obtained after treating the canola gels with gastric pH, showing almost no effect of the pH itself on the protein conformations (not shown).

4.2.1.2 pH 8 gel

One example of 10 hours gastric digestion of the **pH 8 gel** is presented on **Figure 4.13**, showing essentially a variation at large *q*, as for the pH 11 gel. The corresponding master diagram, shown on **Figure 4.14**, contains, besides the **Gas 10h** (3 z; *closed circles*), also **Gas2x** (10 h kinetics, 3 *z,* with double dose of pepsin; *triangles*) and a scan on *z* after 10 h of gastric digestion with the gel imbibed with pepsin in cold prior to digestion (*open circles*). All those gastric digestion kinetics show the same protein **re-compaction** tendency, with the biggest effect for the digestion with higher pepsin concentration, resulting in an increase of exponent *n* from ~2.3 to 2.7 and decrease of ξ from ~30 to 25 Å. Initially pre-unfolded proteins of this gel seemed to reform more compact domains, larger than the size of individual or the correlation length of the unfolded proteins. Interestingly, the infusion with pepsin in cold, before the digestion in optimal conditions, resulted in very similar parameters than its equivalent with no infusion.

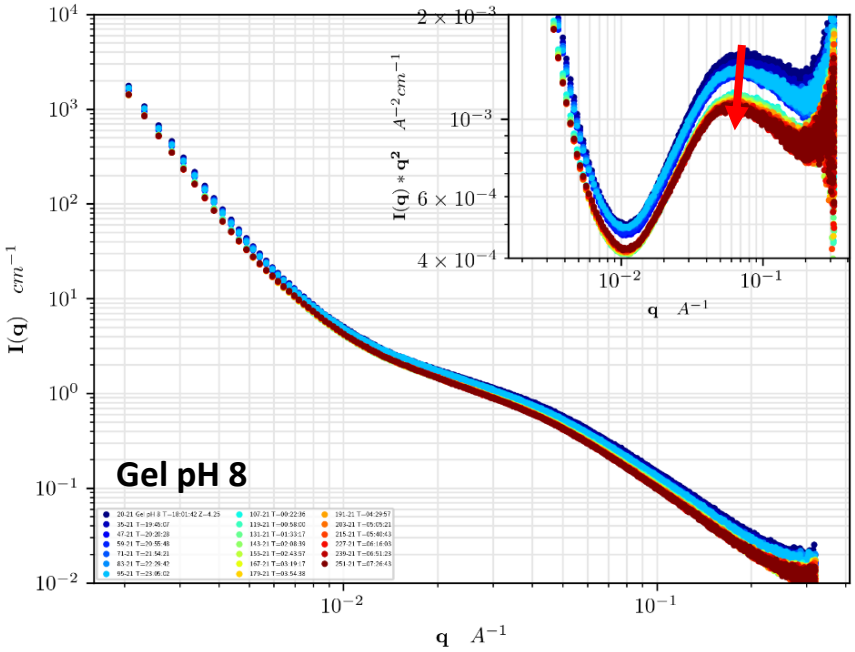

Figure 4.13 SAXS spectra presenting the digestion kinetics of canola protein pH 8 gel for one *z* position in the capillary. Spectra were recorded every 30 min. Colors denote the digestion time and red arrow shows its direction. Inset: Kratky representations of the same data.

On **Figure 4.14b**, shows the effect of longer (**30 hours**) gastric digestion (open circles), nicely confirming the continuation of the re-compaction trend by reaching the highest exponent of ~3.2 (marked by 1. on the diagram). This effect must be a result of the enzymatic attack, since it was not observed upon the gastric pH only (no enzyme). It is, however, strikingly different/opposite from the trends observed for pH 11 gel. Remarkably, the even longer gastric digestion (**96 hours with renewed enzymes**) resulted in changing of the former pattern direction to an unfolding, with a decrease of the exponent back to 2.5 and increase of ξ to as much as 40 Å (this step is marked by 2. on the diagram). This reveals an additional complexity of the gastric digestion process. The resultant unfolded intermediates are then experiencing decrease in size, primarily along with continued unfolding, and finally with a slight re-compaction (ξ ~24 Å and n ~ 2.4). The final protein residues are smaller than initially. Additionally, we showed three points describing the protein states in the liquid digesta, obtained after this long (96 h) digestion step: they represent small and much extended structures.

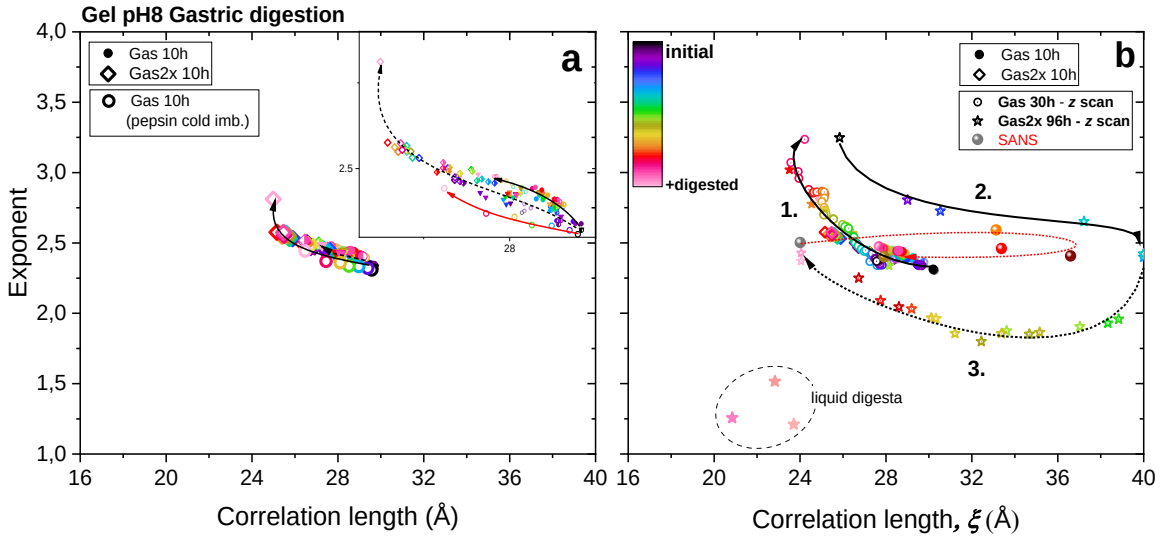

Figure 4.14 Diagram presenting temporal evolution of high *q* scattering parameters (exponent *n* as a function of the correlation length ξ) for the pH 8 gel; each point represents one SAXS curve. **a)** 10-hours gastric digestion kinetics (filled circles, 3 *z*); 10-hours gastric digestion kinetic with pepsin imbibed in cold (open circles, 1 *z*); 10-hours gastric digestion kinetic with double dose of pepsin (triangles, 2 *z*). **b)** scan of the capillary after 30 h of gastric digestion (open circles); after 96 h of digestion (stars); SANS results for 15, 30, 45 and 120 min of gastric digestion (closed circles; data of ref.). Colors represent the digestion state from black (initial) to light pink (most digested state for each experiment). Arrows indicate the evolution directions for clarity.

Compared to the SANS results (reminded by the points with a red arrow on **Figure 4.14**), the above presented data of gastric digestion appear more complete, in the meaning that they fill the time gap between 45 and 120 min of the SANS data. However, the initial points for SANS and SAXS are different (as in the case of pH 11 gel). Moreover, we have to keep in mind that the protocols of digestion are different. SANS and SAXS "times" cannot be thus compared directly. In spite of that, the evolution with time of the protein states follows the same paths. This is very satisfying about the significance of these measurements.

4.2.1.3 Large aggregates in pH 8 and pH 11 gels

At low *q,* 10 hours of gastric digestion yield very weak effects: a very small decrease for the pH 8 gel, and, somehow opposite, a slight increase for pH 11 gel. It is only after 96 hours of digestion, for which the gel state changed to a liquid digesta (visually observable), that a decrease in intensity was visible, with a change from q^{-4} to q^{-3} power-law, indicating the disruption of the large aggregates and decrease of their internal density (see **Figure A2.1**, **Appendix 2**).

Summary of gastric digestion studied by SAXS

Gastric digestion of proteins in capillary conditions could be monitored up to the complete gel dissolution (liquid digesta), but for very long digestion times (96 hours) - much longer than with more in *in vivo*-like SANS protocol.

Correlation length ξ and exponent *n* parameters, which describe the **high *q* scattering**, were shown in forms of master diagrams. The deeper the *z,* the shorter was the corresponding apparent time for the digestion effect:

Gastric digestion of the **pH 11 gel** (with initially folded proteins), showed:

1) unfolding,
2) apparent decrease in characteristic size (scission).

This was coherent with the SANS results, but with shifted ξ values, explainable by differences in contrast.

Gastric digestion of the **pH 8 gel** (with initially unfolded proteins), resulted, on the contrary, in a slight re-compaction, seen likewise for Gastric 15 min in SANS.

For the longest digestion times, the process showed 3 steps:

1) re-compaction, also visible in SANS,
2) re-unfolding to a mid-state with large ξ also visible in SANS,
3) final decrease in the correlation size, throughout continued unfolding and re-compaction of the protein structures/digestion residues.

Eventually, for the two gels, the protein residues after very long-digestion (liquid digesta) were similar (ξ~20 Å, n < 2).
Additionally, a higher enzyme concentration prolonged the protein unfolding.

During 10 h of digestion, the aggregates scattering varied only slightly, but in an opposite way for the pH 8 and the 11 gel.
Only after long digestion (liquid digesta, here after 96 h), a clear decrease in intensity and the power-law decay from q^{-4} to q^{-3} was visible, indicating disruption of large aggregates in both gels.

4.2.2 Gastro-intestinal digestion

We now continue with the presentation of the SAXS results, with a focus on the intestinal digestion. We monitored the digestion kinetics during 3.5 hours of gastric digestion, followed by 15.5 hours of intestinal digestion, with additional 2-hours step with freshly prepared intestinal enzymes. We first focus on the evolution of proteins (high q range) and then, on the evolution of the large aggregates (low q range).

4.2.2.1 Gastro-intestinal digestion at the protein scale

Gel at pH 11: central experiment

Figure 4.15a presents an example of such a ''full kinetics'' for the pH 11 gel, with each spectra representing the gel's state at given digestion time (with 35 min interval) at given z. **Figure 4.15b** shows the z scan on the capillary at the end of the digestion. Similarly to the gastric digestions described in the precedent paragraph, we present here the high q fitting parameters (***ξ, n,*** *intensity* ***A***) on master diagrams shown in **Figure 4.16a-b**. Owing to the digestion progressing in the gel with time in a diffusion-reaction manner, we observed, again, the same protein states gathered very nicely on the master curves, appearing delayed in time for z positions further from the gel surface. These master curves strongly reinforce our observations.

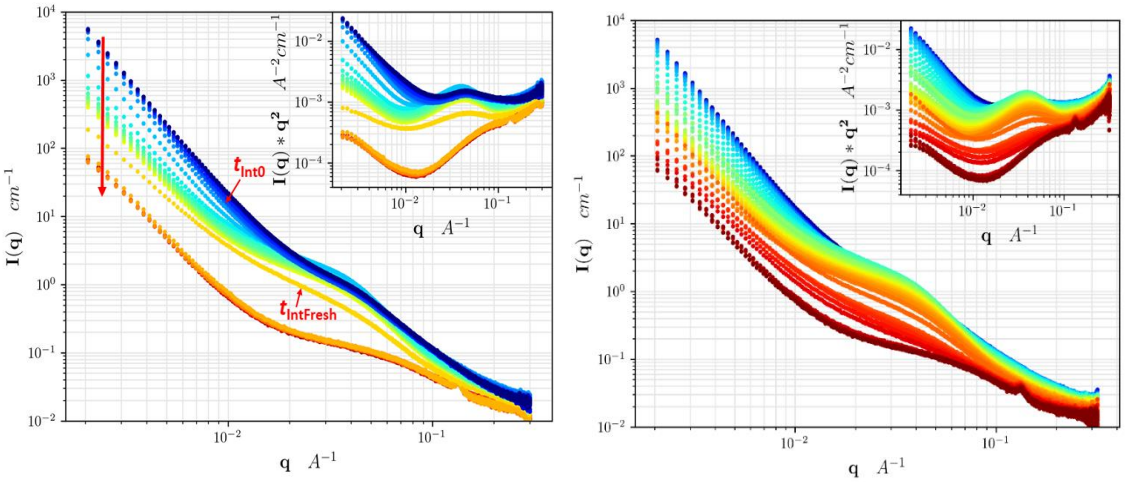

Figure 4.15 Left) SAXS spectra presenting the digestion kinetics of canola protein **gel at pH 11**, for 1 capillary position *z* (closest to the gel surface), recorded every 35 min. Colors denote digestion time and red arrow shows its direction; first 4 curves present 2.2 h of gastric digestion, 5th curve - injection of intestinal juice (after 3.5 h of gastric digestion), and the following curves - 15.5 h of intestinal digestion, plus 2 h with fresh enzymes (Fig. 1 in ref. 2). **Right)** *z* scan on 46 positions on the capillary (7 mm, with 150 µm intervals) after 15.5h of intestinal digestion. Insets: Kratky plots of the same data.

On these master diagrams, containing the best fitting parameters for several (*z*, *t*) pairs, we could hence reconstruct a complete intestinal digestion process.

Here, the gastric step was limited to 3.5 h before initiating the intestinal digestion, so for similar digestion times, gastro-intestinal digestion was more complex than the gastric digestion presented before.

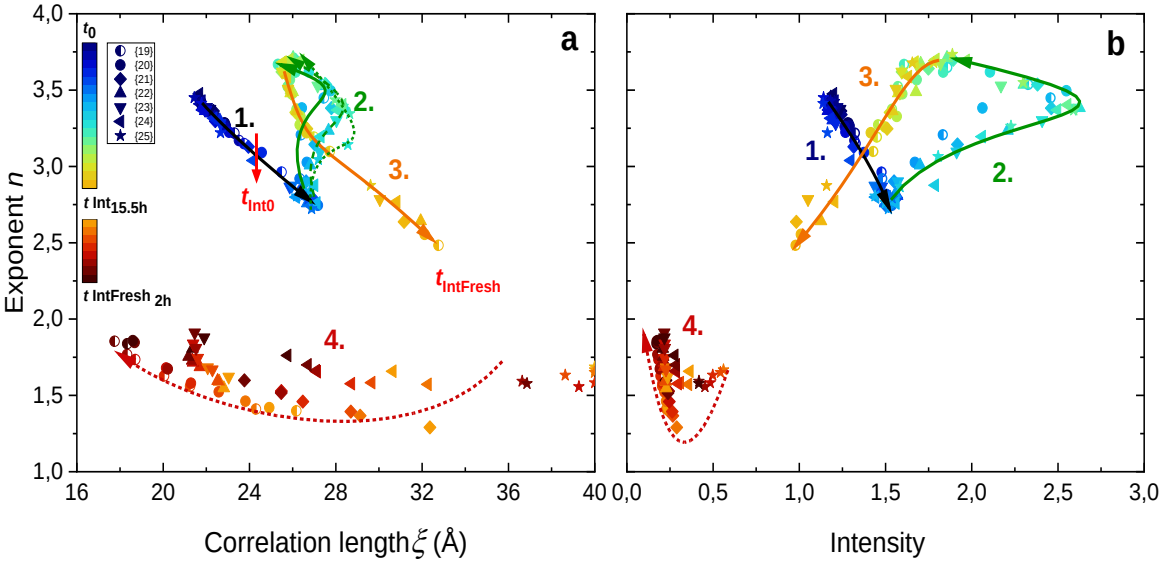

Figure 4.16 Diagrams presenting the evolution during gastro-intestinal digestion (gastric only until 3.5 h = t_{int0}, after which intestinal juice was added - red arrow, up to 15.5 h) of **pH 11 gel**, with the fitting parameters (***ξ***, ***n***, ***intensity***) describing the structural changes at the scale of proteins. **a)** exponent ***n*** as a function of correlation length ***ξ***. **b)** exponent ***n*** as a function of ***intensity***. The shapes of the symbols correspond to 7 different ***z*** positions in the capillary (19-25, with a 150 µm interval) and colors correspond to the digestion time as in **Figure 4.15a**. Numbers indicate the 4 characteristic steps of digestion and arrows - the evolution directions. (Figure 2 in ref. 2).

Intestinal digestion for this pH 11 gel comprised also of 4 successive steps (including a back-and-forth evolution of the proteins). Each of the steps, rather extensive in description, will be presented separately for clarity.

1st step: Protein unfolding

During the 3.5 h of gastric digestion, we recorded only relatively small, but visible and undoubted, changes in the scattering intensity: a decrease of *n* from initial 3.5 to 3.2 and a slight increase of *ξ* from 22 Å to 24 Å, both indicating that the protein unfolding has started. We know from the results just shown, that a complete gastric digestion takes much longer times. This unfolding trend continues, increasingly faster after injection of intestinal juice (red arrow t_{Int0} in **Figure 4.16a** at t_{Gas}= 3.5 h), with *ξ* reaching ~27 Å and *n* 2.8 in the first 35 min of intestinal digestion ($t_{Int0.5h}$). However,

when looking at the intensity diagram (**Figure 4.16b**), we can see, conversely to what was observed in gastric digestion, its slight increase. This gives us a precious indication that the observed features are not only a result of an unfolding of the proteins in the mesh (which would decrease intensity via hydration), but rather correspond to the local aggregation, arising from partially unfolded proteins. Such local aggregation is favored when the pH changes i) from initial 11 to gastric 2, where both component proteins (cruciferin and napin) likely cross their IEP, favoring their unfolding and further interactions and ii) from 2 to the intestinal pH 7, when they can attract each other due to their opposite charges.

2nd step: Re-compaction/Aggregation

Shortly after the intestinal juice was added, we observed a much more evident change in the spectra, seen accurately on the inset (Kratky plot) of **Figure 4.15** with appearing of a sharper maximum (lighter blue curve). The variation of exponent *n* changed here the direction for an increase, reaching a maximum value of ~ 3.8 at t_{Int4h}. This indicated a re-compaction of the pre-unfolded structures from the 1st step, to structures with even higher compactness than in the not-digested samples. This re-compaction step is coherent with the SANS results, where the same exponent *n* ~3.8 was obtained. However, here, we attained additional information, as follows. In the digestion diagram, we can discriminate 2 sub-steps of the protein re-compaction process (*n* increase): the first one, where the intensity increases noticeably (up to 2.5 time the initial value) and the second one, where it decreases. We can imagine that the proteins were here re-forming local aggregates along with their simultaneous contraction. This can explain why ξ did not vary much, especially for the upper *z* positions (where digestion progressed the most). This apparent contraction was undoubtedly provoked by the enzymatic scission, since it did not appear due to only pH change (step 2. on **Figure 4.16)**. Interestingly, the ξ increase was correlated with deeper *z* positions: we can observe some more sinuous paths in the (ξ, *n*) diagram

(marked by 3 green curves[4]. It can be interpreted as a formation and growth of local aggregates/assemblies, appearing before their enzymatic digestion (thus contraction with size ξ reduction), in the sub-step 2. Indeed, for the deeper *z*, the protein unfolding could have continued for longer time, giving a possibility for additional interactions with smaller protein fragments, which were cleaved from the network and could diffuse upwards.

Two more factors could influence this slowing down of digestion rate downwards the capillary, i.e. i) slower enzymatic diffusion through such altered local structure and ii) decrease of enzymatic activity with time. At last, the final compaction state was independent on the digestion kinetics in this 2nd step, i.e. the parameters (ξ, *n*, *intensity*) reached the same values for all *z*.

3rd step: Unfolding/Disaggregation

After reaching the maximum compactness at t_{Int4h} (*n* ~3.8), the ongoing evolution of the local structures came back to an unfolding, as seen through lower $q^2I(q)$ slope (*n* ~2.5), closer to a plateau towards higher *q*. The anew decrease of *n* together with the increase of ξ makes a sort of loop in the (ξ, *n*) diagram. However, contrary to the 1st step, here, the intensity was gradually reduced. This suggests a disaggregation on the local scale, through enzymatic hydrolysis, and transformation into more extended protein structures. This process was continuing up to 15.5 h of the intestinal step, with a slower rate. Such slowing down is not intuitive: one would rather expect its acceleration due to facilitated enzymatic access to the unfolded protein substrates. We propose that this effect was overpowered by the decreased enzymatic activity at these long digestion times.

[4] During this entire step, the fitting parameters (***ξ***, ***n***, ***intensity***) allowed to assume a non-overlapping proteins regime. It was more explained in Chapter 3.

At the end of this 3rd step, the local protein structure was described by the highest ξ of 33 Å, *n* of 2.5 and an intensity back at value before the digestion. ξ approached the size of very unfolded proteins obtained after chemical denaturation (see **Figure 3.5** in Chapter 3), assuming $R_g^2 = 3.\xi^2$. The overlapping concentration would be 0.64g/cm^3, such that unfolded proteins are still under *c**. Thus, the decrease of intensity is not due to interpenetration but to a lower protein mass in the mesh. Besides, the exponent *n* of 2.5 indicates that the correlations at intermediate scale are still present, suggesting a kind of branched polymers. At the end of this step, we therefore assume that the digestion residues are ramified clusters of sequences of proteins of rather extended conformations, polydisperse in mass.

4th step: Protein scission

After 15.5 h of intestinal digestion, fresh pancreatic enzymes were added. This rapidly provoked a disappearance of the cruciferin's form factor oscillation in the $q^2I(q)$ plots (inset of **Figure 4.15**) reaching *n* as low as 1.8. This value is found for very unfolded structures resembling linear polymer chains in a good solvent[3] (similar to our result of chemical protein denaturation presented in section 3.1.2). In the same time, intensity is largely reduced and ξ decreases gradually. This could be due to strong interpenetration of protein chains if they were long enough, but again, we exclude this option: it is more likely caused by the gradual enzymatic hydrolysis of the larger protein fragments. The resulting ξ of ~18 Å can indeed correspond to the size of small peptides (with ~5 amino acids, assuming 3.5 Å per one) and agrees with a peptidomic study showing that most peptides in human jejunum (middle intestinal part) are comprised of between 2 and 14 amino acids[4]. Such a final renewed digestion efficiency was probably driven by the higher activity of fresh enzymes, enhanced by a better access of the enzymes to peptide bonds of very unfolded proteins. To end this description, at the end of the intestinal digestion, the protein residues likely resemble small, extended fragments of low mass, which diffuse in liquid digesta. The complete gastro-intestinal digestion process of the pH 11 gel is presented in **Figure 4.17**.

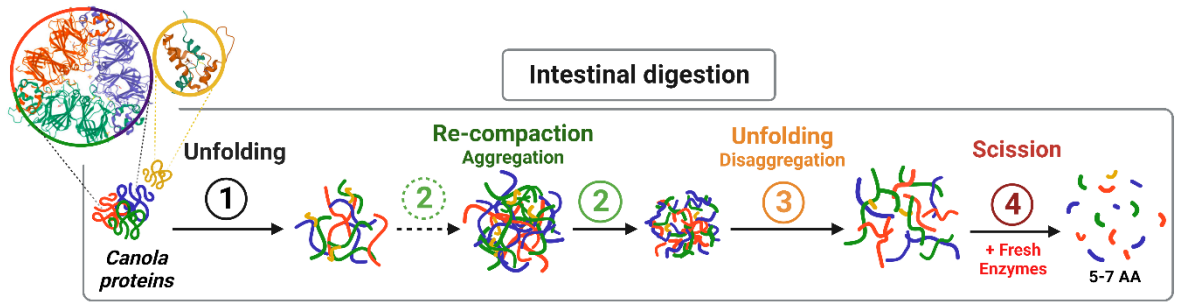

Figure 4.17 Schematic representations of the gastro-intestinal evolution of the canola proteins conformation in the gel prepared at pH 11, showing 4 successive steps. Cruciferin is shown by the three-colored protein and napin is shown in yellow (the proteins PDB structures are showed for clarity).

Gel at pH 11: complementary experiments

Effect of longer gastric phase. We compare intestinal digestion (8.5 h) of pH 11 gels performed after different gastric experiments: **3.5 hours** (presented in the section above) and **12 hours** with double dose of pepsin (Gas2x 12h)[5]. See the comparison in **Figure A1.6**, **Appendix 1**.

The results showed that the level of the protein unfolding before intestinal digestion (here n = 3.2 and ξ = 24 Å for **Gas 3.5h,** and n = 2.9 and ξ = 27 Å for **Gas2x 12h**) can influence the kinetics and extent of the following intestinal step. Namely, for Gas2x 12h (where proteins were more unfolded), a greater protein unfolding was continued primarily, followed by a re-compaction (to n ~ 3.7). For the same duration ($t_{Int2.5h}$), Gas 3.5h sample was described by n = 3 and ξ ~ 26 Å, and it reached the re-compaction level of n 3.7 only after ~1.5 h more. At $t_{Int8.5h}$ (unfolding/disaggregation stage), Gas2x 12h reached structures of n = 2.6 ξ ~36 Å, while Gas 3.5 h - of n = 3 and ξ ~28 Å. Hence, intestinal digestion was more effective after a longer gastric step. We could also notice here that no "loop" behaviour (in 3rd step described above) was observed

[5] Both samples were measured at the equivalent positions; closest to the gel surface.

for the more unfolded sample, pointing out at reduced complexity of its digestion process.

Bile salts. Additionally, the use of bile salts showed a positive impact on the intestinal digestion efficiency. For digestion without bile (Gas2x 10h, with pre-unfolding similar to that of Gas2x 12h), during 8.5h, with a slight unfolding and re-compaction steps, a lower disaggregation level was reached (ξ of 32 Å instead of 36 Å for Gas2x 12h digested with bile), as shown in **Figure A1.7**, **Appendix 1**.

Summary for gastro-intestinal digestion of the pH 11 gel

- Initially folded proteins of the pH 11 gel experienced complex behavior in gastro-intestinal conditions, involving forth and back evolutions (unfolding, re-compaction and unfolding) before the final scission.
- A longer gastric step shortened the following intestinal digestion, through a more complete unfolding.
- Application of fresh enzymes on pre-unfolded proteins gave more potent/faster hydrolysis.
- Bile salts improved intestinal digestion at the proteins scale.
- Very long gastric digestion times (96 h) attained similar results to the more potent pancreatic enzymes (~18 h).

Gel at pH 8: central experiment

Figure 4.18 shows gastro-intestinal digestion kinetics of the **pH 8 gel**, in analogy to the formerly presented gel, with 3.5 h of gastric step followed by 15.5 h of intestinal digestion plus 2 h with fresh enzymes. The evolution pattern (**Figure 4.19**) partially resembles the one of the pH 11 gel. The first difference lays in the 1st step, which for the folded proteins (pH 11) constituted the unfolding, and here it is omitted, since unfolding of the proteins has already occurred during the gel's heat-formation.

1st step: Weak scission and re-compaction

The initially unfolded proteins (n = 2.3, ξ ~30 Å) first underwent a **weak re-compaction**, as shown by a decrease in ξ (to 26 Å) and a minor increase in n (to 2.4), along with some **scission or disaggregation** (an intensity decrease from 1.6 to 1.3). This step is similar to the continuous gastric digestion discussed in section 4.2.1.2.

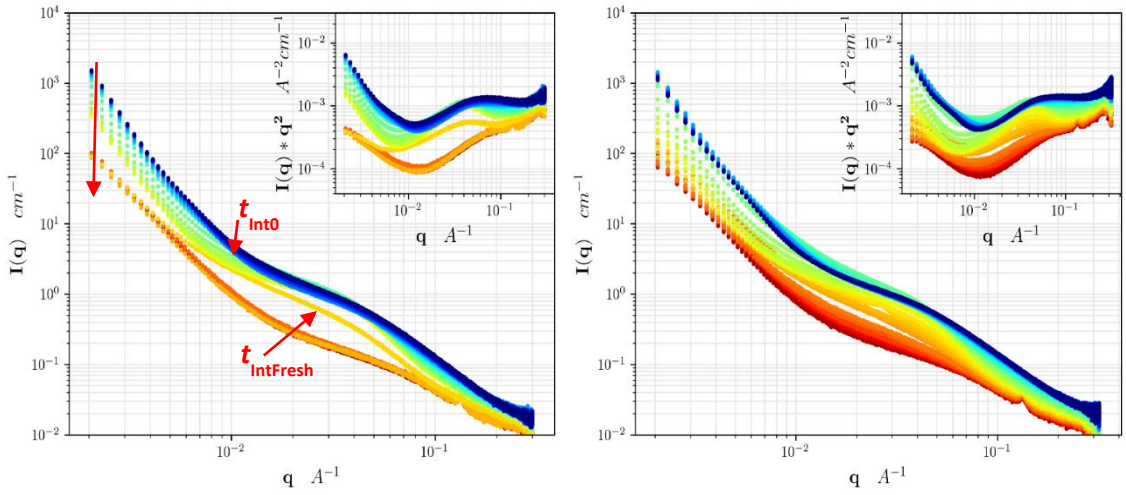

Figure 4.18 Left) SAXS spectra presenting the digestion kinetics of canola protein **pH 8 gel** for one *z* capillary position (closest to the top gel surface). Spectra were recorded every 35 min. Colors denote the digestion time and red arrows are showing its direction; first 4 curves present 2.2 h of gastric digestion step, 5th curve the injection of intestinal juice (after 3.5 h of gastric digestion), and the following curves are for 15.5 h of intestinal digestion, plus 2 h with fresh intestinal enzymes. **Right)** z scan on 46 positions on the capillary (7 mm, with 150 µm intervals) after 15.5 h of intestinal digestion. Insets: Kratky representations of the same data.

2nd step: Re-compaction/ Weak Aggregation

In a 2nd step, the behavior of the proteins catches up with the one observed for the pH 11 gel at the beginning of intestinal digestion. The proteins experience here mostly **re-compaction**, showed by a visible increase of *n*. A sinuosity of $n(\xi)$ of this 2nd step is marked by the green curve. The trends of ξ and intensity are parallel, with a change firstly to an increase and then to a decrease, which can represent a slight protein aggregation[6] before the stronger re-compaction (up to *n* 3.3, as in SANS). Compared to the pH 11 gel, the intensity variations are here however limited, therefore we deduce that not as many "local aggregates" formed during this re-compaction step.

3nd step: Unfolding

The local structures experienced a new decrease in *n* and an increase in ξ, however, in this case, with only a slight decrease in intensity (at the beginning of this step) - read as the local structures **unfolding** and disaggregation, limited by the lower amount of local aggregates formed previously. Here, especially at the beginning, the path of the *n* decrease was smoother than in for the pH 11 gel (no loop-like behavior on the (ξ, n) diagram), which could result from the difference between the unfolding and its combination with disaggregation. This step is very similar to the 3rd step for the for the digestion of the pH 11 gel, treated with the longer gastric pre-digestion (Gas2x 10h or 12h); this similarity comes from the closer initial states of the proteins (unfolding achieved either by heating or longer gastric step). At last, ξ increased to 38 Å, being still considered as the protein size, with slightly higher level of unfolding, compared to the pH 11 gel at the end of its 3rd step.

[6] We still stay below the overlapping concentration.

4th step: Scission

After that, the intestinal juice was replaced with a fresh one and a strong decrease in ξ, n and intensity was observed (as in the case of the pH 11 gel), being an effect of the enzymatic scission on very unfolded proteins. At this digestion step, the differences between the initial structures of the two gels disappeared and the resulting protein residues were of similar size range and extension level. However, a small distinction can be remarked in the case of the pH 8 gel, i.e. that its digestion seemed to be effective on more z positions (faster digestion progression). The schematic process of gastro-intestinal digestion of the proteins in this pH 8 gel is represented in **Figure 4.20**.

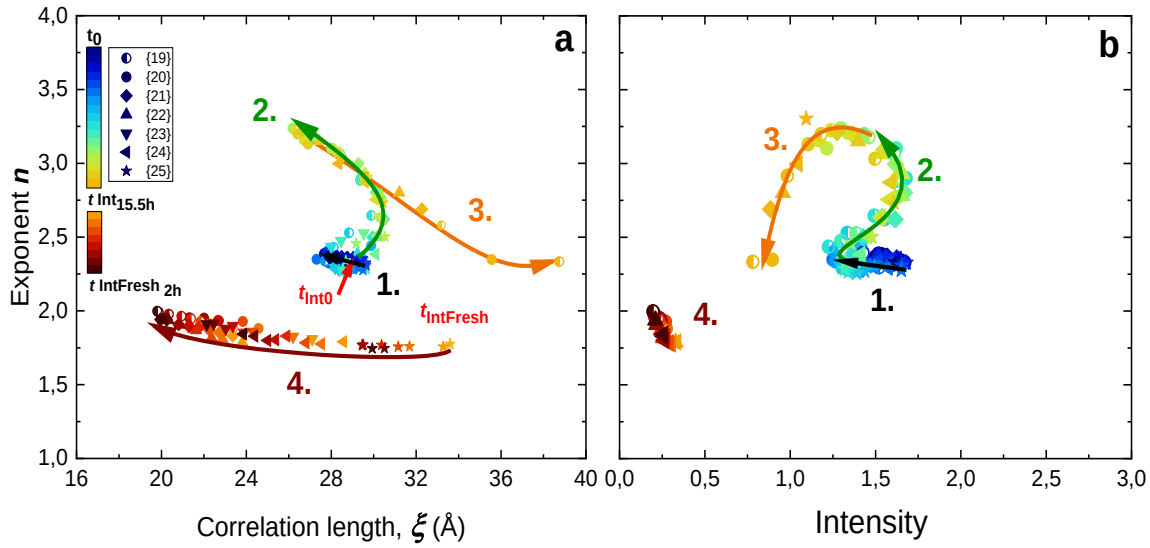

Figure 4.19 Diagram presenting temporal evolution of high q scattering parameters for **pH 8 gel**: each point represents one SAXS curve. **a)** exponent n as a function of correlation length ξ. **b)** exponent n as a function of intensity. Symbols represent 7 different z positions in the capillary (from 19 (closest to the surface to 25, with a 150 µm interval) and colors – the digestion time as in **Figure18a**. Numbers indicate the 4 characteristic steps and arrows – the evolution directions, for clarity.

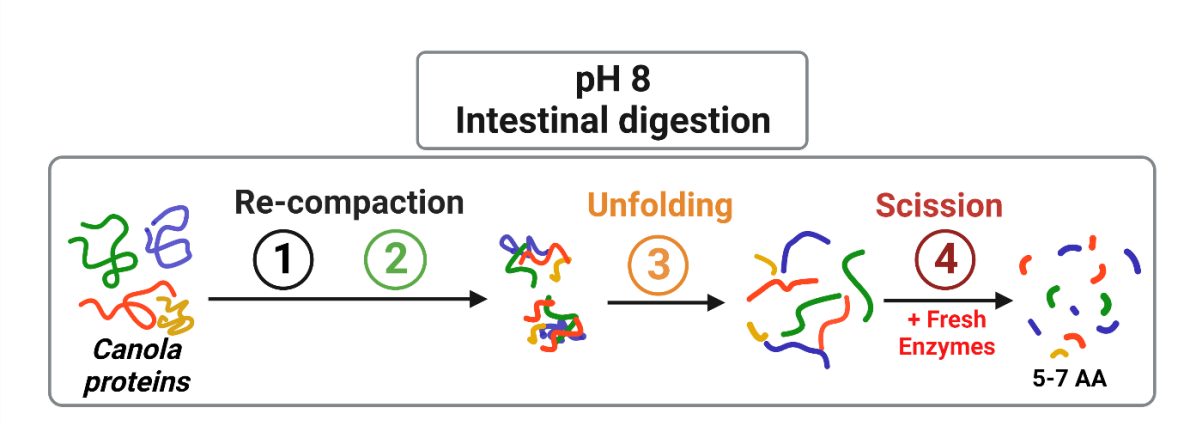

Figure 4.20 Schematic representations of the evolution of the canola proteins conformation in the gel prepared at pH 8, showing 4 successive steps. Cruciferin units are shown by green, orange and purple color and napin is shown in yellow.

Gel at pH 8: complementary experiments

Effect of longer gastric phase.

Interestingly, intestinal digestion of the pH 8 gel, performed after 12 h of gastric digestion with double concentration of pepsin (**Gas2x 12h)** (with partly re-compacted proteins at the starting point), resulted in the same level of re-compaction (to ***n*** ~3.3) but higher level of the subsequent unfolding (up to 36 Å, instead of 33 Å as for **Gas3.5h**) after 8.5 h (see **Figure A1.8**, **Appendix 1**).

Bile salts. We also got the information about the digestion without bile salts: it resulted primarily in similar re-compaction, however with not much variations in ξ (sinuosity of the 2nd step), compared to the digestion with bile. The final structures were less unfolded/disaggregated, reaching n of 2.9 and 35 Å instead of 2.5 and 36 Å (with bile) (see **Figure A1.9**, **Appendix 1**). Here again, the use of bile salts improved the intestinal digestion.

Bile salts peak. After addition of fresh intestinal enzymes, for both gels, we could see the appearance of a new SAXS feature - a small peak around q = 0.133 Å^{-1}, coming most likely from bile salts present in intestinal juice. At this digestion stage, the sample exhibited visually more-liquid state. The unveiling of this peak in liquid-like

sample may be due to their possible conjugation to some free amino acids, released into the after the protein hydrolysis and arrangement into some crystalline phases with long-range structural order. We could have observed well such bile peaks on the capillary scan after a 96 h intestinal digestion (**Figure A1.10**, **Appendix 1**), with its growth, starting from the most liquid sample and getting bigger in less digested *z* position. It suggests that, in the liquid digesta, bile salts can be too diluted to conjugate with free AA, while in deeper *z* positions, where their concentration is higher, and also the gel is sufficiently digested to release AA, bile can be able to conjugate with them.

Summary for intestinal digestion of the pH 8 gel

- Initially unfolded proteins of the pH 8 gel skipped the 1st unfolding step, observed for the initially more folded pH 11 gel.
- The next processes looked similar but of smaller amplitude of the re-compaction/unfolding.
- The final step (scission) was very similar for the two gels.
- The longer gastric step prior to intestinal digestion shortened the following intestinal digestion, through a more complete unfolding (as for the pH 11 gel)

4.2.3 Digestion at the large aggregates scale

Alongside the local conformational changes, we looked at the aggregates size range (above 100 nm), corresponding to the low *q* scattering. Both gels showed initially strong upturns towards lower *q*, with exponent close to 4, characterizing strongly aggregated and compact gels parts (see Chapter 3). **Figure 4.21** shows the variations of the best fit parameters describing large aggregates (a prefactor ***C***, an indicative correlation length Ξ (the real value is too large to be measured), and the exponent ***m***) for the pH 11 gel (as example), and **Figure 4.22** shows intensity and exponent *m* for the pH 11 (blue) and pH 8 (green) gels, for comparison.

Decrease of the intensity. During the intestinal digestion, a continuous low *q* intensity decrease was observed for both gels (**Figure 4.15** and **Figure 4.18**), with progressively slower rate. It could be attributed to a decrease in their specific area (by size growth) or/and number fraction (less aggregates of same size). To make the distinction, we need to determine the aggregates size, for which we have only an apparent value Ξ within this *q* range, suggesting actually their size growth (see **Figure 4.21** for the pH 11 gel).

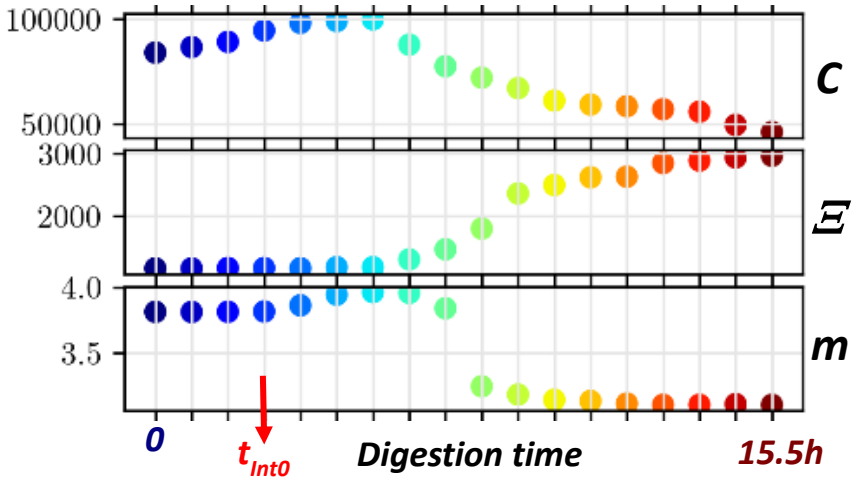

Figure 4.21 Variation of the low *q* parameters extracted from the fitting of the digestion kinetics curves with the two Lorentzian function for pH 11 gel. Each point represent one digestion curve at one *z* position of the capillary. Colors indicate the digestion time, up to 15.5 h of intestinal digestion.

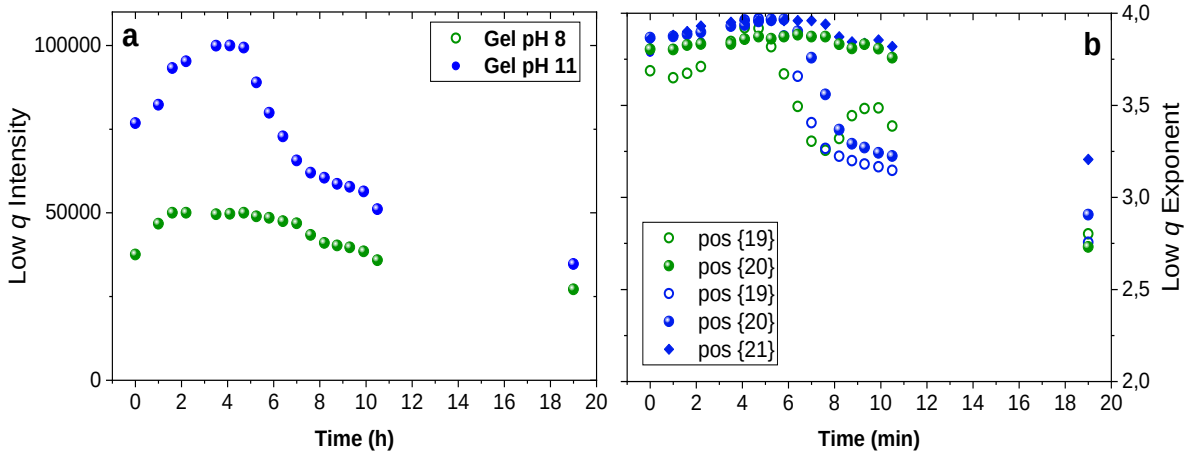

Figure 4.22 Variation of the low *q* parameters extracted from the fitting of the digestion kinetics curves with the two Lorentzian function, for pH 11 (blue points) and pH 8 (green points) gels. **a)** intensity factor ***C*** as a function of digestion time at one z position of the capillary. **b)** exponent ***m*** as a function of digestion time for different *z* positions (19 = closest to the gel surface, 20 and 21 with 150 μm interval).

Let us try to compare the two gels. For the pH 11 gel (initially scattering more), the reduction in low *q* intensity was, surprisingly, stronger: it dropped in total from 5700 to 70 cm^{-1} (by factor 80) at lowest *q* (0.002 $Å^{-1}$), to compare with a drop from 1570 to 90 cm^{-1} for the pH 8 gel. Moreover, we noted some important differences: the pH 8 gel's intensity decrease rate was lower and quasi-constant in time. It was especially visible for $0.006 < q < 0.02$ $Å^{-1}$, suggesting suppression of some intermediate-size aggregates. That could arise from the different level of protein unfolding. Since the aggregates of the pH 11 gel are composed of rather folded proteins, they could crosslink through less reactive protein sites, and be more easily dismantled than for pH 8 gel, where unfolded proteins have more linking opportunities. This would explain the slower decay for the pH 8 gel. Altogether, we could have quite different levels of heterogeneity, with initially different aggregates size and structure. These distributions would become more homogeneous at large digestion times.

Moreover, the degradation of large aggregates could be linked with the high *q* intensity increase observed during local protein structures unfolding and re-compaction steps: the digested protein fragments, released from the aggregates, would re-assemble

together into new structures. Indeed, this was observed only for the pH 11 gel. For the pH 8 gel, some middle-size aggregates could be re-formed, as seen in **Figure 4.18** (right hand side, *z* scans, $10^{-2} < q < 3\ 10^{-2}$ Å^{-1}, on turquoise curves). This could also restrain further deconstruction.

In summary, beyond the first glance, there may be large differences in aggregates of the two gels. This will be re-examined in Chapter 5, owing to neutron imaging and confocal microscopy results.

Decrease of exponent m. The second observation was the progressive change of the intensity power-law towards from around q^{-4} to a q^{-3} decay (**see Figure 4.22**), reflecting a loosening of the internal structure of the aggregates, i.e., objects of lower fractal dimension, with increased interfacial roughness. Here again, the decay of *m* for the pH 11 gel was faster compared to the one of pH 8 gel, for which a smoother initial variation of *m* occurred, followed by its stronger decrease.

For both gels, an addition of fresh pancreatic enzymes resulted in a general reduction of the scattering intensity (observed on **Figure 4.15** and **Figure 4.18**), showing an increased degradation of the less dense aggregates by more active enzymes. However, some signal coming from the aggregates was still present in the two gels after about 20 h of the gastro-intestinal digestion.

Only after very long digestion times (96 h), we reached a clear destruction of the protein aggregates. That was shown by a decrease of the scattering intensity, but also visually, by the liquid-like state of the digested samples (see **Figure A2.2**, **Appendix 2**).

A link with rheological properties of the gels. This has been discussed in the light of SANS data in section 4.1.3. Here, the different geometry of the sample limits the strength of the comparison, but the low *q* data are more provided with information. During intestinal digestion, the neat decrease observed in low *q* SAXS signal (degradation of the large aggregates) agrees with the neat progressive decrease of the viscoelastic moduli. In parallel, in gastric digestion, both the moduli and the low *q* SAXS

showed rather limited variations. We nevertheless evidenced, after closer look, some differences between the two gels (slight but opposite variation of the low *q* scattering).

4.1.1.3 Diffusivity: estimation from SAXS capillary scanning

The spatio-temporal SAXS measurements (on many (*z, t*) curves) allowed additionally estimating the diffusivity "activity" of digestive juice in the gel. The pH and enzyme concentration in a scanned volume was time dependent, by the temporal mass transfers of the digestive solution inside the gel. A very simplistic estimation of the diffusivity activity of enzymes could be obtained by assuming a Fickian diffusion in one dimension, described by:

$$D = (z_1 - z_2)^2 . \Delta t^{-1} \quad \textbf{(4.1)}$$

with z_1 being the depart position in the capillary and z_2 the position to which the digestive juice has diffused[7].

To estimate the rate of the digestive juice diffusion, we used two approaches:

In the first one, we regrouped pairs of superposing (z_1, t_1) and (z_2, t_2) curves, hence $\Delta t = t_2 - t_1$, and we found an example value of $\boldsymbol{D}$ **=1.29 10^{-11} m^2.s^{-1}** for gastric digestion, using **Equation 4.1**. This value for our 10% w/v gels is comparable to the literature values for pepsin diffusion coefficient in whey protein gels, i.e. D_{pepsin} = 1.9 10^{-11} m^2.s^{-1} for 15% w/v gel and D_{pepsin} = *1.2* 10^{-11} m^2.s^{-1} for 20% w/v gel[5]. As a matter of fact, since we have many (*z, t*) pairs, it would be necessary to develop an automatic routine to find superposing (*z, t*) pair curves. Therefore, the above value of *D* is not the real diffusion coefficient of the enzyme but only its rough estimation.

In the second approach, we focused on the variations at local scale, i.e. by looking at the variations with time *t* of the high *q* correlation length ξ (z_i, *t*) and exponent *n* (z_i, *t*) for different z_i positions. We observed that it was possible to translate the curves for

[7] Note that the chosen z_1 was not the real depart point of the gastric juice diffusion and the calculated diffusion coefficient was linked to the digestion state.

the different z_i along the abscissa t, by a value $\Delta t(z_i)$, which is the same for both $\xi(z_i, t)$ and $n(z_i, t)$. We used two ways:

1) linear translation: $t(z_i) = t_{real}(z_i) + \Delta t(z_i)$. The result was good until certain z values (not shown).
2) superposition in logarithmic scale leading, which gave a better master curve (see **Figure 4.23**).

Figure 4.24 presents the results of these calculations using **Equation 4.1**, with D values for pH 11 gel (triangles) and pH 8 gel (circles), as a function of the distance z_2.

We can see that diffusivity changes depending on the state of digestion: it is the highest when z_2 is close to the surface. The decrease in D can be due to i) the structural changes in the sample resulting from the digestion, e.g. a softer (more digested) gel easier to diffuse in, and ii) aging and therefore decreased enzymatic activity for longer digestion time (hence with a gradient decrease downward the capillary). However, since the estimated enzymatic diffusion is measured through the digestion reaction, we cannot decouple the changes of structure and enzymatic activity. We assume that both factors are influencing the resulting diffusivity.

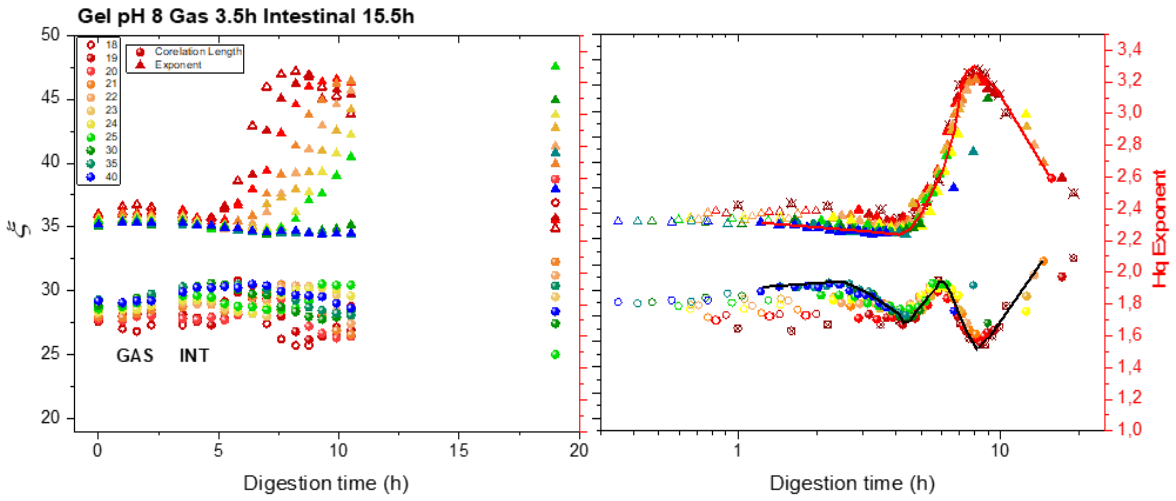

Figure 4.23 High q fitting parameters, $\xi(z_i)$(circles) and $n(z_i)$ (triangles) as a function of digestion time (3.5 h gastric and 15.5 h intestinal) for pH 8 gel (**left**) and different z_i positions. Same data after a horizontal translation on logarithmic scale (**right**).

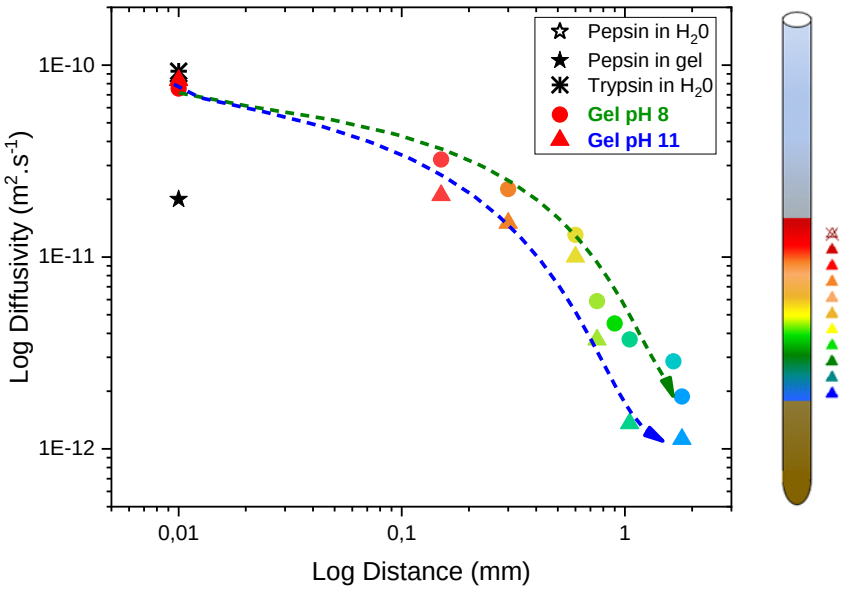

Figure 4.24 Diffusivity of gastro-intestinal juices (pepsin and pancreatic enzymes) as function of the distance from z_1 ("at" the surface of the initial gel) to z_2 positions in the capillary (denoted by different colors, as indicated on the capillary scheme) for the pH 11 gel (triangles) and the pH 8 gel (circles). The solid lines are guides for eyes. The values of pepsin in H_2O and in gel (red stars) are literature values from [5] and trypsin in H_2O from [6] (black star).

The diffusivity curves for the two gels are rather similar. In the upper part of the capillary (most digested gels), the diffusivity is around 8 $x10^{-11}$ $m^2.s^{-1}$, resembling the value of pepsin in water (red star in **Figure 4.24**) and being below the value for trypsin in water (black star). These high values of *D* indicate the liquid state of those most digested parts of the samples. The initial microstructure of the gel slightly affected the enzymatic diffusion: for pH 8 gel, in which proteins were already unfolded before digestion, diffusivity "activity" values are larger than for the pH 11 gel, in which proteins were more globular. Similar observations were shown for milk protein gels: pepsin diffusion was dependent on the crosslinking density and microstructure and affected the digestion rate[57].

To end this part, let us comment about the logarithmic superposition: it can just be a "trick" because it allows a better superposition. It may also open new points of view, which will not be developed here, but the object of modeling efforts by E. Lutton et al.

Meanwhile, on the experimental side, future prospects of the work on enzymatic diffusion could be focused on trials to separate the effects of changes in structure and enzymatic activity.

4.3 Secondary structures: Wide-Angle X-Ray Scattering (WAXS)

Besides exploring the range of protein molecules, we also monitored the lower length scales (higher *q*, from 0.2 $Å^{-1}$ to 2 $Å^{-1}$), which correspond to intramolecular distances inside the protein structure, including secondary structures. **Figure 4.25** shows changes induced by long gastro-intestinal digestion of the pH 8 gel (Gas30h Int96h), from the least digested part in the capillary (purple) to the most digested one (pink). In this *q* range, most of the structural information in the scattering data appears in the form of low intensity oscillations, with the *q*-values of their maxima which could correspond to correlation distances (mean nearest-neighbor distances between/within proteins). Indeed, as shown in chapter 3, due to the heat-gelation, the canola protein solution at pH 8 lost already some oscillations at 0.31 and 0.4 $Å^{-1}$ and most of the distinction for the 0.52 and 0.7 $Å^{-1}$ (see **Figure 3.14**) coming from the cruciferin's form factor and different secondary structures, respectively[8,9,10,11].

Some typical values found in the literature of the correlation peak positions and their possible structural origins, are presented in **Table 4.2.**

Table 4.2 Correlation peak positions and corresponding distances in secondary structures of proteins.

Peak position ***q*** *($Å^{-1}$)*	***Distance*** ***d*** *(Å)*	***Structural origin***
0.52	12.1	Protein submaxima/ Interactions between α-helices[10,]
0.6	**10.5**	**Diameter (α-helices center-to-center)**[12]
0.69	9.1	Secondary structures/β-sheets (9.08 Å)[11]
0.8	7.9	*d* between atoms in secondary structures[8,11]
	7	Pleat distance (2 residue separation)[12]
	5.4	Pitch (distance between turns in α-helix; 3.6 AA)[12]
1.34	**4.7**	**Strand-to-strand distance (in β-sheets)** [11,12]

In the digested **pH 8 sample**, we could have distinguished two correlation oscillations, at 0.6 and 1.34 $Å^{-1}$. Based on these characteristic lengths and the literature data, we suggest that the oscillations originate from α-helices (precisely center-to-center distance) and β-sheets (strand-to-strand distance)[12].

The gradual disappearance of those oscillations in more digested capillary parts (**Figure 4.25**, marked by the arrow) can correspond to the disruption of those secondary structures. Suppression of peak at 0.6 $Å^{-1}$ (helices) occurred earlier in the digestion than suppression of the maximum at 1.34 $Å^{-1}$ (strands). We can deduce that α-helices are less resistant to the digestion than β-sheets. The latter were indeed described as more stable structures[13]. Moreover trypsin does not preferentially cleave peptide bonds with proline residues (-Arg-Pro- and -Lys-Pro-), making them more resistant to proteolysis[14]. In addition, Pro are not likely found in α-helices (due to steric hindrance), whereas β-strands are composed of Pro and Gly. From the literature[15], we know that a higher percentage of β-sheet is not favourable for *in vitro* digestibility.

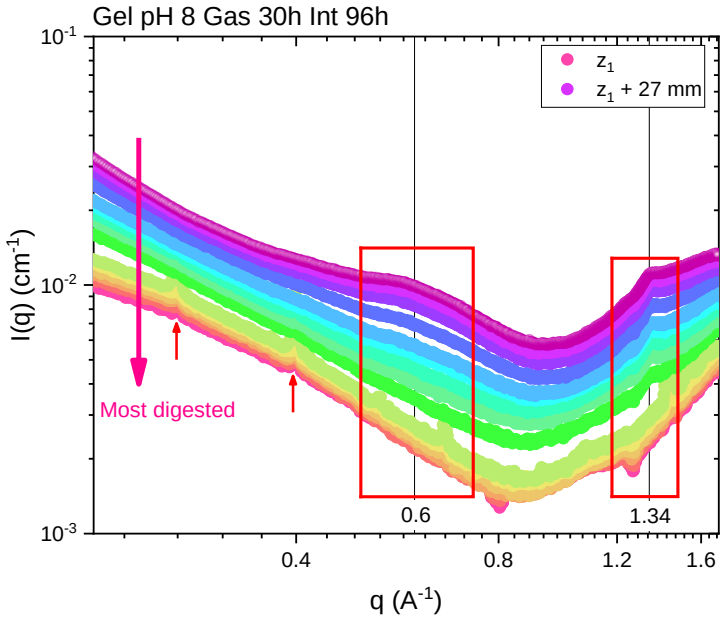

Figure 4.25 WAXS spectra for the pH 8 gel digested for 30 h in gastric and 96 h in intestinal conditions. The colors designate different z positions on the capillary, corresponding to the digestion state: from purple (least digested, z_1 = gel's surface) to pink (most digested, 27 mm downward the capillary). The pink arrow indicates the digestion progress. The oscillations are marked by red frames. 2 red arrows (at 0.23 and 0.4 $Å^{-1}$) point at the bile salt peaks.

Interestingly, the onset of the changes in secondary structures (suppression of the peak at 0.6 $Å^{-1}$) coincided with the **onset of the re-compaction step** observed in SAXS (see **Figure 4.26b**, blue curve and **Figure 4.27**). This suggests that during the **re-compaction** step, α-helices got disrupted by enzymatic scission. The fluorescence spectra on protein solutions showed an exposure of tryptophan residues to the solvent during intestinal digestion attributed to its release from the protein structures after enzymatic cleavage (not shown). This favors the hypothesis of enzymatic scission leading to the disruption of helices in this digestion step. Concerning the β-sheet oscillation (the peak at 1.34 $Å^{-1}$), their disappearance occurred afterwards, simultaneously with the **unfolding-disaggregation step**.

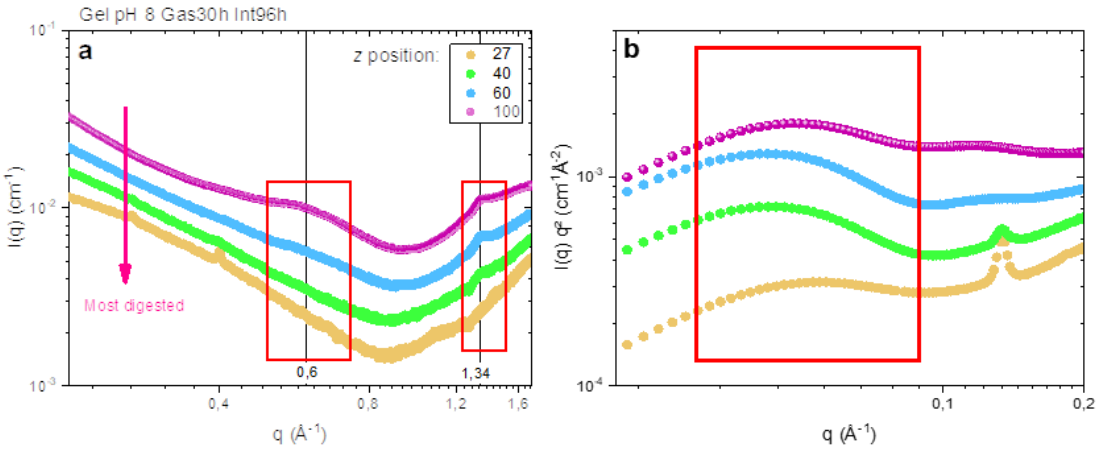

Figure 4.26 a) Chosen WAXS spectra of pH 8 gel digested for 30 h in gastric then for 96 h in intestinal conditions. Colors indicate the state of digestion, from the least (purple) to the most digested (closest to the initial gel's surface; light yellow); interval between 1 z position is 300 µm. The arrow shows the digestion progression, for clarity. The two oscillations (at 0.6 and 1.34 $Å^{-1}$) are marked inside red frames. **b)** the lower *q* data in Kratky representation (corresponding to the conformation of proteins).

Looking at the digested **pH 11 gel**, we remarked the same oscillations at 0.6 $Å^{-1}$ (α-helices) and 1.34 $Å^{-1}$ (β-sheets) in the least digested parts in the capillary (**Figure 4.27**). As for the digested pH 8 gel, their disappearance was progressing along the digestion, with the earlier suppression of helices compared to sheets. It also occurred during the re-compaction of the protein structures (dark blue curve, **Figure 4.28**).

In both digested samples (but more visibly in the pH 11 gel), we noted the appearances of one peak at 0.4 $Å^{-1}$ and around 0.23 $Å^{-1}$. Those peaks are identified as coming from bile salts (described in 4.2.2.1), and we can similarly observe their growth upon digestion - interestingly, it coincides with a vanishing of the second oscillation (at 1.34 $Å^{-1}$) and appearance of more such peaks (**Figure 4.28**, dark yellow curve). This can indicate binding of the bile to protein fragments/free amino acids, released after digestion, and formation of different-sized phases.

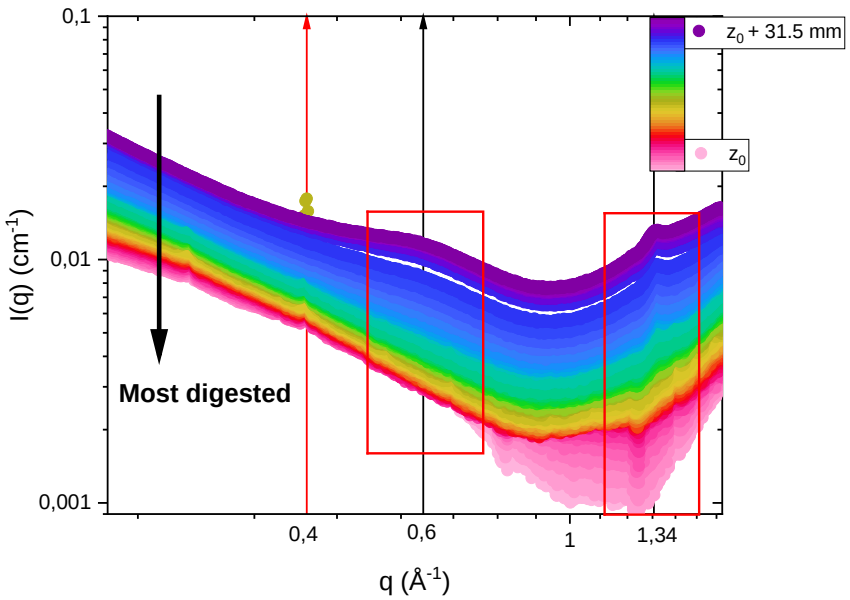

Figure 4.27 WAXS spectra of pH 11 gel digested for 30 h in gastric then for 96 h in intestinal conditions. Colors indicate the state of digestion, from the least digested (purple) to the most digested (light pink). The arrow shows the digestion progression, for clarity. The oscillations are localized inside red frames.

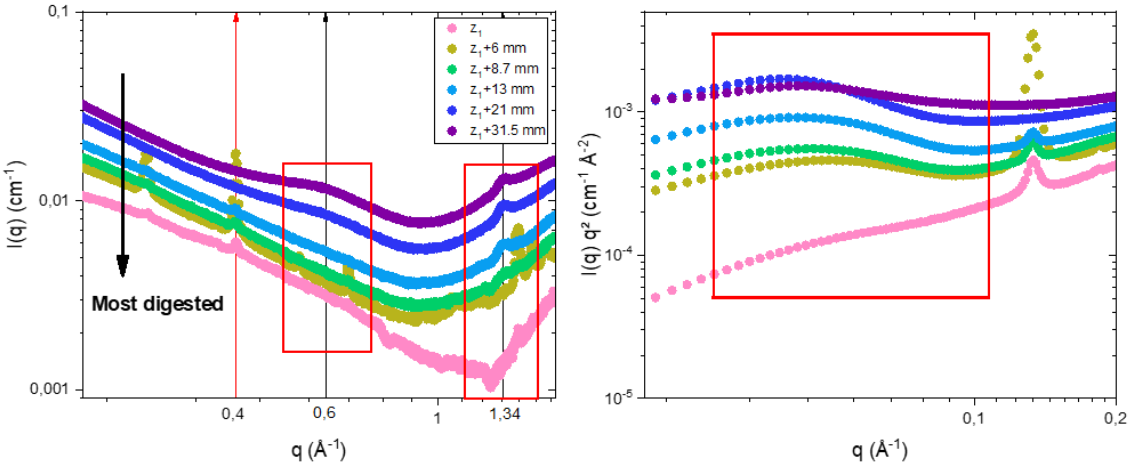

Figure 4.28 WAXS spectra of pH 11 gel digested for 30 h in gastric then for 96 h in intestinal conditions. Colors indicate the state of digestion, from the least (purple) to the most digested (closest to the initial gel's surface; light yellow); interval between z positions is 300 µm. **Left)** The arrow shows the digestion progression, for clarity. The two oscillations (at 0.6 and 1.34 $Å^{-1}$) are marked inside the red frames. **Right)** the same measurements showed in lower *q* (corresponding to the conformation of proteins).

Summary WAXS

- In both pH gels, we have distinguished two oscillations, at 0.6 and 1.34 $Å^{-1}$, identified as originating from α-helices and β-sheets correlation distances.
- The gradual disappearance of those oscillations upon digestion likely corresponds to the disruption of those protein secondary structures.
- Disruption of α-helices occurred earlier than of β-sheets, suggesting the higher resistance of β-sheets towards proteolysis.
- Suppressions of α-helices and β-sheets coincided with the re-compaction and unfolding-disaggregation steps observed in SAXS, respectively.

4.4 Summary and final remarks

Synchrotron SAXS allowed precise monitoring of structures of canola protein gels during *in situ* gastro-intestinal digestion, inside capillary cells, i.e., with 1D enzymatic diffusion without flow or agitation.

Compared to the rheology-SANS protocol, with 3D enzymatic diffusion, being closer to *in vivo* conditions, digestion of the gels was slower. A strong intestinal digestion effect, i.e. the proteins re-compaction and degradation of their aggregates, appeared in about 3 hours (with 30 min of preceding gastric digestion) to compare with 5 min for SANS.

Despite these differences, we found indisputable similarities in the protein conformational evolutions. (ξ, n, intensity) diagrams allowed direct visualization of sizes and shapes of the proteins. SAXS complemented and confirmed the main digestion steps observed by SANS, with much more detailed and precise manner. Digestion in capillary eliminated the difficulties in the analysis of the SANS intensities, because of the uncertainties of the sample volume, caused by erosion during intestinal digestion of the gels. Even though the capillary conditions are not the *in vivo* ones, they allow an access to the complexity of the digestion processes unattainable previously (especially the multistep intestinal digestion).

One main result is that tuning the initial canola protein structure, through the choice of the solvent pH during the gel preparation (see Chapter 3) had a significant effect during digestion:

- For initially folded structures (pH 11 gel), gastric digestion initiated unfolding, certainly useful to the further enzymatic action.
- For both gels, the unfolding dominated also the first step of the subsequent intestinal digestion, until being sufficient for the best enzymatic scission.

We evidenced that deconstructions paths are not obligatorily the simplest ones, nor, apparently, the most efficient. E.g., for the pH 8 gel, in which the very first unfolding step was achieved before initiating the digestion, the already unfolded proteins

experienced an opposite trend in gastric conditions, i.e. a slight compaction. This seems contradictory to the digestion facilitation. In addition, the observed further re-compaction of the unfolded structures appeared to be the effect of contraction of the fragments from readily cleaved proteins into denser local structures. This effect seems, again, contradictory to a simple digestion path, since it creates additional effort to dismantle those structures before their final/further cleavage. Nevertheless, this step was repeatedly seen during all intestinal experiments.

We could expect that the initial differences in unfolding are waved out by the subsequent intestinal digestion, but this is true only in part. In the unfolded case, the intestinal process was less complex, since unfolding and strong local aggregation were skipped during the re-compaction step. This resulted in reaching faster the more extended structures, which were then more readily cut into small fragments when fresh enzymes were added.

Due to this complexity, alternative situations of digestion were useful to study, and that is one richness of this work. They may occur in real human life. As a first example, let us quote the case when fresh enzymes were added after already long digestion. This improved the final intestinal efficiency through the ability of the enzymes to better penetrate the interior of the gel network and cleave the unfolded protein fragments.

Another alternate situation is the very long gastric digestion time (96 h with renewed enzymes): although gastric digestion had clearly much lower effectivity, we could reach digestion states similar to the result of 15 h-intestinal digestion. It is also clear that a double concentration of pepsin helped in stronger digestion effects for both gels. All this reassures us about the activity of the digestive enzymes.

It was also interesting to validate that the absence of bile salts reduced the rate of intestinal digestion (although no lipids were involved).

On the large/medium aggregates scales (low q), gastric digestion induced a slight intensity decrease for the unfolded-protein gel, and, on the contrary, a slight increase for the folded-protein gel. This observation could be linked with the gastric-induced

increase of the moduli of this gel. Intestinal juice had a more powerful effect on the aggregate degradation, compared to the gastric juice, suggesting that the aggregates degradation could be responsible for a decrease of the elastic modulus during the intestinal digestion. Surprisingly, faster degradation was achieved for the more aggregated, folded-protein gel, seen in SAXS. We propose that it might be due to differences in connectivity between the aggregates, possibly related to the differences in their protein unfolding and reactive sites accessibility for the crosslinking.

Additional estimation of the diffusivity of the digestive juice gave similar values between the two pH gels (slightly higher for the gel with initially unfolded proteins). An example value for gastric juice was found to be of 1.29 10^{-11} $m^2.s^{-1}$.

Exploration of the wider *q* range enabled identification of additional features of the canola protein gels structures, namely intramolecular secondary structure distances, and their alterations during gastro-intestinal digestion. However, monitoring of those structures by WAXS remains challenging and requires better procedures for background subtraction.

The main application of this work is the understanding that, by modulating the initial conformation of proteins, one can influence the process and kinetics of their gastrointestinal digestion. Hence, the initial state of food (here proteins) could be adapted to the variations of pH and enzyme activities, characteristics of each individual.

References

[1] Napieraj, M., Brûlet, A., Lutton, E., Randrianarisoa, U., Boire, A., Boué, F. (2022). Monitoring food structure in plant protein gels during digestion: Rheometry and Small Angle Neutron Scattering studies. *Food structure,* 32, 100270. doi: 10.1016/j.foostr.2022.100270.

[2] Napieraj, M., Brûlet, A., Lutton, E., Perez, J., Boué F. Understanding digestion of protein gel using synchrotron X-Ray Scattering, submitted *to Food Hydrocolloids, Short Communications*, March 2023.

[3] Calmettes, P. et al. (1993). How random is a highly denatured protein? *Biophysical Chemistry,* 53, 105-114. doi: 10.1016/0301-4622(94)00081-6.

[4] Santos-Hernández, M., Miralles, M., Amigo, L., Recio, I. (2018). Intestinal Signaling of Proteins and Digestion-Derived Products Relevant to Satiety. *Journal of Agricultural and Food Chemistry*, 66 (39), 10123-10131. doi: 10.1021/acs.jafc.8b02355.

[5] Luo, Q., Borst, W.J., Westphal, A.H., Boom, R.M. et Janssen, A.E.M. (2017). Pepsin diffusivity in whey protein gels and its effect on gastric digestion. *Food Hydrocolloids*, 66, 318-325. doi: 10.1016/j.foodhyd.2016.11.046.

[6] Squire, P.G., Himmel, M.E. (1979). Hydrodynamics and protein hydration. *Archives of Biochemistry and Biophysics*, 196 (1), 165-77.

[7] Thévenot, J., Cauty, C., Legland, D., Dupont, D., & Floury, J. (2017). Pepsin diffusion in dairy gels depends on casein concentration and microstructure. *Food Chemistry*, 223, 54-61. doi: 1016/j.foodchem.2016.12.014.

[8] Hirai, M., Iwase, H., Hayakawa, T., Miura, K. & Inoue, K. (2002). Structural hierarchy of several proteins observed by wide-angle solution scattering. *J. Synchrotron Radiat*., 9, 202–205.

[9] Makowski, L. et al. (2008). Molecular crowding inhibits intramolecular breathing motions in proteins. *J. Mol. Biol*., 375, 529–546.

[10] Phan-Xuan, T., Bogdanova, E., Millqvist Fureby, A., Fransson, J., Terry, A.E., Kocherbitov, V. (2020). Hydration-Induced Structural Changes in the Solid State of Protein: A SAXS/WAXS Study on Lysozyme. *Molecular Pharmaceutics*, 8, 17 (9), 3246-3258. doi: 10.1021/acs.molpharmaceut.0c00351.

[11] Chelvanayagam, G., Knecht, L., Jenny, T., Benner, S., Gonnet, G. (1998). A combinatorial distance-constraint approach to predicting protein tertiary models from known secondary structure. *Folding and Design*, 3 (3) 149-160. doi: 10.1016/S1359-0278(98)00023-6.

[12] Makowski, L. (2010). WAXS – going beyond SAXS. Northeastern University Boston. https://www.embl-hamburg.de/biosaxs/courses/embo2010/slides/waxs-makowski.pdf.

[13] Henzler Wildman, K.A., Lee, D.K., Ramamoorthy, A. (2002). Determination of alpha-helix and beta-sheet stability in the solid state: a solid-state NMR investigation of poly(L-alanine). *Biopolymers*, 15, 64 (5), 246-54. doi: 10.1002/bip.10180.

[14] Savoie, L., Charbonneau, R., Parent, G. (1989). In vitro amino acid digestibility of food proteins as measured by the digestion cell technique. *Plant Foods for Human Nutrition*, 39 (1), 93-107. doi: 10.1007/BF01092406.

[15] Bai, M., Qin, G., Sun, Z., Long, G. (2016). Relationship between Molecular Structure Characteristics of Feed Proteins and Protein In vitro Digestibility and Solubility. *Asian-Australas J Anim Sci*., 29 (8), 1159-65. doi: 10.5713/ajas.15.0701.

Chapter 5 Imaging of gastrointestinal digestion of canola protein gels at micrometer scale

---

In Chapter 4, we focused on the accessible q range by SANS/SAXS, from 2 10^{-3} to 0.3 $Å^{-1}$, to study the evolution of proteins and aggregates structures during digestion. Those kinetic experiments combined with the high flux of synchrotron gave a large amount of data and their treatments and analysis required a lot of efforts and time. Yet, we did not attain the information on the sizes of very large aggregates forming the gels. On the synchrotron beam lines, it is possible to cover a broad q range and reach small q values down to 10^{-3} $Å^{-1}$, if the experiments are performed in several instrument configurations, as shown in **Figure 5.1**, with the SAXS spectra for the initial canola protein gels. However, q of 10^{-3} $Å^{-1}$ was not small enough to investigate size range of our gels' aggregates (>0.1 micron): the slopes of the SAXS curves are about -4 for the two gels; they do not tend to a plateau. Access to larger length scales (USAXS) has not been possible.

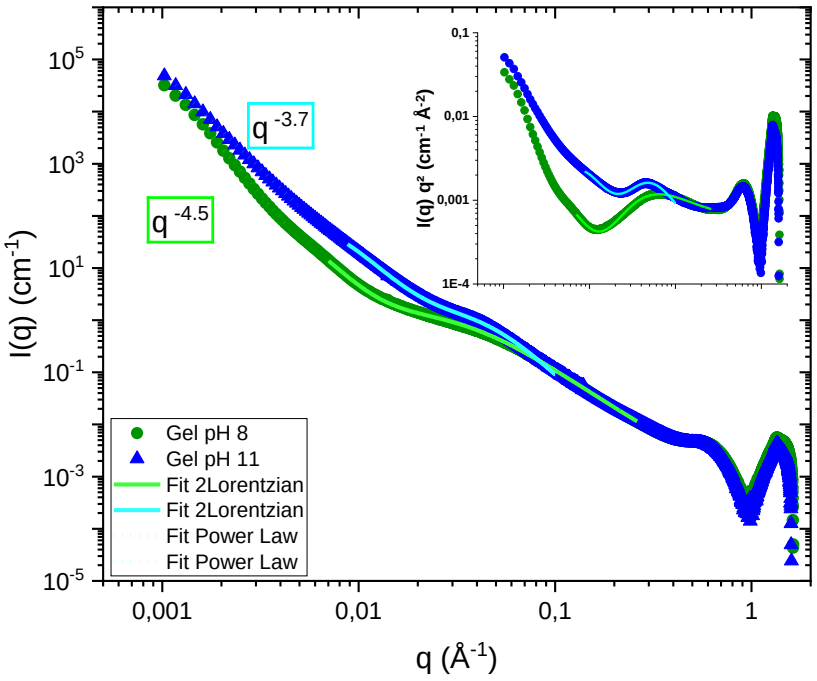

Figure 5.1 SAXS spectra of the pH 8 gel (green) and the pH 11 gel (blue) before digestion. They naturally superimpose on a wide *q* range. The solid lines represent the 2 Lorentzian function fits (see Chapter 4) describing the local protein structure. The dashed lines are the power low fits in the low *q* curves describing larger aggregates.

Information at the micron scale were obtained in this thesis through imaging techniques, upon simulated gastric and intestinal conditions, which we will present in this chapter:

- Neutron Scattering Imaging and confocal fluorescence imaging gave us information about sizes and shapes of the micron-sized protein aggregates after different digestion steps.
- Synchrotron UV-fluorescence imaging allowed the *in situ* monitoring of 100-200 µm gel pieces during digestion.

5.1. Neutron Dark-Field Imaging

Figure 5.2 presents images of different protein gels (c=100 g/L): two from canola (on the top) and from potato and milk (on the bottom). On the right-hand side, we can see their corresponding dark field images (DFI) on the grey scale, measured for one (from 15) sample-to-grating distance (corresponding to the q vector and so the correlation length ξ). A darker image (canola protein gel prepared at pH 8) corresponds to a larger scattering at this q, leading to stronger loss of intensity, much stronger than for the other samples. This canola gel must contain larger volume fractions of micron-size scattering objects, compared to the rest[a].

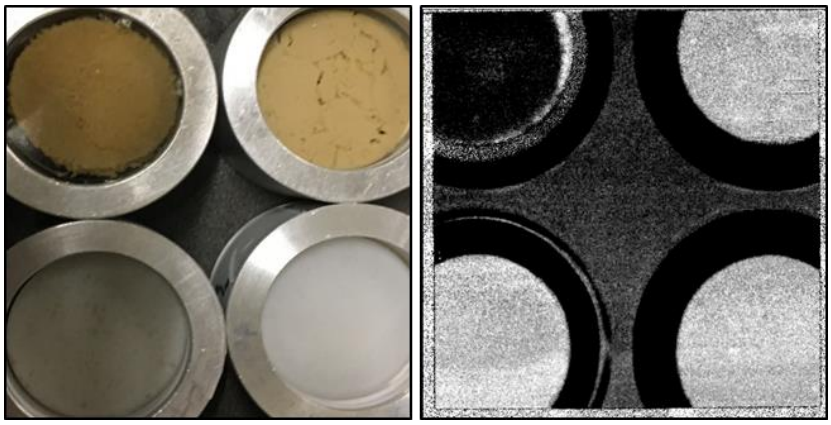

Figure 5.2 Left) Images of 4 different protein gels (100g/L) in circular cells (∅40 mm); top - canola gels, bottom left- potato, bottom right - milk. **Right**) Corresponding Dark Field Images measured at the same gratings distance (corresponding to one value of q).

5.1.1 pH 8 and pH 11 gels before digestion

Differences in protein conformations, arising from the sample's preparation pH, coupled with the heat treatment, could likely affect the size and internal structure of the large-size protein aggregates, contributing to the DFI contrast. Indeed, more non-covalent interactions between the unfolded protein regions, plus additional attraction

[a] Skim milk (no fat droplets) contains 0.1 μm size casein micelles, see Ref. Kim, Y., Valsecchi, J., Oh, O., Kim, J., Lee, S.W., Boué, F., Lutton, E., Busi, M., Christopher, G., Strobl, M. (2022). Quantitative neutron dark-field imaging of milk – a feasibility study. *Applied Sciences*, 12(2), 833. doi: 10.3390/app12020833.

between napin and cruciferin at pH 8, could lead to formation and growth of differently-structured aggregates, than ones formed by the folded proteins at pH 11. On **Figure 5.3** we can compare the DFI signal of the canola protein gels prepared at pH 8 and pH 11 before digestion:the DFI contrast of the pH 11 gel was lower.. This was observed in successive sessions of measurements on ICON beamline in PSI. Since the concentration of proteins in the two gels before digestion was the same, depending on what the DFI scattering contrast originates from, the sample would exhibit a stronger DFI contrast if composed of bigger aggregates, or inversely, pores between them, which directly relates to a larger volume fraction.

In rheology, we have observed that the modulus of the pH 8 gel was lower than the one of the pH 11. This means that the micrometric aggregate size of these gels is not the most important parameter governing their elastic properties. Much probably, as noted in Chapter 4, the local unfolded conformations of the proteins in the pH 8 gel and the folded ones in the pH 11 gel can explain the differences between the moduli.

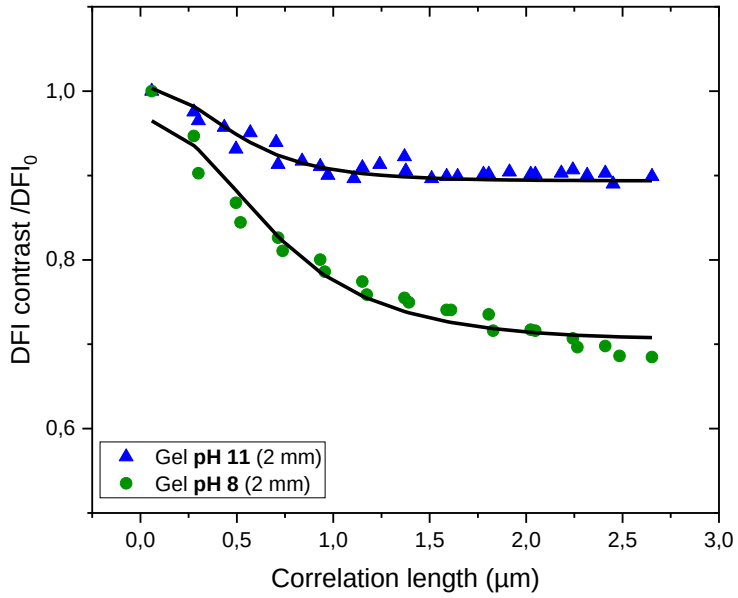

Figure 5.3 Dark Field Imaging (DFI) contrast as a function of correlation length ξ for canola protein gels (100g/L) at pH 8 (**green**) and pH 11 (**blue**), with 2 mm thickness; solid lines are fits by projected real-space correlation functions of the polydisperse hard-sphere model for protein aggregates.

5.1.2 pH 8 gel after digestion

Figure 5.4a presents Dark Field Imaging (DFI) signal as a function of the correlation length ξ for canola gels prepared at pH 8 after gastric and gastro-intestinal digestion. The black curve corresponds to the **gel before digestion**: it is described by relatively high DFI contrast (i.e. loss of amplitude of the interferometer fringes) in the observed ξ range, decreasing to a plateau for larger ξ values. This plateau corresponds to the total scattering cross section; it is low due to the presence of larger volume fractions and/or larger sizes of some scattering objects.

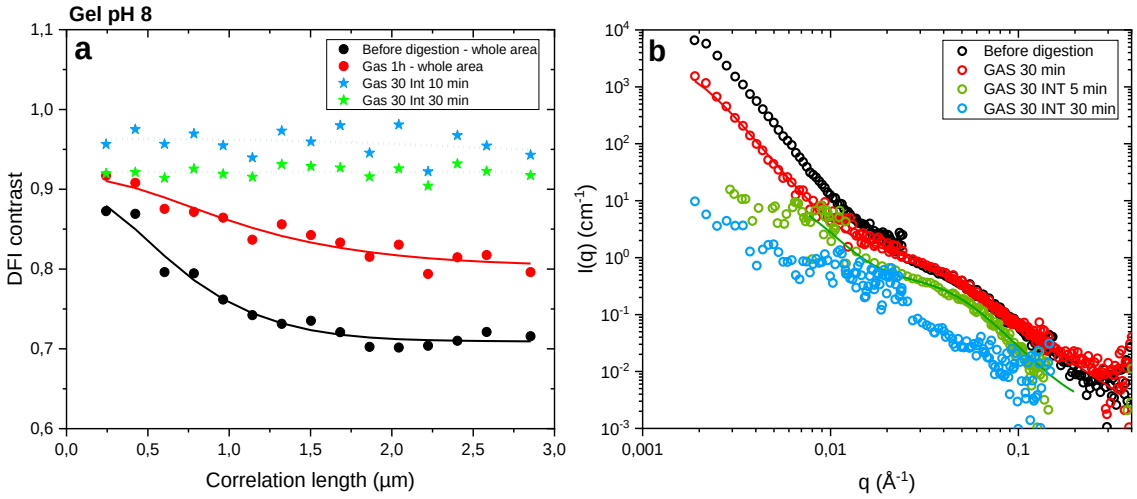

Figure 5.4 a) Dark Field Imaging (DFI) signal, averaged over the whole imaged sample area, as a function of correlation length ξ for canola gels prepared at pH 8 (with 1 mm sample thickness); before digestion (black), after 30 min of gastric digestion (red) and after gastric 30 min plus intestinal digestion 10 min (green) and 30 min (blue); solid lines are the hard-sphere fits. **b**) SANS of the same types of canola protein gels before digestion (black), after 30 min of gastric digestion (red), followed by 5 min (green) or 30 min (blue) of intestinal digestion, for analogy.

The ξ value at which the curve starts to rejoin the plateau is grossly the characteristic size, here around 1-2 µm. The curve's decrease is here not very steep, with rather an extended bending region, suggesting an important polydispersity (see below for quantitative values).

For the red curve, corresponding to the gel **after 30 min in gastric conditions**, the drop in DFI has already visually decreased in magnitude, with a slower decay, indicating a decreased volume/number fraction (concentration) or/and size of the scattering objects. This is expected for the digested sample.

After **10 min** of the subsequent **intestinal digestion** (green curve), the DFI (ξ) became almost completely flat, representing a fast vanishing of the low angle scattering from the protein aggregates in intestinal juice. Such a curve can also be read as a homogenization of the network, resulting from the aggregates dismantling and their reduction to smaller-size objects, or their lower concentration. This effect was even more pronounced after **30 min** of intestinal digestion (blue curve). In fact, the accuracy of the measurements was here too weak to definitely quantify any differences.

Such vanishing of the DFI decay upon digestion can be related to the decrease of the low *q* SANS, which was observed after digestion of the same gels with applying the same digestion protocol (see **Figure 5.4b**, with the same colors representing gastric and gastro-intestinal steps). As observed repeatedly in successive ICON sessions, intestinal digestion was very powerful in large aggregates degradation. The aggregates size and/or their number were already too small to be detectable in the ξ range probed by the neutron DFI technique.

5.1.3 Fitting DFI (ξ) curves: pH 8 and pH 11 gels after gastric digestion

We assumed the scattering objects in the gels to be spherical (form factor of spheres) interacting aggregates (structure factor of hard spheres). Thus, in order to obtain their sizes, we fitted the DFI(ξ) curves with a hard-sphere model[1], taking in account a size distribution, which improved the quality of the fits. The lines on **Figure 5.5a** represent the best fits and the resulting radii distributions of the spheres are shown in **Figure 5.5b**. Mean sizes and widths of the log-normal radii distributions are reported in **Table 5.1**.

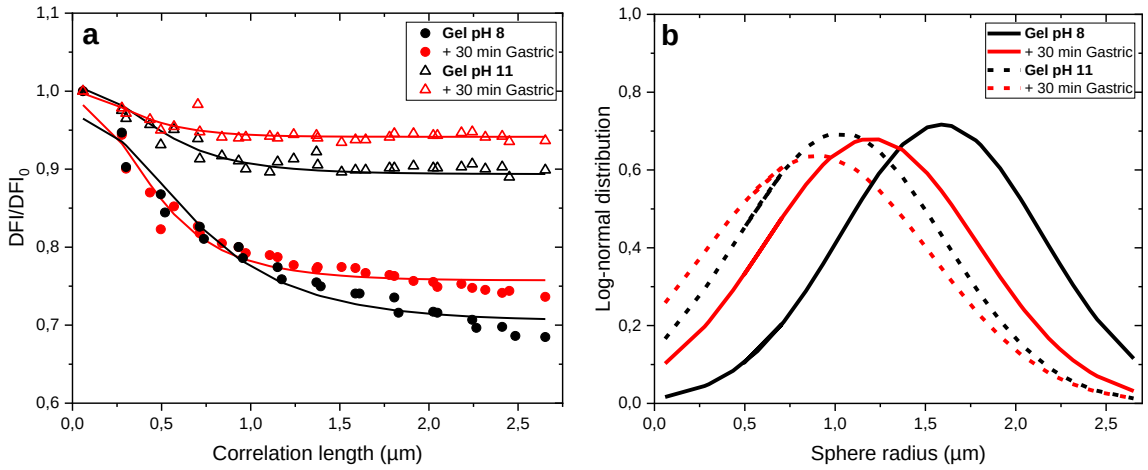

Figure 5.5 a) DFI contrast as a function of correlation length for canola protein gels (with 2 mm sample thickness), prepared at pH 8 (circles) and pH 11 (triangles); before digestion (black) and after 30 min of gastric digestion (red); solid lines represent fits by projected real-space correlation functions of the polydisperse hard-sphere model for protein aggregates. **b**) log-normal distribution of the spherical radii of the protein aggregates (radius width), derived from the fits in **a)**, with solid lines for the pH 8 and dashed lines for the pH 11 gel.

Table 5.1 Fitting parameters derived from polydisperse hard-sphere model for canola protein gel samples. Sample thickness was of 2 mm.

Sample	***Background***	***Scale***	***Radius (µm)***	***Radius width (µm)***
pH 8 no digestion	0.7	1.3	1.58	0.35
pH 8 Gas 30 min	0.7	0.8	1.20	0.49
pH 11 no digestion	0.9	0.3	1.03	0.56
pH 11 Gas 30 min	0.9	0.1	0.90	0.70

The fitting results show that i) the aggregates of the pH 8 gel were initially larger (~1.58 µm) compared to the pH 11 sample (~1.03 µm), and ii) the gastric digestion provoked a decrease of the aggregates size of the two gels. As a matter of fact, the aggregates size of the pH 8 gel decreased after 30 min of gastric digestion to ~1.2 µm, i.e. by 25% while for the pH 11 gel, they were initially smaller, but decreased only slightly to ~0.9 µm, by 12.5 %. This could be compared to the observations from rheology and SAXS, where the pH 11 gel was more resistant to gastric digestion than the pH 8 gel. However, one must stay careful in conclusions due to a clear lack of accuracy in this matter.

5.2 Confocal Fluorescence Imaging

Confocal Laser Scanning Microscopy (CLSM) was used to also explore the microstructures of the canola protein gels (pH 8 and pH 11) upon gastric and intestinal digestion. Images of the gels at initial states, after 30 min gastric and after additional 30 min of intestinal digestion are shown in **Figure 5.6** (with 20x objective) and **Figure 5.7** (with 63x and 100x objective). Those images were chosen as the most representative for each sample.

As can be noted from these figures, the microstructures of both canola gels resemble, in some extend, a microphase separation with rather dense regions of spherical-like protein aggregates/agglomerates (identified as intensely fluorescent areas, proportional to the protein concentration). Therefore, the previous assumption of a distribution of spherical aggregates, giving the origin of the DFI contrast, was justified. Within the chosen intensity scale[b], what can be clearly observed **before digestion** is the existence of the small, point-like aggregates, of sizes around 1 μm, which we will call "micronic aggregates", connected within the network. The question arises of how exactly these aggregates are connected, which is an issue when the gel modulus is concerned. To help to answer this question, 3D imaging trials were performed, but unfortunately, their detailed analysis, allowing the information about the aggregates connectivity, requires more work. It therefore stays as a perspective work.

[b] The darker regions may appear more illuminated when adjusting the intensity contrast. It is therefore difficult to conclude that they do not contain non-aggregated proteins, arranged as in a solution (which emits a diffuse light all over the picture frame).

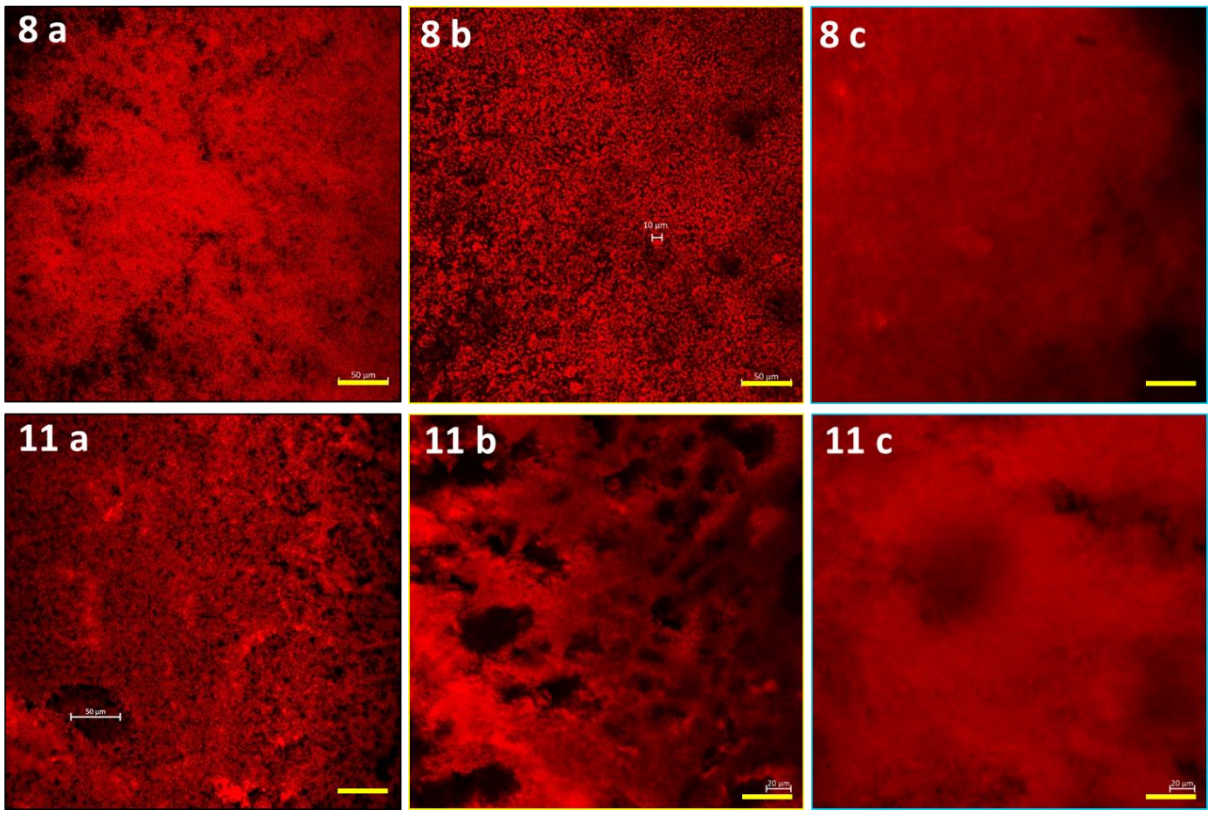

Figure 5.6 CLSM images of heat-set canola protein gels (c=100 g/L), at pH 8 (upper row) and pH 11 (down row); **a**) in the initial state, **b**) after 30 min of gastric digestion and **c**) adding 30 min of intestinal step. The yellow scale bar on the images width of the image is 50 µm. Taken with 20x objective.

pH 8 gel. Let us go into more detail, starting by the pH 8 gel. In the initial state, it shows a very dense assembly of small spheres, covering all the space (see **Figure 5.6a**). Those structures of a few pixels (1-2 µm size) can be better seen in **Figure 5.7a**. Such sizes confirms the trends obtained from DFI curves fittings.

Upon gastric digestion, more areas of lower fluorescence with some larger holes (dark areas with less protein content) appeared, giving a clear effect that the assembly of micronic aggregates was less dense: the strongly fluorescent points can be easily separated by eye, due to more numerous and wider dark spaces in between them. The measurements at the smaller length scales (**Figure 5.7b**) are easier to analyze: we can see the effect of gastric digestion through a decrease of the concentration of the micronic aggregates, resulting in a structure containing smaller-size, point-like aggregates, sometimes agglomerated inside some larger "islands" (of lower fluorescence intensity). The background fluorescence signal between the

distinguishable aggregates and aggregates "islands" seems to be more intense, compared to the state before digestion, as if it contained a larger amount of proteins/protein residues, diffused outwards the digested aggregates. Gastric digestion provoked some disconnection between the aggregates, which could explain, in the framework of gel elasticity, the observed slight decrease of the gel modulus in gastric conditions (see Chapter 4). On the image at x100 scale (**Figure 5.7c**), we can more precisely see the shapes of the separated micronic aggregates, which seem to be slightly bigger than on the 63x scale. One needs to keep in mind that we could be in a particular region of the gel, not representing the whole aspect of the sample.

pH 11 gel. The initial structure of the pH 11 gel (**Figure 5.6a**) seems to rely upon smaller point-like aggregates, with some stronger fluorescing (i.e. more aggregated) regions and low fluorescing holes, both having sizes from~5 to 50 μm and being heterogeneously distributed over the imaged space, seen better in **Figure 5.7a**.
Upon gastric digestion, the gel structure appears more dense (apart from formation of very large (~50 μm) pores, (see **Figure 5.6b**). The fraction of small spherical holes seen so far (i.e. before digestion) is however lower. This apparent increase in density of the observed gel could be a result swelling. Swelling of this gel under gastric pH (without enzyme) was recorded in **Appendix 3** (**Figure A3.1**). In the contrary to the pH 8 gel, here, in **Figure 5.7b** and **c**, we cannot visually distinguish the shapes of the micronic aggregates, because of their smaller apparent size and denser aggregation. On the other hand, we can distinguish (especially from **Figure 5.7c**), some heterogeneously distributed regions/points of higher-density aggregation (stronger fluorescence). In this sample, we can see a rather retained connectivity within the network and the slower structure digestion evolution, suggesting that this gel was more resistant towards gastric juice action (30 min), compared to the pH 8 gel.

Upon **intestinal digestion** (**Figure 5.6c**), both gel structures experienced homogenization, seen by a dissolution of the distinct micronic aggregates, appearing as buried inside a homogenous medium, similar to a protein solution (not shown). The

aspects of the two gels became very similar. This confirms the powerful action of pancreatic enzymes, compared to pepsin, which was observed also throughout previous experiments (i.e. by the decrease of the scattering signal of the aggregates in SAS (Chapter 4) and by DFI imaging).

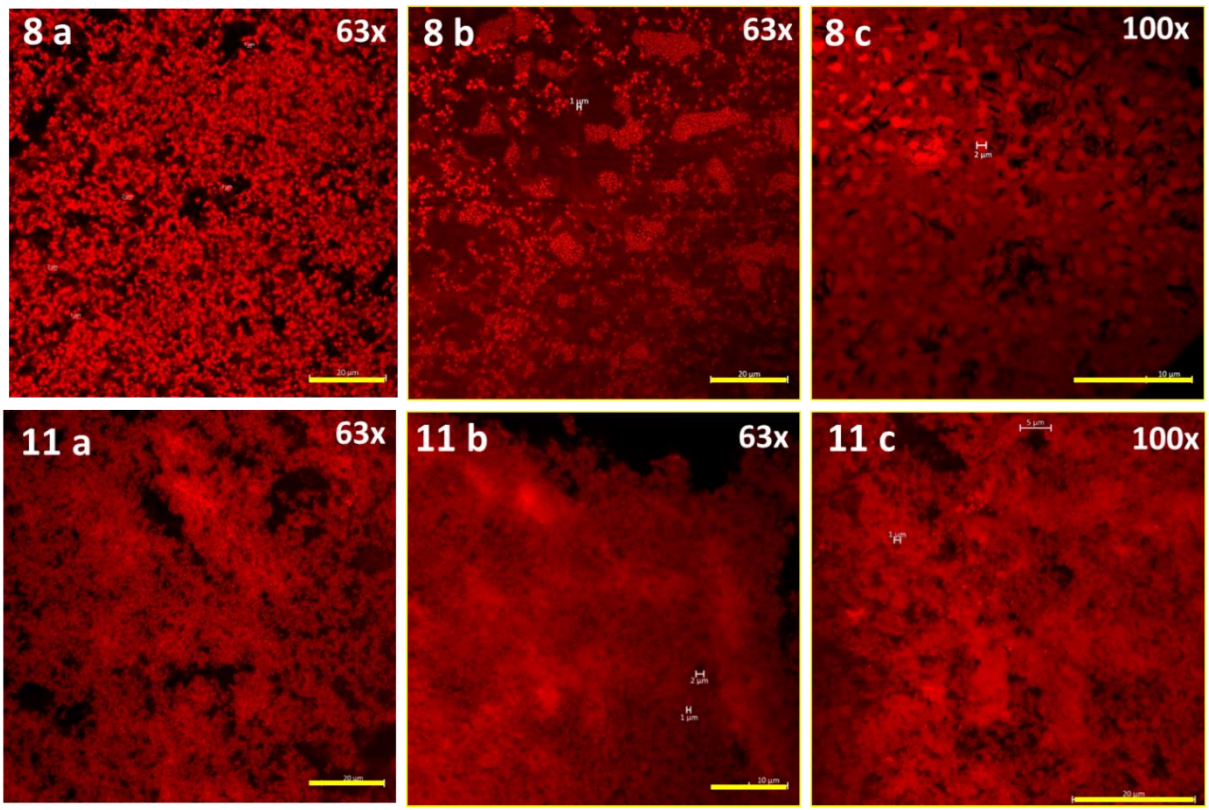

Figure 5.7 CLSM images of heat-set canola protein gels (c=100 g/L), at pH 8 (upper row) and pH 11 (down row); **a**) in the initial state (63x objective), **b**) after 30 min of gastric digestion (63x objective) and **c**) after 30 min of gastric digestion (100x objective). The yellow scale bar on the images is 20 μm.

Sizes of aggregates. At large scale (> 50 μm), the images are heterogeneous, which renders the analysis more difficult and requires better exploration of the whole sample. An opportunity which remains on a safer ground is to measure the sizes of the micronic aggregates. We obtained these sizes and their distributions by measuring the Feret's diameters of the aggregates from the segmented confocal images. The results are shown in **Figure 5.8** (for pH 8 gel) and **Figure 5.9** (for pH 11 gel) and summarized in **Table 5.2**. The initial sizes were of ~1.5 μm for pH 8 gel and ~1 μm for the pH 11

gel. The smaller size of the aggregates for the latter is in agreement with the previously presented DFI results.

In both samples, the aggregates sizes decreased after 30 min of gastric step: by ~1 μm for the pH 8 gel and by ~0.4 μm for the pH 11 gel. This, again, indicates the higher resistivity of the latter gel, arising not from the size of its aggregates but rather their interconnection. These results are in reasonable agreement with the values obtained from the DFI analysis. After the additional 30 min of intestinal digestion, the aggregates further decreased to sizes of ~0.2 μm - the same for both samples, reflecting the visually recorded homogenization of the samples.

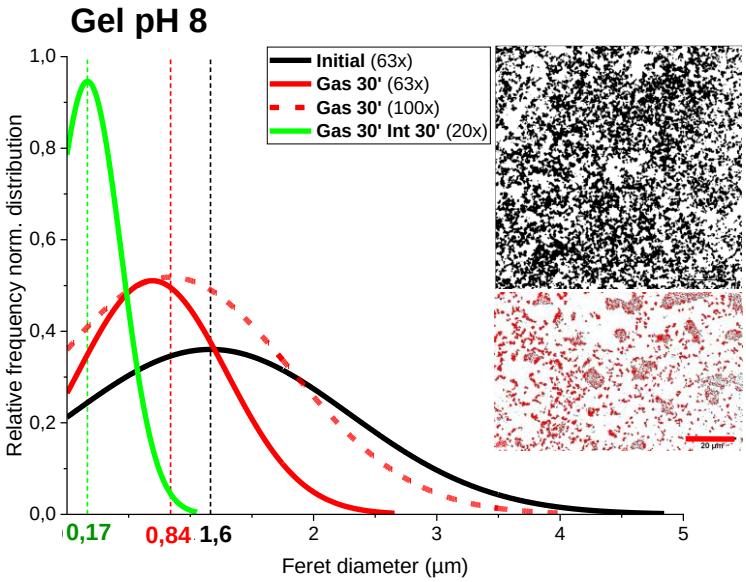

Figure 5.8 Distribution of the Feret's diameter derived from images in **Figure 5.7** (initial 63x and gastric 63x and 100x) and from **Figure 5.6** (intestinal 20x) for pH 8 gel, calculated by *ImageJ* software. The images inside the graphs show segmented aggregates in the initial states (black) and after gastric digestion (red) (with the same scale bars of 20 μm, marked on the right bottom by red line). The black curve represents the initial state, the red ones – after 30 min of gastric digestion and the green one – after additional 30 min of intestinal digestion. The mean of the distribution represents the highest relative frequency value, related to the number of measured sizes on the chosen area of variable size and to a probability distribution; the standard deviation (SD) determines the height and width of the symmetrical plot.

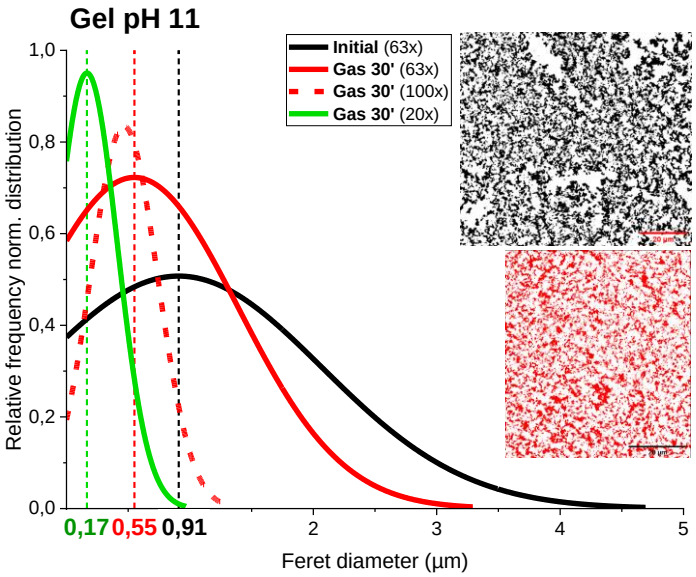

Figure 5.9 Distribution of the Feret's diameter derived from images in Figure 5.7 (initial 63x and gastric 63x and 100x) and from **Figure 5.6** (intestinal 20x) for pH 11 gel, calculated by *ImageJ*. The images inside the graphs show segmented aggregates in the initial states (black) and after 30 min of gastric digestion (red) (with the same scale bars of 20 µm). Black curve represents the initial state, the red ones – after 30 min of gastric digestion and green one – after additional 30 min of intestinal digestion.

Tableau 5.2 Average values of the ferret's diameters and standard deviations (SD) for micronic aggregates, obtained from the image analysis from **Figure 5.6** and **Figure 5.7**.

Sample	***<Feret's diameter> (µm)***	***SD (µm)***
pH 8 - no digestion	1.64	1.13
pH 8 - Gas 30 min	0.69	0.60
pH 8 - Gas 30 Int 30 min	0.17	0.27
pH 11 - no digestion	0.91	1.16
pH 11 - Gas 30 min	0.55	0.80
pH 11 - Gas 30 Int 30 min	0.17	0.25

In summary, these preliminary experiments, using confocal fluorescence microscopy to follow the microstructure of the canola protein gels after gastro-intestinal digestion, were successful. They confirm our views of the gel structures, with quantification of their micronic aggregates sizes, and show differences in density of the aggregates between the two gel samples throughout the digestion.

5.3 Synchrotron Deep-UV Fluorescence Imaging

A synchrotron deep-UV microscopy with the use the auto-fluorescence of tryptophan residues in proteins, made it possible to monitor *in situ* the evolutions of protein gel degradation upon simulated gastric and intestinal digestion, without the need to use fluorescent dyes. We obtained 2D structural information at length scales of 10-1000 µm.

5.3.1 Gastric digestion

Figure 5.10 shows a typical example of an observed process of gastric digestion (80 min) of a piece of gel, here ~200 µm-sized piece of the pH 8 canola protein gel[c]. Two types of microscopy were performed during the same sequence of observations: visible light (transmission) and fluorescence analysis. The fluorescence signal is denoted on the images by the grey level, with whiter tone indicating a stronger signal. In our experiments, fluorescence varies linearly with protein concentration[2].

After injection of gastric solution, we observed an increase of fluorescence signal in the whole field of view of the camera, coming from the fluorescence of pepsin proteins. Despite their small concentration, pepsin contributed visibly to the fluorescent signal, because of the 1.5 mm thickness of the liquid in the infusion cell (being relatively important when comparing to <100 µm gel thickness).

[c] Due to difficulty in obtaining not interrupted image sequences during digestion, we present here only one complete digestion sequence for one gel type; in other trials, the observed sample did move outside the field of view of the camera, at some point after injection of digestive juices, ruining the further experiment.

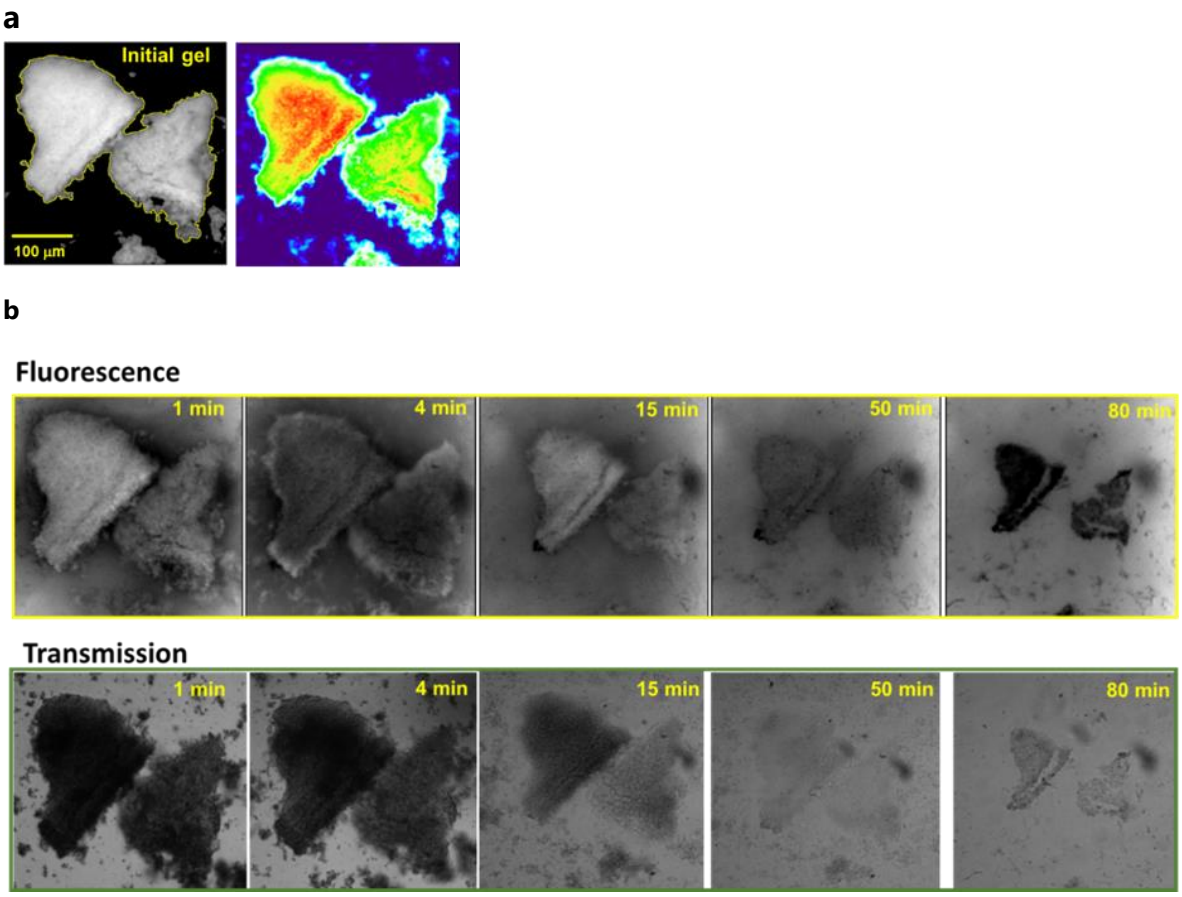

Figure 5.10 a) Fluorescence images of the canola protein gel pieces (pH 8) before digestion, chosen for further analysis; yellow lines correspond to the ROI's selection; the scale bar is 100 µm; the artificially colored image presents more clearly the thickness heterogeneity of the initial gel pieces. **b**) Sequence of gastric digestion of the same gel pieces (same size scale as in image a), in fluorescence (**top row**) and transmission mode (**bottom row**); minutes indicate the times after addition of the gastric juice, preceded with 20 min of photobleaching period (illumination by UV light without digestion). The image contrast was re-adjusted after addition of the gastric juice, to improve further visualization; afterwards the contrast was not changed anymore.

By focusing at the signal given by the two gel pieces, we distinguished the following steps: **1)** an instant swelling, followed by **2)** an ingression of gastric fluid, starting from the borders of the gel (stronger fluorescence at 4 min) towards inside the gel, **3)** a subsequent hydrolysis (dissolution of the gel), and **4)** a shrinking with a simultaneous expel of digested materials from the degraded gel piece into the surrounding liquid.

1) The initial 1-4 min, swelling was likely provoked by the acid pH of the gastric fluid, which increased electrostatic repulsion. It was also detected after soaking the gels at the pH 2 HCl solution, as a control experiment (see **Appendix 3**).

2) In the second step, an increase of the fluorescence signal was observed, starting from the gel's edges and progressing inside the gel. This increase should not be read as the higher protein concentration/or pepsin accumulation specifically on the gel's edges but to the fact that the gel was initially thinner at edges (thicker in the middle part) as we will see in **Figure 5.12**. Upon digestion, the thinner parts became even more transparent, therefore letting passing through more fluorescent light from the background solution.

3) Between 4 and 15 min, the diffusion-digestion towards the inside of the gel was progressing until the gastric juice permeated the entire gel, simultaneously with a decrease in size (dissolution/erosion) of the gel.

   a. The dissolution and higher transparency of the gel, starting from the edges and progressing inside the gel could more simply be seen on the corresponding transmission images.

   b. The fluorescence signal at the outer rims of the gel increased, being an indication of the release of the digestion residues/dry matter loss into the surrounding liquid.

   c. The fluorescence signal of the gel was then slowly decreasing along with the reduction in size of the gel, indicating a slowing down but still ongoing digestion. Remember that the loss of fluorescence due to digestion was simultaneous with the loss of fluorescence of tryptophan residues due to the so-called "photobleaching" phenomenon. On the other side, the fluorescence signal outside the gel stayed constant, due to the diffusive and convective motion of the fluorophores (enzymes, proteins) in the solution and their arrival in the field of view illuminated by the UV light, without being prior photobleached. The result is that the gel appeared darker than the outside solution, although it was still fluorescing (see at 50 min).

4) In the last step, from the 50 min, the slow but ongoing shrinking of the gel occurred, up to the end of the sequence (80 min), where the less-fluorescent residual gel (compared to the background solution) with internal fissures was left over. We assume that the apparent gel shrinking occurred due to the protein digestion and residues release from it.

The schematic process of gastric digestion of the piece of the protein gel is schematically shown in **Figure 5.11**.

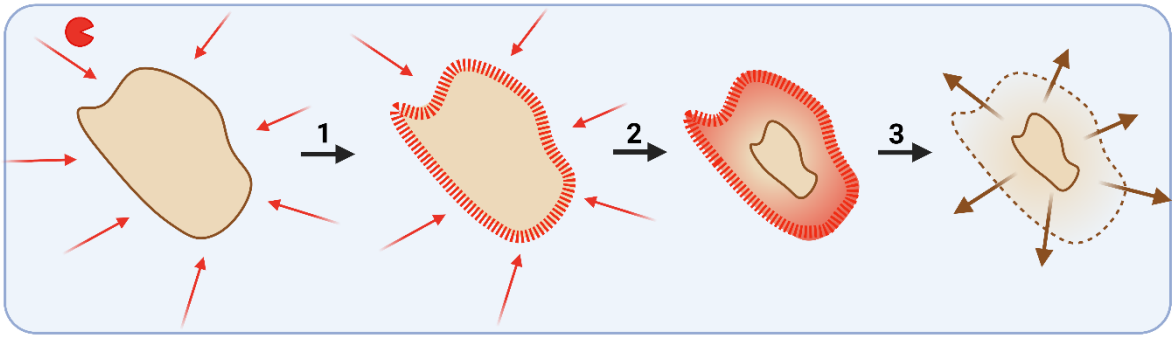

Figure 5.11 Schematic representation of the erosion/digestion processes of a piece of canola protein gel (shown by brown color) during gastric digestion; the black arrows with numbers show the direction of the process with time; the red color represents the pepsin enzyme and its progression, with red arrows showing its diffusion inside the gel with time; the brown arrows at the 3rd step represent the diffusion of the digested protein residues outside the piece of gel.

The digestion of a piece of gel could also be seen by looking at the changes in the gel's profiles. The fluorescence intensity was plotted along the horizontal line going through the solution (120 μm and the gel (190 μm), as shown in **Figure 5.12**. The corresponding profiles (marked by different colors on the graphs) correspond to different digestion times. After the initial increase of the fluorescence in the surrounding liquid above the gel (**Figure 5.12a**, from black to red and blue curves), due to pepsin injection, the gel's surface started to experience erosion by gastric juice. This can be seen from both the corners of the gel (by increase of the signal due to better transmission though the thinner edges), and from the middle surface (by decrease of the signal due to loss of fluorescing matter) (**Figure 5.12b**). The erosion-like digestion continued, together with

some gel's shrinking (see an increase of the signal of the pink curve in **Figure 5.12c**), and diffusion of the residual matter to the liquid, seen further by a decrease of the fluorescence in the middle and its increase on the gel corners (yellow to purple curve in **Figure 5.12c**).

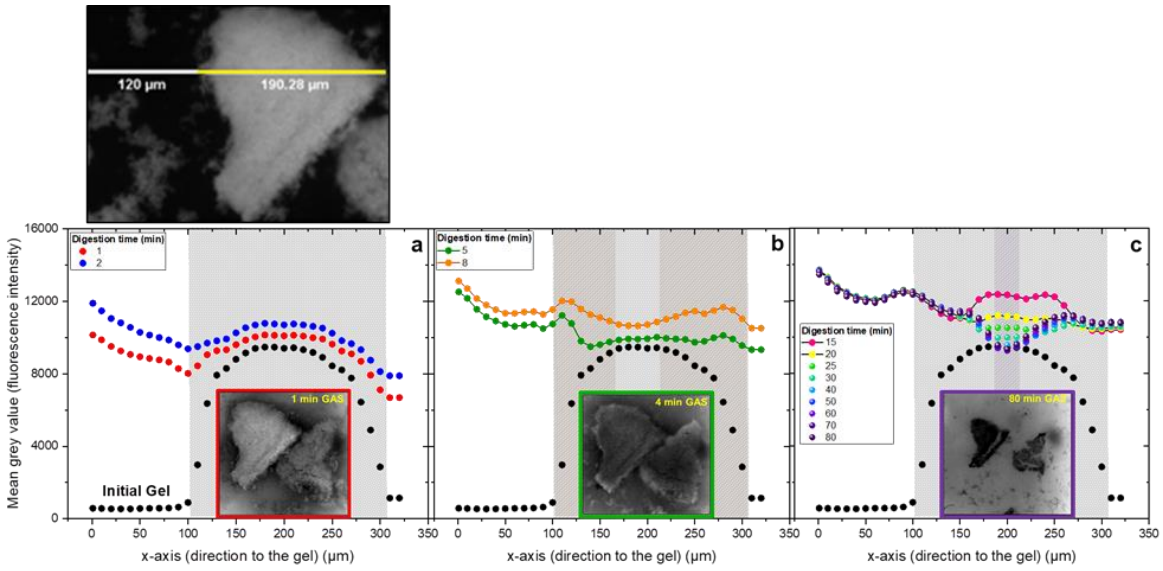

Figure 5.12 Top) Fluorescence image of the initial canola protein piece of gel (pH 8). The horizontal line indicates the location of the follow-up of the digestion of the gel. **Bottom**) Fluorescence profiles and image obtained **a**) at the initial state, after 1 and 2min of gastric digestion, **b**) at the initial state, after 5 and 6min of gastric digestion, **c**) at the initial state and from 15 up to 80 min of gastric digestion. The digestion times are indicated on the different graphs by different colors.

Pepsin propagation inside the gel. **Figure 5.13** shows the mean fluorescence intensity plotted against time, measured for areas differently distant from the edge of the gel up to 100 µm towards its middle part. This can be read as a translation at fixed positions in time of the former **Figure 5.12**.

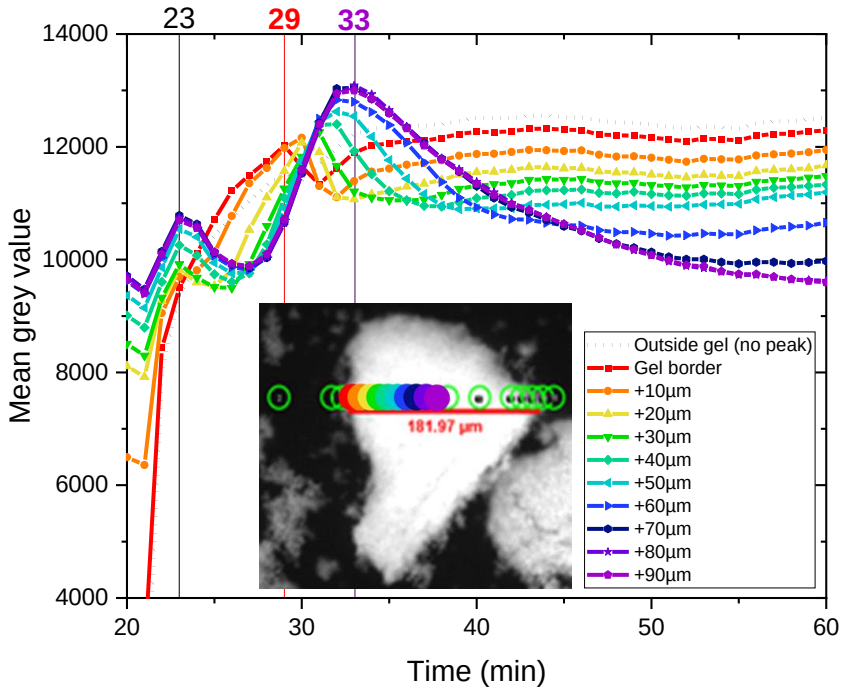

Figure 5.13 Image of a piece of gel (pH 8) and mean grey values as a function of duration of gastric digestion measured on circular area (radius 10 µm) at different distances on a horizontal axis of this piece of gel (from the gel's border (red) to the gel's middle part (purple), with 10 µm distance between each); black dotted line is for an area outside the gel. The times marked at the 3 fluorescence peaks correspond to: appearance of pepsin in the field of view (23 min), arrival of the pepsin-erosion to the gel border at the red circle (29 min), arrival of the pepsin-erosion to the middle of the gel at the purple circle (33 min). Note that 20 first min were without digestion and only with photobleaching.

1/ For the fluorescence intensity outside the gel (black dashed curve), we observed the continuous increase of the fluorescence signal with time, up to ~35 min[d] and its further stabilization[e].

2/ For the area at the edge of the gel (**red curve**), we could notice an increase of the fluorescence signal due to the pepsin's diffusion over this area, up to 9 min after the

[d] The first 20 min was the time given for the gel to photobleach, before injecting the gastric solution.

[e] The constant mean fluorescence value of the solution is due to the stochastic movement of the pepsin and digestion residues in the solution in the experimental cell, also outside the illuminated field of view, thus overcoming the photobleaching effect.

injection of the gastric juice to the cell. It resulted in a dissolution/erosion on this measured area, thus was followed by the fluorescence decrease (less protein material). After this 1st peak decay, some slighter fluorescence increase was observed – it resulted from the diffusion of the protein digestion residues outward the digested gel.

3/ For the inner areas, entering towards inside of the gel, two peaks could be distinguished. The 1st peak, at 3 min after injection of gastric juice (23 min on the graph), corresponds to the arrival of the gastric juice on the top of the gel (giving the fluorescence increase) followed by the gel's digestion from the top and the effect of photobleaching (fluorescence decay)

The 2nd peak, which appearance depends on the distance from edge of the gel (e.g. ~33 min for the area 100 µm from the border, **purple curve**), corresponds to the progression of the pepsin's diffusion into this area and its erosion-like action, resulting in the gel thinning and the fluorescence increase. The decay from this peak relates to the digestion of the gel area plus its photobleaching. The longer decay, for the area in the middle of the gel (purple curve), compared to the edge (red curve), reflects an incomplete dissolution of the middle gel area (see the residual gel at 80 min in Figure 5.9), compared to the dissolved edge of the gel, fluorescing, as described above, due to the diffusive and convective motion of the fluororescent material.

By measuring the times of the arrival of pepsin (2nd peak) to the different successive areas on the gel (e.g. 29 and 33 min, distant by 90 µm), we could estimate the average rate of propagation of pepsin in the gel to **22.5 µm.min^{-1}** (3.7 10^{-7} m.s^{-1}).This value corresponds to a Fickian diffusion coefficient of **~ 9.7 10^{-12} m^2.s^{-1}**. This value is purely indicative and does not correspond to only a simple diffusion of the enzyme, but is related to the observed digestion. It is, however, in reasonable agreement with the literature values for pepsin diffusion coefficient of 1.2 10^{-11} m^2.s^{-1} in 20% w/v whey protein gels[3]. It is also close to the average value obtained for pepsin diffusion reaction in capillary, 1.29 10^{-11} m^2.s^{-1} (see Chapter 4).

Finally, we present in **Figure 5.14** the changes of the mean fluorescence intensity (black curve), the area (blue curve) and the estimated protein content (orange curve), i.e. area x fluorescence, of the two gel pieces during gastric digestion.

The **fluorescence** is an average value over the precise area of the two gel pieces (as shown in **Figure 5.10a**). Its decay correspond to the digestion kinetics of the gel plus the effect of the fluorophore photobleaching. After the fluorescence peak discussed above, we have a quick decay by 12% in 10 min followed by a much slower one.

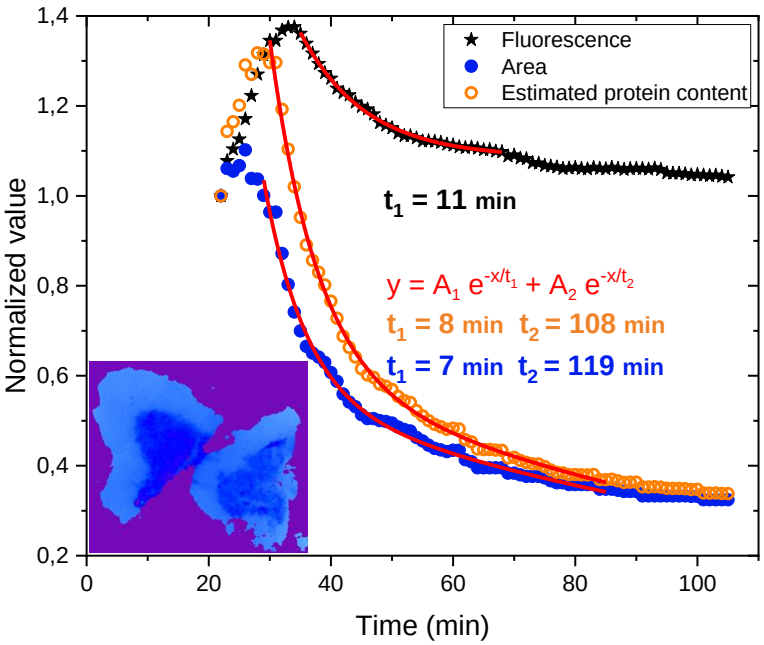

Figure 5.14 Changes with gastric digestion time of the area *S* (blue), the mean fluorescence intensity <*I*> (black), measured directly from the images, and protein content C_{prot}=<*I*>/*S* (orange) of the two canola protein gel pieces (pH 8). All values have been normalized to unity at time "zero" (after 20 min of photobleaching). The red solid lines represent the exponential fittings of the data. The image shows the difference between the initial gel area (lighter blue) and after 80 min of gastric digestion (darker blue).

Regarding the precise **area** of the gel pieces, its important decrease, by 70% in total, confirms the predominance of surface erosion mechanism; except for the size reduction and some enhancement of internal fissures, the initial shape of gel pieces was rather preserved. The area decreased the most (by 40%) during the first 10 min

after the initial swelling of the gel. The remaining slower decay suggests some limitation in efficiency of the gastric digestion.

Through the variation of the fluorescence and area, we could follow the average **protein content**, illustrating the combined kinetics of the size reduction and internal digestion, mostly influenced by the size reduction (see **Figure 5.14**, **orange curve**), with the first 10 min step leading to ~ 50% decrease in protein content

In summary:

- Gastric digestion of the pieces of canola gel was rather slow: after 80 min, they were still visible.
- Surface erosion (i.e. hydrolysis of the proteins located at the gel surface) appears as the major mechanism of gastric digestion, with lower effect of the ingression by pepsin cleaving inside of the gel.
- The resistance of the piece of gel towards a complete digestion could be due to a combined effect of the gel shrinking and pepsin diffusion limitation plus aging of pepsin with time.

5.3.2 Intestinal digestion

Figure 5.15 presents an example of a sequence of images during 36 min of intestinal digestion of canola protein gel (without gastric step before). We can distinguish some differences from the process of gastric digestion: here, the gel experienced some **swelling** and then rapid **disintegration** until its **complete dissolution** (with visible gel structure digestion proceeding not only by the outer erosion but also by the inner one). This complete process required one hour, being much faster compared to gastric digestion. The fluorescence level of the initial piece of gel was gradually reducing (yellow frame), with simultaneous expel of digested residual material, giving an increase of the fluorescence outside the piece of gel (red frame).

A visual observation of the whole area of the experimental infusion cell at the end of the digestion, containing initially many gel pieces, revealed that the whole volume was "washed" out: no more gel pieces of a few microns were observable.

This accelerated gel dissolution could have been due to the rapid swelling of the gel. Indeed, it could help the convective and diffusive influx/transport of the enzymes, allowing the gel's digestion also from the inside. The two mean features observed here, swelling and a kind of immediate dissolution of the gel, are in qualitative agreement with the results of digestion of the canola protein gels in capillaries, deduced from the SAXS measurements. They correspond respectively to the 3rd step (unfolding disaggregation) and the 4th step (final scissions resulting in small peptides) of intestinal digestion described in Chapter 4.

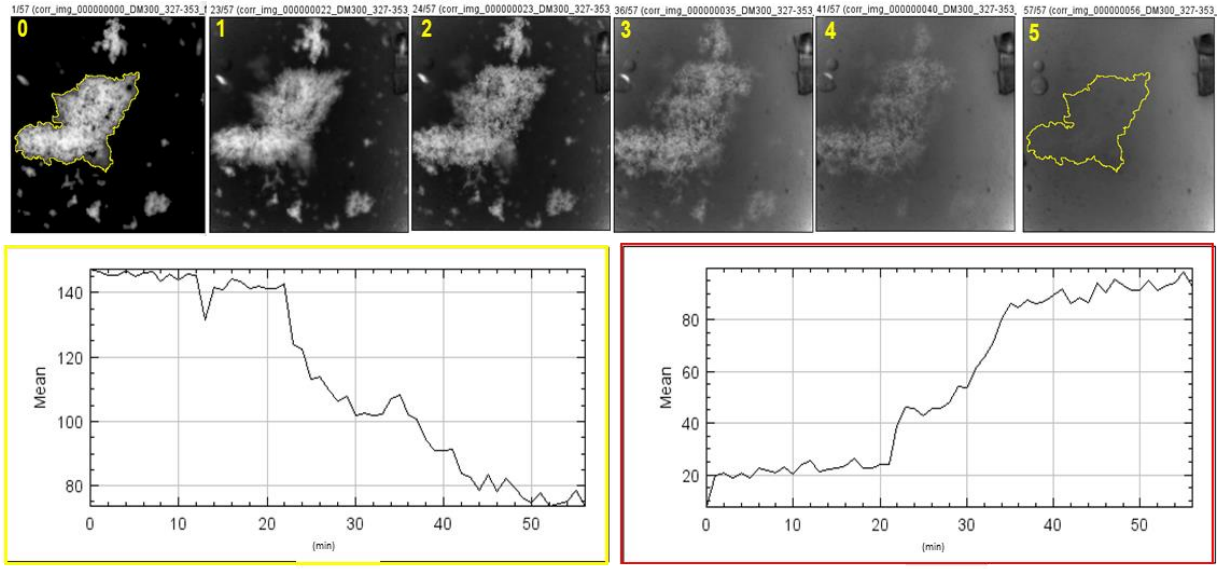

Figure 5.15 Sequence of fluorescence images of canola protein gel during intestinal digestion. **Top**) Images of one piece of gel. Yellow numbers on the images: **0**) the initial gel; **1**) 2 min; **2**) 3 min; **3**) 15 min; **4**) 25 min; **5**) 40 min after intestinal juice injection. **Bottom**) Mean intensity profiles as a function of time (20 min of bleaching, then intestinal juice injection): yellow frame– for the area inside the gel piece; red frame – for the area outside the piece of gel.

Summary and conclusions

In this chapter, we focused on exploring through different imaging techniques, the **microstructural** changes at the **micronic/supra-micronic** size range of canola protein gels (prepared at pH 8 and pH 11), induced by the gastric and intestinal digestion conditions,

Neutron imaging allowed to distinguish the sizes of the protein aggregates of the studied gels. The dominating structures of ~1-2 μm, being initially smaller for the pH 11 gel, experienced reduction in size during gastric digestion, with stronger effect for the pH 8 gel. Intestinal digestion was very powerful in the aggregates degradation, with an important scattering signal reduction observed already after 10 min.

Those results were confirmed by **confocal imaging**, which helped to refine our estimate of the sizes (to ~1-1.5 μm, again, smaller for the pH 11 gel), and to identify the spherical shapes of the protein aggregates, which was only assumed for the neutron imaging analysis. It also confirmed the trends of i) the aggregates size reduction upon 30 min of gastric digestion (by ~1 μm for pH 8 and 0.5 μm for pH 11 gel); ii) a further decrease to <0.2 μm for both gels after additional 30 min of intestinal digestion; iii) the potency of intestinal digestion for faster aggregates degradation, seen as homogenization of the networks. The differences between the behaviors of the two gels upon intestinal digestion vanished, confirming our previous conclusions from SAS (neutron and X-rays) experiments. In addition, confocal imaging allowed us to better explain the opposite evolutions of the elastic moduli of the two gel samples during gastric digestion. Indeed, after the gastric digestion step, the concentration of the aggregates and their connectivity for the pH 8 gel decreased, while, inversely for the pH 11 gel, the microstructure seemed locally more dense (with smaller sizes of the pores) and retained connectivity between the aggregates. The disconnection between the aggregates for the pH 8 gel could explain the decrease of its elastic modulus. On the contrary, the increased apparent density of the protein rich regions, together with the retained aggregates connectivity in the pH 11 gel, could indeed result in the increase of the modulus of this gel.

In situ monitoring of the digestion of $(100\text{-}200)^3$ μm^3 pieces of gel by **Synchrotron fluorescence imaging** showed supra-micronic processes throughout the gastric digestion, i.e. gel's swelling (related to the harsh pH decrease), enzymatic diffusion, gel's shrinking and release of proteins and digestion residues from the gel. The observed decrease in the gel size, with almost unchanged shape suggested that the **enzymatic surface erosion** was the predominant digestion mechanism. Intestinal proteolysis was much faster, including swelling followed by **definite dissolution** of the gel, as also observed in our previous experiments (rheology and SAS).

References

[1] SasView: https://www.sasview.org/docs/user/models/hardsphere.html

[2] Itagaki, H. (2000). Chapter 3 - fluorescence spectroscopy. In Toyoichi Tanaka editor, Experimental Methods in Polymer Science, *Polymers, Interfaces and Biomaterials*, 155–260. Academic Press, Boston.

[3] Luo, Q., Borst, W.J., Westphal, A.H., Boom, R. M. and Janssen, A.E.M. (2017). Pepsin diffusivity in whey protein gels and its effect on gastric digestion. *Food Hydrocolloids*, 66, 318-325. doi: 10.1016/j.foodhyd.2016.11.046.

CONCLUSION

Despite an increasing interest in protein consumption, the digestive behavior of proteins, in native or processed states, has not yet been fully explored. In this thesis, we focus on the digestion of the main canola seed proteins, napin and cruciferin, having together a great potential for being included in human diet.

We studied the protein structures, mainly in gels, and their transformations during gastrointestinal digestion at different scales: ranging from a few nanometers (protein size), through a few microns (aggregate size), to a few tens of microns (chewed food size).

Starting from canola protein solutions, we showed that processing affects the initial structure of proteins. High temperature (95°C) treatment induced denaturation of canola proteins, their aggregation and crosslinking, yielding stable, elastic gel networks. **The choice of the pH of the protein solution combined with the heat-treatment** allowed us to obtain protein networks of different structures, having different elastic moduli and degrees of protein folding: the preparation of the gel in alkaline pH enabled to preserve the folded structures of the proteins and gave a higher modulus to the resulting gel, compared to the neutral pH preparation.

Continuing with gels, this work led to several main findings regarding digestion.

Thanks to a **novel approach to study *in vitro* protein digestion based on the use of Small-Angle Scattering (SAS) techniques** (SANS in disk-shaped/half-cm gel pieces and SAXS in capillary cells), we provided previously unexplored nanostructural information about protein behaviors during digestion. SANS, in spite of a different sample shape, confirmed the very detailed information from SAXS, which allowed to construct **diagrams showing complex but reproducible digestion patterns of proteins**. The observed mechanisms included unfolding, re-compaction, local aggregation, disaggregation and scission (cleavage) of proteins.

Differences in digestion appeared between the gels due to different initial pH.

The level of the protein unfolding before digestion, affected the conformational evolutions of the proteins during digestion:

- when proteins did not undergo complete denaturation during the primary (pH and heat) processing, the secondary processing (by the enzyme and pH conditions of the stomach) provoked a complementary unfolding of the protein structures;
- when the proteins were already pre-unfolded by the primary processing, their re-compaction occurred.

The more complete digestion process was achieved for gastro-intestinal conditions: the proteins experienced more complex multistep behaviors, with unfolding (dependent of the initial protein state) and strong re-compaction, accompanied with some re-aggregation of the local structures - a signature effect observed in all intestinal digestion experiments, with different amplitude depending on the initial state of the gel. Because of this effect, the digestion had to be reinforced by additional structure unfolding and disaggregation. This result can be of importance *in vivo* from the point of view of final nutrient efficiency. It would be interesting to investigate deeper this feature, by changing, for example, the ratio of cruciferin/napin (which have a different isoelectric point).

At the end of such gastro-intestinal digestion kinetics, the final digestion products (small peptides) from different gels resembled each other by size and shape. We have therefore succeeded to reach the stage close to a complete digestion. It is interesting to point out that, for very long times of only gastric digestion, the complete digestion could also be reached.

Comparing the kinetics of gastric and intestinal digestions between the different protein gels, the ones with compactly folded proteins and stronger networks (prepared at alkaline pH) showed slower digestion rates, attributed to more difficult enzymatic penetration and proteolysis.

The structure effects on digestion were also seen when comparing the gels to native protein solutions. Digestion of folded proteins in native solutions showed significantly faster digestion rates. In other terms, although heating provoked a partial protein unfolding, it did not facilitate the enzymatic digestion; because the induced protein aggregation and network formation had a predominating role on the gels resistance.

The **second part** of this thesis work concerned the **large protein aggregates**, being likely important for the gel states. Firstly, by the use of the scattering (SANS), during both gastric and intestinal digestion, we observed a decrease of the aggregates signal for both pH 8 and pH 11 gels, which could be attributed - even though this assumption is not the only one possible (see below), to a decreasing number/specific area of the aggregates. Secondly, we focused on different complementary **imaging techniques**. We first observed differences in the aggregates structure between the gels formed at alkaline or neutral pH. Micron-sized, spherical aggregates could be detected by fluorescence confocal imaging and quantified, as well as by neutron Dark Field Imaging (DFI), giving, consistently, smaller sizes for the pH 11 gel. Under gastric digestion, the DFI from these aggregates strongly decreased while confocal microscopy images showed their decrease in size. Under intestinal digestion, a rapid homogenization into small aggregates was achieved. Therefore, **the results from those three techniques are consistent** with each other in respect of (i) a decrease of the aggregates size and (ii) a constant or decreasing aggregates volume fraction during both gastric and intestinal digestion.

Concerning the **connectivity between these large aggregates**, it **could not be directly revealed through the scattering information**. Meanwhile, the confocal imaging may help: the images of the pH 11 gel showed more connected structure (the micronic aggregates seemed to be less separated from each other than in the pH 8 gel). This became more important in gastric digestion. On the other hand, intestinal digestion step worked in a similar way for the two gels, inducing the structure homogenization. Nevertheless, no direct assumption on the connectivity could be

made based on those 2D images. We assumed that the large aggregates dissolved and disconnected in a "sea" of unconnected individual proteins.

Together with the protein network structures, **rheology** showed differences between the two preparation pH gels. The most striking appeared upon gastric digestion, namely the opposite time variations of the elastic modulus of the folded and unfolded protein gels. They were likely to be due to changes on the scale of the local protein conformation (unfolding or compaction), in parallel with possible effect from the structure (aggregates) at larger scale discussed above. In this context, the gastric step can be an important driving factor of protein digestion.

From what above, it arises that, whereas we have explored well the structure on the scale range of the proteins, **some weaker points appear** in the exploration of the scale of large aggregates, their relation with rheology and difficulty in conciliation of the information from different techniques, which seemed to be related to the sample spatial heterogeneity. We discuss that now.

Firstly, a more precise quantification of the large protein aggregates and their transformation during *in situ* digestion experiments is needed. Information on their size was not directly accessible in the *q* range of SAXS/SANS measurements.

A second difficulty, despite our efforts and the numbers of techniques used in this thesis work, was the lack of connectivity information to link rheometry results with the structure:

- we assumed that the contribution to the elastic modulus came principally from the connected proteins, both in gastric phase, which showed differences in local structure between the two gels, simultaneous with the differences in rheology, and in intestinal phase, where proteins unfolded and were cleaved into small peptides;
- however, the behavior of the large aggregates could also be linked to the decay of the modulus. As said above, from neutron DFI and confocal imaging we could see that aggregates decreased in size already during gastric digestion, with confocal images of the pH 11 gel showing more connected structure between micronic

aggregates. This information is in agreement with the variations of the modulus observed for the two gels.

More generally, the use of different techniques (rheometry, SAXS, SANS and *in situ* imaging), involved different states of the digested sample heterogeneity:

- in rheometry, the 2-hours intestinal digestion of one gel sample resulted in a gel and a solution part. However, the digestion was done *in situ* thus all the sample was measured; we could therefore fear that the modulus was not homogenously distributed, impairing its average measure at these long times;
- in SANS, neutron and confocal imaging, on the reverse, after the digestion, only gel parts, not the solution fraction, of the samples were recovered for the measurements;
- in SAXS, thanks to *in situ* digestion and scanning of the capillary sample, we could measure both the solution and gel part of the digested samples, depending on the position in the capillary (all digested material stayed in the cell). Interestingly, SAXS results showed behaviors similar to the ones observed in SANS, but for much longer times in SAXS; it concerned both the local scale of protein conformation as well as the aggregates scale (notably the decrease in low *q* intensity).

  These differences in digestion rates can be due to the fact that in capillary SAXS we follow the progressive diffusion of the enzyme from outside to inside and the reaction without expulsion of the residues outside the scattered volume. Meanwhile, for SANS, as well as for DFI and rheometry, the cylindrical samples were soaked in cold enzymatic juice first and let be digested also from the inside, with a simultaneous expulsion of the digestion residues. In this case, the role of the surface erosion was more important than in SAXS.
- **at even larger scale**, the progressive erosion of the surface of the gel was evidenced already in the gastric phase, by UV-fluorescence microscopy during the real-time *in situ* monitoring of the digestion of "200 µm" pieces of a gel. The erosion was fast enough to dominate over the diffusion, at least above a given penetration length. Meanwhile, the penetration of the enzymes was influenced by the structure

of the gel. Intestinal digestion was very rapid for such micrometric size sample. In spite of that, we could however catch that the "fluffy" morphology was evolving towards a more holed structure.

In summary, the use of those different sample geometries may seem not satisfactory because connecting the different results is difficult. This was the tribute to pay for an extended multiscale study, which permitted to focus on different stages of the digestion.

Recommendations for future works are therefore proposed:

- future synchrotron SAS studies should concentrate on lower *q* range (USAXS), in order to resolve the structure and size of the protein aggregates in initial material, their fate and possibly new (re)formation on protein digestion;
- confocal imaging could be a good direction to obtain information about the aggregate connectivity within the gel networks. Here, it will be necessary to develop a sophisticated analysis of the 3D confocal images (already acquired);
- it would be also interesting to study the local protein structures (secondary structures, tryptophan environment) **in the gels** (requiring very thin cells) during *in situ* digestion by methods of Circular dichroism, UV-absorbance and fluorimetry, in relation to SAS.

Prospects concern first **other foods**. As mentioned in Chapter 1, there is an increased demand for protein-based products, particularly from plant sources. In this direction, the existing results (not presented in this manuscript) on potato proteins and napin and cruciferin from canola (separately) will be analyzed. They can be extended to answer questions like: by how much do all plant proteins differ in properties in gastrointestinal conditions? Our methods can easily apply as well to more widely investigated animal proteins (e.g. milk, egg and meat) and their modification by processing.

Initially disrupted structure by processing (at variance with structuration by heat-treatment), is also a direction for future study, to verify its effect on facilitated digestion.

Modeling of the gastrointestinal process will close the list here. Such work has been started by Evelyne Lutton, using data obtained during this thesis, mainly from SAXS and fluorescence imaging. Concerning diffusion and reaction of the enzymes inside the protein gels, our results show apparent diffusion coefficient for pepsin of 1-1.3 10^{-11} m^2. s^{-1}, obtained from SAXS, with some echo in fluorescence imaging of erosion. This value can give an indication for the start, completed by FRAP measurements with marked enzymes. In reality, we were witnesses of a concurrence of convection, diffusion, swelling of the gel, reaction, surface erosion and expulsion of the digestion residues. This complexity can be taken care of by using so-called Agent Based Models, more flexible than the Equations based (EDP) ones, and simpler than molecular dynamics. This may enable us to tackle the problem of the different digestion evolutions which do not scale the same with gel size.

Concerning **more direct applications**, the results presented in this thesis would allow, for example, to design or optimize new protein-based foods with specific nutrient digestion behaviors or rates, adapted to different physiological functionalities, e.g. controlling the sensation of satiety, by consuming structured foods with slowed digestion rates.

Appendices

APPENDIX 1: Complementary figures

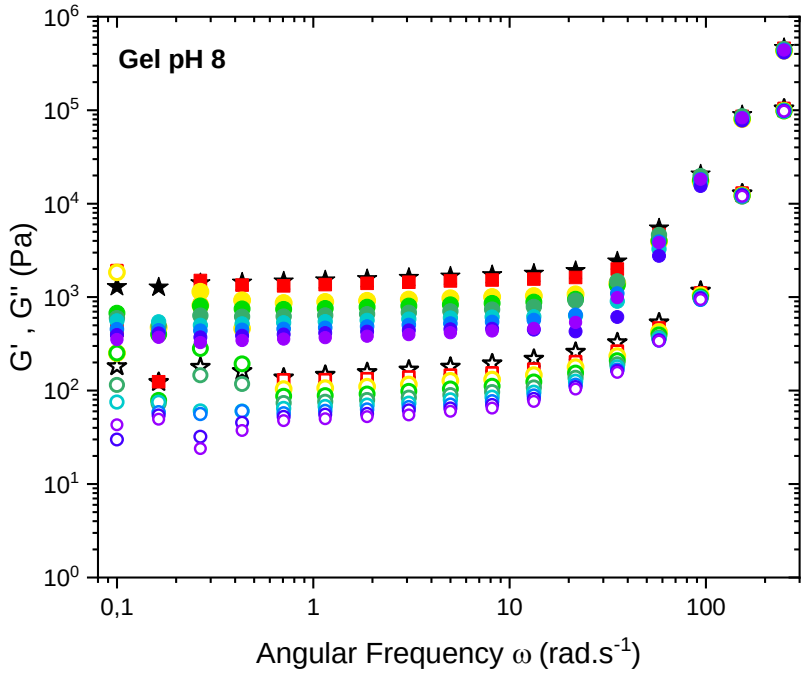

Figure A1.1 Example of frequency sweep curves (storage moduli (*G'*, closed symbols) and loss moduli (*G''*, open symbols) as a function of oscillating frequency for the canola gel (100 g/L) prepared at pH 8 during the digestion process. Each curve represents a different stage of digestion: before digestion (black), 30 min of gastric step (red), then intestinal digestion kinetics during 60 min with 10 min interval (yellow t_0 to purple $t_{60\ min}$). Notice that above ω of 50 $rad.s^{-1}$, all of the curves show the same strong increase of the moduli.

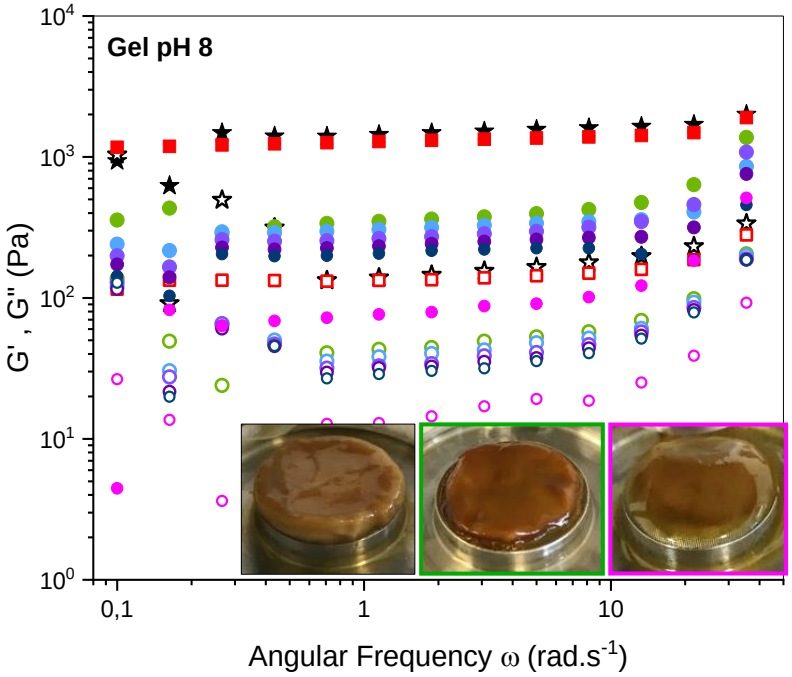

Figure A1.2 Frequency sweep curves for canola gel (100 g/L) prepared at pH 8 (storage moduli (*G'*, closed symbols) and loss moduli (*G''*, open symbols) as a function of oscillating frequency (from 0.1 to 50 rad.s^{-1}), during the digestion process. Each curve represents a different stage of digestion: before digestion (black), 30 min of gastric step (red), then intestinal digestion (60 min kinetics with 10 min interval) after 1 h of intestinal step[1] (green $t_{60\ min}$ to magenta $t_{120\ min}$). The images show the visual states of the gels during intestinal digestion: after 20 min (curve not shown), after 1 h (corresponding to the green curve), after 2 h of intestinal digestion (corresponding to the magenta curve).

[1] The 1st hour of intestinal digestion was performed *in-vitro* (in a Falcon tube), then the digestion that was continued *in-situ* (and recorded) on the rheometer for the 2nd hour.

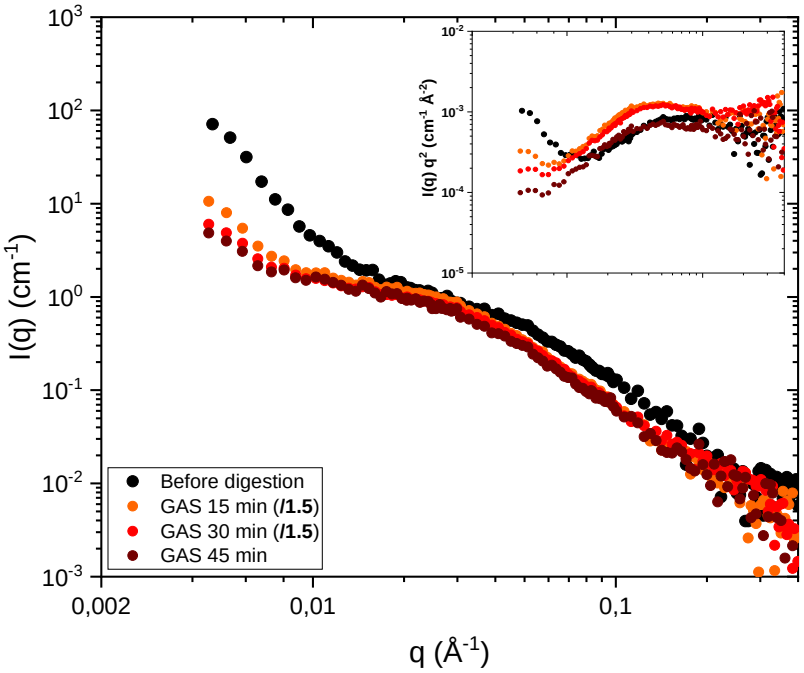

Figure A1.3 Small-Angle Neutron Scattering of canola gels (100 g/L) prepared at **pH 8**: initial gel (black); after 15 min of gastric digestion (orange); after 30 min of gastric digestion (red); after 45 min of gastric digestion (brown). The curves for gastric 15 min and 30 min were divided by a prefactor 1.5^2 for a better visualization on a common plot. Inset: Kratky representations of the same data (without the prefactor).

[2] The intensity level variations occurred due to a poor control of the sample volume in the neutron cell when filling it with digested gel pieces, sometimes resulting in their de-swelling, which lead to an increase of the concentration and thus of the scattering intensities. It did not affect much the shape of the curves.

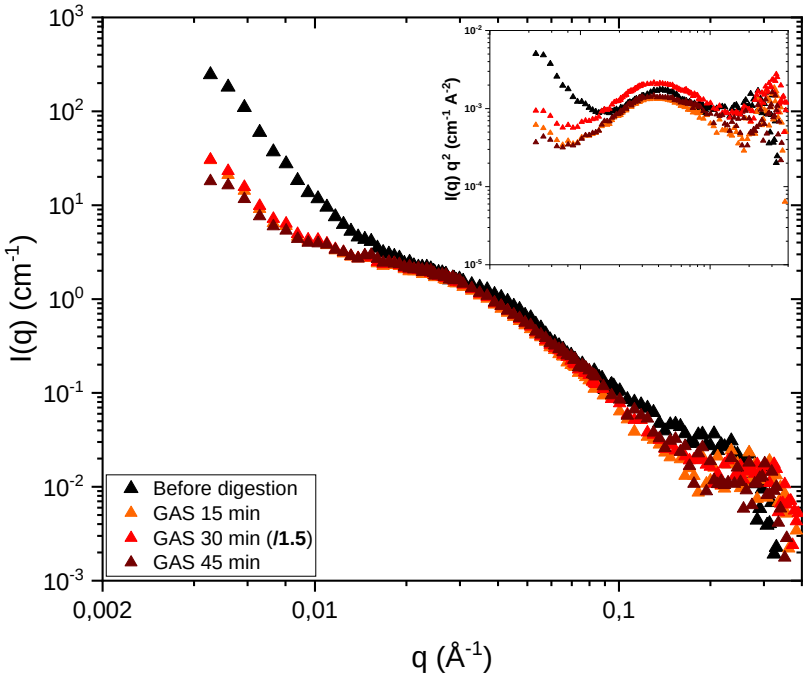

Figure A1.4 Small-Angle Neutron Scattering of canola gels (100 g/L) prepared at pH 11: initial gel (black); after 15 min of gastric digestion (orange); after 30 min of gastric digestion (red); after 45 min of gastric digestion (brown). The curves for gastric 15 min and 30 min were divided by a prefactor 1.5[3] for a better visualization on common plot. Inset: Kratky representations of the same data (without the prefactor).

[3] The intensity level variations occurred due to a poor control of the sample volume in the neutron cell when filling it with digested gel pieces, sometimes resulting in their de-swelling, which lead to an increase of the concentration and thus the scattering intensities. It did not affect the shape of the curves.

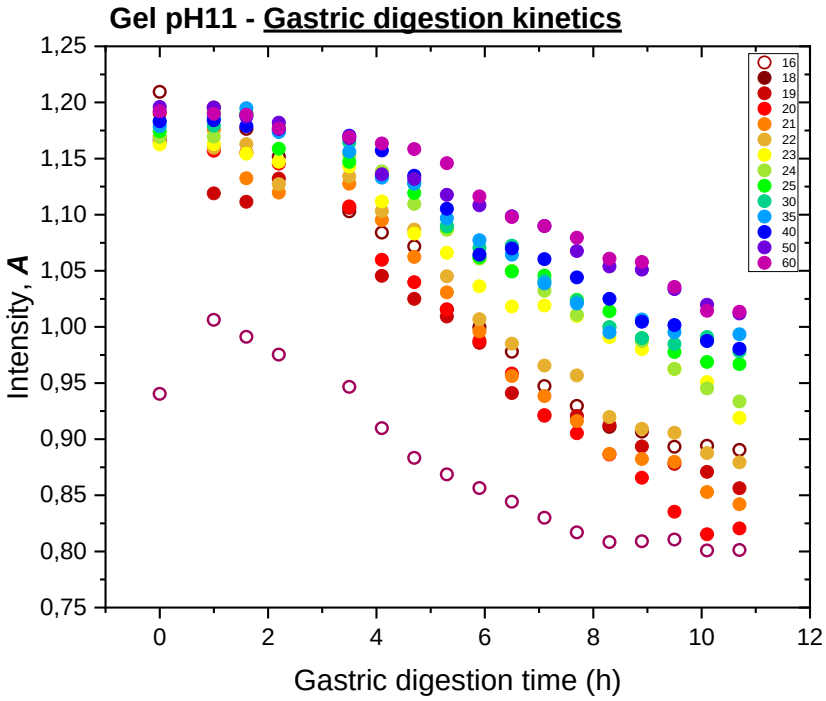

Figure A1.5 Evolution of the high *q* fit parameter ***A*** as a function of gastric digestion time for canola protein gel prepared at pH 11. Each point represents one SAXS curve. The colors represent different z positions in the capillary from 16 (at the gel's surface) to 60 (at 6.6 mm downward), with a 150 µm interval. Points at t=0 weres measured before digestion. The gastric juice was added at the 2nd points.

We can notice the same decreasing trend of the intensity ***A*** with digestion time, accelerating from around the 4th hour of digestion. The stronger (faster) intensity decay was observed for the *z* positions closest to the gel's top surface (closest to the gastric juice).

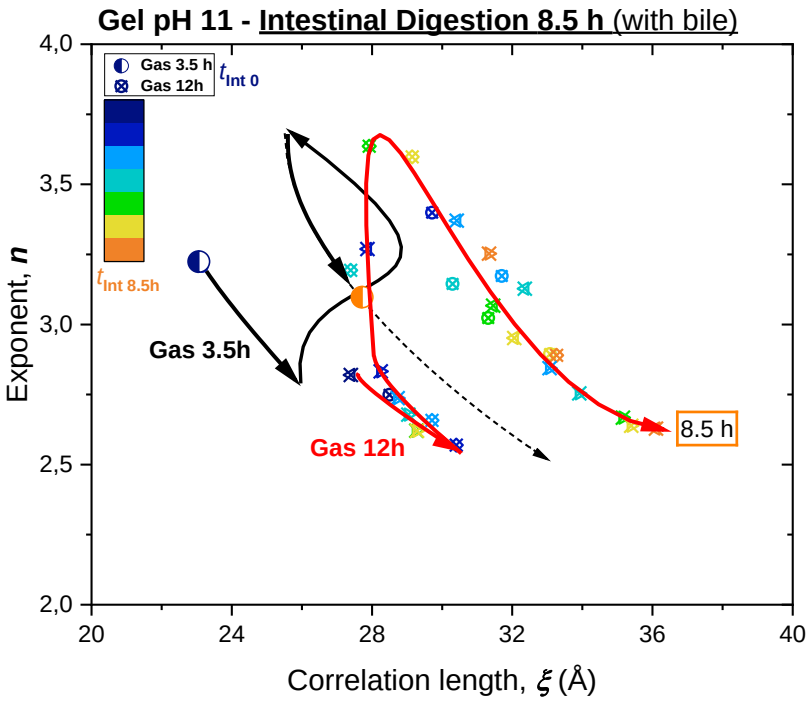

Figure A1.6 Effect of longer gastric step on the intestinal digestion. Diagram presenting the temporal evolution of high *q* fit parameters (exponent ***n*** as a function of the correlation length ξ) for canola gel prepared at pH 11, submitted to intestinal digestion during 8.5 h. Each point represents one SAXS curve. The colors represent different intestinal digestion times, from t_0 (dark blue) to 8.5 h (orange) of intestinal digestion. Diagrams of two gel samples are shown:

1) after 12 h of gastric digestion **Gas 12h** (crossed symbols), which evolution during intestinal digestion is marked by **red arrows**. 3 different crossed symbols show 3 capillary positions *z*, (from the closest to the gel's surface downward, with a 150 µm interval)
2) after 3.5 h of gastric digestion **Gas 3.5h** (double circles) – only two points (t_0 and plus 8.5 h of intestinal digestion) at 1 capillary position closest to the gel's surface, with the full evolution path marked by **black arrows**.

We can see an enhanced effect of longer (12h) gastric step before initiating the intestinal digestion, i.e. reaching of the more unfolded/disaggregated structures (larger ξ and lower ***n***) after 8.5 h of intestinal digestion.

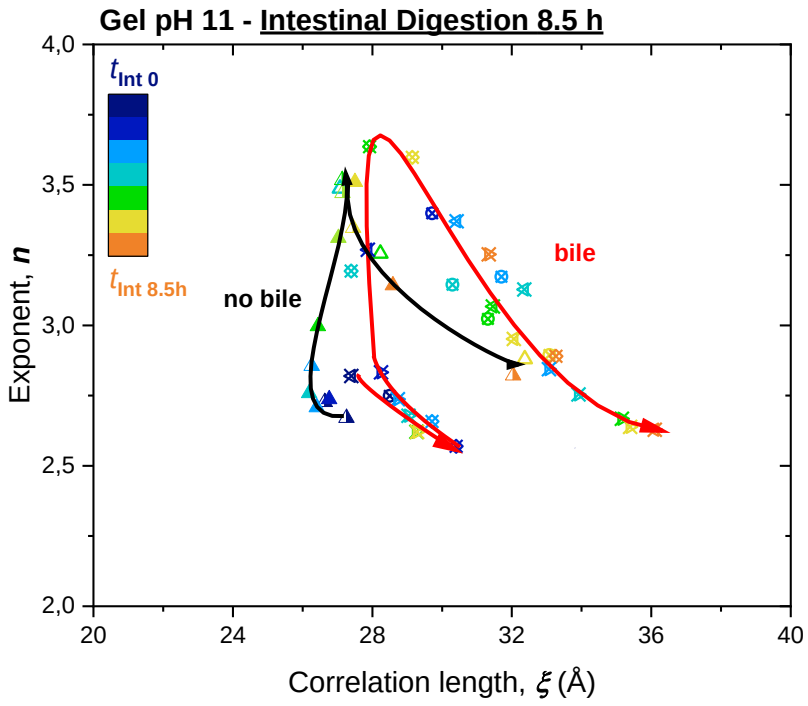

Figure A1.7 Effect of bile salts on the intestinal digestion. Diagram presenting the temporal evolution of high *q* fit parameters (exponent ***n*** as a function of the correlation length *ξ*) for canola gel prepared at pH 11, submitted to intestinal digestion during 8.5 h. Each point represents one SAXS curve. The colors represent different intestinal digestion times, from t_0 (dark blue) to 8.5 h (orange) of intestinal digestion. Diagrams for two gel samples are presented, digested after 10/12h of gastric step by intestinal juice with or without bile salts:

1) **with bile** (crossed symbols), which evolution during intestinal digestion is marked by **red arrows**;
2) **without bile** (triangles), which evolution during intestinal digestion is marked by **black arrows**. 3 different crossed symbols for each sample show 3 capillary positions *z*, (from the closest to the gel's surface downward, with a 150 µm interval);

We can see an enhanced final effect of bile in the intestinal juice on the digestion, i.e. reaching of the more unfolded/disaggregated structures (larger ξ and lower ***n***) after 8.5 h of intestinal digestion.

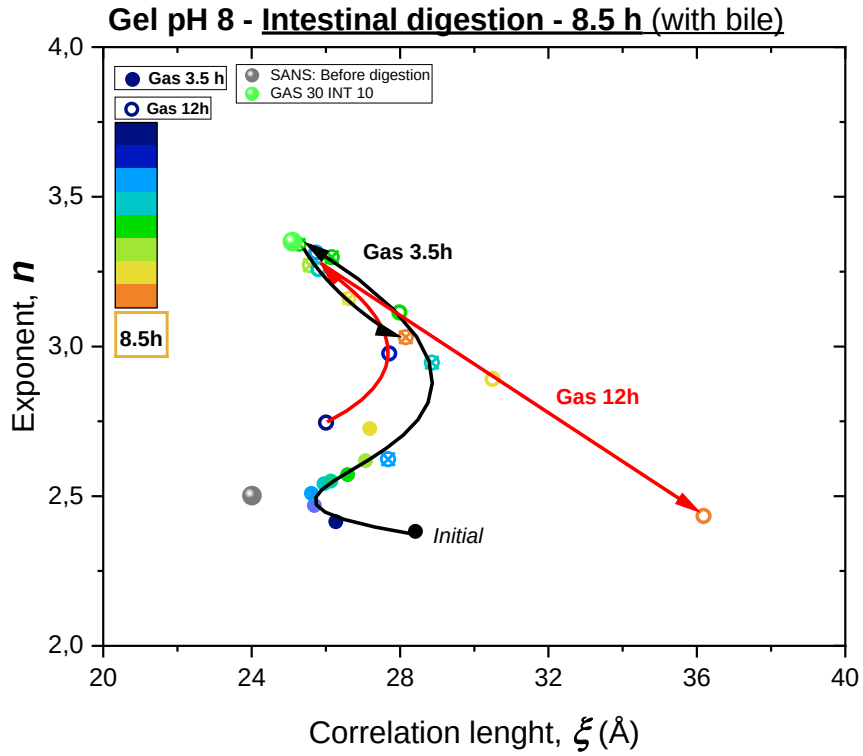

Figure A1.8 Effect of longer gastric step on the intestinal digestion. Diagram presenting the temporal evolution of high *q* fit parameters (exponent ***n*** as a function of the correlation length ξ) for canola gel prepared at pH 8, submitted to intestinal digestion of 8.5 h. Each point represents one SAXS curve. The colors represent different intestinal digestion times, from t_0 (dark blue) to 8.5 h (orange) of intestinal digestion.

Diagrams for two gel samples are presented:

1) after 12 h of gastric digestion (**Gas 12h** -open circles), which evolution during intestinal digestion is marked by **red arrows**, measured on 1 capillary position (closest to the gel's surface);
2) after 3.5 h of gastric digestion (**Gas 3.5h**), which evolution during intestinal digestion is marked by **black arrows**. 2 different symbols show 2 capillary positions *z*: the closest to the gel's surface (crossed circles) and 300 µm downwards (closed circles). Black initial point is the reference state before digestion.

Additionally, 2 points for SANS results for the pH 8 gel are shown: before digestion (big lighter black circle) and after 30 min of gastric then 10 min of intestinal digestion[4] (big lighter green circle) – showing the same level of compactness (***n***=3.3) reached during the intestinal step. We can see an enhanced effect of longer (12 h) gastric step before initiating the intestinal digestion, i.e. reaching of the more unfolded/disaggregated structures (larger ξ and lower ***n***) after 8.5 h of intestinal digestion.

[4] Digested in *in vitro* conditions (Falcon tube), not in a capillary.

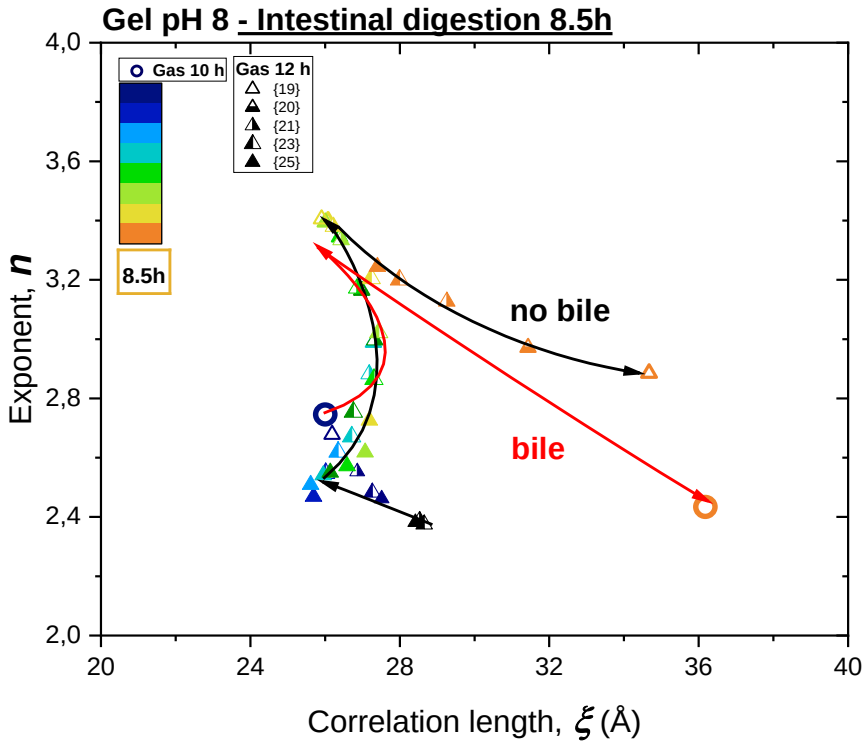

Figure A1.9 Effect of bile salts on the intestinal digestion. Diagram presenting the temporal evolution of high *q* fit parameters (exponent ***n*** as a function of the correlation length ξ) for canola protein gel prepared at pH 8, submitted to intestinal digestion of 8.5 h. Each point represents one SAXS curve. The colors represent different intestinal digestion times, from t_0 (dark blue) to 8.5 h (orange) of intestinal digestion.

Diagrams for two gel samples are presented, digested by intestinal solution with or without bile salts, after 10/12h of gastric step:

1) **with bile** (open circles), which evolution during intestinal digestion is marked by **red arrows**; only two points (t_0=Gas 10 h and after Int 8.5 h) for 1 capillary position (closest to the gel's surface), with the full evolution path marked by **red arrows**.
2) **without bile** (triangles), which evolution during intestinal digestion is marked by **black arrows;** 5 different crossed symbols show 5 capillary positions *z*: from z = 19 (closest to the gel's surface downwards to z = 25, with a 150 µm interval.

We can see an enhanced effect of the intestinal digestion with bile, i.e. reaching amore unfolded/disaggregated structures (larger ξ and lower ***n***) after 8.5 h of intestinal digestion.

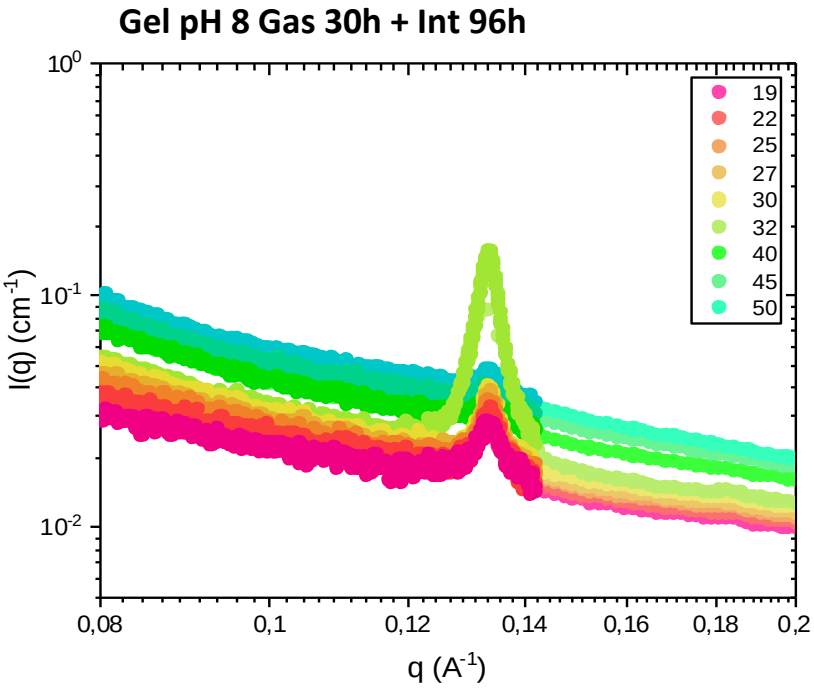

Figure A1.10 High *q* range of SAXS spectra of canola protein gel (100 g/L) prepared at pH 8, after 30 h of gastric and 96 h of intestinal digestion. We observe a peak at q = 0.13 $Å^{-1}$, which appears in the very digested sample part (visually liguid digesta, z= 19 – pink color), and its progressive increase at less digested sample positions (z =32 - light green). No peak was observed for even less digested positions (z from 40 to 50). Interval between 2 z positions was 300 µm. This peak most likely comes from bile salts present in intestinal juice and can indicate its conjugation to some free amino acids, released into the after the protein hydrolysis and arrangement into some crystalline phases with long-range structural order. The same feature was also observed during the intestinal digestion of the pH 11 gel.

APPENDIX 2: Long gastric and intestinal digestions

We investigated by SAXS the effect of **very long gastric and intestinal digestions** of canola protein gels. For these experiments, the protein gels in capillary cells were digested about 100 h. We performed vertical scanning of the capillaries (associating the *z* positions closer to the gel surface with the biggest degree of digestion).

We observed a progressive destruction of the protein aggregates, through a decrease of the low *q* scattering intensities and curves slopes (seen more precisely that in experiments showed in Chapter 4). In the most digested sample parts, large fraction of proteins was present in the liquid phase, representing a relatively low mass fraction of the gel.

Figure A2.1 shows the SAXS spectra for the **pH 8 gel after 96 h of gastric digestion**. The presented capillary positions *z* correspond to already very digested states: from the most digested part of the capillary with the lowest scattering signal (pos2) to the less digested position(pos40).

Figure A2.2 shows the SAXS spectra for the **pH 8 gel after 30 h of gastric digestion plus 96 h of intestinal digestion**. The presented capillary positions *z* correspond to different states: from the most digested part of the capillary with the lowest scattering signal (19) to the least digested (100). Positions from 19 to 40 are considered as the liquid digesta.

Similar effects of aggregates destruction during both long gastric and long intestinal digestion were also observed in digestion of the pH 11 gel (not shown).

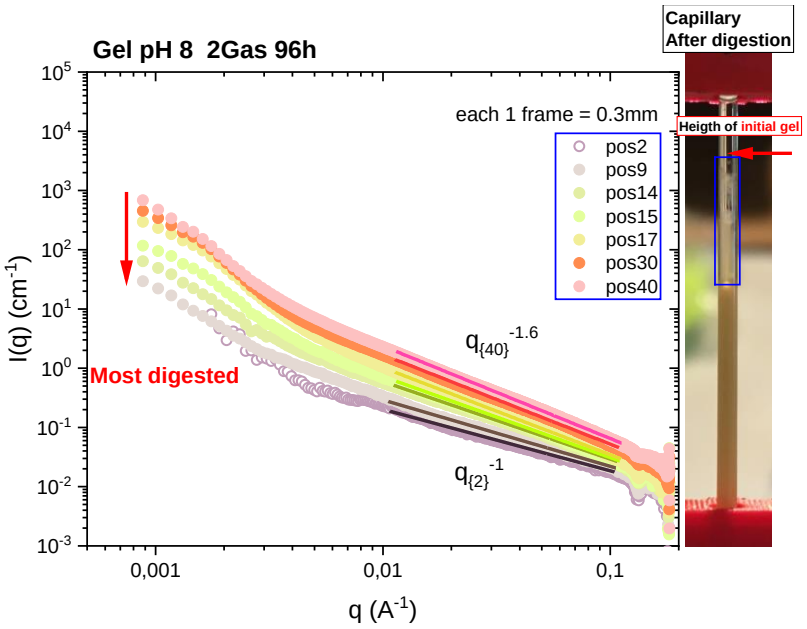

Figure A2.1 SAXS spectra for the pH 8 gel after 96 h of gastric digestion with renewed gastric juice. The presented capillary positions z correspond to already very digested states: from the most digested position of the capillary with the lowest scattering signal (pos2) to the less digested position (pos40), with 300 µm interval between two successive positions. A similar effect of aggregates destruction was also observed in the digestion of the pH 11 gel.

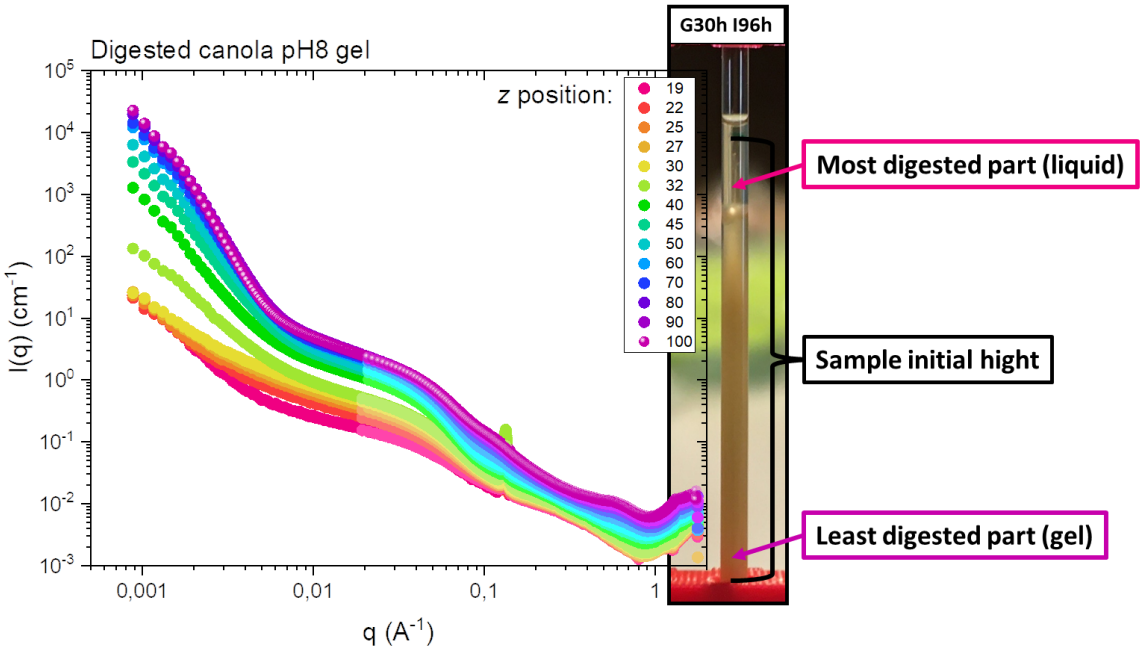

Figure A2.2 SAXS profile of the canola protein gel, digested with gastric juice for 30h then with intestinal juice for 96h. The colors represent different positions in the capillary: from the most digested position (19, pink – liquid state) to the least digested position (100, purple – gel state), with 300 µm interval between two successive positions

APPENDIX 3: Canola gel swelling in gastric pH 2

We performed some imaging experiments on the canola protein gels under control gastric pH conditions (~pH 2) but without pepsin enzyme, thus verifying solely the effect of the very acidic condition on the gel structures.

Confocal fluorescence imaging. In **Figure A3.1**, we can see a fluorescent piece of canola protein gel prepared at pH 11 in initial state (left-hand side) and after 30 min in HCl solution of pH 2 (right-hand side). We can see an increase in size of this piece of gel, indicating swelling of the network, caused by acid-induced repulsion of the proteins of the gel.

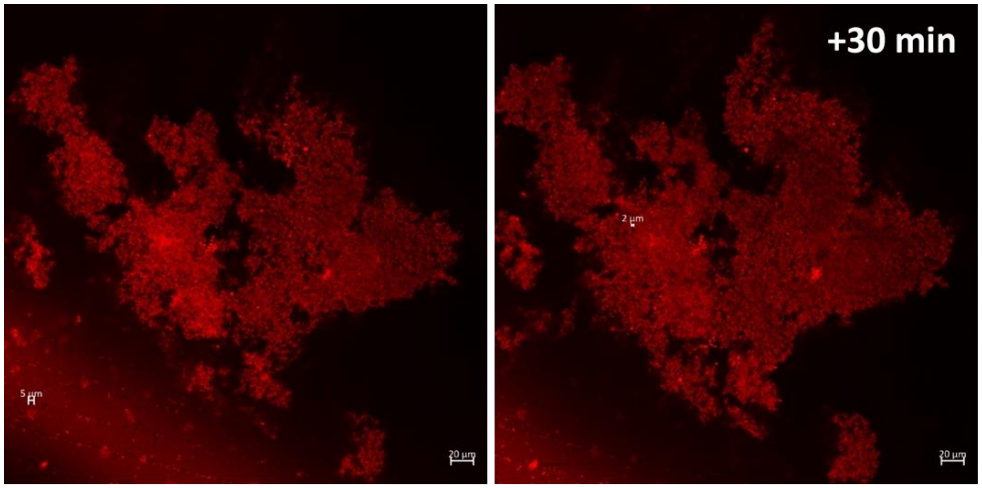

Figure A3.1 Confocal fluorescence images of a piece of canola protein gel (100 g/L) prepared at pH 11, with fluorescent dye Rhodamine B, showing the effect of swelling of the gel after 30 min in HCl solution (at pH 2). The contrast levels are the same. The scale bar is 20 µm.

Deep UV-fluorescence imaging. Figure A3.2 shows a fluorescent canola protein gel at pH 8 in the initial state (left-hand side) and after 20 min in HCl solution of pH 2 (right-hand side). We can see some increase of the size of the gel piece, indicating a swelling of the network. The auto-fluorescence intensity of the gel did slightly decrease due to the photobleaching of the gel piece.

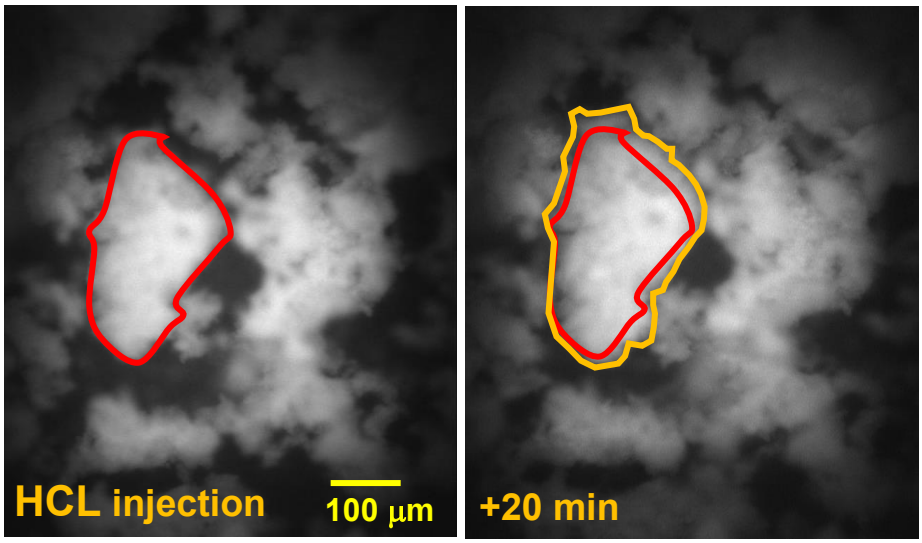

Figure A3.2 Deep UV-fluorescence images of the canola protein gel (100 g/L) prepared at pH 8, showing the effect of swelling of the gel after 20 min in HCl solution (at pH 2). The contrast levels are the same. The scale bar is 200 µm.

APPENDIX 4: Digestion of canola protein solutions

Small-Angle X-ray Scattering

We also performed SAXS experiments on canola protein solutions at pH 8 and pH 11during gastric and intestinal digestion.

Figure A4.1 shows the SAXS curves of proteins solutions after 1 hour of gastric digestion (red curves), followed by 30 min of intestinal digestion for the canola protein solutions at pH 8 (circles) and pH 11 (triangles). The effects of both gastric and intestinal digestion were the same for both pH solutions (no difference also in the initial samples).

After 1 h of gastric digestion, proteins have lost their native conformations (partially lost of the oscillation of the form factor of the hollow cylinder), due to unfolding and or subunits dissociation, similar to the effect of heat-triggered unfolding. Concerning the low q range, we could also see some increase of the low q upturn, due to the acid-induced aggregation/phase separation – the effect was observed also after the HCl addition to the protein solutions. This effect did not occur in the digestion of the corresponding gels. The following intestinal digestion provoked further, more pronounced unfolding of protein structures, with almost complete vanishing of the oscillations due to the compact protein structure. No protein re-compaction step, repeatedly observed upon intestinal digestion of the protein gels (presented in Chapter 4), was observed. In compare to the digestion of protein in gel networks, the digestion of proteins in solutions was significantly faster (see comparison on **Figure A4.2**). Altogether, we can consider the gel structures to have a stabilizing effect against the pH-enzymatic hydrolysis.

In summary, in solutions, canola proteins experienced during gastro-intestinal conditions:

- **unfolding** similar to the heat-triggered one,
- much **faster hydrolysis than in gels**.

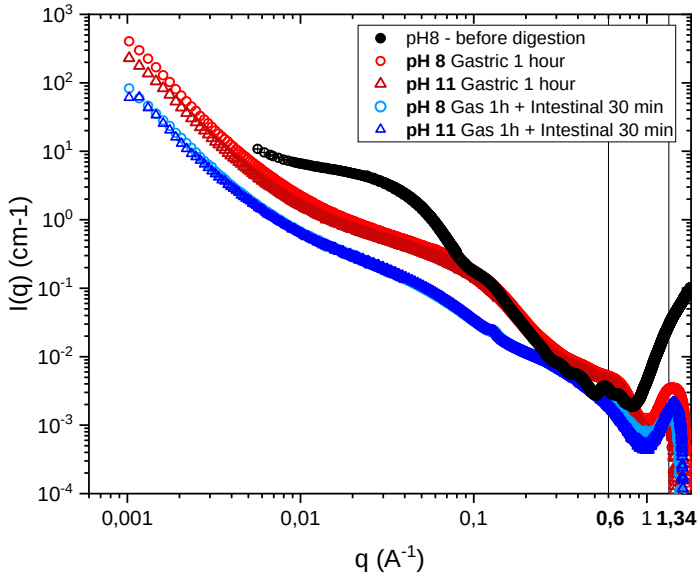

Figure A4.1 Canola protein solutions at pH 8 (circles) and pH 11 (triangles) after 1 h of gastric digestion (red) followed by 30 min of intestinal digestion (blue). The black curve represents an initial pH 8 solution. Concentration of protein for sample before digestion and for samples with digestion was 100g/L but for intestinal digestion, the samples were diluted with intestinal solution, thus reducing the concentration to 50g/L. The increased signal at q > 1 $Å^{-1}$ comes from the non subtracted buffer signal.

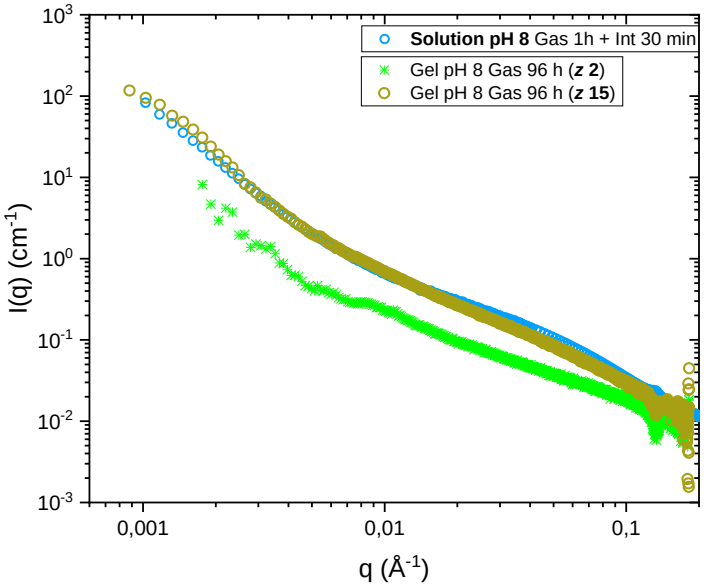

Figure A4.2: Solution at pH 8 after 1 h of gastric digestion and 30 min of intestinal digestion (from Fig. A4.1), compared to the corresponding gels after 96 h of gastric digestion, measured at the gel's surface (light green) and 4 mm downwards the capillary (dark green).

APPENDIX 5: Estimation of degree of hydrolysis (DH)

To complete the structural study on digestion of the canola protein gels and solution and answer questions about the digestion rates, we performed the digestion experiments of small (mm-size) canola protein gel pieces and quantified the degree of their protein enzymatic hydrolysis (see Material and Methods in Chapter 2).

We could see differences in digestion kinetics between the pH 8 and pH 11 gels, as well as a distinct effect for digestion proteins in native solution. **Figure A5.1** shows the percentage of protein hydrolysis as a function of digestion time, for 2 h of gastric step (red symbols) and 2 h of subsequent intestinal step. First of all, a great difference could be noticed between the digestion efficiency for protein solution and protein gels, with much slower hydrolysis (release of peptides) in case of the latter, especially in the gastric step (after 2 h of gastric digestion, around 7 fold higher %DH was obtained for the native solution in compare to the gels). The digestion kinetics of canola proteins in the **native solution** can be characterized by relatively fast initial hydrolysis, as if the proteins were readily hydrolyzed when attacked by the proteases, followed by slower subsequent stage, in which a large part of the proteins was digested and the enzymatic activity was decreased. After 2 h of subsequent intestinal step, the native solution displayed a DH ~90%, which is close to a complete hydrolysis of the protein into single amino acids.

Whereas, in **case of the gels**, a much slower initial gastric hydrolysis was observed, which then started slightly to accelerate. After 2 h of subsequent intestinal step, the protein gels displayed DH of 50-60 %, corresponding majority of dipeptides.

The difference between the digestion of proteins in gels and in the native solution likely results from the harder access of the enzyme to the substrate, caused by the steric hindrance of the gel network for the diffusive enzyme ingression, as well as the egression of peptides.

Moreover, we can distinguish some difference in the digestion kinetics between the two different gels. The **pH 8 gel**, comprised of partially unfolded proteins, exhibited faster hydrolysis rate, already in gastric step, reaching 50% higher degree of hydrolysis

after 2h, compared to the **pH 11 gel**, with compactly folded proteins. Since pepsin likely cleaves between the hydrophobic residues buried in less accessible protein cores, the unfolded proteins would naturally facilitate the digestion.

The differences between gastric and intestinal digestion steps lay in different efficiencies of pepsin and pancreatic enzymes, with the latter ones having more cleavage sites and thus providing higher digestibility.

The differences seen in the intestinal digestion between the two pH gels can be related to the differences in digestion of the corresponding gels observed by SAS, i.e. the formation of some intermediate "local aggregates" in the pH 11 gel, which can disturb the fluidity of hydrolysis and result in some slowing down, as observed at about 2-3h of the intestinal digestion for the pH 11 gel.

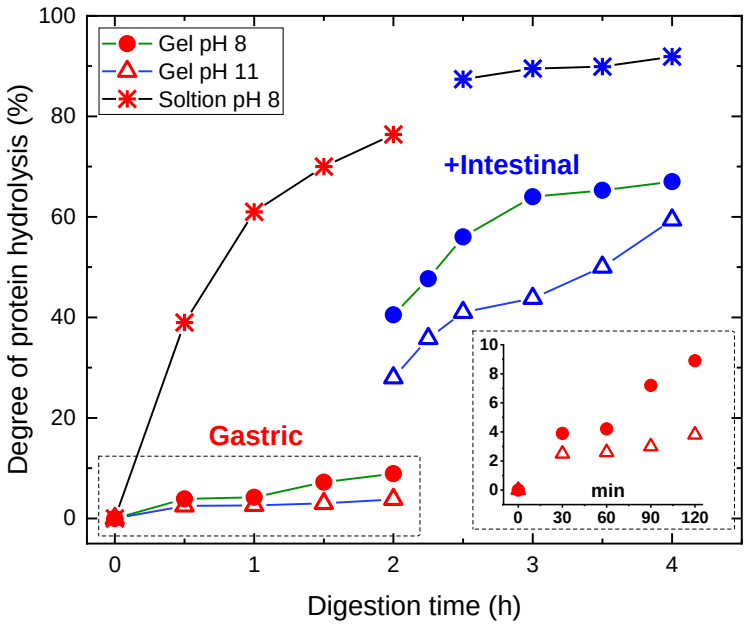

Figure A5.1 Degree of protein hydrolysis as a function of time, during 2 h gastric (red) and then 2 h of intestinal (blue) digestion; for canola protein native solution (~pH 8) (starred symbols) and canola protein gels, prepared at pH 8 (circles) and pH 11 (open triangles), at the same protein concentration (100g/L).